FACULTAD DE CIENCIA Y TECNOLOGÍA

Departamento de Química

Centro de Investigación en Síntesis Química

Área de Química Orgánica

TESIS DOCTORAL

Photocontrol of Antibacterial Activity

Memoria presentada en la Universidad de La Rioja para optar al grado de Doctor en Química por:

Elena Contreras García

Septiembre 2020

FACULTAD DE CIENCIA Y TECNOLOGÍA

Departamento de Química

Centro de Investigación en Síntesis Química

Área de Química Orgánica

D. DIEGO SAMPEDRO RUIZ, Profesor Titular de Química Orgánica del Departamento de Química de la Universidad de La Rioja,

CERTIFICA:

Que la presente memoria titulada "**Photocontrol of Antibacterial Activity**", ha sido realizada en el Departamento de Química de La Universidad de La Rioja bajo su dirección por la Graduada en Química **Dña. Elena Contreras García** y autoriza su presentación para que sea calificada como Tesis Doctoral.

Logroño, septiembre de 2020

Fdo. Diego Sampedro Ruiz

Agradecimientos

Hace varios años que decidí iniciar esta etapa en el mundo de la investigación científica. Entonces era una estudiante de grado que no tenía muy claro en que rama de la química centrar su interés, pero finalmente me decidí por la fotoquímica. Me gustaría empezar esta parte de la tesis agradeciendo a mi tutor **Diego** por acogerme en el grupo y darme la oportunidad de realizar mis trabajos fin de estudio, así como esta tesis doctoral. También por permitirme desarrollar mis ideas a lo largo de la tesis y evolucionar como investigadora. A **Pedro**, el jefe supremo del grupo, por motivarme siempre a seguir por el camino de la investigación.

A **Miguel Ángel** quiero darle las gracias por su versatilidad dentro y fuera del laboratorio. Por saber estar ahí en los buenos momentos de celebración, pero lo que es más importante en los malos, teniendo siempre palabras amables y mensajes de apoyo. MA gracias por ejercer de psicólogo de grupo.

Debo admitir que durante todos estos años ha habido momentos buenos y momentos malos, estos últimos generalmente asociados con la parte científica. No es fácil dedicar tu tiempo y esfuerzo a un trabajo que da alguna alegría, pero conlleva muchos fracasos en el camino. A pesar de todo, si doy las gracias por algo es por la gente que he conocido y que han hecho que esta experiencia sea inolvidable.

En primer lugar, me gustaría agradecer a mis compañeros de laboratorio. **David** gracias por ser mi maestro, por tener la paciencia de enseñarme desde mi inicio en este mundo. Por hacerme reír cuando bailabas en el laboratorio y llorar cuando cantabas. **Raúl** gracias por ser el técnico de este grupo y sacar a flote el laboratorio. Por ayudarme con los equipos cada vez que te planteaba un problema, y por mantener la calma en medio de la tormenta.

Puede que nuestro grupo no sea el más numeroso, pero para eso tenemos al lado a los Quibis que son los primos-hermanos que siempre están ahí. Gracias **Ali** por ser mi fiel compañera de gym y obligarme a ir cuando prefería echarme una siestita. A **Pablo** por entrar todos los días a darme los buenos días y sacarme una sonrisa. También por venir a perrear cada vez que ponía un temazo en el lab. A **Guille** por hacer del despacho una zona de juegos con las partidas al Triviador. A mi italiana favorita **Xhenti**, que junto con **Iris Alicia** han sido compañeras de largas horas de cotilleo de la casa Slytherin. Y no quiero olvidarme de **Pau** e **Ismael** que también estaban ahí para despotricar siempre que la ocasión lo merecía.

Dentro del grupo de los inorgánicos me gustaría agradecer en primer lugar a **Quintana** por despertarme a las 4 de la mañana para ver los partidos de la NBA (Lebron>Curry). También al fetuccini italiano **Mattia**, **Mónica** (rubia), **Mónica** (morena), **Rebeca** por los buenos momentos que hemos vivido.

Agradecer también a la profesora **Carmen Torres** y su equipo **Carmen Lozano**, **Carla Andrea** y **Laura** por colaborar con el diseño y la ejecución de la parte más biológica de esta tesis, ayudándome con ciertos conceptos con los que quizá los químicos no estamos tan familiarizados.

I want to thank **Prof. Arthur Winter** for allowing me to be part of his group for four months. Thanks for taking into account the idea of this thesis and helping me achieve the objectives I was looking for. I also want to thank the people forming the group, especially **Komadhie**, **Pradeep**, and **Logan**, for making me feel welcome and helping me settle in the new lab.

A mis amigas **Berta**, **Nerea**, **Andrea**, **Alba** les quiero agradecer por estar ahí y obligarme a desconectar del mundo de la química los viernes de cena y los sábados de fiesta. Aunque estos últimos con la edad se van reduciendo. Mención especial para **Andrea** por diseñar la portada de esta tesis.

A mi familia, mis **padres** y **hermano** por su apoyo constante que se ha hecho más necesario estos últimos años y por creer siempre en mí. Por el cariño infinito que me han dado siempre, por educarme y hacerme ser la persona que soy hoy en día.

Por último, quiero dar las gracias a **Edu** por acompañarme durante este largo camino dentro y fuera del laboratorio. Has sido uno de los pilares de mi vida desde mucho antes de que empezara la tesis y espero que lo seas durante muchos años más.

Finalmente quiero agradecer a las entidades financiadoras por el apoyo económico prestado para la realización de esta tesis doctoral. En especial, a la Universidad de La Rioja por el contrato predoctoral FPI-UR y las ayudas a tesis doctorales (ATUR), así como al Ministerio de Ciencia e Innovación por los proyectos CTQ2014-59650-P y CTQ2017-87372-P.

“Don’t waste your time looking back.
You’re not going that way”.

Ragnar Lothbrok – Vikings

Table of Contents

Abstract

This doctoral thesis describes the design, synthesis, and evaluation of compounds whose antibacterial activity can be controlled using light. In the first chapter, a brief historical perspective in photochemistry and the use of light in medical therapy is introduced. From the evolution of these two areas have emerged different alternatives that rely on light stimuli to treat diverse diseases.

The second chapter focuses on some of these alternatives: the photopharmacological approach and the use of photoreleasable protective groups to cage drugs. Photopharmacology is based on bioactive molecules that incorporate in their structure a molecular switch. The photoactive moiety can undergo an isomerization process that induces changes in the molecule properties like dipole moment, geometry, or electronics. These changes can result in isomers with different biological activity. Thus, a reversible system can be created where one isomer presents activity against the desired target while the other does not. On the contrary, the use of a photoreleasable protective group to cage a drug creates an irreversible system. The protective group is linked in a position that renders the drug inactive, upon light irradiation, the drug is released recovering its activity. These two options can help to solve some of the problems that classic pharmacological agents present. More specifically, the work here described is aimed at antibiotic drugs.

The objectives of this thesis are listed in the third chapter.

The fourth chapter focuses on the photopharmacological approach. Several molecules were designed with their structure based on quinolone antibiotics and a molecular switch linked in different positions. The molecular switches employed were based on the hydantoin structure and the pyrrole of the phytochrome chromophore. After their synthesis, their photochemical properties were evaluated. All of them were able to carry out the isomerization process with UV or visible light, and different photostationary states were found. Furthermore, the characteristics of one of the derivatives were studied more in-depth to test its efficiency and stability as a molecular switch. Finally, a study to evaluate possible changes in the activity of the initial isomers and the photostationary states obtained was carried out. The biological study showed that two compounds changed their activity after irradiation.

The fifth chapter describes the caging process of ciprofloxacin, a quinolone antibiotic, using oxime esters. Different oxime parts were synthesized to try to achieve a bathochromic shift in their absorption. The coupling reaction between the oxime and the antibiotic was designed to form an oxime ester at position 3 of ciprofloxacin.

This position is of great importance for the antibacterial activity of the drug. The study of the photochemical properties showed strong absorption in the UV region for all derivatives. The release reaction was successfully induced in all cases with good yields. Moreover, absorption in the visible region was achieved when tetrafluoroboric acid was added to the samples in halogenated solvents. A new band in the blue region of the spectrum appeared, making possible their irradiation with visible light. Finally, to improve the solubility in water of these compounds, one of the oxime esters was trapped in a polymeric micelle, which highly enhanced this property.

Lastly, the sixth chapter also focuses on the caging technique and tries to solve some of the drawbacks that oxime esters present. In this chapter, a new photoreleasable group was employed, known as BODIPY. Several BODIPY structures were synthesized to achieve absorption inside the therapeutic window and make the molecules totally or partially soluble in water. This group was coupled at position 3 of two quinolones antibiotics: nalidixic acid and ciprofloxacin. All photoreleasable quinolones displayed absorption in the visible region varying from the green to the NIR region. Irradiation of the samples with visible light allowed the complete release of the antibiotic part in all cases. Furthermore, their stability and efficiency were evaluated. Finally, a biological study was performed to evaluate possible differences in the activity of the caged and uncaged compound. Results showed a strong deactivation of the antibacterial properties when the BODIPY group was linked to the antibiotic. Upon light irradiation, the activity of the drugs was recovered.

Resumen

Esta tesis doctoral describe el diseño, síntesis y evaluación de compuestos cuya actividad antibacteriana puede ser controlada mediante el estímulo de la luz. En el primer capítulo, se introduce brevemente una perspectiva histórica de la fotoquímica, así como del uso de la luz en la terapia médica. De la evolución de estas áreas han surgido diferentes alternativas que se basan en el estímulo de la luz para tratar diversas enfermedades.

El segundo capítulo se centra en algunas de estas alternativas: el enfoque fotofarmacológico y el uso de grupos protectores fotoliberables para enjaular medicamentos. La fotofarmacología está basada en moléculas con actividad biológica que incorporan en su estructura un interruptor molecular. La parte fotoactiva puede experimentar un proceso de isomerización que induce un cambio en ciertas propiedades de la molécula como el momento dipolar, la geometría o la electrónica. Estos cambios pueden dar como resultado isómeros con diferentes actividades biológicas. Por tanto, se puede crear un sistema reversible donde un isómero presenta actividad contra el objetivo deseado mientras que el otro no. Por el contrario, el uso de un grupo protector fotoliberable para enjaular un medicamento da lugar a un sistema irreversible. El grupo fotoprotector se enlaza en una posición que hace que el medicamento se inactive. Cuando este es irradiado con luz, el medicamento se libera y recupera su actividad. Estas dos opciones pueden ayudar a resolver algunos de los problemas que presentan los agentes farmacológicos clásicos. Más específicamente, el trabajo aquí descrito está dirigido hacia medicamentos antibacterianos.

Los objetivos de esta tesis aparecen descritos en el tercer capítulo.

El cuarto capítulo se centra en el enfoque fotofarmacológico. Se diseñaron varias moléculas con su estructura basada en quinolonas unidas a un interruptor molecular en diferentes posiciones. Los interruptores moleculares empleados se basaron en la estructura de la hidantoína y en el pirrol del cromóforo del fitocromo. Tras su síntesis, se evaluaron sus propiedades fotoquímicas. Todos ellos llevaron a cabo el proceso de isomerización con luz UV o visible, encontrándose distintos estados fotoestacionarios para cada uno de ellos. Además, se estudiaron más a fondo las características de uno de los derivados para comprobar su eficiencia y estabilidad como interruptor molecular. Finalmente, se llevó a cabo un estudio para evaluar posibles cambios en la actividad de los isómeros iniciales y los estados fotoestacionarios obtenidos. El estudio biológico mostró que dos de los compuestos

cambiaron su actividad después de ser irradiados. Los mejores resultados mostraron un cambio de 4 órdenes.

El quinto capítulo describe el proceso de fotoliberación del ciprofloxacino, un antibiótico perteneciente a las quinolonas, usando ésteres de oxima. Se sintetizaron diferentes oximas para intentar conseguir un desplazamiento batocrómico en su absorción. La reacción de acoplamiento entre la oxima y el antibiótico se diseñó para que el éster de oxima se formase en la posición 3 del ciprofloxacino. Esta posición es de vital importancia para la actividad antibacteriana del medicamento. El estudio de las propiedades fotoquímicas mostró una fuerte absorción de todos los derivados en la zona UV del espectro. El proceso de liberación se llevó a cabo satisfactoriamente en todos los casos con buenos rendimientos. Además, se logró la absorción en la región visible del espectro cuando se añadió ácido tetrafluorobórico a las muestras en disolventes halogenados. Se descubrió una nueva banda en la región azul del espectro, lo que hizo posible la irradiación con luz visible. Por último, para mejorar la solubilidad en agua de estos compuestos, uno de los ésteres de oxima fue atrapado en una micela polimérica, lo que mejoro notoriamente esta propiedad.

Finalmente, el sexto capítulo también está centrado en la estrategia de fotoliberación y trata de resolver algunos de los inconvenientes que presentan los esteres de oxima. En este capítulo, se utilizó un nuevo grupo fotoliberable conocido como BODIPY. Se sintetizaron varios BODIPYs con el fin de lograr la absorción dentro de la ventana terapéutica y hacer las moléculas total o parcialmente solubles en agua. Este grupo se acopló en la posición 3 de dos quinolonas: ácido nalidíxico y ciprofloxacino. Todas las quinolonas fotoliberables mostraron absorción en la zona visible del espectro, variando desde la región verde hasta el infrarrojo cercano. La irradiación de las muestras se llevó a cabo con luz visible y permitió la completa liberación del antibiótico en todos los casos. Además, también se evaluó su estabilidad y eficiencia. Por último, se realizó un estudio biológico para evaluar posibles diferencias en la actividad de los compuestos enjaulados y liberados. Los resultados obtenidos mostraron una fuerte desactivación de las propiedades antibacterianas cuando el grupo BODIPY estaba unido al antibiótico. Tras la irradiación con luz, la actividad del medicamento se recuperó. Los mejores resultados mostraron una diferencia de diez ordenes de cambio en la actividad.

Abbreviations and Acronyms

Φ	quantum yield
^{13}C-NMR	carbon nuclear magnetic resonance
^{1}H-NMR	proton nuclear magnetic resonance
Å	angstrom
ACS	American Chemical Society
Boc group	*tert*-butyloxycarbonyl protecting group
BODIPY	boron-dipyrromethene
brs	broad singlet (in NMR spectroscopy)
Calcd.	calculated
CFU	colony-forming unit
CP	ciprofloxacin
d	doublet (in NMR spectroscopy)
DAEs	diarylethenes
DASAs	donor-acceptor Stenhouse adducts
DCM	dichloromethane
dd	doublet of doublets (in NMR spectroscopy)
DIPEA	*N,N*-diisopropylethylamine
DMAP	4-(dimethylamino)pyridine
DMF	*N,N*-dimethylformamide
DMSO	dimethyl sulfoxide
DNA	deoxyribonucleic acid
EC_{50}	half-maximal effective concentration
FDA	Food and Drug Administration
GABA	gamma-aminobutyric acid
GSH	glutathione

HGT	horizontal gene transfer
HPLC	high-performance liquid chromatography
HR ESI-MS	high-resolution electrospray ionization mass spectrometry
IC_{50}	half-maximal inhibitory concentration
IR	infrared
J	coupling constant (in NMR spectroscopy)
LED	light-emitting diode
Levo	levofloxacin
LORR	loss of righting reflex
LOXs	lipoxygenases
m	multiplet (in NMR spectroscopy)
MBC	minimum bactericidal concentration
MC	merocyanine
MEK-1	mitogen-activated protein kinase 1
MIC	minimum inhibitory concentration
NIR	near-infrared
NOESY	nuclear Overhauser effect spectroscopy
NPV	net present value
PDT	photodynamic therapy
PPG	photoreleasable protective group
ppm	parts-per-million
PSS	photostationary state
PTFE	polytetrafluoroethylene
q	quartet (in NMR spectroscopy)
qd	quartet of doublets (in NMR spectroscopy)
quint	quintet (in NMR spectroscopy)
RGB	red green and blue

s	singlet (in NMR spectroscopy)
SP	spiropyran
t	triplet (in NMR spectroscopy)
TBTU	*O*-(benzotriazol-1-yl)-N,N,N’,N’-tetramethyluronium tetrafluoroborate
TEA	triethylamine
TFA	trifluoroacetic acid
THF	tetrahydrofuran
t_R	retention time (in high-performance liquid chromatography)
UV	ultraviolet
Vis	visible
vs.	*versus*
δ	chemical shift
ε	molar extinction coefficient
λ	wavelength

Chapter 1

Introduction and Historical Perspective

1.1 Photochemistry: early discoveries and evolution

Reactions induced by light are significantly older than life itself. Solar radiation is the fundamental energy source in Earth evolution, from its accretion phase till now. It is safe to say that photochemistry on our planet started as soon as the dust began to settle.[1]

Solar energy has been used by people since the beginning. First humans used it as a source of light and heat. Egyptians were able to use solar light inside the pyramids to build the tombs thanks to mirrors. It is widely believed that Archimedes, also employing mirrors, could destroy the Roman fleet in the battle of Syracuse.

Besides making use of the physical interactions of light with materials, some pioneer scientists realized that light could also interact with the chemical nature of them. Several sunlight-induced changes in the appearance of materials or their functionality were noticed. Some examples are the bleaching effect on dyed fibers, the preservation of paintings,[2] or the peeling and fading in exterior paints.

The use of sunlight for laboratory experiments is documented as early as 1599 when Conrad Gesner described "*The maner of Distilling in the Sunne*".[3] Fifty years later, John French designed two setups based on the heat capacity of different materials to rectify spirits.[4]

In the 18th century, Priestly observed two photoreactions in two different fields: inorganic chemistry and photosynthesis. Upon exposing partially filled vials of nitric acid to sunlight, he noted a change in the liquid's color due to the formation of nitrogen dioxide.[5] Priestly is also given credit for discovering the basic principles of photosynthesis. Following his steps, in 1804 Nicholas Theodore de Saussure demonstrated the influence that light has in plants to consume water and carbon dioxide and to produce oxygen.[6]

In the following decades, several scientists contributed either by choice or by chance to the development of photochemistry. Some of the first reactions discovered were light-induced halogenations, [2+2]-cycloadditions, photoreductions of carbonyl compounds, photodimerizations, and geometric isomerizations.

Regarding organic compounds and photochemistry, the photoreaction of santonin might be the first one discovered. In 1834, Hermann Trommsdorff reported that upon exposure of santonin to sunlight, the color changed from white to yellow, followed by a crystal burst.[7] Furthermore, he studied how different wavelengths affected the reaction using a prism. He realized that the yellow crystals only appeared

after irradiation with direct sunlight and also with blue and violet rays, but interestingly, not with yellow, green, or red beams.

At the end of the 19th century, photochemistry was a small field of the expanding science of chemistry. Only a limited number of reactions were discovered, and the sun was the only light source.

At the beginning of the 20th century, Ciamician and Silber began a methodical investigation of photochemical reactions. Thanks to their effort, photochemistry began to be considered a major branch of chemistry. They discovered photopinacolization, intramolecular cycloadditions, and both α- and β-cleavage, which later proved to be of immense importance for the development of molecular photochemistry.

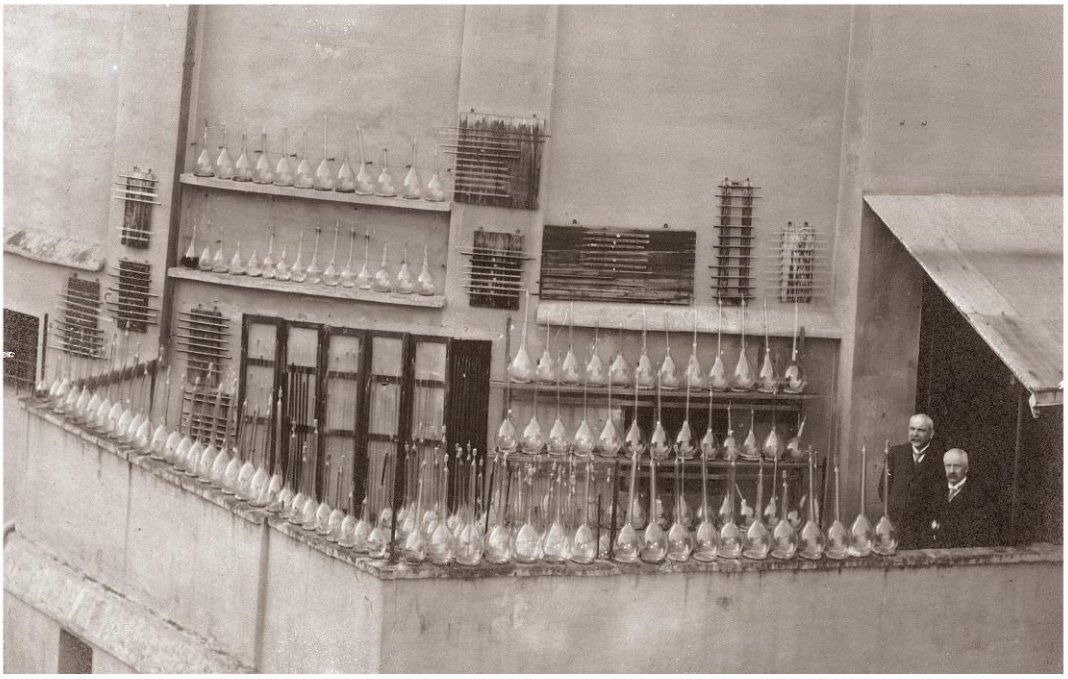

Figure 1. Giacomo Ciamician and Paolo Silber on the roof of the chemistry building in Bologna. In order to perform photochemical experiments, samples were exposed to sunlight. Reprinted with permission from Sistema Museale di Ateneo. ©Copyright 2020 - ALMA MATER STUDIORUM.

The value of their work not only consisted of the number of new photoreactions they discovered but also in Ciamician's effort to compile all the work established to date in the area of photochemistry. Ciamician drew a visionary picture of future applications of light-driven reactions in organic synthesis as well as in industry.

1.2 The use of light in medical therapy

Phototherapy has been employed since ancient times as a treatment for different diseases. Through sunlight exposure, people were treated for several conditions, from locomotor disorders to an array of skin diseases. There are manuscripts as old as Papyrus Ebers, which recorded the treatment of vitiligo through the ingestion of a boiled extract from a weed growing in the Nile Delta, followed by sun exposure.[8]

Modern phototherapy was possible thanks to achievements made by a few scientists. Isaac Newton discovered the color wheel using a prism to split a light beam into seven basic colors. Friedich Wilhelm Herschel discovered in 1800 the sun's infrared spectrum. One year later, Johann Wilhelm Ritter and William Hyde Wollaston discovered the ultraviolet radiation.[9] At the end of the 19th century, the transition from heliotherapy to artificial phototherapy was possible thanks to the development of electric sources of irradiation.

In 1877, Downes and Blunt proved that sunlight has a bactericidal effect and could kill *Bacillus anthracis*.[10] In 1896, Finsen, aware of this effect, developed a "chemical rays" lamp to treat lupus vulgaris successfully.[11] The importance of this discovery must be remarked because, at that time, no anti-inflammatory or antibiotic drugs were available. In 1903, due to the relevance of his research, Finsen was awarded the Nobel Prize in medicine.

At the beginning of the 20th century, a new form to use light with medical purposes was created. By combining a light source, a photosensitizer, and tissue oxygen, photodynamic therapy was able to treat malignant tumors of the skin and subcutaneous tissue.[12]

A few years later, in 1956, Sister Jean Ward observed that sunshine decreased neonatal jaundice, which in conjunction with tests made by hospital biochemists,[13] led to the use of light as an effective therapy for infantile hyperbilirubinemia.[14] Nowadays, exposure to sunlight or UV light keeps being the treatment of choice for newborns with this condition.

More modern uses of light for medical applications include photopharmacology and optogenetics. Both methodologies enable light-induced manipulation of cellular activity. To accomplish this objective, they use optically active components that are introduced into the desired target. In optogenetics, photoreceptors are introduced at the genetic level, enabling the control of diverse biological networks. In contrast, photopharmacology relies on photochromic compounds that need to be externally supplied.

1.3 References

1. Canuto, V. M.; Levine, J. S.; Augustsson, T. R.; Imhoff, C. L.; Giampapa, M. S., The young Sun and the atmosphere and photochemistry of the early Earth. *Nature* **1983,** *305* (5932), 281-286.
2. Price, D. S., XXXVIII.—On the action of light upon sulphide of lead, and its bearing upon the preservation of paintings in picture galleries. *Journal of the Chemical Society* **1865,** *18* (0), 245-249.
3. Gesner, C., *The Practise of the New and Old Phisicke*. London, 1599; p 23-24.
4. French, J., *The Art of Distillation*. T. Williams: London, 1653.
5. Priestly, J., *Experiments and observations on different kinds of air* J. Johnson: London, 1775.
6. Ihde, A. J., *The Development of Modern Chemistry*. Dover Publications: 1984.
7. Trommsdorff, H., Ueber Santonin. *Annalen der Pharmacie* **1834,** *11* (2), 190-207.
8. Millington, G. W. M.; Levell, N. J., Vitiligo: the historical curse of depigmentation. *International Journal of Dermatology* **2007,** *46* (9), 990-995.
9. Roelandts, R., Bicentenary of the discovery of the ultraviolet rays. *Photodermatology, Photoimmunology & Photomedicine* **2002,** *18* (4), 208-208.
10. Downes, A. H.; Blunt, T. P., Researches on the effect of light upon bacteria and other organism. *Proceedings of the Royal Society* **1877,** *26*, 488-500.
11. Finsen, N. R., Om Anvendelse i Medicinen af koncentrerede kemiske Lysstraale. [On the application in medicine of concentrated chemical rays of light]. *Gyldendalske Boghandels Forlag* **1896**.
12. Jesionek, A.; Tappeiner, H. v., Die Behandlung der Hautkarzinome mit fluoreszierenden Stoffen. *Deutsches Archiv für klinische Medizin* **1905,** *82*, 223-226.
13. Dobbs, R. H.; Cremer, R. J., Phototherapy. *Archives of Disease in Childhood* **1975,** *50* (11), 833-836.
14. Influence of Light on the HyperbilirubinÆmia of Infants. *The Lancet* **1958,** *271* (7030), 1094 - 1097.

Chapter 2

Literature Review

2.1 An insight into antibiotics

Antibiotics are one of the most important milestones in medicine. Although the first antibiotics were discovered in the early 20th century, they were used for a long time before. It is a fact that Egyptians used honey and bread on which filamentous fungi grew, to treat wounds and burns.[1] At the end of the 19th century, several scientists noticed that some bacteria could inhibit others. Louis Pasteur and his colleague François Joubert observed in 1877 that the growth of *Bacillus anthracis* was inhibited when co-cultivated with common aerobic bacteria. Even though these observations had been made, no antibacterial molecule was purified. It was in 1909 when Paul Ehrlich discovered arsphenamine, an arsenic derivative active against *Treponema pallidum*, which causes syphilis.[2] The antibiotic was marketed in 1911 with the name Salvarsan®, later Mapharsen®. A few years later, in 1930, Gerhard Domagk discovered that sulphanilamide,[3] a molecule synthesized 22 years before by Paul Gelmo,[4] had antibiotic activity. This molecule was commercialized under the name Prontosil®.

Antibiotics are not a human invention as they are produced by microorganisms such as *Streptomyces* or fungi as weapons to eliminate bacteria that are competing for the same resources.[5] First antibiotic agents were isolated from natural secretions of environmental bacteria or fungi. Moreover, natural products isolated from microorganisms have been the source of most antibiotics currently on the market.[6] In 1941, Selman Waksman coined the term antibiotic to describe those natural molecules that could inhibit the growth of bacteria.[7] Nowadays, this term has been expanded to include also synthetic products with similar activity.

Research and development of new antibiotic agents seem to be a major issue. The majority of the marketed antibiotics in recent years are based on natural chemotypes. Between 1982 and 2002, 70 out of 90 antibiotics commercialized had their origin in natural products.[6] Most of the remaining products belonging to quinolones. Research on synthetic antibiotics is decreasing due to a poor return on investment.[8] Meanwhile, the research of natural products is following the same tendency because of the lack of success. As shown in figure 1, the number of new compounds that reach the market has been steadily decreasing to reach the critical number of only 2 specialties approved by the FDA for the period 2008-2012.[9]

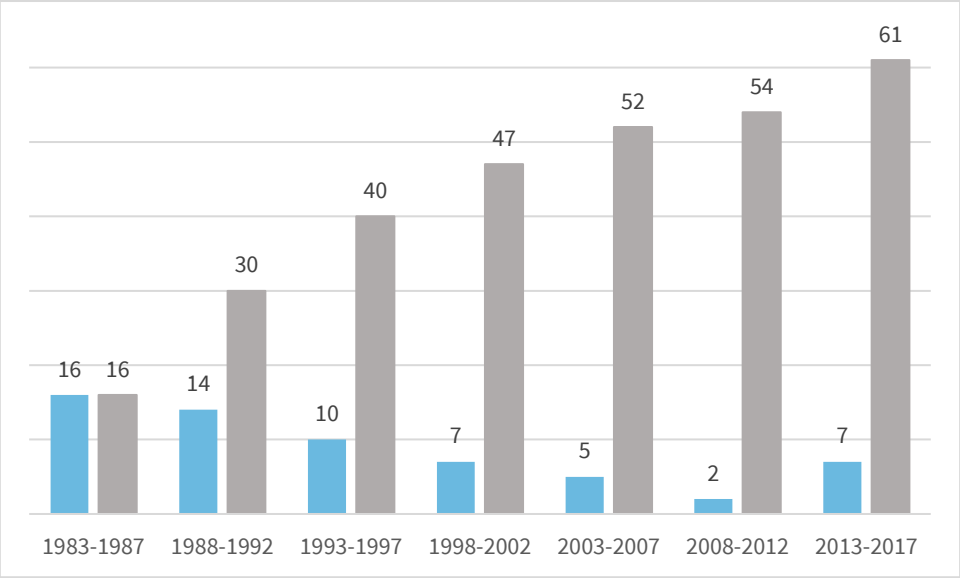

Figure 1. Evolution of the FDA-approved antibiotics since 1983. In blue, the new antibiotics approved during that time interval. In grey, the total amount of antibiotics approved from 1983 until the year specified. Data obtained from reference 9.

2.2 The problem of antibiotic resistance

While the discovery of new antibiotics keeps decreasing, the problem with antibiotic resistance is rising to a dangerously high level. Antibiotic resistance occurs when bacterial pathogens develop defense mechanisms against different antibiotics used for their treatment. These resistant bacteria receive the name of "superbugs". Examples of these superbugs are *Staphylococcus aureus* (MRSA) and *Mycobacterium tuberculosis* among Gram-positive bacteria and *Klebsiella pneumoniae* among Gram-negative bacteria. The rising of these superbugs is a major global healthcare problem in the 21st century.

Although now accessible to the majority of the population in developed countries, antibiotics were initially scarce and very expensive, only restricted for use by the military during World War II.[10] Over time, new formulations were developed, and the manufacturing processes were simplified, making antibiotics accessible to a large number of people. Seen at that time as miraculous drugs, they were used to treat even the most common and trivial types of infections, many of these, non-bacterial in nature. One could think that this mistake would have been corrected over the years, with a better knowledge of how these drugs work. However, the use of antibiotics to treat non-bacterial infections is currently one of the main reasons of antibiotic resistance.

The first cases of antibacterial resistance appeared in the late 1930s and the 1940s, soon after introducing the first antibiotic classes, sulfonamides, and penicillin.

Sir Alexander Fleming warned in 1945 that inappropriate use of penicillin could drive to the selection of resistant "mutant forms" of *Staphylococcus aureus*, which later could lead to more severe infections in the host or the people that the host was in contact.[11] He was right, and after a year of widespread use of this drug, several strains of this bacterium became resistant to penicillin. Only a few years later, over 50% were no longer susceptible to this antibiotic.[11] Unfortunately, this was not only an isolated case as further discoveries of new antibiotics were also followed by this threat.[12]

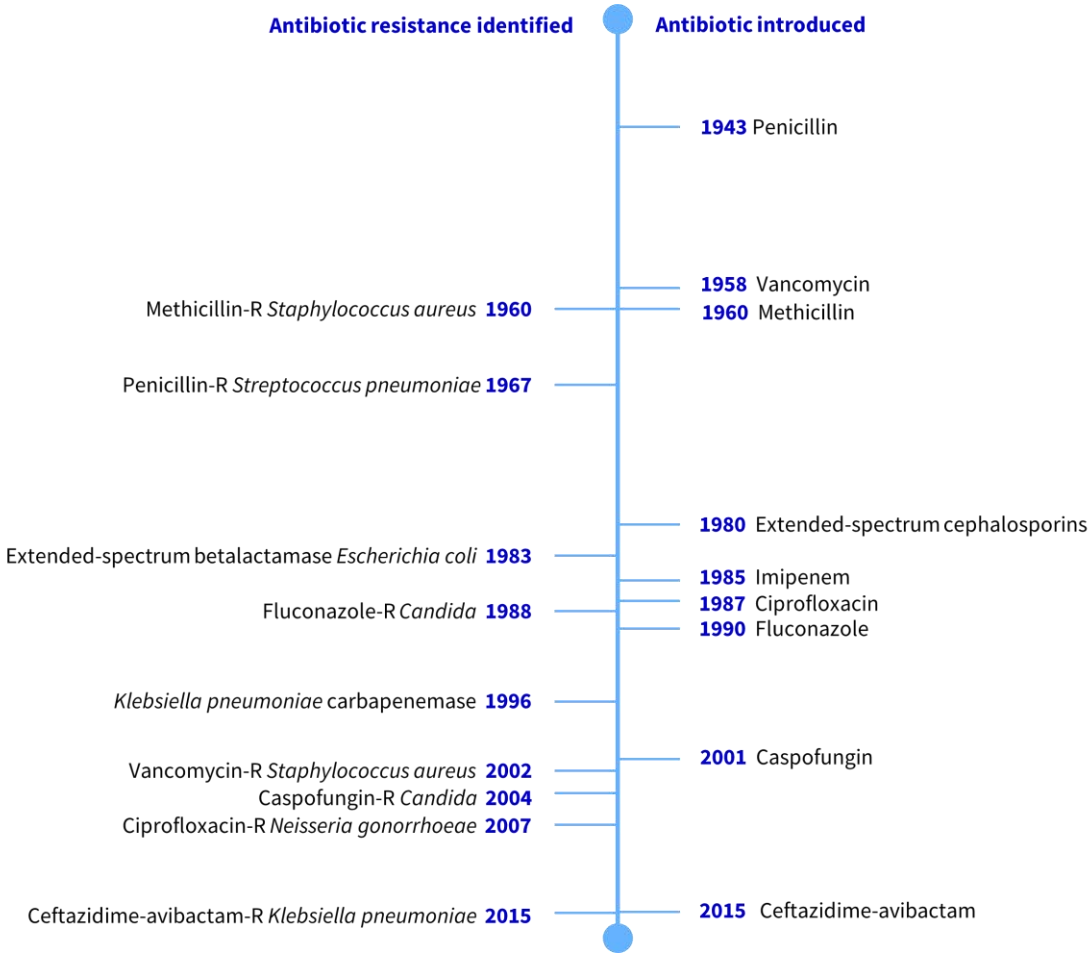

Figure 2. Timeline representing how resistance appears after a new antibiotic is introduced in the market. Data obtained from reference 12.

Therefore, what in the beginning could look like the eradication of most common infectious diseases from humanity with the discovery of antibiotics, soon tended to indicate that we were moving in the opposite direction, facing a future with a growing number of resistant bacteria responsible of new epidemics.

For the most part, bacterial resistance is developed at the genetic level. Meaning if a bacterium generates antibiotic resistance, the genetic make-up of the previously susceptible bacteria has to change, either via mutation or by the

introduction of new genetic information. To this day, there are still many unknowns about how bacteria develop resistance, but significant efforts are being made to expand knowledge on this subject. Recent studies have led to the identification of many genes that are responsible for intrinsic resistance to antibiotics of different classes.[13-14]

It is estimated that in Europe, 33000 people die each year due to multidrug-resistant bacterial infections, which cost over € 1.5 billion annually in healthcare costs and productivity losses.[15] In the United States, more than 2.8 million people are infected with antibiotic-resistant bacteria annually, with 35000 deaths as a direct result.[12] By 2050, it is expected that the number of deaths attributable to resistance to antibiotics will approach the number of 10 million people per year, more than road traffic accidents or even cancer.[16]

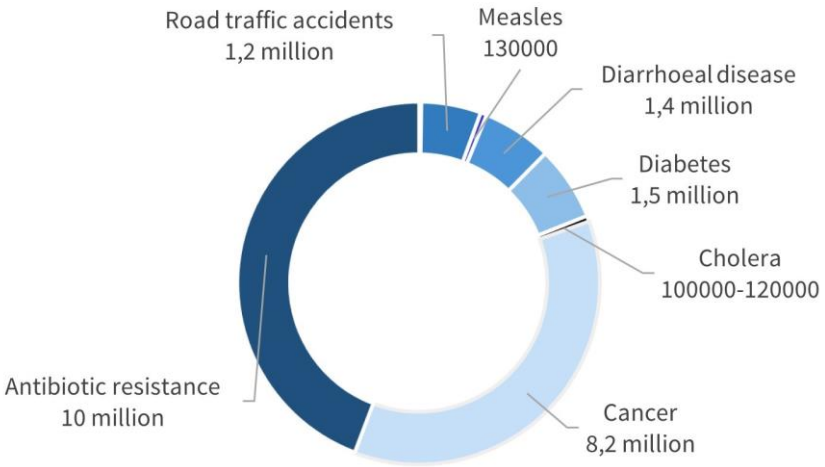

Figure 3. Graphic displaying the estimated causes of death by 2050. Data obtained from reference 16.

Different factors can contribute to this problem. In the following paragraphs, the most relevant will be discussed.

As mentioned before, consumers have an important role when it comes to antibiotic resistance. The overuse of these drugs drives the evolution of resistance. Antibiotics remove drug-sensitive competitors, leaving resistant bacteria behind to reproduce as a result of natural selection.[17]

Incorrectly prescribed antibiotics also contribute to the promotion of resistant bacteria. Studies have shown that choice of agent, treatment indication, or duration of antibiotic therapy is incorrect in many cases.[16, 18] Incorrectly prescribed antibiotics have questionable therapeutic benefits. Drug intake in lower concentrations such as

subinhibitory or subtherapeutic ones can promote the development of resistance by supporting genetic alterations, like changes in gene expression, horizontal gene transfer (HGT), and mutagenesis.[19]

Of course, other factors are critical besides the way antibiotics are prescribed and consumed. In both the developed and developing world, antibiotics are widely used to prevent diseases and promote growth in animals raised for food.[16] An estimated 80% of these drugs sold in the United States are directed to livestock.[20] The transmission route for resistant bacteria may occur through direct or indirect contact. Direct contact happens after humans have been exposed to animals and biological substances (such as blood, feces, urine, saliva, milk, and semen) and enhances the easy and rapid dissemination of resistant bacteria from host-to-host. In addition, the human population can be indirectly exposed to this threat via contact or consumption of contaminated food products.[21-22] The sequence in which this happens is explained next: first, the antibiotic is administrated to the animal, killing or suppressing susceptible bacteria, allowing the resistant ones to survive and thrive; then, resistant bacteria are transmitted to human through food; finally, these bacteria can cause infections once they are present in the human body. But these are not the only way bacteria go from animal to human, the agricultural use of antibiotics also affects the environmental microbiome.[22-23] Up to 90% of the antibiotics given to livestock are excreted in urine and stool, and then widely dispersed through fertilizer, groundwater, and surface runoff.[22]

Another element that should not be overlooked is the antibacterial products sold for hygienic or cleaning purposes accompanied by excessive utilization of them. Cleaning for hygiene purposes does not necessarily imply applying antimicrobial products that may increase antibiotic resistance in the microbiome. Consequently, immune-system versatility can be compromised, possibly increasing morbidity and mortality due to infections that would not usually be virulent.[24]

Because antibiotics are used to treat punctual infections, which means relatively short periods of treatment, these drugs are not as profitable as others that treat chronic conditions like diabetes or asthma.[25-26] A cost-benefit analysis by the Office of Health Economics in London estimated the net present value (NPV) of a new antibiotic in $50 million, while the value for a drug used to treat neuromuscular disease is $1 billion.[20] When comparing these two values, it is clear why pharmaceutical companies prefer to invest in other types of drugs. Besides antibiotics been short-time treatments, the price of these drugs is relatively low compared to others on the market.

With these data in mind, it is evident that the problem of antibiotic resistance is one of the most serious threats to human health today. Although this fact has been demonstrated, and the message has grown stronger in recent years, it seems like a large part of the world population is not taking it seriously. Believing that this increasing threat can be solely solved by the development of new drugs is illusory. As long as a new antibiotic reaches the market, the risk of resistance is nearly inevitable. The solution to this issue is not as simple as to correct one thing but a global endeavor. It is necessary to educate people in order to change old and wrong behaviors. By doing so, we can extend the useful life of these meds. Besides, a more considerable economic effort by private and public industry is crucial to discover new types of antibiotics or maybe new ways of administration and to have a better knowledge of bacteria. Without research, there is not future.

2.3 Photopharmacology

Photopharmacology is a new and growing area of medicine. While classic pharmacotherapy offers the possibility to cure diseases and alleviate symptoms through the administration of drugs, it also presents many problems that are a major concern. The administration of conventional drugs is often followed by unwanted or adverse effects due to the lack of selectivity.[27] Consequently, poor selectivity lowers the threshold level of toxicity, limiting the allowed dose of the desired drug to inferior concentrations of the active compound.[28] The problem with selectivity is also one of the reasons why many new drugs in clinical research are discarded.[29] Increasing selectivity is not an easy task because the treatment of some diseases must rely on targets present in both healthy and diseased tissues.[28] Not less serious is the problem of drug resistance, explained in previous paragraphs for antibiotics.

These drawbacks can be solved by designing a method that allows drug delivery in a specific part of the body. Light is a powerful tool to achieve this goal because it presents many advantages such as very high spatiotemporal precision, facile control over the intensity and wavelength, and lack of residues. The combination of these two concepts, photochemistry and pharmacology, is known as photopharmacology.

2.3.1 Photodrugs requirements

Photopharmacological agents are bioactive molecules that have been modified to include a synthetic molecular switch in their structure.[30] Thus, photopharmacology is focused on the design, synthesis, study, and application of drugs whose activity can

be regulated by light. As if drug development were not hard enough, this new field of pharmacology adds some difficulties that will be explained next.

First of all, it is important to differentiate between the types of change that light can induce in the photoactive part of the molecule, which might be reversible or irreversible. Reversible molecules can be interconverted between two or more states upon light stimulus through several cycles without losing their properties. Controlling the activity of biomolecules in a reversible manner can be accomplished including a molecular switch in their structure. Two types of photoswitches have been used in photopharmacological applications. The first group includes molecular switches that can be interconverted between *cis* and *trans* isomers, azobenzenes being the most common. The second group includes those that are interconverted between open and closed forms. By using this reversible strategy, two isomers of the biomolecule are obtained, allowing the possibility to create an "on/off" system. For this to happen, the isomerization process must be able to take place once the biomolecule is attached to the molecular switch. Besides, the structural change in the molecule upon irradiation should be big enough to produce a difference in the activity of the two isomers.

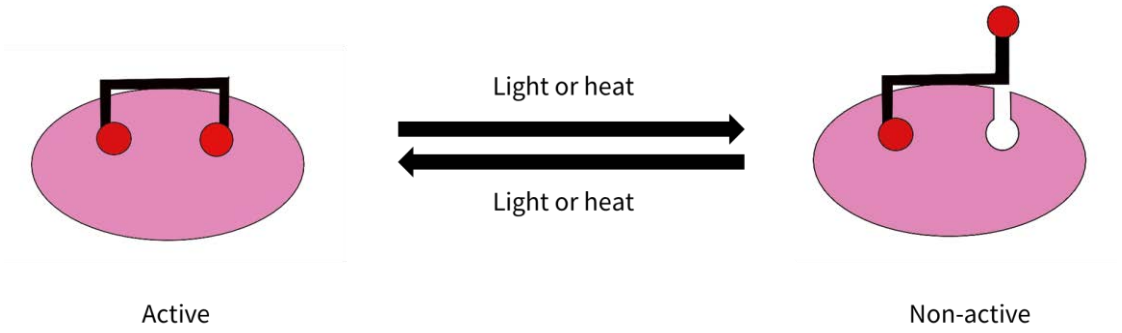

Figure 4. Illustrative example of a molecular switch with biological activity. On the left, the active isomer is able to interact with the target. On the right, when the isomerization process takes place either by light irradiation or thermally, the inactive isomer obtained is unable to interact with the target. Reversion can be carried out with light irradiation or thermally.

On the contrary, irreversible strategies to photocontrol bioactive molecules are based on the cage strategy. These molecules contain a photoreactive moiety covalently attached to an active compound in a way that renders the ligand inert to its target receptor. This means that once the caged compound is exposed to light irradiation, the active molecule is released and cannot come back to the initial form.

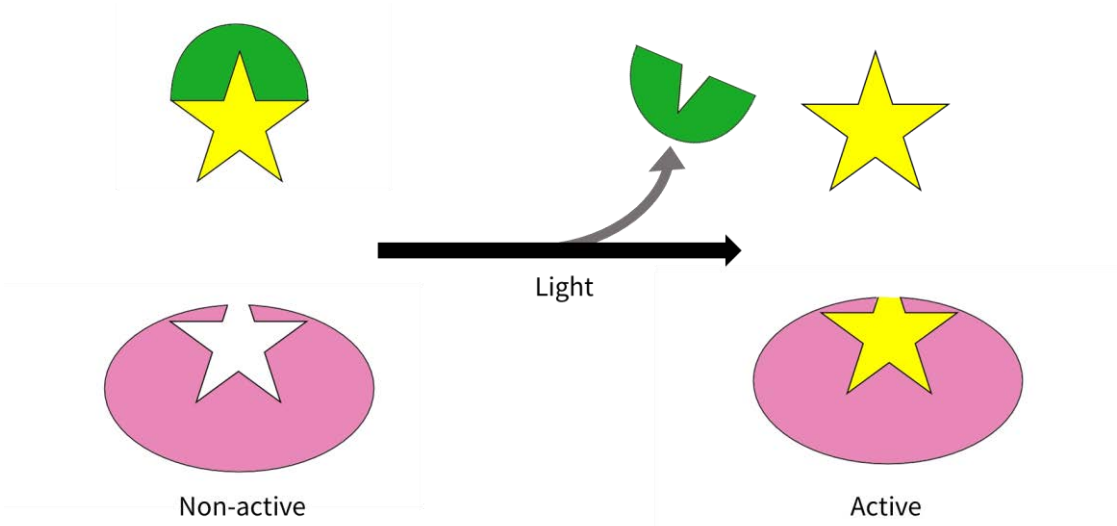

Figure 5. Illustrative example of a caged compound. On the left side, the bioactive molecule activity is being blocked. Upon light irradiation, the photoactive moiety (represented in green) is released, and the activity of the biomolecule (represented in yellow) is recovered.

As of yet, it is not clear whether this last group can be considered inside the photopharmacological approach. Some researchers only consider molecular switches because of their reversible properties compared to caged compounds. Others, however, recognize both strategies, reversible and irreversible, to be part of this field. For this reason, the work here presented will separate both groups in different sections.

Drugs structure is designed and optimized to get the maximum potency and efficacy.[31] One of the first things to consider when doing modifications to introduce the photoactive moiety is that biological activity needs to be retained in at least one of the states. Changes in the structure of bioactive molecules will potentially lead to a decrease in the activity. In order to solve this problem, further optimization of the photoactive compounds will need to be performed to obtain the best results of potency and efficacy. Always considering that one of the states of the photodrug should be active while the other should not present activity against the target.

When the drug is linked to the photoactive moiety, its photochemical properties must be considered. To achieving good performance, the molecular switch should fulfill a number of criteria. The most relevant are listed below:

- Active isomer: ideally, the thermodynamically favored state should be the inactive form of the drug. This would allow the direct administration of the drug without previous steps of deactivation. After administration, the isomerization process would be induced to activate the drug where needed.

- Conversion of the initial isomer to the photoisomer: in the interest of obtaining the highest difference of activity between the initial state and the final one, the isomerization process must be efficient. Considering that this process allows going from the active to the inactive isomer or vice versa, higher percentages of conversion from one isomer to the other are desired.
- Quantum yield: this value relates the number of molecules of photoisomer obtained with the number of photons absorbed at the irradiation wavelength by the molecular switch. The quantum yield is also related to the effectiveness of the process of isomerization, so high values are preferred.
- Reversion process: since molecular switches can go from one state to the other reversibly, reversion from the thermodynamically less stable isomer to the stable one should be performed until completion. Hence, restoring the properties of the initial isomer.
- Stability: the isomerization process should be stable for an infinite number of cycles with no degradation of the molecule since these systems are expected to be switched on/off repeatedly. High stability implies retaining the properties of the system for several cycles. Besides, it is important to avoid the formation of non-desired products that might be toxic to the biological environment.

Another crucial factor is the type of light necessary to carry out the irradiation of the photodrug. When designing the photoactive part, it is possible to make some modifications in the structure with the purpose of changing the absorption spectrum. Wavelength selection is aimed towards the red region of the spectrum in order to avoid phototoxicity and to improve tissue penetration.

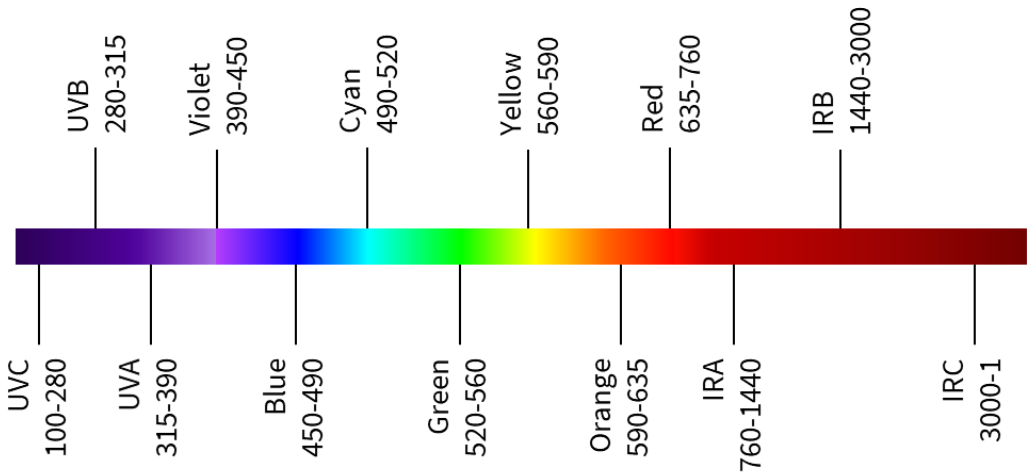

Figure 6. Ultraviolet, visible, and infrared light spectrum. Wavelengths displayed from 100 nm (UVC) to 1 mm (IRC).

The toxicity of UV light has been studied and prove to be carcinogenic.[32] It also can cause mutations[33] and can induce cell apoptosis.[34] Therefore, considering this information, UV light should be avoided when working with living tissues, which means that UV light absorbing photodrugs should not be used for biological applications involving direct irradiation. Besides UV light toxicity, this type of irradiation barely offers tissue penetration.[35-36] The depth of penetration of light into tissues is limited by both optical scattering and absorption by endogenous chromophores. Inside the visible region of the spectrum, light absorption is bigger for the longer wavelengths. While the depth of penetration varies with the tissue type, it is assumed that red light can reach up to 1 cm. Moving up to longer wavelengths, light's maximum penetration can be achieved using wavelengths around 800 nm corresponding with the IRA region. This light can penetrate into skin 2 cm,[37] which makes it the ideal light source for biological applications. Wavelengths longer than 1200 nm are absorbed by water.[38] Thus, the therapeutic window of the skin is restricted between 600 to 1200 nm.

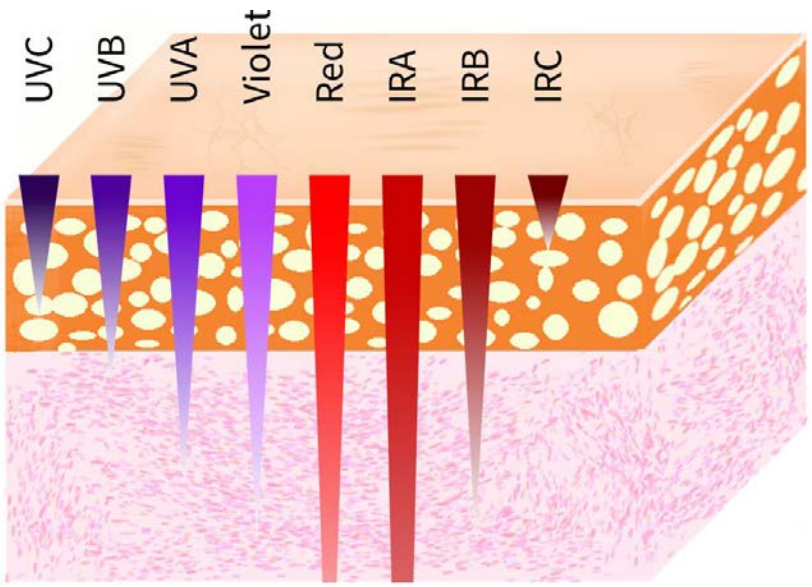

Figure 7. Image showing the tissue penetration for different types of light from UVC to IRC. Data obtained from reference 35.

Reversible systems present an additional factor to consider when working with photodrugs. Once the irradiation of the sample has been carried out, it is important to consider the process that the molecule undergoes in order to come back to the initial state. This process can be performed either through irradiation with a different wavelength or thermally. Preferences in the way reversion is performed will depend on the specific application of the photodrug.

For the first option, the ideal scenario would be that the two isomers presented absorption in different regions of the spectrum. This would ensure the irradiation of each isomer separately, allowing higher photostationary states (PSS).

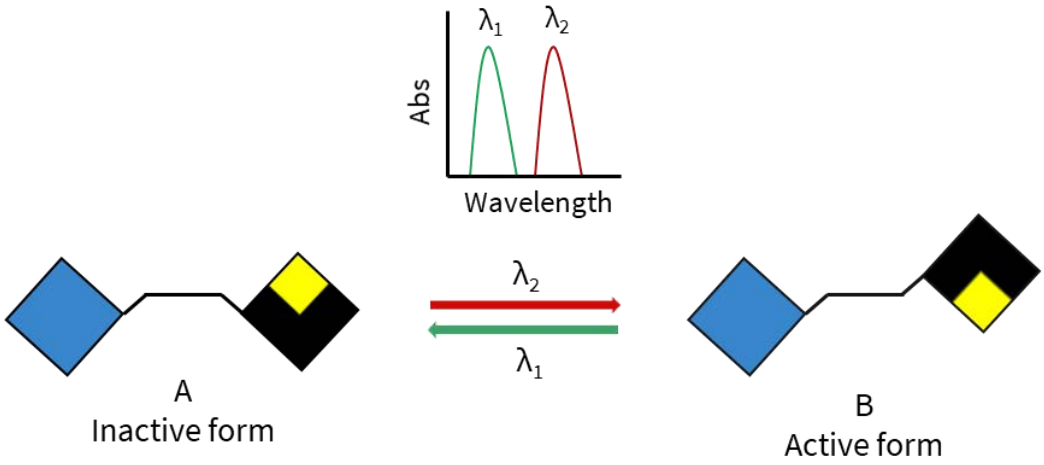

Figure 8. Illustrative example of a molecular switch based on *cis*/*trans* isomerization linked to a bioactive molecule. Form A being the inactive one which upon light irradiation with λ_2 can be converted to the active form B. Reversibility can be achieved when irradiating form B with λ_1 to obtain form A.

The second option is a thermal way. After irradiation, conversion from isomer B to isomer A can be completed heating the sample, since this last one is the thermodynamically stable isomer. Thermal relaxation opens the possibility of temporal control of the drug activity.[39] The photopharmaceutical agent can be activated before administration and completely turned into the inactive form by the time it is excreted thanks to body temperature, maintaining the activity enough time to find the target if the half-life is appropriately chosen.

By combining both methods, light irradiation and thermal relaxation, a variety of scenarios can be created in order to control the activity of the biomolecule.[39]

When working in biological applications, it is essential to address the solubility and stability of the compounds in the cellular environment. The molecules should be total or partially soluble in water in their different states. This will ensure no precipitation once they are introduced in the environment. The degradation of the molecules is a possibility either via enzyme-mediated[40] or glutathione (GSH)-mediated reduction.[41-43] This last one, been the most studied since the concentration of GSH in cells can reach up to 10 mM.[44]

Finally, the toxicity of the photopharmaceutical agents should be considered, studying not only the photodrug and its different forms but also the possible sub-products that can occur when irradiating the samples in biological environments.

2.3.2 Advantages and limitations of photodrugs

Although there is still a long way to go, significant accomplishments have been made in the field of photopharmacology. There are several advantages to this new way of drug administration. For instance, the selectivity it could offer when treating only the specific part of the body where the disease is localized, instead of been present in some parts where its activity can be not beneficial. By targeting the specific area, the dose of the drug could be adjusted and increased without the threat of adverse effects. In addition, the total amount of active compound present in the body will be lower than with conventional drugs, because it is only active in a small region, which could help with the problem of drug resistance. Related to this problem is also the environmental buildup of drugs. By using light-activated drugs, it is possible to deactivate them before being expelled of the body when using a reversible strategy. Figure 9 shows a representation of the different approaches herein described.

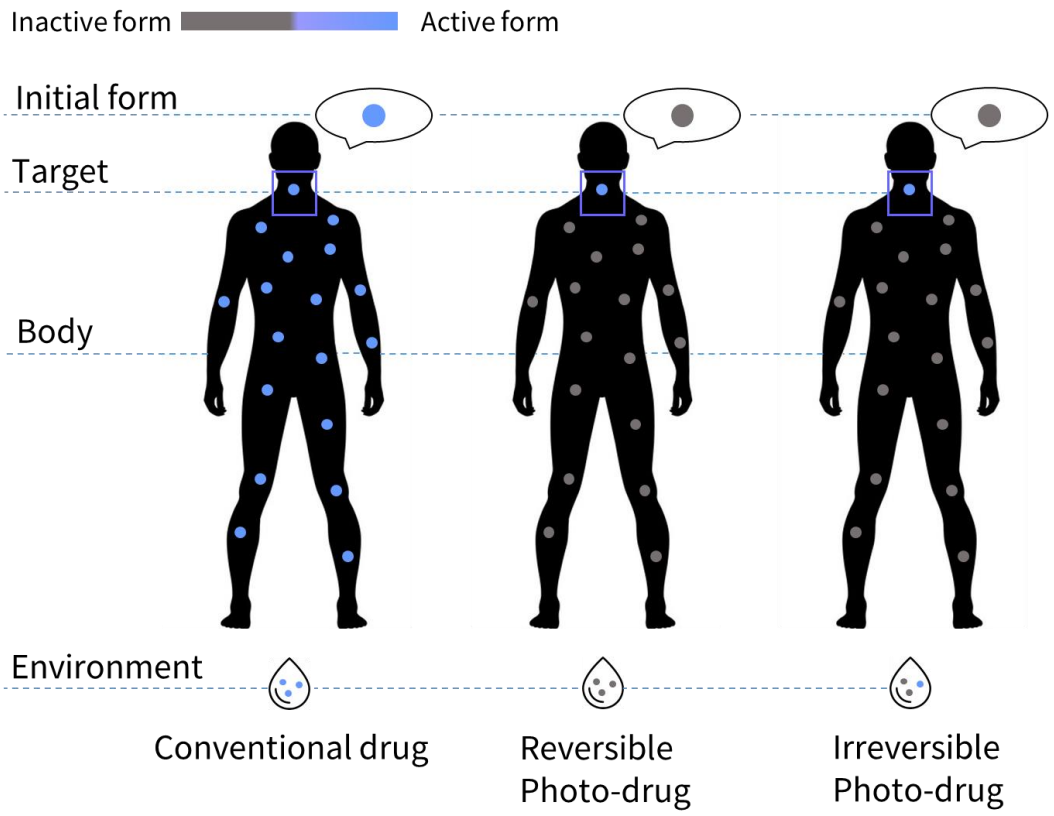

Figure 9. Representation of oral intake for different types of drugs. Conventional drugs are active in their initial form, spreading through the body and finally excreted. Reversible photodrugs could be administrated in their inactive form and switched to the active form only in the specific target where the disease is localized. Finally, they could be switched off again, leaving no active residues to be expelled. Irreversible photodrugs could be administered in their inactive form and released in the affected area. Eventually, only a small fraction of the active molecule would be eliminated.

Designing biomolecules that can be controlled by light is not an easy task, and the most crucial requirements have been explained in previous paragraphs. After obtaining the photodrug, one of the main challenges is how to deliver light in the part of interest. As mentioned before, light penetration can reach up to 2 cm into tissue when working with IRA light. With this knowledge, a classification of the different targets in the human body can be made.[30] Class 1 includes the most superficial organs, easily accessible by light like skin and eyes. Class 2 covers those organs that can be accessible by endoscopy such as gastrointestinal (GI) tract, mouth and throat, sinuses, respiratory system, cervix, and biliary tract. Class 3 organs are those that are lying just below the skin, making them accessible to light irradiation without the need of incision. Examples of this class are thyroid, testicles, lymph nodes, and muscles and bones lying just under the skin. Class 4 consists of organs accessible through minor incision like peritoneum, liver, ovaries, stomach, intestines, and prostate. Finally, in class 5 belong organs only accessible through major incision such as brain and bone marrow.

Besides having this limitation, photopharmacology should only be considered when the disease is localized in a specific target, not when it is spread through the body.

2.4 Previous works in photopharmacology

Photopharmacology has experienced a big development in the last decade. Although being a relatively new field, it has aroused interest in the scientific community, and considerable efforts are being made to begin the clinical phase. Related to these advances, are those made in the way light is delivered.[45] Photodynamic therapy can help in this area because it presents the same problem, but contrary to photopharmacology, it is well established. Therefore, photodynamic therapy devices could be adapted and employed to control the activity of drugs. Delivering light to a specific target where the disease is localized can be achieved by combining suitable light sources and optimal fiber optic delivery devices.

Even though photopharmacology is a new area with a lot to discover, many examples can be found in the literature, which will be discussed in the next paragraphs. These examples will include the most recent advances in the control of the activity of bioactive molecules using light.

Gaining control of a biomolecule in a reversible way can be accomplished by combining the active molecule with a molecular switch. There are many types of molecular switches, but the most commonly used for biological applications are two types: based on *cis*/*trans* isomerization and those that can be interconverted between open and closed forms. With that being said, azobenzenes are, without a doubt, the most widely used thanks to their properties that will be explained next. Regarding the election of the bioactive molecule, a variety of them can be found in the bibliography.

2.4.1 Azobenzenes

Azobenzenes were discovered in the mid-1800s.[46] Originally employed in the dye industry as synthetic coloring agents, their properties as molecular switches were unnoticed until several years later. In 1937, Hartley discovered that azobenzenes could go from the *trans* to the *cis* isomer when they were irradiated with UV light.[47] In order to recover the initial isomer, it is necessary to either irradiate with blue light or leave the sample in the dark. The process of isomerization can be steadily repeated, without product decomposition or other side reactions, making azobenzenes stable during several cycles, and therefore a good choice for their use as molecular switches. The robustness of the photoisomerization process even when the initial molecule is

modified to introduce new groups,[48] as well as the ease of the synthetic procedure that can be customized to obtain a huge variety of derivatives, make azobenzenes a popular photoswitch in diverse fields. In addition, it should be noted that the end-to-end distance of each isomer is significantly different. The distance between the *trans* and *cis* isomer among the carbons at the *para* positions changes by approximately 3.5 Å,[48] which makes azobenzenes extremely interesting for the control of certain types of biomolecules. Finally, the isomerization process occurs on picoseconds, a timescale suitable for biological processes that are usually slower.

Pioneers in this field were the group of Erlanger and Nachmansohn. They studied azobenzenes-based inhibitors of acetylcholinesterase in 1969 and 1971 respectively.[49-50]

More recently, in 2012, Trauner and co-workers achieved photocontrol of Propofol.[51] Propofol was discovered in 1980 and became the most widely used intravenous general anesthetic.[52] The mechanism of action of Propofol is not fully understood yet, but it is commonly accepted that it induces anesthesia from potentiation of GABA-induced currents. In his work, Trauner synthesized several azo-Propofols. Azo-Propofols are derivatives of Propofol including azobenzenes in their structure and making them photoswitchable versions of the anesthetic.

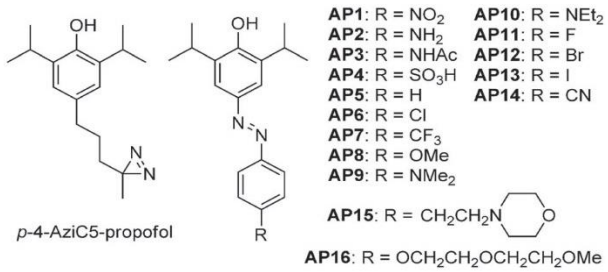

Figure 10. On the left, *p*-4-AziC5 Propofol, a photoreactive derivative of Propofol. On the right AP1-AP16 all of the azo-Propofol derivatives synthesized, AP-2 showing the best results. Reprinted by permission from reference 51. Copyright © 2012 Wiley-VCH Verlag GmbH & Co. KGaA, Weinheim.

To evaluating the anesthetic power, one of the azo-Propofols was tested *in vivo* as well as Propofol. Groups of albino *Xenopus laevis* tadpoles were placed in aqueous solutions containing either Propofol or azo-Propofol and tested every five minutes for the loss of righting reflexes (LORR). The loss of righting reflexes happened in 10 minutes for Propofol and 25 minutes for azo-Propofol. Irradiation of azo-Propofol with UV light shifted the EC_{50} value from 1.1 μM (non-irradiated) to 4.6 μM (irradiated). When tadpoles were exposed to 3 μM of azo-Propofol it produced LORR, and after irradiation with UV light, all of them spontaneously righted themselves. This work is

one of the first examples of a photodrug whose activity can be controlled in a reversible way.

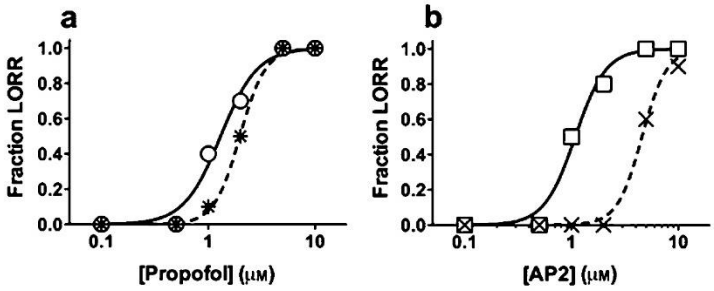

Figure 11. Optical control of anesthetic. a) Effect of Propofol before and after irradiation. Light produces a small shift from 1.1 μM to 2 μM. b) Effect of light in azo-Propofol. Light produces a big shift from 1.1 μM to 4.6 μM thanks to the isomerization process. Reprinted by permission from reference 51. Copyright © 2012 Wiley-VCH Verlag GmbH & Co. KGaA, Weinheim.

In 2013, Feringa and co-workers designed a series of novel molecules that included in their structure a part based on quinolones, known for their antibacterial properties.[53] They exchanged the piperazine unit in the quinolone structure with an aryldiazo moiety. The goal of this project was to modulate the antibacterial activity using light.

Conversion from the *trans* to the *cis* isomer occurred when samples were irradiated with UVA light. Reversion to the initial isomer was carried out with visible light. The isomerization process could be repeated for at least 3 cycles without presenting signs of side products. Some of the molecules displayed a good PSS with >95% *trans* before irradiation and >85% *cis* after irradiation. In order to test the antibacterial activity, *Escherichia coli* CS1562 was used. MIC values between the non-irradiated samples and the PSS proved to be different for some of the compounds, the larger difference been MIC ≥ 64μg ml^{-1} for the non-irradiated (*trans,* mostly) and MIC = 16 μg ml^{-1} for the irradiated form (*cis,* mostly).

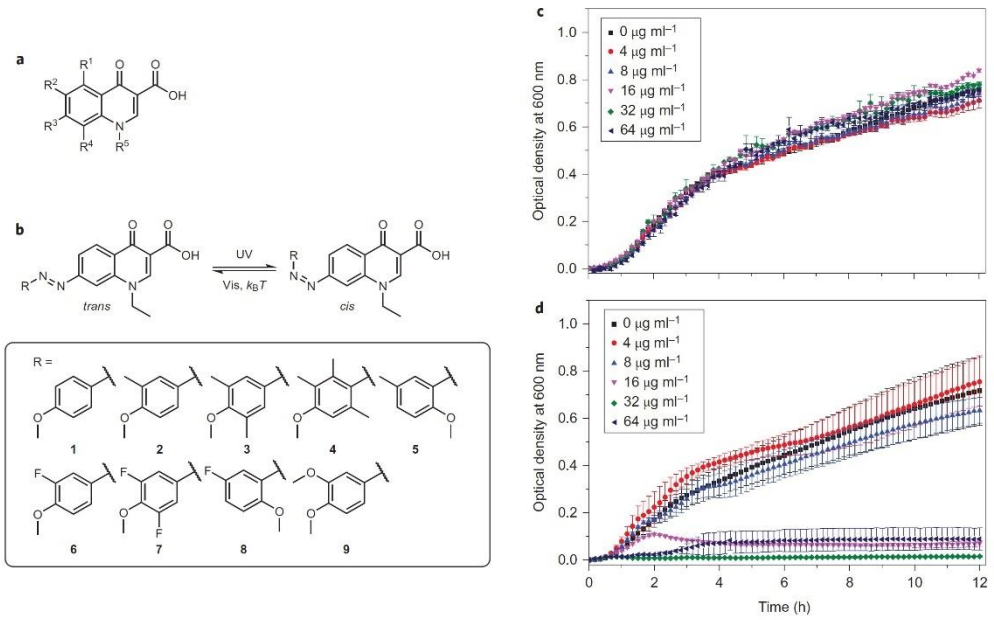

Figure 12. Control of bacterial growth with photoswitchable antibacterial agents. a) Structure of quinolone antibacterial agents. b) Modifications made to introduce azobenzenes in the structure of quinolones and irradiation process. Isomerization to obtain the *cis* isomer was achieved with UV light. Reversion to the *trans* isomer was carried out with visible light or thermally at ambient temperature. c) Growth curve of E. coli CS1562 for the non-irradiated compounds. d) Growth curve of E. coli CS1562 for the irradiated compounds. Reprinted by permission from reference 53. Copyright © 2013, Springer Nature.

Additionally, the pharmacodynamics for the compound with better results were studied. The same type of bacteria was incubated with 40 μg ml^{-1} of the compound in different states: the active form (*cis* isomer), *cis* isomer switched to *trans* after 30 min and *cis* isomer switched to *trans* after 60 min. Results obtained exhibited a similar behavior for the *cis* isomer, and the *cis* isomer switched to *trans* after 60 min. These experiments indicate that the quinolones exhibit their antibacterial effect in the exponential phase.

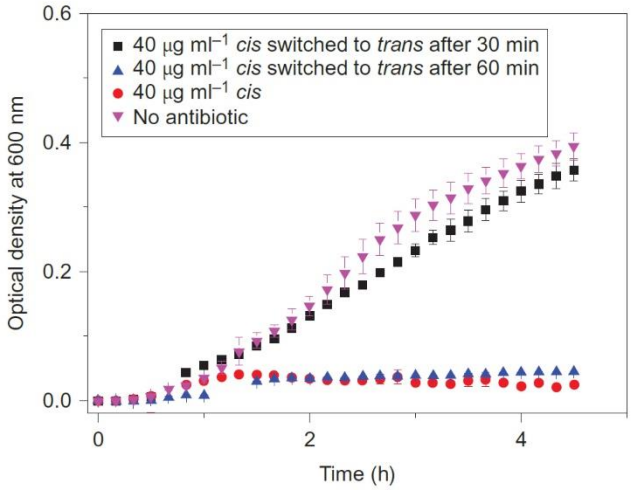

Figure 13. Pharmacodynamic study for the photoswitchable quinolone with better results. Reprinted by permission from reference 53. Copyright © 2013, Springer Nature.

A few years later, in 2017, Feringa and co-workers improved these results by synthesizing derivatives of trimethoprim.[54] Trimethoprim is an antibiotic that belongs to the group of antifolates. They attached several azobenzenes in the trimethoprim core structure, some of them absorbed in the red region of the spectrum. This shift can be achieved with the synthesis of azobenzenes bearing fluoro, chloro or methoxy substituents in all ortho positions of the azo moiety.[55-56] Hence, the isomerization of the molecules was carried out with red light, compatible with biological systems. Differences between the activity of the initial isomer and the PSS were observed for some of the compounds, demonstrating once again that antibacterial properties could be modulated by light. This work opens the possibility for future localized and reversible antibacterial treatments that will present important advantages over the ones currently used.

In 2018, Abell and co-workers designed several peptides based on the structure of gramicidin S.[57] The new derivatives included an azobenzene moiety introduced to gain optical control over the structure of the peptides. Gramicidin S is a natural cyclic peptide with antibiotic properties that have been attributed to its well-defined β-sheet secondary structure and amphiphilic character.[58]

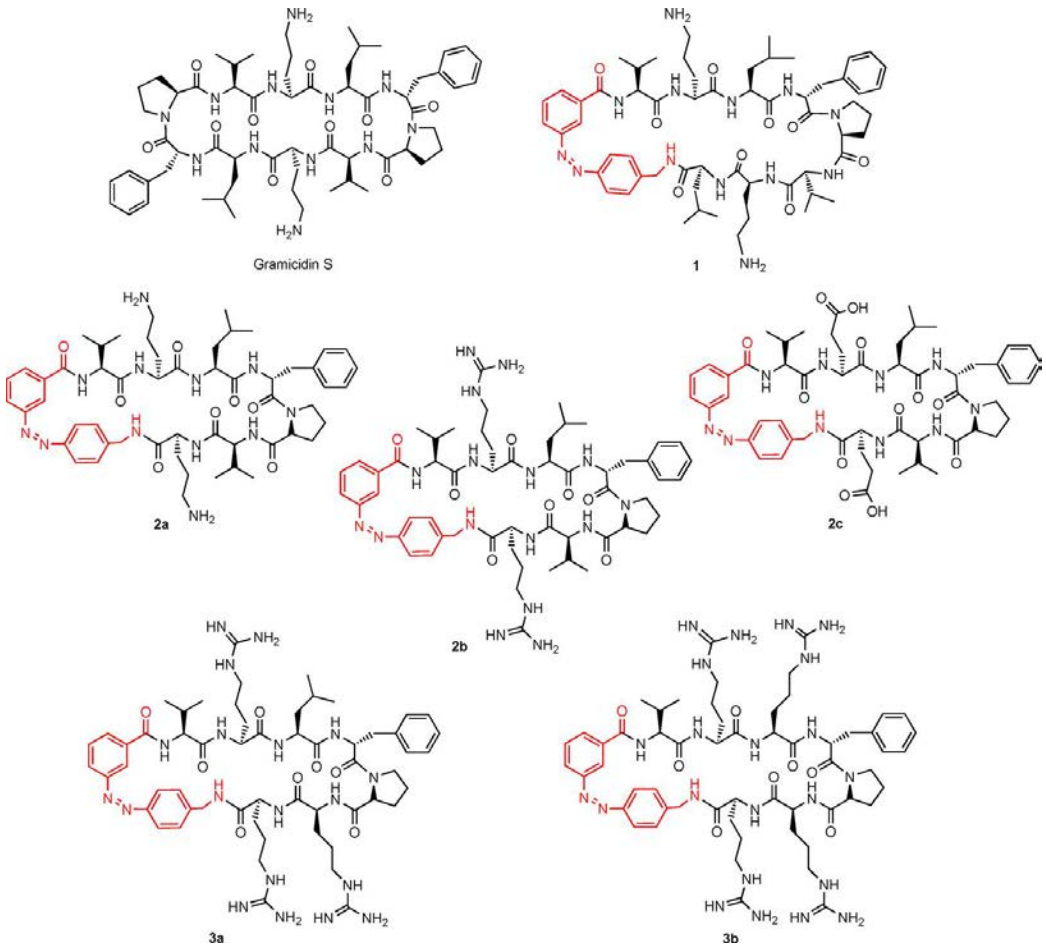

Figure 14. Gramicidin S structure and derivatives synthesized with the azobenzene moiety highlighted in red. Reprinted by permission from reference 57. Copyright © 2018 Wiley-VCH Verlag GmbH & Co. KGaA, Weinheim.

It was expected that one of the isomers of azobenzene, more specifically the *cis* isomer, would maintain the well-defined secondary structure of the peptide and, by doing so, to also maintain the antimicrobial properties. On the contrary, when the azobenzene was in its *trans* form it was expected to disrupt the β-sheet, therefore losing the activity. Additionally, other modifications on the peptide structure were made to check the effect of positive and negative charges on antimicrobial activity. The importance of amphiphilicity was studied by introducing some basic amino acids residues into the peptide backbone.

The thermally stable isomer for all the peptides was the *trans* isomer. Irradiation with UVA light (352 nm) allowed isomerization to the *cis* form with PSS values varying from 90-64%. Conversion from the *cis* to the *trans* form was carried out with visible light (405 nm) with PSS between 88-66%. To checking the secondary structure of the peptides, ^{1}H NMR studies were performed. It was determined that *cis* isomers presented a better-defined β-strand structure than *trans* isomers in all cases.

The antimicrobial activity was tested against *S. aureus* ATCC 49775. Although MIC values for all the synthesized peptides were higher than for gramicidin S (MIC 2 μg ml^{-1}), which means a lower activity than the natural peptide, differences between *cis* and *trans* isomers were observed in some cases. Peptides **2a** and **2b** in their *cis* forms were 4 times more active than in their *trans* forms, with the more potent being **2b**-*cis* (MIC 32 μg ml^{-1}). This work is a beautiful example of how the structure in peptides is key for their properties and how photochemistry can be used to control them.

In 2019, Szymanski and co-workers designed several $BRAF^{V600E}$ inhibitors with photocontrolled activity.[59] Mutations in BRAF kinase drive the formation of melanoma, the most deadly and challenging type of skin cancer.[60] Nowadays, two types of $BRAF^{V600E}$ inhibitors are used in clinical practice;[61-62] however, both present significant disadvantages. Because these drugs are active in both healthy and cancerous tissue, they can cause cell death in melanoma, whereas in healthy cells, they can also boost the activity and result in increased proliferation, which can lead to the formation of tumors.[63] By introducing azobenzenes in the structure of $BRAF^{V600E}$ inhibitors, it was expected to obtain two forms, one active, to use in cancerous cells and one inactive that would not affect healthy cells.

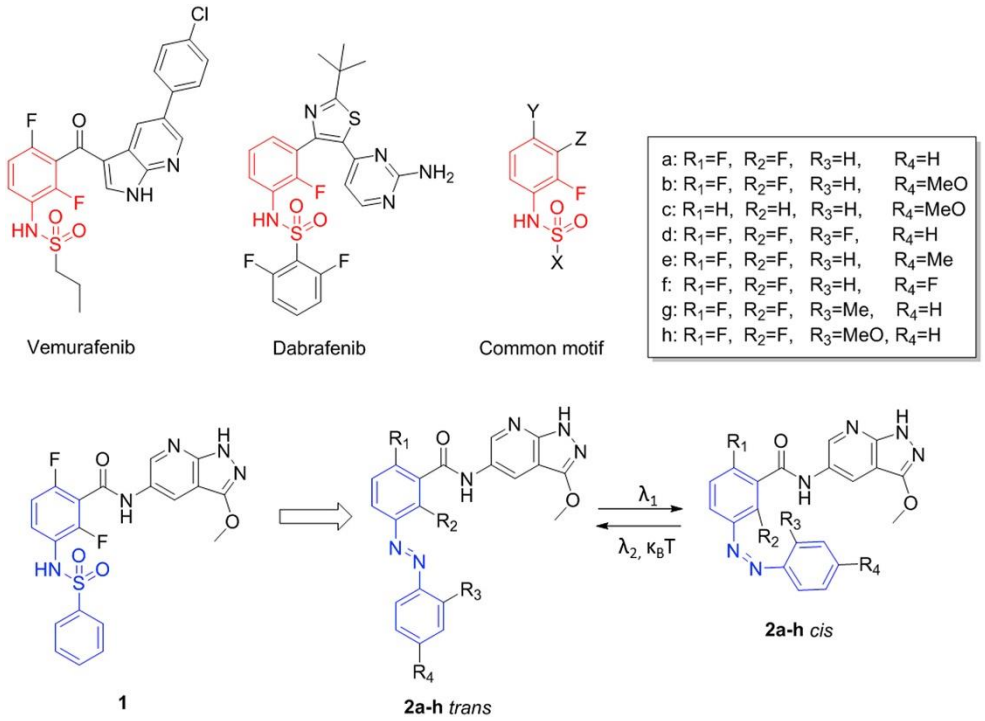

Figure 15. Structures of $BRAF^{V600E}$ inhibitors Vemurafenib, Dabrafenib, and their common motif. On the bottom part, structure of the derivatives synthesized, including the azobenzene moiety highlighted in blue and isomerization process. Reprinted by permission from reference 59. Copyright © 2019 Elsevier Masson SAS.

Different derivatives were synthesized, and their photochemical properties were determined. The irradiation of the samples was carried out using UVA light, and various PSS were found with the values varying between 55-94% of the *cis* isomer. All compounds had relatively long half-lives (> 10 h). In order to check their activity, an assay with purified recombinant $BRAF^{V600E}$ with inactive MEK-1 as a substrate was performed. The compound that presented better results had a difference of 10-fold in activity between the initial isomer and the PSS (*trans* IC_{50} 1.68±0.62 μM, PSS IC_{50} 156±47 nM). In comparison, Vemurafenib, one of the two drugs in trial, presents an IC_{50} of 9.6±3.3 nM. In addition, the reversibility of this compound was demonstrated when, upon thermal re-isomerization, the original activity was recovered. With this project, Szymanski proved how by the introduction of a molecular switch that leads to an "on/off" system, the selectivity of an existing pharmaceutical agent can be potentially improved and, as a result, reduce its adverse effects.

Nowadays, there is a fair amount of published articles focused on the photocontrol of different molecules employing azobenzenes. Moreover, the number of publications related to this line is increasing every year. The possibilities for the reversible control of biomolecules are wide and can be extended from small molecules such as antibiotics[53-54] and ion channel blockers[64-65] to more complex systems like lipids,[66-67] and peptides.[57, 68-69] No matter the size of the system all of them have a common objective, the reversible control of their properties using light. Great achievements have been made to create drugs that can be turned "on/off" in a specific part of the body. These new photodrugs could help solve the problem of drug resistance or avoid the adverse effects of classical drugs in the future. Furthermore, photopharmacology offers fascinating prospects to control more complex functions like vision restoration[70-71] or insulin release.[72-73]

2.4.2 Other molecular switches

It seems obvious that in the field of photopharmacology azobenzenes are the main choice. In fact, in a review published in 2018 by professor Trauner about *in vivo* photopharmacology,[74] of the 123 examples mentioned, only 9 belonged to a distinct type of molecular switch. However, several projects employing a variety of molecular switches can be found for this field like diarylethenes, fulgimides, hemithioindigos, spiropyrans, or donor-acceptor Stenhouse adducts.

The first examples of thermally irreversible photochromic diarylethenes were reported in 1967.[75] Diarylethenes (DAEs), present some advantages on their own, such as really efficient photoisomerization, thermal stability, and fatigue resistance.[76] The isomerization process in DAEs consists of a reversible photochemically induced

cyclization, which consequently changes the electronic properties and flexibility of the molecule. The open-ring form is generally colorless and can be converted to the closed-ring form using UV light. On the contrary, the closed-ring form is generally colored and can be reverted to the open-ring form using visible light. When working with photodrugs, the inactive isomer, and therefore the one administrated should be the closed-ring form. Upon irradiation with visible or near-infrared light, the active form could be obtained.

The photocontrol of peptides with diarylethenes has been studied over the last years. As exposed previously, the natural peptide gramicidin S presents antibacterial properties.[58] The activity of derivatives based on the structure of gramicidin S has been successfully photomodulated by inserting different molecular switches like azobenzenes, synthesized by Abell,[57] or diarylethenes synthesized by Ulrich and Komarov.[77] In 2016 Ulrich and Komarov, inspired by their previous results, decided to synthesize a second-generation of diarylethene-based peptidomimetics to photocontrol their cytotoxic activity against cancer cells lines.[78] Besides the properties as an antibiotic, gramicidin S is highly cytotoxic to prokaryotes and eukaryotic cells and can also inhibit tumor growth *in vivo*.[79]

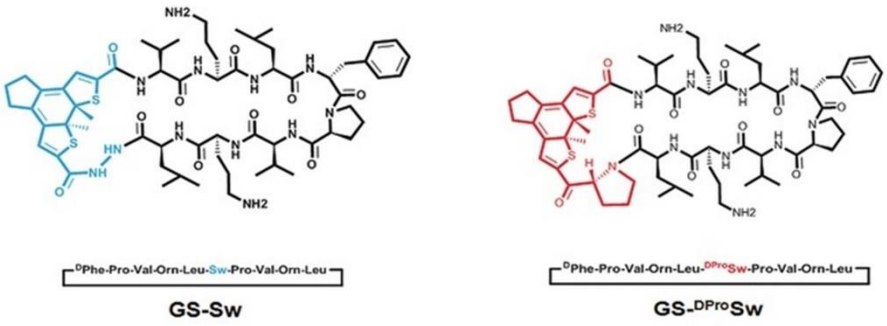

Figure 16. Structures of the peptide mimetics of gramicidin S with the diarylethene unit highlighted in blue and red. On the left (blue), first-generation (GS-Sw) synthesized previously as an antibacterial peptide. On the right (red), second-generation (GS-DProSW) synthesized to study its cytotoxicity in cancer cells. Modified by permission from reference 78. Copyright © 2016 WILEY-VCH Verlag GmbH & Co. KGaA, Weinheim.

Once the analog was synthesized, the cytotoxicity of the two isomers was tested in a standard MTT assay against HeLa and COLO-205 cell lines. Results showed good cytotoxicity for the open-ring form with IC_{50} values very close to those found in the natural peptide. The closed-ring form presented about 5.5-8.0-fold lower cytotoxicity. Encouraged by these promising results and after testing the stability of the analogs in blood and the isomerization process in tumor tissues (> 75% conversion), an *in vivo* experiment was set up using the LLC model in C57B1/6 mice.

After administration of the peptidomimetic in its less active form, mice were locally irradiated with visible light for 20 minutes. The data exhibited a rate of animal survival improved by 60% compared to the control (mice without treatment). Future studies in this line could lead to the development of oxygen-independent PDT for cancer.

In 2018, Yin designed a series of antibacterial agents linked to dithienylethene switches.[80] In a similar way as in the previous work by Feringa,[53-54, 81] it was expected that the properties of the antibacterial agents could be modulated thanks to the photoactive moiety. Norfloxacin and ciprofloxacin were used as antibiotics. The photoswitchable derivatives were synthesized by an amide condensation reaction between the corresponding dithienylethene-mono-carboxylic acid and the secondary amine in the piperazine ring of the antibiotic.

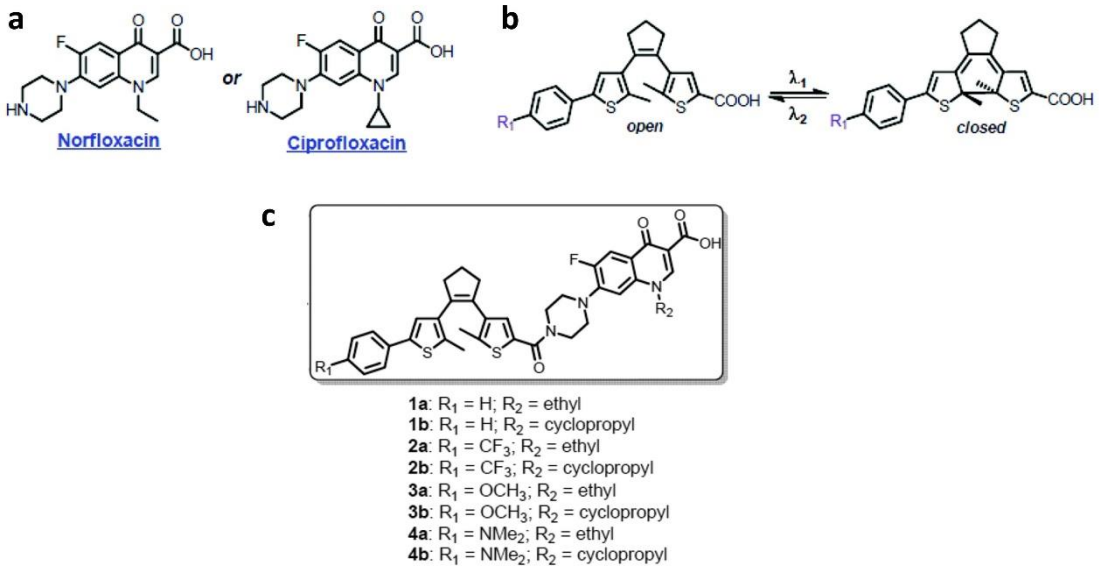

Figure 17. Use of dithienylethene switches for the control of antibacterial activity. a) Structures of the antibiotics employed, norfloxacin and ciprofloxacin which belong to the fluoroquinolone class. b) Isomerization process that dithienylethene undergoes. c) Structure of the derivatives synthesized combining an antibiotic and the molecular switch. Modified by permission from reference 80. Copyright © The Royal Society of Chemistry 2018.

Isomerization from the open-ring to the closed-ring isomer was carried out with UV light (λ = 254 nm), and a change in the color of the sample was observed. The initial isomer presented a yellow color, whereas the final isomer was pink. Reversion from the closed-ring to the open-ring isomer occurred when irradiating with visible light (λ > 402 nm). To test the antimicrobial activity, MIC was determined on *E. coli* and *S. aureus.* The MIC values before irradiation (open-ring form) obtained were 16-32 μg ml^{-1} for *E. coli* and 8-32 μg ml^{-1} for *S. aureus*. After irradiation of the samples, differences in the activity of the closed-ring form were observed, the most significant for

compounds **1b** and **3b**, 4 times more active in their PSS (MIC = 2 μg ml^{-1}) versus the initial isomer (MIC = 32 μg ml^{-1}).

Additional examples in the literature include the use of DAEs in photochromic dopamine,[82] enzyme inhibitors[83] and cytotoxic platinum complexes.[84]

As well as with diarylethenes, the isomerization mechanism of fulgimides is a process of cyclization. Fulgimides display excellent photochemical properties like high photostationary states and a really low degradation after several cycles. However, examples with these molecular switches are less frequent. The first article that can be found addressing the incorporation of fulgimides into biological structures was reported in 1992 by Willner.[85] In his project, Willner incorporated a fulgide unit, a precursor of fulgimides, in the structure of concanavalin A in order to modulate the binding of the substrate photochemically. More recent projects include photochromic dopamine receptors[82] and the first peptide containing a fulgimide unit,[86] both published by König and co-workers in 2017 and 2019, respectively.

Another group of molecular switches that are being used for photopharmacological applications is hemithioindigos. Hemithioindigos (HTIs) combine a thioindigo and a stilbene part connected by a double bond responsible for the isomerization. One of the best qualities of HTIs is their red shifted absorption, which makes possible to induce photoisomerization with visible light in both directions *Z* to *E* and *E* to *Z.* Besides, they have high photostationary states, excellent fatigue resistance, and enhanced thermal stability.

In 2006, Kuhn designed a photoswitchable inhibitor of the lipid-peroxidizing lipoxygenases (LOXs).[87] LOXs are implicated in the pathogenesis of bronchial asthma,[88] atherosclerosis,[89] and osteoporosis.[90]

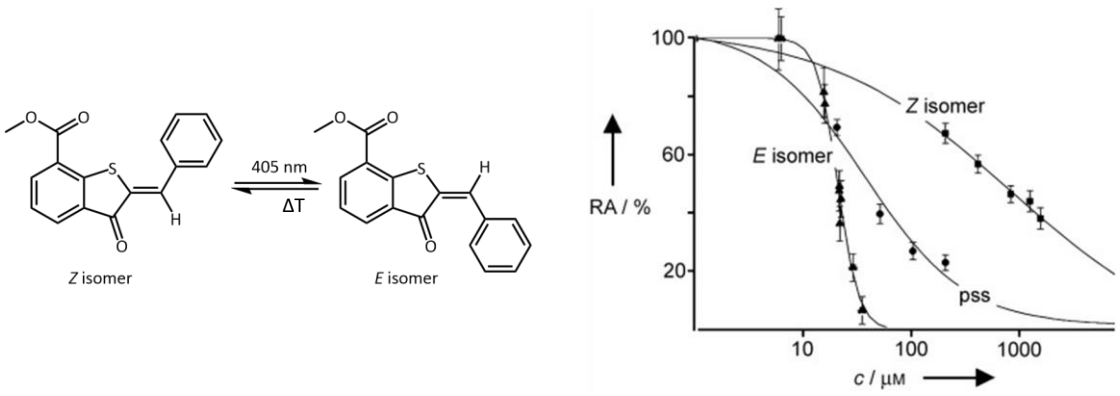

Figure 18. Photoswitchable inhibitor of LOXs and isomerization process. On the right, dose-response curves for inhibition of native rabbit 12/15-LOX for both isomers and PSS. Modified by permission from reference 87. Copyright © 2006 WILEY-VCH Verlag GmbH & Co. KGaA, Weinheim.

The irradiation process of the hemithioindigo was carried out with visible light (405 nm). The PSS obtained presented 62% of photoisomer (*E*). In a first assay, the inhibitory potency of both isomers, purified by HPLC, was tested on purified mammalian 12/15-LOX. As shown in figure 18, *E* isomer was able to strongly inhibit the enzyme. Isomer *Z*, however, appeared to be ineffective. These results prove that hemithioindigos can be a good alternative when designing photodrugs.

The fourth group of molecular switches is spiropyrans (SP). Their photochromism was discovered in 1952.[91] The photoisomerization of spiropyrans takes place through a mechanism of cyclization. The C_{spiro}-O bond in the closed ring form (SP) undergoes heterolytic cleavage upon UV light irradiation, resulting in the formation of a zwitterionic conjugated system, usually called merocyanine form (MC).[92] The change between both forms induces a huge difference in the polarity of the molecule (8-15 D). SP are also sensitive to solvents, pH, temperature, or mechanical stimuli.

In 2011, Önfelt and Andréasson designed a novel photochromic spiropyran with cytotoxic properties.[93] The compound reached a PSS of 60% of the open form when irradiated with UV light. The reverse reaction was induced by visible light (λ > 465 nm) to obtain 100% of the closed form.

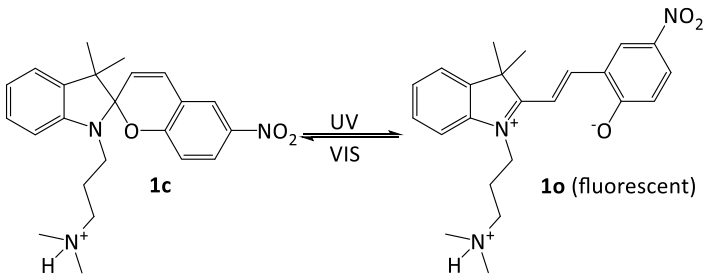

Figure 19. Structure and isomerization process of spiropyran derivative with light-induced cytotoxic activity. Reprinted by permission from reference 93. Copyright © The Royal Society of Chemistry 2011.

Firstly, the cellular uptake was tested using HEK 293 cells. It was proved that only the closed form was able to penetrate the cell membrane, whereas the open form displayed very low penetration, probably associated with changes in polarity. In order to check if the isomerization process was viable inside the cells, the cells containing the closed form were irradiated with UV light. The results were positive, and the cytotoxic effects were evaluated next. The data showed that the initial isomer, the closed form, did not have effect on the cellular survival, but when the cells were irradiated, inducing the photoisomerization, the open form was able to cause cell death. In the future, similar compounds to this spiropyran derivative may be used as substitutive for photodynamic therapy in cancer treatment.

Spiropyrans have also been employed by Feringa and co-workers to achieve light-induced control in antibiotics. It has been previously mentioned how in 2013, Feringa synthesized photoswitchable antibiotics using azobenzenes as molecular switches.[53] In 2015, a similar work was published but with some interesting differences.[81] This time, a commercial antibiotic was chosen, instead of designing a derivative. The antibiotic selected was ciprofloxacin, and the molecular switch was attached in the position of the secondary amine of the piperazine unit. Two types of molecular switches were synthesized, azobenzene and spiropyran.

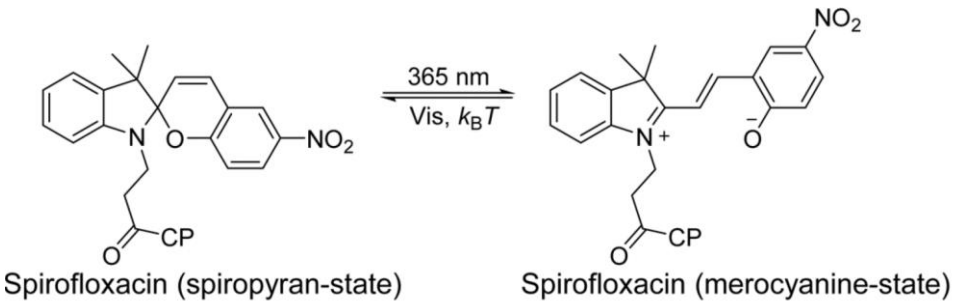

Figure 20. Structure and isomerization process of spiropyran derivative (CP = ciprofloxacin). MC form can be obtained upon irradiation with UV light (λ = 365 nm). Reversion to the SP form is carried out with visible light irradiation or thermal relaxation. Reprinted by permission from reference 81. Copyright © 2015 American Chemical Society.

The spiropyran derivative reached a PSS value of 82% of the MC form when it was irradiated with UV light (λ = 365 nm). To testing the antibacterial properties, MIC values were measured on *E. coli* CS1562 and *M. luteus* ATCC 9341. The results presented differences between both isomers on *E. coli*. Spirofloxacin had a MIC of 1.25 μM when spiropyran was the predominant form (82%). However, when the majority of the compound was in the merocyanine form, the value was 0.625 μM. In this case, spiropyran exhibited better properties than azobenzene as a molecular switch able to induce a change in the activity of ciprofloxacin.

Other biological applications of spiropyrans include the synthesis of a photoresponsive polymeric membrane surface,[94] the first reversible sensor for γ-Glutamyl-cysteinyl-glycine (GSH)[95] or the development of spiropyrans compounds with the ability to interact with G-quadruplex (G4) structures.[96]

Finally, the last group of photoswitches of this section is donor-acceptor Stenhouse adducts, also known as DASAs. DASAs are the newest group of photoswitches herein discussed as they were discovered in 2014 by Read de Alaniz and co-workers.[97-98] The mechanism of isomerization of DASAs has been recently proposed.[99] It is a really complex pathway in which photochemistry is only responsible for a part of the overall process. In a simpler way, it could be described as a cyclization

process. Irradiation of the strongly colored elongated triene form with visible light, leads to the formation of a colorless cyclopentenone, producing a large structural change. Reversion from the cyclopentenone to the triene form can be carried out with thermal relaxation exclusively. In the presence of polar solvents like water or methanol, DASAs undergo cyclization albeit slowly even without the presence of light.[100]

As has been described, molecular switches are commonly employed to create an "on/off" system with different bioactive molecules. However, the use of DASAs for pharmacological applications could be more directed towards drug release. These compounds suffer a big change in structure and polarity when they are irradiated. Such a molecular contraction can be used to disrupt aggregates. In 2016, Read de Alaniz and co-workers designed a DASA with a hydrophilic tail at the donor end, and long alkyl chains on the 1,3-dialkyl barbituric acid acceptor, creating an amphiphile that could assemble into micelles.[101] When the aqueous samples were irradiated with visible light (530-570 nm), isomerization of the DASA was induced, which resulted in the non-amphiphilic form leading to the disassembly of micelles. This was demonstrated by using Nile red to study micelle behavior.

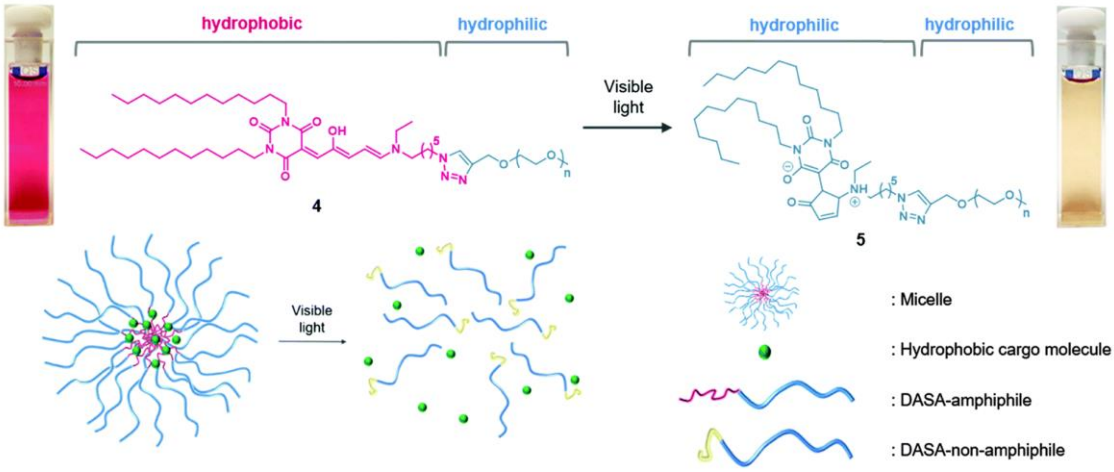

Figure 21. On the top, isomerization process of DASAs. The hydrophobic part is highlighted in pink and the hydrophilic part in blue. On the bottom, simulation of micelle formation in an aqueous medium to encapsulate hydrophobic cargo. Upon irradiation with visible light, the disruption of micelles is triggered, and the cargo molecules released. Modified by permission from reference 101. Copyright © The Royal Society of Chemistry 2016.

Finally, micelles were loaded with paclitaxel, a drug used for the treatment of different types of tumors. Samples were incubated with MCF-7 cells to verify the controlled release of the drug from the micelle. Results proved that paclitaxel was successfully delivered to the cancer cells when samples were irradiated, triggering the release of the drug. Consequently, a decrease of 46% in the viability of cells was

observed. Samples kept in the dark displayed a significantly lower cell death because the chemotherapeutic agent remained inside the micelles. This work presents new possibilities for molecular switches, not only as tools to induce a change in the activity of a biomolecule but also as new materials for the construction of light-activated micelles. The approach of Read de Alaniz is related to the next section of this thesis in which the strategy of photocaged compounds will be discussed.

In these paragraphs, the most used molecular switches in the field of photopharmacology have been considered. Some of them, like azobenzenes, discovered long ago and with a large number of articles in the bibliography. Others, like DASAs, have been recently designed, and their applications remain to be explored.

Although big steps have been made in the right direction, some properties remain to be improved. If photopharmacology aspires to be a modern alternative to classic pharmacotherapy, the development of new structures more compatible with biological systems is necessary. Another decisive factor is trying to achieve a more significant difference in activity between both forms of the molecule. In order to fulfill these criteria, the field of photopharmacology is quickly evolving. The research of molecular switches intended to control pharmacological agents has not reached its peak yet as new structures are currently being studied for their future application in this area.[102-103]

Table 1. Photophysical properties of most used molecular switches in photopharmacology.[104] Modified from reference 104.

Molecular switch	Mechanism	λ_{irr} (*O*/*E*)[a]	λ_{irr} (*C*/*Z*)[a]	Thermal stability[b]/ Thermal half-life	Fatigue resistance (aqueous solution)[c]	Switching effect
Azobenzenes	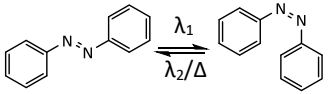	310-440 nm	420-900 nm	- / days	+	conformation, dipole moment
DAEs	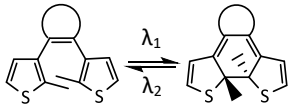	230-300 nm	530-980 nm	+	+	rigidity, electronics
Fulgimides	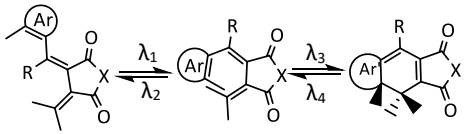	270-481 nm	470-825 nm	+	+	rigidity, electronics
HTIs	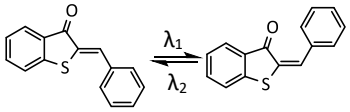	480-514 nm	400-415 nm	- / hours	+	conformation, dipole moment
Spiropyrans	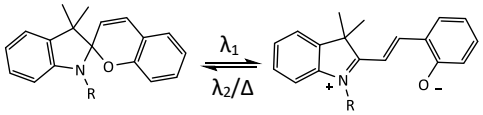	320-380 nm	440-660 nm	- / hours	-	conformation, polarity
DASAs	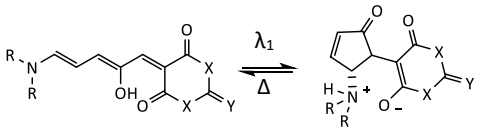	450-700 nm	n/a[d]	- / minutes	n/a	geometry, polarity

[a]: λ_{irr} = irradiation wavelength employed to obtain *O*→*C* / *E*→*Z* or *C*→*O* / *Z*→*E*. [b]: + → thermally stable, - → thermally unstable. [c]: + → several cycles of isomerization performed without sign of decomposition in aqueous solution. - → no reversible switching in aqueous solution. n/a → non-applicable. No data available for fatigue resistance in water due to spontaneous cyclization in polar solvents like water. [d]: Reversion from the closed to the open form only possible via thermal relaxation.

2.5 Photoreleasable groups

Photoreleasable protective groups (PPGs), also called photoremovable, photocleavable or photoactivatable, are another important tool that provides spatial and temporal control over bioactive molecules. Light activation of pharmacological agents in an irreversible way presents an alternative to photopharmacology and can be achieved with the photocaging technique. This approach is based on the modification of a known drug, in order to covalently attach the PPG in a critical position, which renders the molecule inactive. When the caged compound is irradiated, the PPG is removed, and the drug recovers its activity. This process is irreversible, meaning when the drug is cleaved, reversion to the initial inactive form is not possible (see figure 5).

The use of PPGs to create bioactive molecules that can be activated in specific targets where the disease is localized offers a new way of drug administration.

2.5.1 Requirements of a photocage in biological applications

The requirements for a photocage are slightly less strict than those previously exposed for molecular switches because it is an irreversible system. Therefore, reversion processes do not have to be considered. In this case, the caged compound should not present activity, and the release process should be efficient, allowing the total release of the active compound in shorts amounts of time and without forming any photoproduct other than the desired. Regarding the rest of the requirements, most of them match the ones explained in section 2.3.1.

The PPG should have strong absorption at wavelengths compatible with the therapeutic window (between 600 and 1200 nm) to prevent phototoxicity and allow maximum tissue penetration.

The photoreaction should be clean, avoiding the formation of non-desire products. High quantum yields of release are preferred. The quantum yield is equal to the number of released molecules divided by the number of photons at the irradiation wavelength, therefore higher quantum yields mean better release efficiencies. Ideally, the photochemical byproducts once the release takes place should be transparent at the irradiation wavelength. Thus, preventing competitive absorption, which would entail a decay in the release efficiency.

Besides, the PPG should be soluble in cellular environments as it is being tested for biological applications. Stability in this environment is required prior to and during

the photolysis. Furthermore, PPG toxicity should be studied before and after the release takes place.

2.5.2 Advantages and limitations of photocages

As well as with the photopharmacological approach, the use of photocages for the release of drugs implies several advantages over traditional methods.

This new administration method provides a solution to common problems such as low selectivity, drug dosage, and adverse effects. Attaching a photoreleasable group to a pharmacological agent allows the controlled photorelease of the active form in a specific target. Consequently, the drug would be in its inactive form in the rest of the body, where its effect could be damaging, which would improve remarkably the selectivity of the agent. Improved selectivity would allow a better adjustment in drug dosage. Higher doses could be used in the affected part only, removing the adverse effects in the other healthy areas.

Whereas when working with molecular switches the activity of the compounds once the photoactive moiety has been attached must be re-evaluated and will be potentially affected, the use of PPGs does not affect to the final activity of the molecule, making them an easier option to control the activity of biomolecules.

However, the irreversible character of PPGs removes the option of deactivation after the damaged area has been treated. Small fractions of the active drug will face the process of elimination and could possibly affect the organs involved, such as kidney and liver. After the elimination, these fractions will end in the environment, but at a much lower concentration than with conventional administration (see figure 9).

2.5.3 Previous works in drug photorelease

Photoreleasable protective groups have been widely studied over the last decades, becoming of great interest in delivering bioactive molecules through light stimulus.

Traditional PPGs based on nitrobenzyl, nitroanilide, or phenacyl moieties are responsive to UV light, which has been extensively explained to be not compatible with biological applications. Nevertheless, the uncaging reaction implies the dissociation of the covalent bond formed between the PPG and the leaving group, which requires energy. UV light is more energetic than visible light, and thus, it is easier to break a bond with UV light that with visible. Despite this fact, scientists, encouraged by the potential use of PPGs in biological fields, have reported several PPGs working with visible light over the last years. This section will be focused on these recent

advances in the design of photocages. More specifically, in the photorelease using organic structures that directly release the substrate with single-photon absorption. However, it should be mentioned that the release of molecules with visible light can also be achieved by other methods, like via photoinduced electron transfer,[105-106] via metal-ligand photocleavage[107-108] or by using photosensitizers.[109-111]

Coumarins were first employed as a photoreleasable group by Givens in 1984.[112] Some of their properties include high molar absorption coefficients, fast release rates, good stability, and fluorescent properties, which can help monitor the reaction course. Besides, their structure can be modified in order to improve their solubility in aqueous media. First coumarins were responsive to UV light, but during these past years, new and improved versions have been synthesized with absorption in the visible region.

In 2006, Hayashi, Kiso, and co-workers synthesized the first photoresponsive prodrug of paclitaxel.[113] Paclitaxel has been described in previous examples as one of the most important drugs in cancer therapy. A derivative of coumarin was carbamate-linked to suppress the pharmacophore activity.

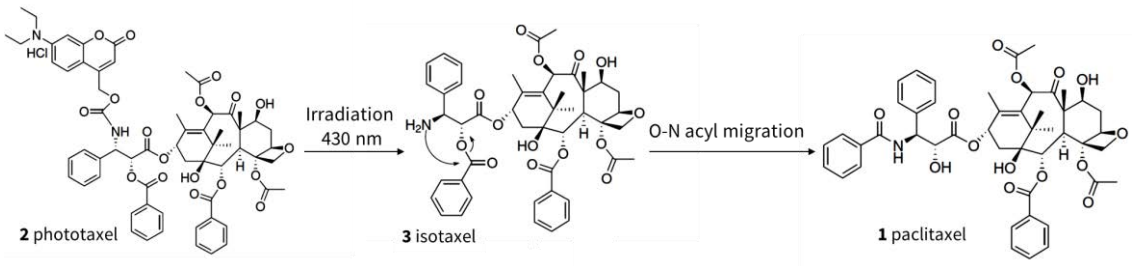

Figure 22. Release mechanism of paclitaxel caged with a coumarin PPG. First step is the irradiation with visible light (430 nm) of compound **2**. The coumarin unit is removed to obtain prodrug **3**. Second step involves O-N intramolecular acyl migration of **3** to obtain paclitaxel **1**. Modified by permission from reference 113. Copyright © 2006 Elsevier Ltd.

Prodrug **2** was irradiated with visible light (λ = 430 nm), and the release was followed by UV-Vis absorption spectrum and HPLC. Paclitaxel was released with a 69% yield in 30 minutes. This value might be related to partial decomposition of prodrug or the intermediate due to their photoinstability. The prodrug was observed to be stable in solution in the absence of light for at least 1 month, and in solid state up to 4 months.

New advances in the design of coumarins were made by Kele and co-workers in 2019.[114] They described the synthesis of a new class of coumarins with shifted absorption toward the red region. In addition, these new structures showed good water solubility and high release yields.

Another group that presents promising properties as PPG for future biological applications are quinones. The use of quinones as PPG was reported by Steinmetz for the first time in 2005.[115] Quinones have maximum absorption in the green region, but the band can extend to the red region. Thus, the release can be carried out with red light (626 nm).[116] Besides, their structure can be modified in order to gain water solubility. Compared to coumarins absorbing in the visible region, quinones display lower molar extinction coefficients ($\varepsilon_{coumarins}$ = 30000-40000 $M^{-1}cm^{-1}$ *vs.* $\varepsilon_{quinones}$ = 1900-2600 $M^{-1}cm^{-1}$)[114, 116] but improved quantum yields ($\phi_{coumarins}$ = 0.14-1.09 % *vs.* $\Phi_{quinones}$ = 0.27-5.7 %).[114, 116] Nowadays, quinones have only been employed to release small organic molecules.[115-117] However, given their good properties, they are a promising candidate for the release of bioactive molecules.

Perhaps one of the most studied photocages in the last years is BODIPYS. This family of chromophores offers tunable absorptions throughout the visible/near-IR region (450-800 nm), high molar absorption coefficients (30000-80000 M^{-1} cm^{-1}),[118] and known biological compatibility.[119] Furthermore, they have a sharp absorption profile that would not interfere with the wavelengths required for fluorescence observation, which allows the visualization of caged compounds. In addition, the structure of BODIPYs is quite versatile, and several positions can be employed to link the cargo molecule, as shown in figure 23.

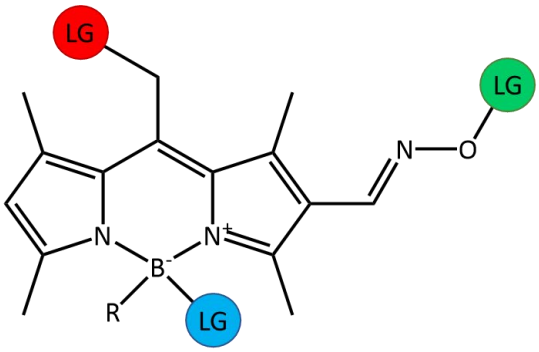

Figure 23. Possible positions in the BODIPY structure where the leaving group (LG) can be linked. In blue, photo-caging at the 4-position.[120] In red, *meso*-position photo-caging.[118] In green, N-O cleavage photo-caging.[121]

BODIPYs were used for the first time as photocages in 2014 when Urano and co-workers serendipitously discovered that 4-aryloxy BODIPY derivatives were photocleavable at the 4-position by visible light irradiation.[120] In order to apply this new role of BODIPYs in a biological study, they chose histamine, which plays an important role in many physiological processes, as the cargo molecule. The terminal amine group of histamine was caged with BODIPY through a benzyloxycarbonyl linker.

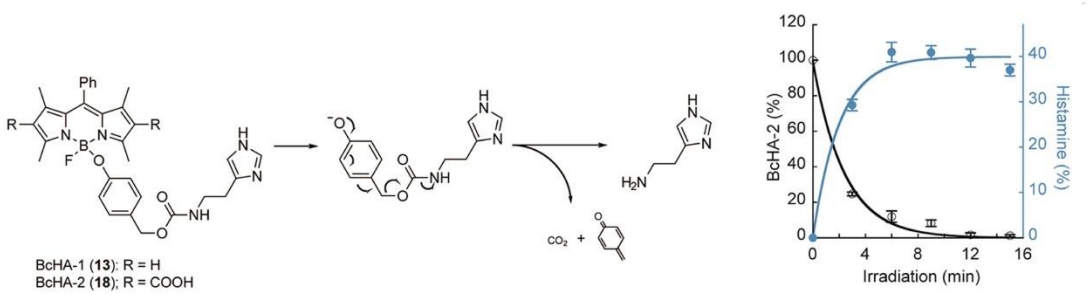

Figure 24. Release process for the BODIPY linked to histamine (**13** and **18**). Upon light irradiation with visible light (475-490 nm), the phenolate group is released and further decomposes to produce free histamine. On the right, time course of **18** consumption (in black) and histamine production (in blue) when irradiated. Adapted with permission from reference 120. Copyright © 2014 American Chemical Society.

In vitro studies were performed on HeLa cells. Although **13** exhibited good photocleavability, it failed to stimulate the cells, probably due to mismatched localization of the caged compound and target receptor. As for **18**, *in vitro* irradiation showed a release yield of 40%.

BODIPY caging at the 4-position was also employed by Chakrapani and co-workers to uncage levofloxacin, a known fluoroquinolone.[122] The synthesized BODIPY incorporating levofloxacin linked through a B-O bond (BDP-Levo) had a release yield of 31%. To testing the antibacterial activity of BDP-Levo, assays were performed in *Staphylococcus aureus*. Results displayed a clear inhibition of bacteria growth for the samples containing BDP-Levo once the samples were exposed to light. Samples kept in the dark did not show growth inhibition. As was demonstrated, the strategy of uncaging can be employed to achieve the controlled release of antibiotics.

A second position for photocaging in the core of BODIPY was discovered in 2015 by the groups of Weinstain[123] and Winter.[124] The new *meso*-substituted BODIPY proved to be effective for the release of small organic molecules with green light and proved to have higher release yields than those reported at the 4-position. A few years later, in 2018, Winter and co-workers expanded the range of absorption to the NIR region with new structures.[118] This new position has also been used for biological applications like the release of hydrogen sulfide,[125] or an anticancer drug.[126]

Recently, a third position for photocaging has been reported by Zhang and co-workers.[121] They described a new BODIPY oxime ester as a new platform to uncage aromatic and aliphatic carboxylic acids. Green light irradiation allows the cleavage of the weak N-O bond. In order to demonstrate the application of this new position in drug delivery, an anticancer drug was photouncaged.

Photocages have been used longer than molecular switches to regain control of bioactive molecules by light. However, the problems they face are similar to the ones previously explained for photodrugs. While there is a vast amount of photoprotective groups, only a few are responsive to visible light. Besides, other properties like water solubility or release efficiency need to be improved if they want to substitute classic pharmacological agents in the near future. For this reason, the design of new photoremovable groups that are compatible with biological applications has raised the interest of researches over the last few years.

2.6 References

1. Marija, P.; Zlata, J.; Aleksandar, K.; Miloš, P.; Dušanka, D.; Sanja, M.-S., Burns treatment in ancient times. *Medicinski pregled* **2013,** *66* (5-6), 263-267.
2. JONES, H. W., Report of a Series of Cases of Syphilis Treated by Ehrlich's Arsenobenzol at the Walter Reed General Hospital, District of Columbia. *The Boston Medical and Surgical Journal* **1911,** *164* (11), 381-383.
3. Domagk, G., Ein Beitrag zur Chemotherapie der bakteriellen Infektionen. *Deutsche Medizinische Wochenschrift* **1935,** *61* (07), 250-253.
4. Gelmo, P., Über Sulfamide der p-Amidobenzolsulfonsäure. *Journal für Praktische Chemie* **1908,** *77* (1), 369-382.
5. Stadler, M.; Dersch, P., *How to Overcome the Antibiotic Crisis*. Springer: 2016.
6. Newman, D. J.; Cragg, G. M., Natural Products as Sources of New Drugs from 1981 to 2014. *Journal of Natural Products* **2016,** *79* (3), 629-661.
7. Sciences, N. A. o., *Biographical Memoirs*. The National Academies Press: Washington, DC, 2003; p 387.
8. Projan, S. J., Why is big Pharma getting out of antibacterial drug discovery? *Current Opinion in Microbiology* **2003,** *6* (5), 427-430.
9. Duval, R. E.; Grare, M.; Demoré, B., Fight Against Antimicrobial Resistance: We Always Need New Antibacterials but for Right Bacteria. *Molecules* **2019,** *24* (17), 3152.
10. Lerner, P. I., Producing Penicillin. *New England Journal of Medicine* **2004,** *351* (6), 524-524.
11. Wormser, G. P.; Bergman, M. M., The Antibiotic Paradox: How the Misuse of Antibiotics Destroys Their Curative Powers, 2nd Edition By Stuart B. Levy Cambridge, Massachusetts: Perseus Publishing, 2002. *Clinical Infectious Diseases* **2003,** *36* (2).
12. CDC, Antibiotic resistance threats in the United States, 2019. **2019**.
13. van Hoek, A.; Mevius, D.; Guerra, B.; Mullany, P.; Roberts, A.; Aarts, H., Acquired Antibiotic Resistance Genes: An Overview. *Frontiers in Microbiology* **2011,** *2* (203).

14. Sandner-Miranda, L.; Vinuesa, P.; Cravioto, A.; Morales-Espinosa, R., The Genomic Basis of Intrinsic and Acquired Antibiotic Resistance in the Genus Serratia. *Frontiers in Microbiology* **2018,** *9* (828).
15. A European One Health Action Plan against Antimicrobial Resistance (AMR). European Commission: 2017.
16. Tackling Drug-resistant Infections Globally: Final Report and Recommendations. *Review on antimicrobial resistance* **2016**.
17. Read, A. F.; Woods, R. J., Antibiotic resistance management. *Evolution, Medicine, and Public Health* **2014,** *2014* (1), 147-147.
18. Luyt, C.-E.; Bréchot, N.; Trouillet, J.-L.; Chastre, J., Antibiotic stewardship in the intensive care unit. *Critical care (London, England)* **2014,** *18*, 480.
19. Viswanathan, V. K., Off-label abuse of antibiotics by bacteria. *Gut Microbes* **2014,** *5* (1), 3-4.
20. Bartlett, J. G.; Gilbert, D. N.; Spellberg, B., Seven Ways to Preserve the Miracle of Antibiotics. *Clinical Infectious Diseases* **2013,** *56* (10), 1445-1450.
21. Founou, L. L.; Founou, R. C.; Essack, S. Y., Antibiotic Resistance in the Food Chain: A Developing Country-Perspective. *Frontiers in Microbiology* **2016,** *7* (1881).
22. Kumar, K.; Gupta, S. C.; Chander, Y.; Singh, A. K., Antibiotic Use in Agriculture and Its Impact on the Terrestrial Environment. *Advances in Agronomy* **2005,** *87*, 1 - 54.
23. Manyi-Loh, C.; Mamphweli, S.; Meyer, E.; Okoh, A., Antibiotic Use in Agriculture and Its Consequential Resistance in Environmental Sources: Potential Public Health Implications. *Molecules* **2018,** *23* (4), 795.
24. Mahnert, A.; Moissl-Eichinger, C.; Zojer, M.; Bogumil, D.; Mizrahi, I.; Rattei, T.; Martinez, J. L.; Berg, G., Man-made microbial resistances in built environments. *Nature Communications* **2019,** *10* (1), 968.
25. Piddock, L. J. V., The crisis of no new antibiotics—what is the way forward? *The Lancet Infectious Diseases* **2012,** *12* (3), 249 - 253.
26. Zhabiz, G.; Omar, B.; Donald Gene, P., Bacteriophage therapy: a potential solution for the antibiotic resistance crisis. *The Journal of Infection in Developing Countries* **2014,** *8* (02).
27. Edwards, R.; Aronson, J. K., Adverse drug reactions: definitions, diagnosis, and management. *The Lancet* **2000,** *356* (9237), 1255 - 1259.
28. Lehár, J.; Krueger, A. S.; Avery, W.; Heilbut, A. M.; Johansen, L. M.; Price, E. R.; Rickles, R. J.; Short Iii, G. F.; Staunton, J. E.; Jin, X.; Lee, M. S.; Zimmermann, G. R.; Borisy, A. A., Synergistic drug combinations tend to improve therapeutically relevant selectivity. *Nature Biotechnology* **2009,** *27* (7), 659-666.

29. Hay, M.; Thomas, D. W.; Craighead, J. L.; Economides, C.; Rosenthal, J., Clinical development success rates for investigational drugs. *Nature Biotechnology* **2014,** *32* (1), 40-51.
30. Lerch, M. M.; Hansen, M. J.; van Dam, G. M.; Szymanski, W.; Feringa, B. L., Emerging Targets in Photopharmacology. *Angewandte Chemie International Edition* **2016,** *55* (37), 10978-10999.
31. Jorgensen, W. L., Efficient Drug Lead Discovery and Optimization. *Accounts of Chemical Research* **2009,** *42* (6), 724-733.
32. Brash, D. E.; Rudolph, J. A.; Simon, J. A.; Lin, A.; McKenna, G. J.; Baden, H. P.; Halperin, A. J.; Pontén, J., A role for sunlight in skin cancer: UV-induced p53 mutations in squamous cell carcinoma. *Proceedings of the National Academy of Sciences of the U S A* **1991,** *88* (22), 10124-10128.
33. Kappes, U. P.; Luo, D.; Potter, M.; Schulmeister, K.; Rünger, T. M., Short- and Long-Wave UV Light (UVB and UVA) Induce Similar Mutations in Human Skin Cells. *Journal of Investigative Dermatology* **2006,** *126* (3), 667 - 675.
34. Aragane, Y.; Kulms, D.; Metze, D.; Wilkes, G.; Pöppelmann, B.; Luger, T. A.; Schwarz, T., Ultraviolet light induces apoptosis via direct activation of CD95 (Fas/APO-1) independently of its ligand CD95L. *Journal of Cell Biology* **1998,** *140* (1), 171-182.
35. Anssi Auvinen; James Bridges; Kenneth Dawson; Wim De Jong; Philippe Hartemann; Arne Hensten; Peter Hoet; Thomas Jung; Mats-Olof Mattsson; Hannu Norppa; Jean-Marie Pagès; Ana Proykova; Eduardo Rodríguez-Farré; Klaus Schulze-Osthoff; Joachim Schüz; Mogens Thomsen; Vermeire, T., Health Effects of Artificial Light. EU Publications: 2012.
36. Ash, C.; Dubec, M.; Donne, K.; Bashford, T., Effect of wavelength and beam width on penetration in light-tissue interaction using computational methods. *Lasers in Medical Science* **2017,** *32* (8), 1909-1918.
37. Frazier, C. C., Photodynamic Therapy in Dermatology. *International Journal of Dermatology* **1996,** *35* (5), 312-316.
38. Kalka, K.; Merk, H.; Mukhtar, H., Photodynamic therapy in dermatology. *Journal of the American Academy of Dermatology* **2000,** *42* (3), 389-413.
39. Velema, W. A.; Szymanski, W.; Feringa, B. L., Photopharmacology: Beyond Proof of Principle. *Journal of the American Chemical Society* **2014,** *136* (6), 2178-2191.
40. Zbaida, S., The Mechanism of Microsomal Azoreduction: Predictions Based on Electronic Aspects of Structure-Activity Relationships. *Drug Metabolism Reviews* **1995,** *27* (3), 497-516.

41. Beharry, A. A.; Wong, L.; Tropepe, V.; Woolley, G. A., Fluorescence Imaging of Azobenzene Photoswitching In Vivo. *Angewandte Chemie International Edition* **2011,** *50* (6), 1325-1327.
42. Kumar, P.; Laughlin, S. T., Chapter Seven - Modular activatable bioorthogonal reagents. In *Methods in Enzymology*, Shukla, A. K., Ed. Academic Press: 2019; Vol. 622, pp 153-182.
43. Stricker, L.; Böckmann, M.; Kirse, T. M.; Doltsinis, N. L.; Ravoo, B. J., Arylazopyrazole Photoswitches in Aqueous Solution: Substituent Effects, Photophysical Properties, and Host–Guest Chemistry. *Chemistry – A European Journal* **2018,** *24* (34), 8639-8647.
44. López-Mirabal, H. R.; Winther, J. R., Redox characteristics of the eukaryotic cytosol. *Biochimica et Biophysica Acta (BBA) - Molecular Cell Research* **2008,** *1783* (4), 629 - 640.
45. Yoon, I.; Li, J. Z.; Shim, Y. K., Advance in Photosensitizers and Light Delivery for Photodynamic Therapy. *Clinical Endoscopy* **2013,** *46* (1), 7-23.
46. Noble, A., III. Zur Geschichte des Azobenzols und des Benzidins. *Justus Liebigs Annalen der Chemie* **1856,** *98* (2), 253-256.
47. Hartley, G. S., The Cis-form of Azobenzene. *Nature* **1937,** *140* (3537), 281-281.
48. Beharry, A. A.; Woolley, G. A., Azobenzene photoswitches for biomolecules. *Chemical Society Reviews* **2011,** *40* (8), 4422-4437.
49. Bartels, E.; Wassermann, N. H.; Erlanger, B. F., Photochromic Activators of the Acetylcholine Receptor. *Proceedings of the National Academy of Sciences* **1971,** *68* (8), 1820-1823.
50. Deal, W. J.; Erlanger, B. F.; Nachmansohn, D., Photoregulation of biological activity by photochromic reagents, III. Photoregulation of bioelectricity by acetyl choline receptor inhibitor. *Proceedings of the National Academy of Sciences* **1969,** *64* (4), 1230-1234.
51. Stein, M.; Middendorp, S. J.; Carta, V.; Pejo, E.; Raines, D. E.; Forman, S. A.; Sigel, E.; Trauner, D., Azo-Propofols: Photochromic Potentiators of GABAA Receptors. *Angewandte Chemie International Edition* **2012,** *51* (42), 10500-10504.
52. Vanlersberghe, C.; Camu, F., Propofol. In *Modern Anesthetics*, Schüttler, J.; Schwilden, H., Eds. Springer Berlin Heidelberg: Berlin, Heidelberg, 2008; pp 227-252.
53. Velema, W. A.; van der Berg, J. P.; Hansen, M. J.; Szymanski, W.; Driessen, A. J. M.; Feringa, B. L., Optical control of antibacterial activity. *Nature Chemistry* **2013,** *5* (11), 924-928.

54. Wegener, M.; Hansen, M. J.; Driessen, A. J. M.; Szymanski, W.; Feringa, B. L., Photocontrol of Antibacterial Activity: Shifting from UV to Red Light Activation. *Journal of the American Chemical Society* **2017,** *139* (49), 17979-17986.
55. Bléger, D.; Schwarz, J.; Brouwer, A. M.; Hecht, S., o-Fluoroazobenzenes as Readily Synthesized Photoswitches Offering Nearly Quantitative Two-Way Isomerization with Visible Light. *Journal of the American Chemical Society* **2012,** *134* (51), 20597-20600.
56. Samanta, S.; Beharry, A. A.; Sadovski, O.; McCormick, T. M.; Babalhavaeji, A.; Tropepe, V.; Woolley, G. A., Photoswitching Azo Compounds in Vivo with Red Light. *Journal of the American Chemical Society* **2013,** *135* (26), 9777-9784.
57. Yeoh, Y. Q.; Yu, J.; Polyak, S. W.; Horsley, J. R.; Abell, A. D., Photopharmacological Control of Cyclic Antimicrobial Peptides. *ChemBioChem* **2018,** *19* (24), 2591-2597.
58. Prenner, E. J.; Kiricsi, M.; Jelokhani-Niaraki, M.; Lewis, R. N. A. H.; Hodges, R. S.; McElhaney, R. N., Structure-Activity Relationships of Diastereomeric Lysine Ring Size Analogs of the Antimicrobial Peptide Gramicidin S. *The Journal of Biological Chemistry* **2004,** *280*, 2002-2011.
59. Hoorens, M. W. H.; Ourailidou, M. E.; Rodat, T.; van der Wouden, P. E.; Kobauri, P.; Kriegs, M.; Peifer, C.; Feringa, B. L.; Dekker, F. J.; Szymanski, W., Light-controlled inhibition of BRAFV600E kinase. *European Journal of Medicinal Chemistry* **2019,** *179*, 133-146.
60. Ugurel, S.; Röhmel, J.; Ascierto, P. A.; Flaherty, K. T.; Grob, J. J.; Hauschild, A.; Larkin, J.; Long, G. V.; Lorigan, P.; McArthur, G. A.; Ribas, A.; Robert, C.; Schadendorf, D.; Garbe, C., Survival of patients with advanced metastatic melanoma: The impact of novel therapies. *European Journal of Cancer* **2016,** *53*, 125-134.
61. Kim, G.; McKee, A. E.; Ning, Y.-M.; Hazarika, M.; Theoret, M.; Johnson, J. R.; Xu, Q. C.; Tang, S.; Sridhara, R.; Jiang, X.; He, K.; Roscoe, D.; McGuinn, W. D.; Helms, W. S.; Russell, A. M.; Miksinski, S. P.; Zirkelbach, J. F.; Earp, J.; Liu, Q.; Ibrahim, A.; Justice, R.; Pazdur, R., FDA Approval Summary: Vemurafenib for Treatment of Unresectable or Metastatic Melanoma with the BRAFV600E Mutation. *Clinical Cancer Research* **2014,** *20* (19), 4994-5000.
62. Rutkowski, P.; Blank, C., Dabrafenib for the treatment of BRAF V600-positive melanoma: a safety evaluation. *Expert Opinion on Drug Safety* **2014,** *13* (9), 1249-1258.
63. Adelmann, C. H.; Ching, G.; Du, L.; Saporito, R. C.; Bansal, V.; Pence, L. J.; Liang, R.; Lee, W.; Tsai, K. Y., Comparative profiles of BRAF inhibitors: the paradox index as a predictor of clinical toxicity. *Oncotarget* **2016,** *7* (21).

64. Mourot, A.; Kienzler, M. A.; Banghart, M. R.; Fehrentz, T.; Huber, F. M. E.; Stein, M.; Kramer, R. H.; Trauner, D., Tuning Photochromic Ion Channel Blockers. *ACS Chemical Neuroscience* **2011,** *2* (9), 536-543.
65. Schoenberger, M.; Damijonaitis, A.; Zhang, Z.; Nagel, D.; Trauner, D., Development of a New Photochromic Ion Channel Blocker via Azologization of Fomocaine. *ACS Chemical Neuroscience* **2014,** *5* (7), 514-518.
66. Liu, X.-M.; Yang, B.; Wang, Y.-L.; Wang, J.-Y., Photoisomerisable cholesterol derivatives as photo-trigger of liposomes: Effect of lipid polarity, temperature, incorporation ratio, and cholesterol. *Biochimica et Biophysica Acta (BBA) - Biomembranes* **2005,** *1720* (1), 28-34.
67. Frank, J. A.; Moroni, M.; Moshourab, R.; Sumser, M.; Lewin, G. R.; Trauner, D., Photoswitchable fatty acids enable optical control of TRPV1. *Nature Communications* **2015,** *6* (1), 7118.
68. Glock, P.; Broichhagen, J.; Kretschmer, S.; Blumhardt, P.; Mücksch, J.; Trauner, D.; Schwille, P., Optical Control of a Biological Reaction–Diffusion System. *Angewandte Chemie International Edition* **2018,** *57* (9), 2362-2366.
69. Broichhagen, J.; Podewin, T.; Meyer-Berg, H.; von Ohlen, Y.; Johnston, N. R.; Jones, B. J.; Bloom, S. R.; Rutter, G. A.; Hoffmann-Röder, A.; Hodson, D. J.; Trauner, D., Optical Control of Insulin Secretion Using an Incretin Switch. *Angewandte Chemie International Edition* **2015,** *54* (51), 15565-15569.
70. Hüll, K.; Benster, T.; Manookin, M. B.; Trauner, D.; Van Gelder, R. N.; Laprell, L., Photopharmacologic Vision Restoration Reduces Pathological Rhythmic Field Potentials in Blind Mouse Retina. *Scientific Reports* **2019,** *9* (1), 13561.
71. Laprell, L.; Hüll, K.; Stawski, P.; Schön, C.; Michalakis, S.; Biel, M.; Sumser, M. P.; Trauner, D., Restoring Light Sensitivity in Blind Retinae Using a Photochromic AMPA Receptor Agonist. *ACS Chemical Neuroscience* **2016,** *7* (1), 15-20.
72. Broichhagen, J.; Schönberger, M.; Cork, S. C.; Frank, J. A.; Marchetti, P.; Bugliani, M.; Shapiro, A. M. J.; Trapp, S.; Rutter, G. A.; Hodson, D. J.; Trauner, D., Optical control of insulin release using a photoswitchable sulfonylurea. *Nature Communications* **2014,** *5* (1), 5116.
73. Broichhagen, J.; Frank, J. A.; Johnston, N. R.; Mitchell, R. K.; Šmid, K.; Marchetti, P.; Bugliani, M.; Rutter, G. A.; Trauner, D.; Hodson, D. J., A red-shifted photochromic sulfonylurea for the remote control of pancreatic beta cell function. *Chemical Communications* **2015,** *51* (27), 6018-6021.
74. Hüll, K.; Morstein, J.; Trauner, D., In Vivo Photopharmacology. *Chemical Reviews* **2018,** *118* (21), 10710-10747.

75. Kellogg, R. M.; Groen, M. B.; Wynberg, H., Photochemically induced cyclization of some furyl- and thienylethenes. *The Journal of Organic Chemistry* **1967,** *32* (10), 3093-3100.
76. Irie, M., Diarylethenes for Memories and Switches. *Chemical Reviews* **2000,** *100* (5), 1685-1716.
77. Babii, O.; Afonin, S.; Berditsch, M.; Reiβer, S.; Mykhailiuk, P. K.; Kubyshkin, V. S.; Steinbrecher, T.; Ulrich, A. S.; Komarov, I. V., Controlling Biological Activity with Light: Diarylethene-Containing Cyclic Peptidomimetics. *Angewandte Chemie International Edition* **2014,** *53* (13), 3392-3395.
78. Babii, O.; Afonin, S.; Garmanchuk, L. V.; Nikulina, V. V.; Nikolaienko, T. V.; Storozhuk, O. V.; Shelest, D. V.; Dasyukevich, O. I.; Ostapchenko, L. I.; Iurchenko, V.; Zozulya, S.; Ulrich, A. S.; Komarov, I. V., Direct Photocontrol of Peptidomimetics: An Alternative to Oxygen-Dependent Photodynamic Cancer Therapy. *Angewandte Chemie International Edition* **2016,** *55* (18), 5493-5496.
79. Okamoto, K.; Tomita, Y.; Yonezawa, H.; Hirohata, T.; Ogura, R.; Izumiya, N., Inhibitory Effect of Gramicidin S on the Growth of Murine Tumor Cells in vitro and in vivo. *Oncology* **1984,** *41* (1), 43-48.
80. Li, Z.; Wang, Y.; Li, M.; Zhang, H.; Guo, H.; Ya, H.; Yin, J., Synthesis and properties of dithienylethene-functionalized switchable antibacterial agents. *Organic & Biomolecular Chemistry* **2018,** *16* (38), 6988-6997.
81. Velema, W. A.; Hansen, M. J.; Lerch, M. M.; Driessen, A. J. M.; Szymanski, W.; Feringa, B. L., Ciprofloxacin–Photoswitch Conjugates: A Facile Strategy for Photopharmacology. *Bioconjugate Chemistry* **2015,** *26* (12), 2592-2597.
82. Lachmann, D.; Studte, C.; Männel, B.; Hübner, H.; Gmeiner, P.; König, B., Photochromic Dopamine Receptor Ligands Based on Dithienylethenes and Fulgides. *Chemistry – A European Journal* **2017,** *23* (54), 13423-13434.
83. Falenczyk, C.; Schiedel, M.; Karaman, B.; Rumpf, T.; Kuzmanovic, N.; Grøtli, M.; Sippl, W.; Jung, M.; König, B., Chromo-pharmacophores: photochromic diarylmaleimide inhibitors for sirtuins. *Chemical Science* **2014,** *5* (12), 4794-4799.
84. Presa, A.; Brissos, R. F.; Caballero, A. B.; Borilovic, I.; Korrodi-Gregório, L.; Pérez-Tomás, R.; Roubeau, O.; Gamez, P., Photoswitching the Cytotoxic Properties of Platinum(II) Compounds. *Angewandte Chemie International Edition* **2015,** *54* (15), 4561-4565.
85. Willner, I.; Rubin, S.; Wonner, J.; Effenberger, F.; Baeuerle, P., Photoswitchable binding of substrates to proteins: photoregulated binding of .alpha.-D-mannopyranose to concanavalin A modified by a thiophenefulgide dye. *Journal of the American Chemical Society* **1992,** *114* (8), 3150-3151.

86. Lachmann, D.; Konieczny, A.; Keller, M.; König, B., Photochromic peptidic NPY Y4 receptor ligands. *Organic & Biomolecular Chemistry* **2019,** *17* (9), 2467-2478.
87. Herre, S.; Schadendorf, T.; Ivanov, I.; Herrberger, C.; Steinle, W.; Rück-Braun, K.; Preissner, R.; Kuhn, H., Photoactivation of an Inhibitor of the 12/15-Lipoxygenase Pathway. *ChemBioChem* **2006,** *7* (7), 1089-1095.
88. Samuelsson, B.; Dahlen, S.; Lindgren, J.; Rouzer, C.; Serhan, C., Leukotrienes and lipoxins: structures, biosynthesis, and biological effects. *Science* **1987,** *237* (4819), 1171-1176.
89. Kühn, H.; Chan, L., The role of 15-lipoxygenase in atherogenesis: pro- and antiatherogenic actions. *Current Opinion in Lipidology* **1997,** *8* (2), 111-117.
90. Klein, R. F.; Allard, J.; Avnur, Z.; Nikolcheva, T.; Rotstein, D.; Carlos, A. S.; Shea, M.; Waters, R. V.; Belknap, J. K.; Peltz, G.; Orwoll, E. S., Regulation of Bone Mass in Mice by the Lipoxygenase Gene Alox15. *Science* **2004,** *303* (5655), 229-232.
91. Fischer, E.; Hirshberg, Y., Formation of Coloured Forms of Spirans by Low-temperature *Journal of the Chemical Society* **1952,** (0), 4522-4524.
92. Lukyanov, B. S.; Lukyanova, M. B., Spiropyrans: Synthesis, Properties, and Application. (Review). *Chemistry of Heterocyclic Compounds* **2005,** *41* (3), 281-311.
93. Nilsson, J. R.; Li, S.; Önfelt, B.; Andréasson, J., Light-induced cytotoxicity of a photochromic spiropyran. *Chemical Communications* **2011,** *47* (39), 11020-11022.
94. Nayak, A.; Liu, H.; Belfort, G., An Optically Reversible Switching Membrane Surface. *Angewandte Chemie International Edition* **2006,** *45* (25), 4094-4098.
95. Heng, S.; Zhang, X.; Pei, J.; Abell, A. D., A Rationally Designed Reversible 'Turn-Off' Sensor for Glutathione. *Biosensors* **2017,** *7* (3), 36.
96. Livendahl, M.; Jamroskovic, J.; Hedenström, M.; Görlich, T.; Sabouri, N.; Chorell, E., Synthesis of phenanthridine spiropyrans and studies of their effects on G-quadruplex DNA. *Organic & Biomolecular Chemistry* **2017,** *15* (15), 3265-3275.
97. Helmy, S.; Leibfarth, F. A.; Oh, S.; Poelma, J. E.; Hawker, C. J.; Read de Alaniz, J., Photoswitching Using Visible Light: A New Class of Organic Photochromic Molecules. *Journal of the American Chemical Society* **2014,** *136* (23), 8169-8172.
98. Helmy, S.; Oh, S.; Leibfarth, F. A.; Hawker, C. J.; Read de Alaniz, J., Design and Synthesis of Donor–Acceptor Stenhouse Adducts: A Visible Light Photoswitch Derived from Furfural. *The Journal of Organic Chemistry* **2014,** *79* (23), 11316-11329.
99. Zulfikri, H.; Koenis, M. A. J.; Lerch, M. M.; Di Donato, M.; Szymański, W.; Filippi, C.; Feringa, B. L.; Buma, W. J., Taming the Complexity of Donor–Acceptor Stenhouse

Adducts: Infrared Motion Pictures of the Complete Switching Pathway. *Journal of the American Chemical Society* **2019,** *141* (18), 7376-7384.

100. Lerch, M. M.; Di Donato, M.; Laurent, A. D.; Medved', M.; Iagatti, A.; Bussotti, L.; Lapini, A.; Buma, W. J.; Foggi, P.; Szymański, W.; Feringa, B. L., Solvent Effects on the Actinic Step of Donor–Acceptor Stenhouse Adduct Photoswitching. *Angewandte Chemie International Edition* **2018,** *57* (27), 8063-8068.
101. Poelma, S. O.; Oh, S. S.; Helmy, S.; Knight, A. S.; Burnett, G. L.; Soh, H. T.; Hawker, C. J.; Read de Alaniz, J., Controlled drug release to cancer cells from modular one-photon visible light-responsive micellar system. *Chemical Communications* **2016,** *52* (69), 10525-10528.
102. Hoorens, M. W. H.; Medved', M.; Laurent, A. D.; Di Donato, M.; Fanetti, S.; Slappendel, L.; Hilbers, M.; Feringa, B. L.; Jan Buma, W.; Szymanski, W., Iminothioindoxyl as a molecular photoswitch with 100 nm band separation in the visible range. *Nature Communications* **2019,** *10* (1), 2390.
103. Lentes, P.; Stadler, E.; Röhricht, F.; Brahms, A.; Gröbner, J.; Sönnichsen, F. D.; Gescheidt, G.; Herges, R., Nitrogen Bridged Diazocines: Photochromes Switching within the Near-Infrared Region with High Quantum Yields in Organic Solvents and in Water. *Journal of the American Chemical Society* **2019,** *141* (34), 13592-13600.
104. Lachmann, D.; Lahmy, R.; König, B., Fulgimides as Light-Activated Tools in Biological Investigations. *European Journal of Organic Chemistry* **2019,** *2019* (31-32), 5018-5024.
105. Falvey, D. E.; Sundararajan, C., Photoremovable protecting groups based on electron transfer chemistry. *Photochemical & Photobiological Sciences* **2004,** *3* (9), 831-838.
106. Borak, J. B.; Falvey, D. E., Ketocoumarin dyes as electron mediators for visible light induced carboxylate photorelease. *Photochemical & Photobiological Sciences* **2010,** *9* (6), 854-860.
107. Zayat, L.; Noval, M. G.; Campi, J.; Calero, C. I.; Calvo, D. J.; Etchenique, R., A New Inorganic Photolabile Protecting Group for Highly Efficient Visible Light GABA Uncaging. *ChemBioChem* **2007,** *8* (17), 2035-2038.
108. Shell, T. A.; Shell, J. R.; Rodgers, Z. L.; Lawrence, D. S., Tunable Visible and Near-IR Photoactivation of Light-Responsive Compounds by Using Fluorophores as Light-Capturing Antennas. *Angewandte Chemie International Edition* **2014,** *53* (3), 875-878.
109. Atilgan, A.; Tanriverdi Eçik, E.; Guliyev, R.; Uyar, T. B.; Erbas-Cakmak, S.; Akkaya, E. U., Near-IR-Triggered, Remote-Controlled Release of Metal Ions: A Novel

Strategy for Caged Ions. *Angewandte Chemie International Edition* **2014,** *53* (40), 10678-10681.

110. Gorka, A. P.; Nani, R. R.; Zhu, J.; Mackem, S.; Schnermann, M. J., A Near-IR Uncaging Strategy Based on Cyanine Photochemistry. *Journal of the American Chemical Society* **2014,** *136* (40), 14153-14159.
111. Nani, R. R.; Gorka, A. P.; Nagaya, T.; Kobayashi, H.; Schnermann, M. J., Near-IR Light-Mediated Cleavage of Antibody–Drug Conjugates Using Cyanine Photocages. *Angewandte Chemie International Edition* **2015,** *54* (46), 13635-13638.
112. Givens, R. S.; Matuszewski, B., Photochemistry of phosphate esters: an efficient method for the generation of electrophiles. *Journal of the American Chemical Society* **1984,** *106* (22), 6860-6861.
113. Mariusz Skwarczynski; Mayo Noguchi; Shun Hirota; Youhei Sohma; Tooru Kimura; Yoshio Hayashi; Kiso, Y., Development of first photoresponsive prodrug of paclitaxel. *Bioorganic & Medicinal Chemistry Letters* **2006,** *16* (17), 4492 - 4496.
114. Bojtár, M.; Kormos, A.; Kis-Petik, K.; Kellermayer, M.; Kele, P., Green-Light Activatable, Water-Soluble Red-Shifted Coumarin Photocages. *Organic Letters* **2019,** *21* (23), 9410-9414.
115. Chen, Y.; Steinmetz, M. G., Photochemical Cyclization with Release of Carboxylic Acids and Phenol from Pyrrolidino-Substituted 1,4-Benzoquinones Using Visible Light. *Organic Letters* **2005,** *7* (17), 3729-3732.
116. Wang, X.; Kalow, J. A., Rapid Aqueous Photouncaging by Red Light. *Organic Letters* **2018,** *20* (7), 1716-1719.
117. Walton, D. P.; Dougherty, D. A., A general strategy for visible-light decaging based on the quinone cis-alkenyl lock. *Chemical Communications* **2019,** *55* (34), 4965-4968.
118. Peterson, J. A.; Wijesooriya, C.; Gehrmann, E. J.; Mahoney, K. M.; Goswami, P. P.; Albright, T. R.; Syed, A.; Dutton, A. S.; Smith, E. A.; Winter, A. H., Family of BODIPY Photocages Cleaved by Single Photons of Visible/Near-Infrared Light. *Journal of the American Chemical Society* **2018,** *140* (23), 7343-7346.
119. Alford, R.; Simpson, H. M.; Duberman, J.; Hill, G. C.; Ogawa, M.; Regino, C.; Kobayashi, H.; Choyke, P. L., Toxicity of Organic Fluorophores Used in Molecular Imaging: Literature Review. *Molecular Imaging* **2009,** *8* (6), 7290.2009.00031.
120. Umeda, N.; Takahashi, H.; Kamiya, M.; Ueno, T.; Komatsu, T.; Terai, T.; Hanaoka, K.; Nagano, T.; Urano, Y., Boron Dipyrromethene As a Fluorescent Caging Group for Single-Photon Uncaging with Long-Wavelength Visible Light. *ACS Chemical Biology* **2014,** *9* (10), 2242-2246.

121. Sambath, K.; Zhao, T.; Wan, Z.; Zhang, Y., Photo-uncaging of BODIPY oxime ester for histone deacetylases induced apoptosis in tumor cells. *Chemical Communications* **2019,** *55* (94), 14162-14165.
122. Kumari, P.; Kulkarni, A.; Sharma, A. K.; Chakrapani, H., Visible-Light Controlled Release of a Fluoroquinolone Antibiotic for Antimicrobial Photopharmacology. *ACS Omega* **2018,** *3* (2), 2155-2160.
123. Rubinstein, N.; Liu, P.; Miller, E. W.; Weinstain, R., meso-Methylhydroxy BODIPY: a scaffold for photo-labile protecting groups. *Chemical Communications* **2015,** *51* (29), 6369-6372.
124. Goswami, P. P.; Syed, A.; Beck, C. L.; Albright, T. R.; Mahoney, K. M.; Unash, R.; Smith, E. A.; Winter, A. H., BODIPY-Derived Photoremovable Protecting Groups Unmasked with Green Light. *Journal of the American Chemical Society* **2015,** *137* (11), 3783-3786.
125. Štacko, P.; Muchová, L.; Vítek, L.; Klán, P., Visible to NIR Light Photoactivation of Hydrogen Sulfide for Biological Targeting. *Organic Letters* **2018,** *20* (16), 4907-4911.
126. Jang, Y.; Kim, T.-I.; Kim, H.; Choi, Y.; Kim, Y., Photoactivatable BODIPY Platform: Light-Triggered Anticancer Drug Release and Fluorescence Monitoring. *ACS Applied Bio Materials* **2019,** *2* (6), 2567-2572.

Chapter 3

Objectives

This doctoral thesis has as the main goal of designing antibacterial molecules whose properties could be modulated using light as a stimulus. In order to achieve this, a series of secondary objectives have been laid out and are presented next:

- Design of novel structures with potential antibacterial properties that incorporate a molecular switch in their structure. Perform their synthesis, characterization, and finally evaluate their properties which include:
    - The wavelength of absorption of the synthesized molecules. Preferably, in the visible region in order to obtain molecules suitable for biological applications.
    - The solubility in aqueous media, either complete or partial, by employing a certain amount of an organic solvent miscible with water. This will ensure their compatibility with biological studies.
    - The photoswitching behavior, once it is linked to the antibiotic moiety, following the isomerization process to quantify the photoisomer formed.
    - The thermal reversion of the photoswitch once the photoisomer is obtained.
    - The stability of the molecular switch after irradiation through several cycles, to monitor possible products of decomposition.
    - The analysis of the efficiency of the isomerization process.
    - The antibacterial activity of both isomers. Studying possible differences between the initial isomer and the photoisomer.
- Design of new molecules consisting of a photoreleasable protective group and an antibiotic. Carry out their synthesis and characterization to finally evaluate a series of properties, including:
    - The wavelength of absorption. Preferably in the visible region to make them suitable for biological studies.
    - Their solubility in aqueous media, complete or partial by using mixtures of water with other organic solvents.
    - The release of the antibiotic once it has been linked to the photoprotective group and quantification of the process.
    - The possible formation of byproducts when the molecule is irradiated.
    - The thermal stability in the dark.
    - The analysis of the efficiency of the release process.
    - The antibacterial activity of both forms caged and uncaged. Studying possible differences before and after irradiation of the molecules.

Chapter 4

Reversible Control of Quinolone Derivatives

4.1 Introduction

Resistance to antibiotics is one of the biggest healthcare problems of this century. From a chemical point of view, the ways to solve this problem go from the design and synthesis of new antibiotics to the development of new routes of administration. Photopharmacology addresses this last option, employing light as a stimulus to deliver the bioactive compound in a specific target.

In this chapter, the design, synthesis, and study of the photochemical, and antimicrobial properties of new photopharmacological agents will be described. Two components form this reversible system, an antibiotic part, and a molecular switch. Combining both, it is expected to create a system whose antibacterial properties could be optically controlled in a reversible way.

4.1.1 Quinolone antibiotics

In the last decades, quinolones have become some of the most frequently prescribed antibacterials in the world.[1-2] Their increased use is due to a number of characteristics like rapid bactericidal effect against most susceptible organisms and their extraordinary tissue penetration.[3]

The first quinolone was isolated by George Lesher and co-workers in 1962 as a byproduct in the synthesis of chloroquine, an antimalarial agent.[4] Nalidixic acid is not a proper choice for the treatment of systemic infections as it has moderate Gram-negative activity and low oral absorption. However, urinary concentrations are high, making nalidixic acid a perfect antibiotic for the treatment of urinary tract infections (UTIs).[5]

The real breakthrough of quinolones came in the early 1980s when a new generation of these antibiotics was developed. The second generation includes compounds with a fluoro-group at position 6 and a major ring substituent (piperazine or methyl piperazine) at position 7. A detailed representation of the different positions in quinolone antibiotics and their role in the antibiotic activity is displayed in figure 1. These compounds are broad-spectrum, meaning they are active against gram-positive and gram-negative bacteria. In addition, they are well absorbed from the gastrointestinal tract, providing adequate blood levels to allow their use for systematic infections.[6] Examples of this new generation include ciprofloxacin, norfloxacin, and ofloxacin, some of them still used today. In fact, ciprofloxacin remains one of the most commonly prescribed antibiotics.[7]

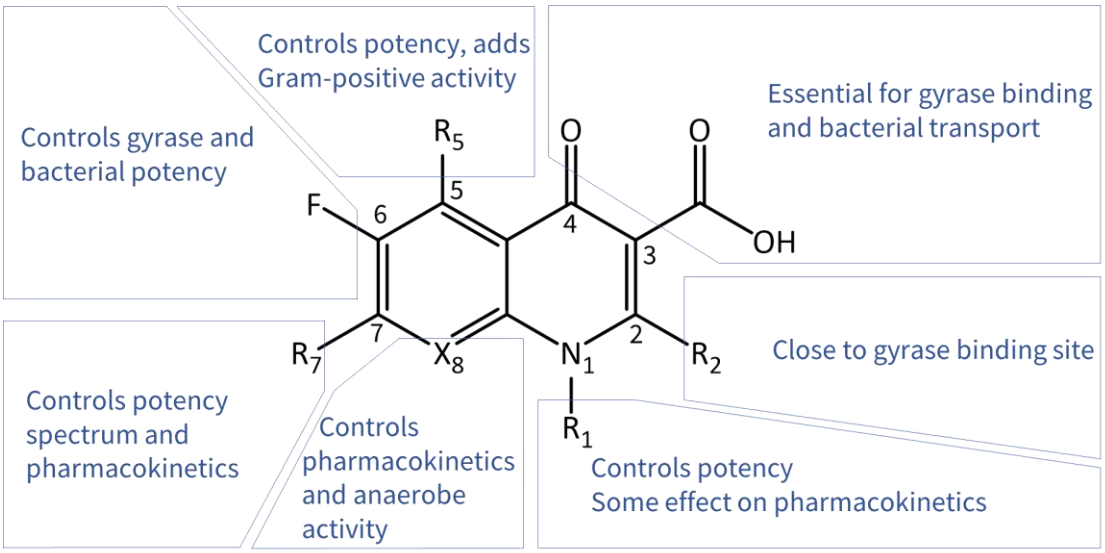

Figure 1. Structure-activity relationship of quinolone antibacterials.[8] Modified by permission from reference 8. Copyright © 1994, The British Society of Antimicrobial Chemotherapy.

Regarding the adverse effects, quinolones are well tolerated and relatively safe. Common adverse effects include gastrointestinal and central nervous system (CNS) effects in 2 to 20 percent of patients treated with quinolones.[9-11] It has also been reported that some quinolones can induce cardiovascular effects such as hypotension or tachycardia. Moreover, they can alter the cardiac rhythm and prolong QT intervals, which may result in fatal ventricular arrhythmias. For this reason, patients with a known predisposition to arrhythmias should avoid these drugs.[9-11]

The mechanism of action of quinolones is based on a rapid inhibition of DNA synthesis by promoting cleavage of bacterial DNA in the DNA-enzyme complexes of DNA gyrase and type IV topoisomerase. Increases in the concentration of enzyme-DNA cleavage complexes result in rapid bacterial death.[6, 12-13]

The problem of antibiotic resistance has been explained in a previous section, and unfortunately, the case of quinolones is not any different. Quinolone resistance is becoming a prevalent clinical issue that is threatening the use of these drugs. Three mechanisms have been identified to be associated with quinolone resistance: target-mediated, plasmid-mediated and chromosome-mediated.[6, 12] An excessive use of these drugs either in the agricultural feed or in clinical medicine will likely reduce the effectiveness of quinolones in the near future.

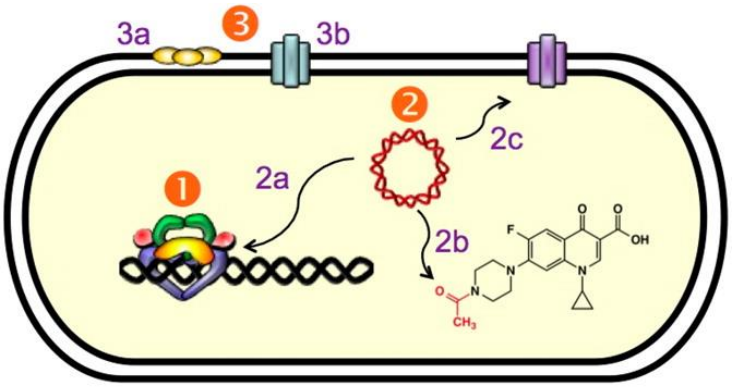

Figure 2. Illustrative example of mechanisms of quinolone resistance. (1) Target-mediated resistance: mutations in gyrase and topoisomerase IV result in weakened quinolone-enzyme interactions. (2) Plasmid-mediated resistance: (2a) Qnr proteins (represented in yellow) decrease topoisomerase-DNA binding and protect enzyme-DNA complexes from quinolones. (2b) Aac(6')-Ib-cr is an aminoglycoside acetyltransferase that acetylates the free nitrogen on the piperazine ring, making quinolones less effective. (2c) Plasmid-encoded efflux pumps decrease the concentration of quinolones in the cell. (3) Chromosome-mediated resistance: (3a) Underexpression of porins in Gram-negative species decreases drug uptake. (3b) Overexpression of chromosome-encoded efflux pumps decreases drug retention in the cell. Reprinted by permission from reference 12. Copyright © 2014 American Chemical Society.

4.1.2 Hydantoin-based molecular photoswitches

Hydantoins, also known as imidazolidine-2,4-diones were discovered by Adolf von Baeyer in 1861.[14] Since then, they have become a subject of interest in diverse areas of science. As a result, more than 3000 research articles and patents in methodological and medicinal chemistry have been published.[15] Hydantoins are present in some natural products[16-18] and are used in organic synthesis,[19-20] coordination chemistry,[21] polymer science[22] and in the design of molecular switches.[23]

Regarding their use as molecular switches, their mechanism of isomerization is based on *Z/E* isomerism, with *E* isomer being the thermodynamically stable state. Their properties include high photostability and fatigue resistance, as they can be interconverted between both isomers for several cycles without apparent decomposition. Besides, they present strong absorption in the UVA region of the spectrum. The reversion process from *Z* to *E* can be carried out with light and in some cases, thermally. Finally, these switches can be easily synthesized.[23]

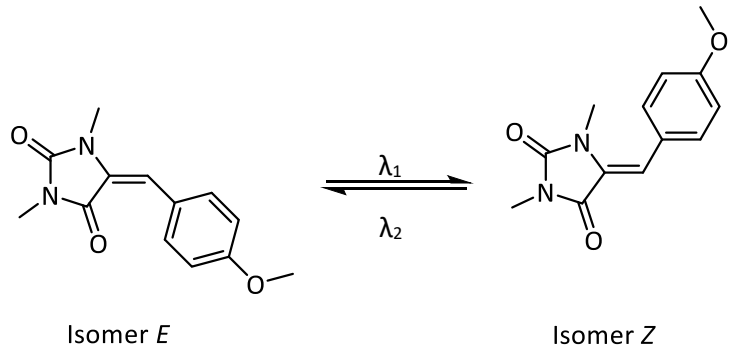

Figure 3. Isomerization process of a molecular switch based on the hydantoin structure. Upon irradiation with λ_1 isomer *Z* is obtained. Reversion to isomer *E* can be performed with λ_2. Adapted by permission from reference 23. Copyright © 2015 American Chemical Society.

4.1.3 Phytochrome-based molecular switches

Phytochromes are an essential group of photoreceptors[24-25] present in plants and microorganisms like bacteria,[26] fungi,[27] and simple molds.[28] They are involved in many light-regulated processes, extending from phototaxis and pigmentation in bacteria to seed germination and flowering in higher plants. The chromophore of phytochrome, also known as bilin, can be interconverted between two states upon light absorption, undergoing *Z*/*E* isomerization.

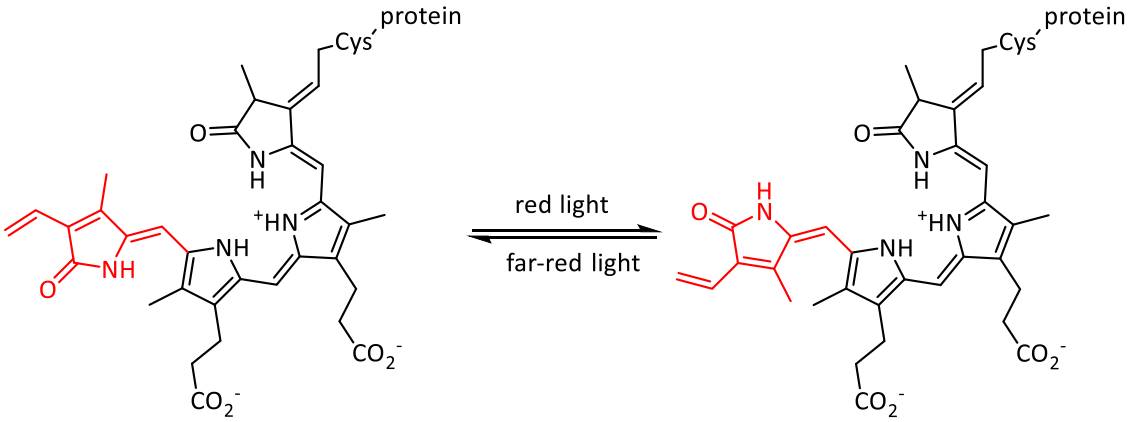

Figure 4. Isomerization process of the phytochrome chromophore. Upon light irradiation, the photoisomerizable part (highlighted in red) can be reversibly interconverted between *Z* and *E* isomers.

By taking inspiration from nature, the pyrrole scaffold in the chromophore of phytochrome responsible for the isomerization can be used as a molecular switch.[29] Interestingly, one of the characteristics of this switch is the presence of hydrogen-bond interactions, which can control the photoisomerization degree. Other properties include their ease of synthesis and strong absorption in the UV region.

4.2 Results

4.2.1 Design of photoswitchable antibiotics

Our molecular design is based on quinolones. Two antibiotic parts have been designed. The first one, inspired in the structure of quinolones like ciprofloxacin or norfloxacin, with the presence of a carbon at position 8 (see figure 5). We envisioned that the antibacterial properties of the molecule could be retained when exchanging the piperazine unit at position 7 either with the hydantoin or the pyrrole of the phytochrome chromophore. By the incorporation of a molecular switch, the molecule becomes photoresponsive, switching between the *Z* and *E* isomers when irradiated. The second antibiotic part is inspired in a naphthyridone, with the presence of a nitrogen atom at position 8 (see figure 5). The structure of nalidixic acid has been modified to incorporate the pyrrole moiety in two different positions. As in the previous case, we anticipated that the introduction of the molecular switch based on the phytochrome chromophore at position 7 would not seriously affect the antibacterial properties. Additionally, the same switch was used at position 3, a critical point for the antibacterial behavior of the molecule. The effect of the molecular switch in this position will be of great importance in future chapters. Once the molecular switches were attached to the antibiotic parts, it was expected that one of the isomers presented a higher antibacterial activity than the other. Thus, creating a reversible system whose antibacterial properties could be controlled using light as a stimulus.

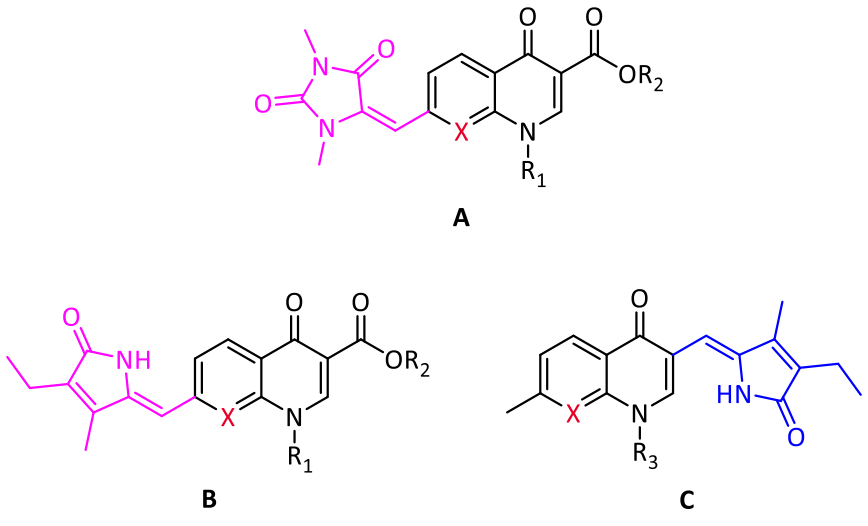

Figure 5. Design of photoswitchable quinolones. Based on hydantoin structure (**A**), based on the pyrrole of the phytochrome chromophore (**B, C**). Position 8 is highlighted in red. Substituents at positions 3 and 7 are highlighted in blue and pink, respectively.

4.2.2 Synthesis

The synthesis of the quinolone derivatives is a long process involving several steps. In these paragraphs, a general overview of the procedure is displayed. A more detailed version can be found in section 4.4.5. The route describing the synthesis of the antibiotic part based on quinolones, with a carbon atom at the 8 position, and its corresponding photoswitchable versions is described in scheme 1.

Scheme 1

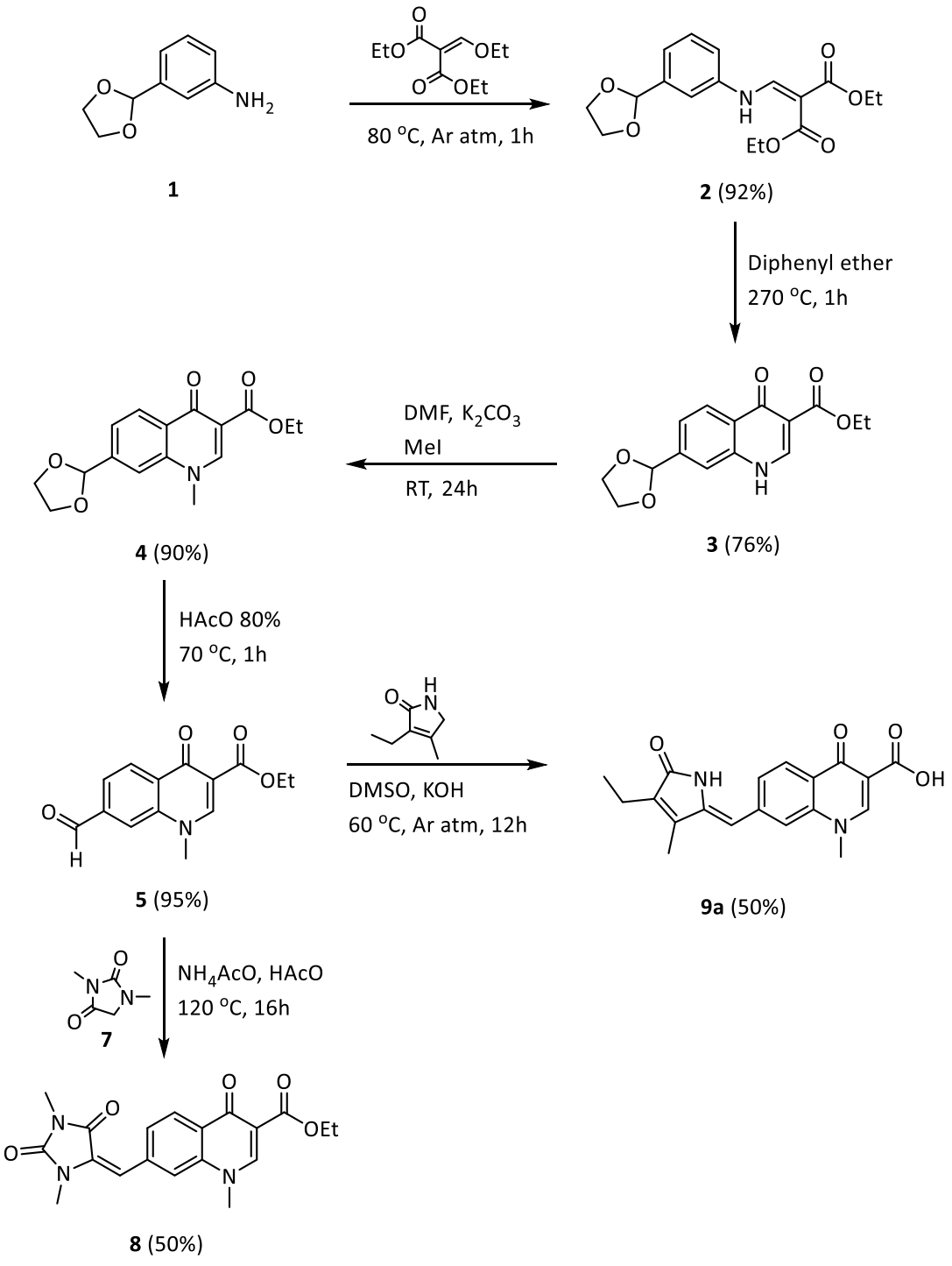

The first step was a condensation between **1** and the malonate that resulted in the enamine **2**. Upon thermal cyclization of **2**, compound **3** was obtained. The secondary amine of **3** was methylated to obtain the tertiary amine **4**, which highly improves its solubility in organic solvents. The final step to complete the antibiotic part was the acetal deprotection to give the aldehyde **5**. Once the antibiotic part was synthesized, two different routes were followed to link the molecular switches. The hydantoin moiety was linked via acid-catalyzed aldol condensation resulting in **8**. The pyrrole based in the phytochrome chromophore was attached via base-catalyzed aldol condensation ending in **9a**. After synthesizing **9a**, its sodium salt derivative **9b** was obtained by the addition of aqueous sodium hydroxide.

The second antibiotic part is based on a naphthyridone with a nitrogen atom at the 8 position. For the synthesis of this part, nalidixic acid was employed, and two modifications were made in its structure to achieve the photoswitchable version. The synthetic route of these derivates is described in scheme 2.

Scheme 2

Procedure A:

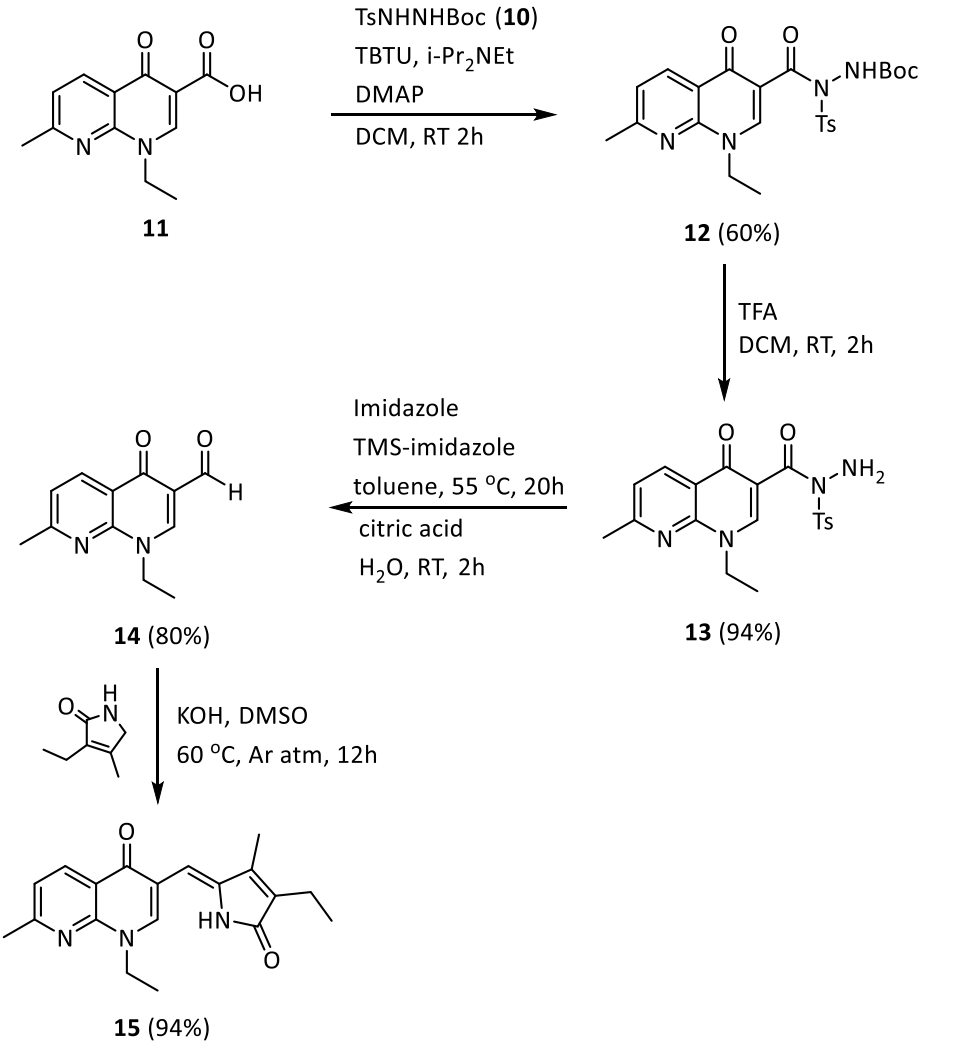

Procedure B:

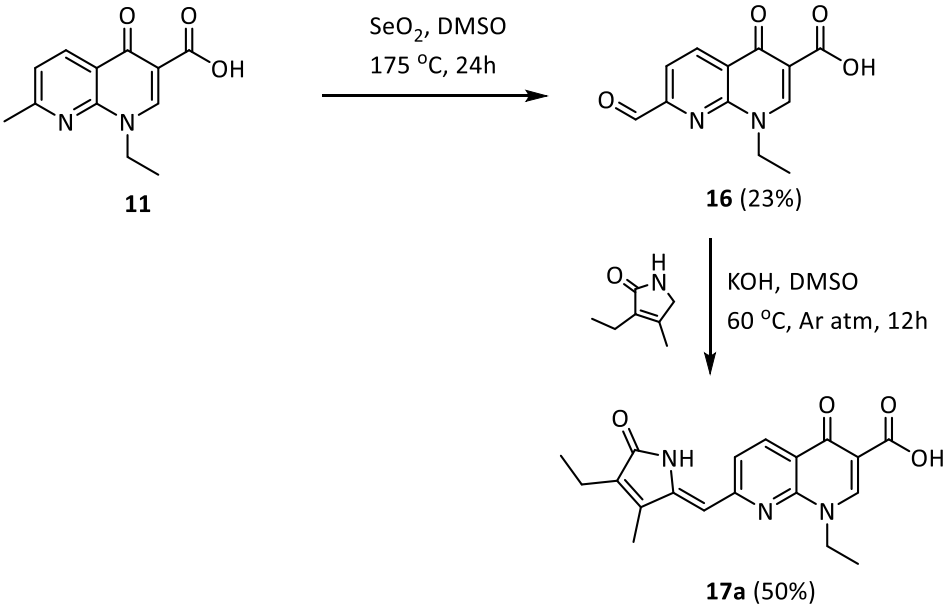

The aldehyde of nalidixic acid in position 3 (procedure A) was synthesized via a modified McFayden-Stevens reaction.[30] Nalidixic acid **11** was condensed with hydrazine **10**, previously synthesized, to form hydrazine **12**. The next step was the removal of the Boc group to give the hydrazine **13**, which can be transformed in the aldehyde **14**. The final step involved a base-catalyzed condensation between **14** and the pyrrole to obtain **15**.

In order to link the photoswitch in position 7 of nalidixic acid, procedure B was followed. Aldehyde **16** was synthesized by selenium dioxide oxidation, and later base-catalyzed condensation allowed the formation of **17a**. After obtaining **17a**, its sodium salt derivative **17b** was synthesized by the addition of aqueous sodium hydroxide.

4.2.3 Photochemical properties

Once the synthesis of the different derivatives was completed, their photochemical properties were studied. Such properties provide crucial information about the requirements and the performance of the diverse molecular switches obtained.

First of all, it is important to know the range of absorption for each photoswitchable quinolone. UV-Vis spectroscopy was employed to record the absorption spectrum of all compounds. Different solvents were used to dissolve the samples according to their solubility. The information obtained from the UV-Vis spectrum allows choosing an adequate light source to induce the photoreaction.

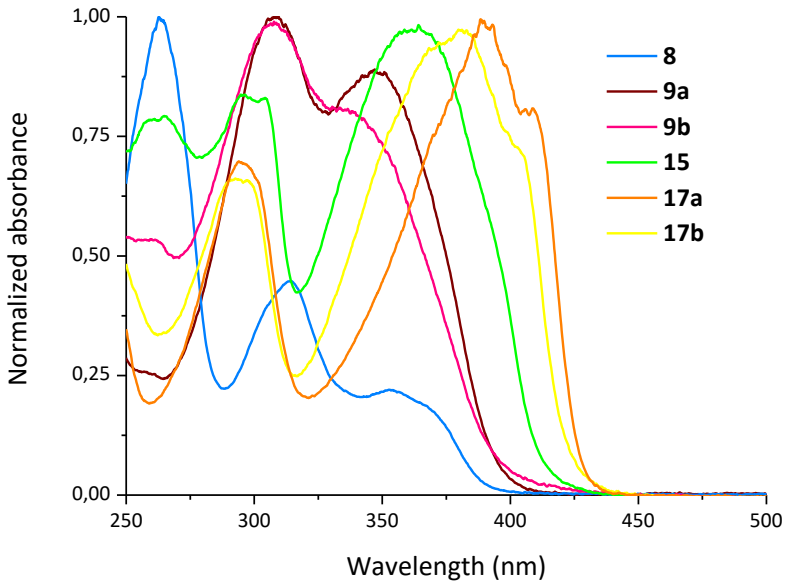

Figure 6. UV-Vis spectra of the different photoswitchable quinolones (**8** and **17a** dissolved in chloroform, **9a** and **15** dissolved in methanol, **9b** and **17b** dissolved in water). All samples were prepared in a concentration close to 5E-5M.

As shown in figure 6, the absorption varies between the UV and the visible region. Compounds **8**, **9a** and **9b** have strong absorption around 300 nm with their bands extending to 400 nm. However, compounds **15**, **17a** and **17b** present absorption in the visible region, with **17a** being the most red-shifted. This difference in the absorption range corresponds to the antibiotic part employed in each case. For those with a carbon at the 8 position, the absorbance could be found in the ultraviolet region. Meanwhile, those whose structure is based on the nalidixic acid, with a nitrogen at the 8 position, displayed absorbance in the visible region. Compounds with the absorption shifted towards the visible region are favored over the ones absorbing only in the UV region, due to better compatibility when working in biological applications. Furthermore, compounds soluble in water, like the sodium salts derivatives **9b** and **17b**, are also preferred over those soluble in organic solvents for the same reason. Additional information obtained from this experiment, like the absorption maximum or the molar extinction coefficient is collected in table 1.

Table 1. Maximum absorption and molar extinction coefficient of photoswitchable quinolones.

Compound	λ_{max} (nm)	ε ($M^{-1}cm^{-1}$)
8	263, 314	23800, 10500
9a	308	21500
9b	308	17400
15	364	44500
17a	391	21800
17b	381	17100

Prior to the irradiation process, it is important to know the initial isomer obtained after the synthesis, also known as the thermodynamically stable. Once the initial isomer is assigned, the isomerization process direction can be established either from *Z* to *E* or from *E* to *Z*, since both of the molecular switches here discussed are based in *Z*/*E* isomerism. To distinguish what isomer is obtained after the synthesis, a two-dimensional magnetic resonance experiment was performed. NOESY data (see Appendix A) reported that the isomer found for the phytochrome chromophore in all cases was *Z* with a signal correlating the vinylic proton and the methyl group in the

pyrrole. For the hydantoin moiety, no signal was observed so based on the data found in the bibliography *E* isomer was assigned.[23]

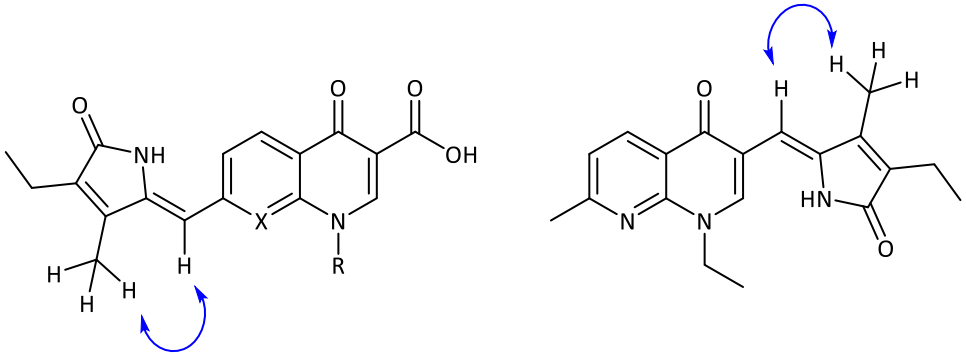

Figure 7. Assignation of the thermally stable isomer of the phytochrome chromophore based molecular switches. Signaled with the blue arrow are the protons that showed a correlation in the NOESY spectrum (see Appendix A).

With this information, the irradiation of the samples was carried out. Knowing the absorption range of the molecules thanks to UV-Vis spectroscopy, two distinct light sources were selected. For the molecules absorbing in the UV region, a 125W medium-pressure Hg lamp was employed. Additionally, the samples were protected with a Pyrex filter to ensure that wavelengths shorter than 290 nm, which may produce undesired reactions caused by more energetic transitions, were eliminated. In one specific case, a quartz filter was used because shorter wavelengths were considered of importance in the isomerization process. For those compounds absorbing in the visible region, a white LED lamp was used to irradiate the samples. The emission spectra of both light sources can be found in figure 8. Compounds were dissolved at 0.1M concentration in different deuterated solvents according to their solubility. The irradiation process was followed by ^{1}H-NMR during short time intervals which allowed to follow the isomerization course until the PSS was reached (see figure 9). The results collected for each photoswitch are described in the next paragraphs.

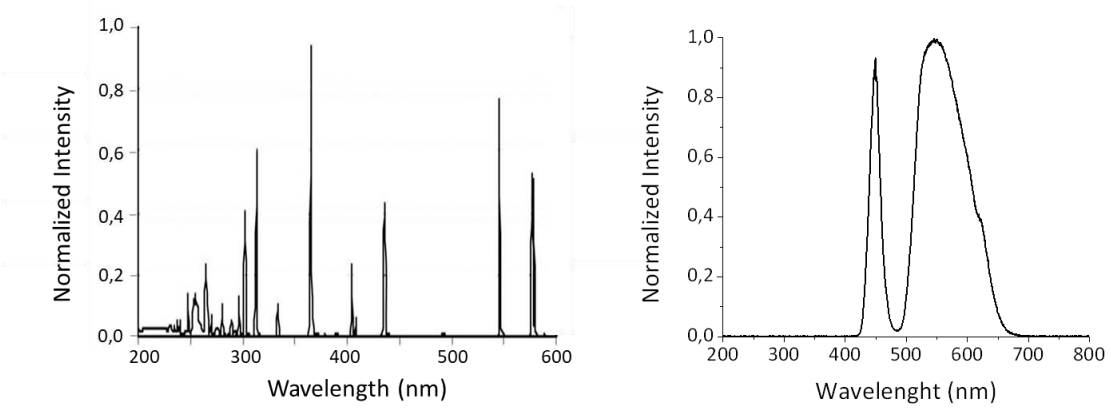

Figure 8. Emission spectra for the irradiation sources employed to induce the isomerization process. On the left, the emission spectrum of medium-pressure Hg lamp; the use of a Pyrex filter removes the shorter wavelengths (λ < 290 nm). On the right, the emission spectrum of a white LED.

Compound **8** was dissolved in deuterated chloroform and irradiated with the 125W medium-pressure Hg lamp since it presented absorption in the UV region. The irradiation was carried out employing two different filters: Pyrex and quartz. As can be seen in figure 6, this molecule presented two bands, the maximum absorption at 263 nm and a smaller band at 314 nm. Hence, the quartz filter ensured that the irradiation covered both bands, and the Pyrex filter only the band present at 314 nm. As expected, the PSS obtained for the Pyrex filter was lower than the one obtained with quartz filter, PSS_{Pyrex} = 31% photoisomer *Z*, PSS_{quartz} = 59% photoisomer *Z*. These results indicate that the band at 263 nm participates in the isomerization process.

Compound **9a** was dissolved in deuterated dimethyl sulfoxide and irradiated with the 125W medium-pressure Hg lamp, considering that it mainly absorbed in the UV region. Additionally, since this compound presented a small absorption in the visible region, a white LED was also employed to induce the photoreaction. Because the maximum absorption appeared at 308 nm, a Pyrex filter was selected for the Hg lamp and the PSS reached 37% of photoisomer *E*. For the white LED the PSS reached a 25% of *E*. In a similar way, the sodium salt **9b** was dissolved in deuterated water and irradiated to give 35% of photoisomer *E* using the Hg lamp.

Compound **15** was dissolved in deuterated methanol and irradiated with the white LED because it presented absorption in the visible region. The PSS showed 41% of photoisomer *E.*

Finally, compound **17a** was dissolved in deuterated chloroform and irradiated with the white LED in the visible region reaching a PSS of 50% photoisomer *E*. The sodium salt **17b** was dissolved in deuterated water to give a PSS of 40% *E*.

Table 2. Summary of data corresponding to the isomerization process of each compound.

Compound	**8**	**9a**	**9b**	**15**	**17a**	**17b**
Solvent	$CDCl_3$	DMSO-D_6	D_2O	CD_3OD	$CDCl_3$	D_2O
Initial isomer	*E*	*Z*	*Z*	*Z*	*Z*	*Z*
PSS(*Z*/*E*)	59:41[a] 31:69[b]	63:37[b] 75:25[c]	65:35[b]	59:41[c]	50:50[c]	60:40[c]
Irradiation time (min)	120[a] 60[b]	25[b] 135[c]	25[b]	90[c]	20[c]	20[c]

[a]: Irradiation with 125W medium-pressure Hg lamp using a quartz filter. [b]: Irradiation with 125W medium-pressure Hg lamp using a Pyrex filter. [c]: Irradiation with white LED.

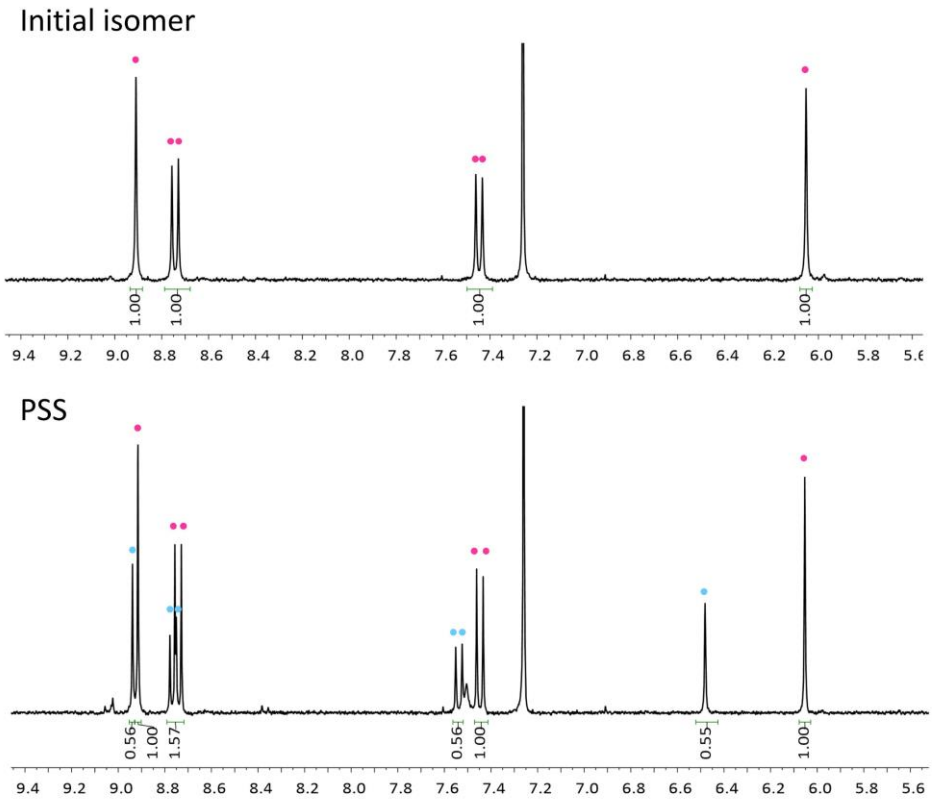

Figure 9. Irradiation process of **17a** followed by ^{1}H-NMR. On the top, ^{1}H-NMR spectrum of the initial isomer. On the bottom, ^{1}H-NMR spectrum of PSS, achieved after irradiation with the corresponding light source. The photoisomer (blue signals) is obtained in different proportions depending on the compound.

After successfully study the isomerization of all the molecular switches synthesized, their thermal relaxation was evaluated. Once the PSS has been reached, reversion to the initial isomer can be achieved thermally, as the photoisomer is the thermally unstable form.

Table 3. Summary of data corresponding to the thermal relaxation of each compound.

Compound	**8**	**9a**	**15**	**17a**
Temperature (°C)	n/a[a]	110	110	45
Time (days)	n/a[a]	3	3	3

[a]: Heating at 60 °C did not show signs of reversion, whereas heating at 70 °C resulted in the sample decomposition.

As can be seen in table 3, thermal relaxation was possible in all cases except for compound **8**, which decomposed at temperatures higher than 70 °C. Compounds **9a** and **15** required harsh conditions to revert to the thermally stable isomer completely. Samples were heated at 110 °C for 3 days in DMSO because of the high-temperature requirement. Compound **17a** was able to revert to the initial isomer under milder conditions, 45 °C for 3 days.

These data demonstrate the high stability of the photoisomers, as they need long periods of heat exposure to achieve thermal relaxation. When thinking in their application in a biological context, the photoisomers could be generated in biological media and keep their activity for extended intervals.

Next, compound **9a** was selected to check its photostability. The sample was alternately irradiated with UV and visible light to switch between PSS_{UV} (37% *E*) and PSS_{Vis} (25% *E*) for several cycles.

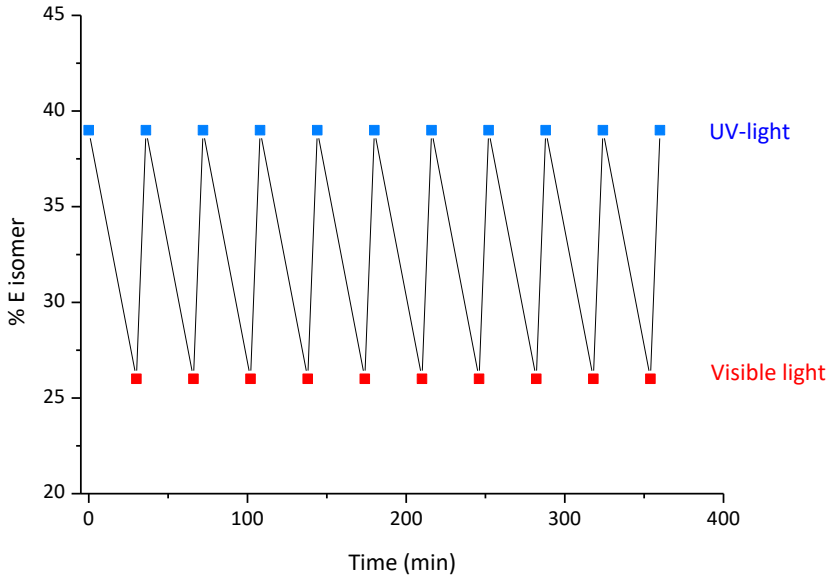

Figure 10. Photostability of compound **9a**. Cycles performed irradiating alternatively between UV light and visible light. The sample was prepared in deuterated DMSO, and isomer *E* was quantified by ^{1}H-NMR.

Derivative **9a** proved to have high stability, and no additional signals of byproducts were observed by ^{1}H-NMR. Thus, it can be stated that **9a** is extremely photostable with no signs of decomposition after several cycles.

Finally, to complete the photochemical study, the quantum yield of **9a** was calculated. This measure relates the number of molecules of photoisomer formed with the number of photons absorbed by the molecular switch, resulting in the number of photons that effectively participate in the rotation of the C=C double bond to induce the photoisomerization. Therefore, this feature gives information about the efficiency of the process, so higher quantum yields are desired.

$$\Phi = \frac{\text{number of molecules formed of photoisomer}}{\text{number of photons absorbed by the molecular switch}}$$

Equation 1. Equation expressing the quantum yield of a photoisomerization process.

The quantum yield of **9a** was calculated using *trans*-azobenzene as an actinometer, following the procedure described in the bibliography.[31] An actinometer is a chemical system that undergoes a light-induced reaction, for which the quantum yield is known accurately. *Trans*-azobenzene was selected as a suitable actinometer due to its wavelength range between 230-460 nm being compatible with the molecule under study. Moreover, *trans*-azobenzene presents a tabulated F value at 313 nm, which is close to the maximum absorption of compound **9a** (308 nm). The

experimental procedure for the measurements of quantum yield is described in section 4.4.3. The calculated value for the quantum yield of **9a** was 0.34, which confirmed the efficiency of the isomerization process $Z \rightarrow E$.

4.2.4 Antibacterial activity

In order to test the antibacterial activity of the photoswitchable quinolones, two parameters were analyzed: minimal inhibitory concentration (MIC) and minimal bactericidal concentration (MBC). MIC is defined as the lowest concentration of a chemical able to prevent visible growth of bacteria. MBC is the lowest concentration of a chemical required to kill a particular bacterium. In other words, MIC is associated with a bacteriostatic effect, whereas MBC is related to a bactericidal effect.

All compounds were tested before and after irradiation. Quinolone sensitive *Escherichia coli* ATCC 25922,[32] was incubated with different concentrations either of the initial isomer or the PSS. MIC values were determined visually (see figure 12), by the presence or absence of turbidity in the well. If the well is clear, it means that the compound studied in that concentration has a bacteriostatic effect, inhibiting the growth of new bacteria. If the well is turbid, it means the opposite. The results obtained for each compound are explained next.

Table 4. MIC and MBC values of photoswitchable quinolones.

Compound	**8**	**9a**	**9b**	**15**	**17a**	**17b**
MIC (μg/ml)	*E*: 128 PSS: 128	*Z*: 16 PSS: 64	*Z*: 8 PSS: 16	*Z*: - PSS: -	*Z*: - PSS: -	*Z*: - PSS: -
MBC (μg/ml)	*E*: 128 PSS: 128	*Z*: 32 PSS: 128	*Z*: 16 PSS: 32	*Z*: - PSS: -	*Z*: - PSS: -	*Z*: - PSS: -

When performing the antibacterial test, ideally compounds should be soluble in water in order to avoid any interference with the cell culture. The use of other solvents can have a bactericidal effect in the bacterium under study. Given the lower water solubility of compounds **8**, **9a**, **15**, and **17a**, different mixtures of methanol and water were employed to dissolve them. In order to eliminate any possible mistake in the results due to the use of methanol in the sample preparation, additional controls were carried out to check the MIC and MBC values of the solvent mixture. Compounds **9b** and **17b** did not need any additional control as they were soluble in water.

The molecular switch based on the hydantoin structure **8** did not show any difference between the initial isomer *E* and its PSS (59% *Z*). Probably because of the presence of an ester group instead of an acid in position 3, which have been described to have a big role in the activity of quinolones.[6]

Inside the group of derivatives synthesized with a molecular switch based on the pyrrole of the phytochrome chromophore, compounds **15**, **17a** and **17b** failed to show antibacterial activity. Compound **15** presumably because of the election of the position to link the molecular switch. In a similar way as with compound **8**, the elimination of the acid group in the quinolone structure induced the loss of the antibiotic properties. However, compounds **17a** and **17b** bear the pyrrole in a different position, which supposedly should not affect so strongly the antibacterial activity (see figure 1).

Compounds **9a** and **9b** proved to have antibacterial activity, and more importantly, different values for the PSS and the initial isomer were observed. Compound **9a** had a four-fold difference in activity ($MIC_{\mathbf{9a}\text{-}Z\ isomer}$ = 16 μg/ml *vs.* $MIC_{\mathbf{9a}\text{-}PSS}$ = 64 μg/ml). Compound **9b** presented a two-fold difference in activity but a lower MIC value than **9a** which indicates higher activity ($MIC_{\mathbf{9b}\text{-}Z\ isomer}$ = 8 μg/ml *vs.* $MIC_{\mathbf{9b}\text{-}PSS}$ = 16 μg/ml). A similar result was observed for the MBC with **9a** and **9b** showing a four-fold and a two-fold difference in activity respectively ($MBC_{\mathbf{9a}\text{-}Z\ isomer}$ = 32 μg/ml *vs.* $MBC_{\mathbf{9a}\text{-}PSS}$ = 128 μg/ml, $MBC_{\mathbf{9b}\text{-}Z\ isomer}$ = 16 μg/ml *vs.* $MBC_{\mathbf{9b}\text{-}PSS}$ = 32 μg/ml). These results are in agreement with the ones obtained for the MIC. It should be mentioned that this difference in activity was achieved despite the PSS having a low proportion of photoisomer, 37% and 35% for **9a** and **9b** respectively. A higher percentage of photoisomer could imply a bigger difference in the activity. Additionally, MIC for nalidixic acid was measured, obtaining a value of 2 μg/ml, which is close to the values obtained for compound **9b-***Z* isomer. In figure 11, a comparative between the MIC of nalidixic acid and the compounds showing better results can be seen.

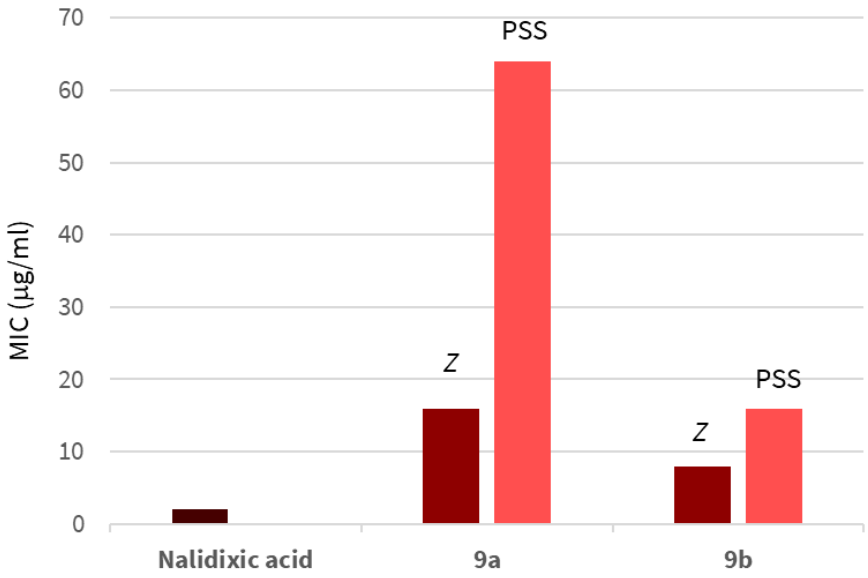

Figure 11. Graphic comparing MIC on *E. coli* ATCC 25922 of nalidixic acid, a commercial antibiotic, *vs.* the compounds showing better results (**9a** and **9b**). In dark red is represented the thermodynamically stable isomer, *Z*. In light red, the MIC value of the PSS, 37-35% *E* isomer.

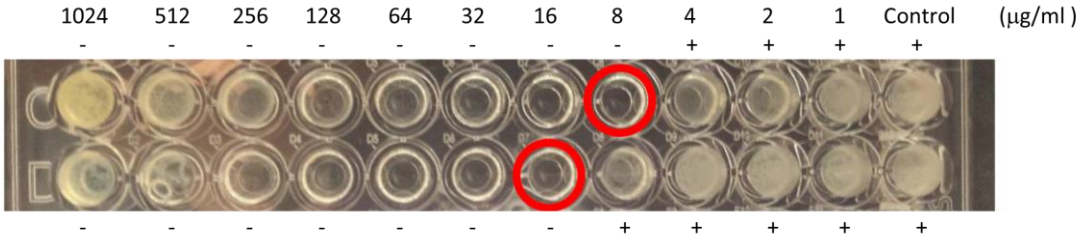

Figure 12. Growth inhibition of *Escherichia coli* ATCC 25922 against compound **9b** in its initial isomer *Z* (top row) and its PSS (bottom row). – indicates the growth inhibition of bacteria in the well, + indicates the growth of bacteria in the well. MIC values are depicted with a red circle.

4.3 Conclusions

In this chapter, a series of photoswitchable quinolones have been presented. The synthetic procedure has been designed to allow the incorporation of different molecular switches in two positions of the antibiotic. Two approaches have been followed to design the antibiotic part. In the first one, this part has been synthesized from scratch, obtaining after 4 steps a quinolone-based unit with an aldehyde group at the 7 position that can be used to link via condensation diverse molecular switches. The second approach employs commercially available nalidixic acid, whose structure has been modified to incorporate an aldehyde group either at position 3, in a one-step route, or at position 7, in 3 steps. After successfully synthesizing six derivatives, their photochemical properties have been evaluated. The irradiation of the photoswitchable quinolones has been carried out either with visible light or with UV

light giving results of 35-59% photoisomer formed. Besides, reversion to the initial isomer by thermal relaxation has been possible in all cases except one. For one of the compounds, additional measurements have been performed, like photostability and quantum yield studies that have proved the good performance of the molecular switch. Finally, the antibacterial activity of the derivatives has been studied. Two of the six compounds have been found to change their activity upon irradiation with visible light. In both cases, the initial isomer presented a higher activity than the PSS. Moreover, one of them presents high water solubility, a property of great importance when working with bioactive molecules. This work presents an alternative to azobenzenes in the photocontrol of antibiotic activity. The prospect to create systems that can be turned on/off upon light irradiation to change the antibiotic activity can be a future solution to the problem of antibiotic resistance or adverse effects.

4.4 Experimental section

4.4.1 Thermal relaxation studies

All compounds were dissolved in deuterated solvents to obtain a concentration of 0.1M. The solvents selected for this study were according to the temperature used to induce the reversion process. Then, irradiation of the samples was carried out with the corresponding light source in each case to obtain the PSS. Finally, reversion to the thermodynamically stable isomer was completed by heating the samples. This process was followed by ^{1}H-NMR until the signals of the photoisomer wholly disappeared.

4.4.2 Photostability study

Compound **9a** was dissolved in DMSO-D_6 to obtain a concentration of 0.1M. The sample was irradiated alternatively using a 125W medium-pressure Hg lamp (UV light) with a Pyrex filter and a white LED (visible light). When irradiated with UV light, a PSS of 37% *E* isomer was obtained, whereas irradiation with visible light allowed the reversion up to 25% of *E* isomer. The irradiation procedure was followed by ^{1}H-NMR, which made possible the quantification of each isomer.

4.4.3 Quantum yield

To measure the quantum yield of compound **9a** *trans*-azobenzene was used as an actinometer. The actinometer allowed calculating the number of photons absorbed by the sample using the following equation.

$$E_p \text{ mol of photons} \cdot cm^{-2} \cdot s^{-1} = \frac{F(\lambda)\ x\ \Delta A_{(358\ nm)}}{t}$$

Equation 2. Equation expressing the number of photons absorbed by the sample.

Where ΔA refers to the change in the absorbance at 358 nm of the *trans*-azobenzene solution when irradiating at 313 nm, and t is the irradiation time responsible for that change. The F factor depends on the wavelength, and it is tabulated for different values in the literature. For this specific case at 313 nm, F has a value of 5.3E-6 einstein·cm^{-2}. The wavelength of irradiation was selected to have the maximum absorption of compound **9a** for an F value present in the bibliography.

First, a solution of *trans*-azobenzene in methanol was prepared so that its absorbance at 358 nm was close to one. This consideration is important to avoid experimental errors since the values of *trans*-azobenzene quantum yields are measured and tabulated for an absorbance close to one at 358 nm. Next, this solution was irradiated in a quartz cuvette at 313 nm using monochromatic light. The irradiation should induce a change in the absorbance at 358 nm close to 0.02. With the data obtained from this measurement, the number of photons absorbed by the sample can be calculated using equation 2.

Then, a solution of **9a** in DMSO was prepared by adjusting the value of absorbance at 313 nm to the one displayed by the actinometer. The solution was irradiated at 313 nm for a period in which the conversion from *Z* to *E* was lower than 20% to avoid absorption by the photoisomer, which would lead to experimental error. This change was quantified by ^{1}H-NMR and allowed to determine the number of molecules formed of photoisomer to calculate the quantum yield by using equation 1 (see section 4.2.3).

4.4.4 Antibacterial activity

All compounds were dissolved in mixtures of methanol/water or directly in water to prepare the stock solution. Serial two-fold dilutions of the stock solution were made in a range of concentrations from 1024 to 1 μg/ml.

MIC was determined by the conventional microdilution method in cation adjusted Mueller-Hinton broth (Becton Dickinson).[33] *Escherichia coli* ATCC 25922 strain was cultured in Brain-Heart Infusion agar (Becton Dickinson) for 24 hours at 37 °C. Overnight colonies were used to prepare an inoculum adjusted to the turbidity of a 0.5 McFarland in sterile saline (equivalent to 1 x 10^8 CFU/ml). This suspension was diluted in cation adjusted Mueller-Hinton broth to give a final organism density of 5 x 10^5

CFU/ml and exposed to serial twofold dilutions of each compound tested (1-1024 μg/ml) with a final volume of 0.1 ml in a 96 well microdilution tray. The MIC value was the lowest concentration of compound where no visible growth was apparent after 20-24 hours of incubation at 37 °C. Untreated samples were included as positive controls of the bacterial growth. Each assay was carried out four times.

MBC was calculated by inoculating in Brain-Heart Infusion agar plates 10 μl of treated cultures without visible growth in MIC assays. The total number of colonies was counted after incubation for 24 hours at 37 °C determining the number of CFU/ml. The MBC value was the lowest concentration of compound able to kill ≥ 99.9% of the initial bacterial inoculum (5 x 10^5 CFU/ml). Each assay was carried out four times.

4.4.5 Synthesis

4.4.5.1 General information

For details about general experimental information, see Appendix, section A.

4.4.5.2 Synthetic procedure

Diethyl 2-(((3-(1,3-dioxolan-2 yl)phenyl)amino)methylene)malonate (2):

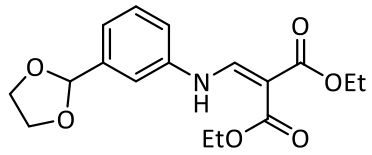

A mixture of acetal **1** (12.1 mmol, 2.0 g) and diethyl ethoxymethylenemalonate (12.1 mmol, 2.6 g) was stirred for 1 hour at 80 °C. During this time, a light argon flow was introduced to the reaction mixture to remove the ethanol formed. Next, the reaction mixture was dissolved in DCM (50 ml) and washed with 1M HCl (50 ml) and brine (50 ml). The organic layer was dried with anhydrous $MgSO_4$, filtered, and the solvent was evaporated *in vacuo* to obtain 3.7 g (92%) of orange oil.
^{1}H-NMR (300 MHz, $CDCl_3$): δ 11.07 (d, *J* = 13.7 Hz, 1H), 8.54 (d, *J* = 13.7 Hz, 1H), 7.37 (t, *J* = 7.8 Hz, 1H), 7.29–7.22 (m, 2H), 7.16–7.10 (m, 1H), 5.79 (s, 1H), 4.35-4.21 (m, 4H), 4.13-4.02 (m, 4H), 1.38 (t, J = 7.0 Hz, 3H), 1.33 (t, J = 7.0 Hz, 3H).

Ethyl 7-(1,3-dioxolan-2-yl)-4-oxo-1,4-dihydroquinoline-3-carboxylate (3):

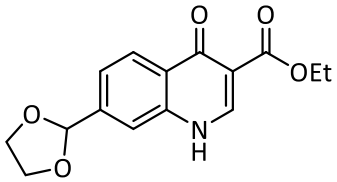

A solution of **2** (5.3 mmol, 1.8 g) in diphenyl ether (10 ml) was added dropwise to a solution of boiling diphenyl ether (50 ml). After heating at 270 °C for 1 hour, the mixture was allowed to reach room temperature, and hexane (200 ml) was added. The resulting solid was filtered to give 1.1 g (76%) of a brown solid.
^{1}H-NMR (300 MHz, DMSO-D_6): δ 8.57 (s, 1H), 8.17 (d, *J* = 7.8 Hz, 1H), 7.68 (s, 1H), 7.45 (d, *J* = 7.8 Hz, 1H), 5.89 (s, 1H), 4.29 – 4.15 (m, 2H), 4.10 – 3.94 (m, 4H), 1.27 (t, *J* = 6.8 Hz, 3H).

Ethyl 7-(1,3-dioxolan-2-yl)-1-methyl-4-oxo-1,4-dihydroquinoline-3-carboxylate (4):

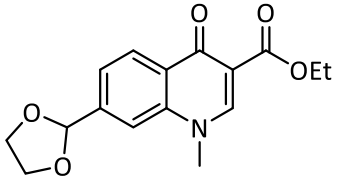

To a solution of **3** (1.6 mmol, 1.5 g) in DMF (10 ml) was added potassium carbonate (4.8 mmol, 0.7 g) and methyl iodide (16 mmol, 2.2 g). The resulting mixture was stirred at room temperature overnight. After that time, DMF was removed *in vacuo*. The solid obtained was dissolved in DCM (50 ml) and washed with H_2O (100 ml). The organic layer was dried with anhydrous $MgSO_4$, filtered, and the solvent was evaporated *in vacuo* to obtain 0.4 g (90%) of a brown solid.
^{1}H-NMR (300 MHz, $CDCl_3$): δ 8.53 (d, *J* = 8.6 Hz, 1H), 8.48 (s, 1H), 7.57-7.51 (m, 2H), 5.93 (s, 1H), 4.39 (q, *J* = 7.1 Hz, 2H), 4.16-4.07 (m, 4H), 3.89 (s, 3H), 1.41 (t, *J* = 7.1 Hz, 3H).

Ethyl 7-formyl-1-methyl-4-oxo-1,4-dihydroquinoline-3-carboxylate (5):

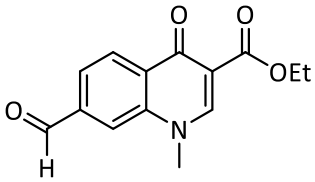

A solution of **4** (0.9 mmol, 0.26 g) in 80% acetic acid (30 ml) was stirred at 70 °C for 1 hour. Next, the solvent was removed *in vacuo*, and 0.21 g (90%) of a brown solid was obtained.

^{1}H-NMR (300 MHz, $CDCl_3$): δ 10.18 (s, 1H), 8.69 (d, *J* = 8.1 Hz, 1H), 8.57 (s, 1H), 7.98 (d, *J* = 1.2 Hz, 1H), 7.91 (d, *J*= 8.1 Hz, 1H), 4.39 (q, *J* = 7.1 Hz, 2H), 3.97 (s, 3H), 1.41 (t, *J* = 7.1 Hz, 3H).

4,5-dihydroxy-1,3-dimethylimidazolidin-2-one (6):

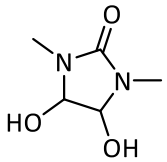

Triethylamine was added dropwise over glyoxal (44 mmol 2.5 g)until pH = 9, keeping the temperature between 25-35 °C. Next, a solution of dimethylurea (44 mmol, 3.8 g) in water (4 ml) was added to the solution. The mixture was stirred for 16 hours at room temperature. After that time, the solvent was removed *in vacuo* to give 6.1 g (96%) of a colorless oil. The oil was used in subsequent steps without further purification.

1,3-dimethylimidazolidine-2,4-dione (7):

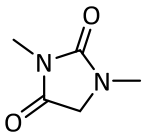

A mixture of **6** (42 mmol, 6.1 g) and sulfuric acid (42 mmol, 1.1 g) was stirred for 6 hours between 95-100 °C. After that time, the reaction was cooled in an ice bath and neutralized with saturated aqueous sodium bicarbonate. The crude was extracted 4 times with EtOAc (50 ml). The combined organic layers were washed with brine (50 ml) twice and dried over anhydrous $MgSO_4$. The solvent was evaporated *in vacuo* to obtain 1.8 g (33%) of a white solid.

^{1}H-NMR (300 MHz, DMSO-D_6): δ 3.76 (s, 2H), 2.71 (s, 6H).

^{1}H-NMR spectrum in agreement with published data.[34]

Ethyl-7-((1,3-dimethyl-2,5-dioxoimidazolidin-4-ylidene)methyl)-1-methyl-4-oxo-1,4-dihydroquinoline-3-carboxy late (8):

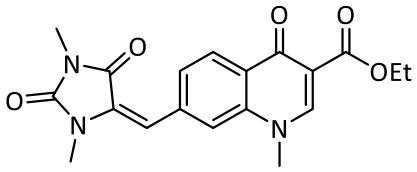

A mixture of aldehyde **5** (0.6 mmol, 0.15 g), ammonium acetate (0.1 mmol, 8 mg), and hydantoin **7** (0.6 mmol, 0.08 g) in acetic acid (5 ml) was stirred at 120 °C for 16 hours. After that time, the solvent was evaporated *in vacuo*. The residue was purified by column chromathography (EtOAc:MeOH 10:0.1), to give 0.11 g (50%) of a yellow solid.
^{1}H-NMR (400 MHz, $CDCl_3$): δ 8.67 (d, *J* = 7.8 Hz, 1H), 8.54 (s, 1H), 7.98 (d, *J* = 1.1 Hz, 1H), 7.92 (dd, *J* = 7.9, 1.2 Hz, 1H), 4.40 (q, *J* = 7.1 Hz, 2H), 3.98 (s, 3H), 2.97 (s, 6H), 1.42 (t, *J* = 7.1 Hz, 3H).
^{13}C-NMR (100 MHz, $CDCl_3$): δ 173.8, 172.7, 170.0, 165.3, 157.2, 150.7, 140.1, 138.8, 132.5, 129.2, 125.8, 116.9, 111.9, 61.1, 51.9, 41.6, 29.8, 25.0, 14.5.
HR-MS (ESI, [M+H]+): Calcd. for C19H19N3O5 + H: 370.1397; Found: 370.1394

7-((4-ethyl-3-methyl-5-oxo-1,5-dihydro-2H-pyrrol-2-ylidene)methyl)-1-methyl-4-oxo-1,4-dihydroquinoline-3-carboxylic acid (9a):

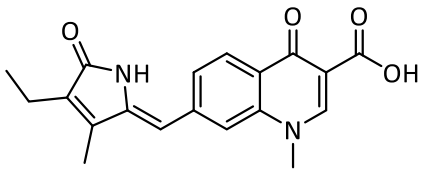

A mixture of aldehyde **5** (1.2 mmol, 0.3 g), 3-ethyl-4-methyl-1,5-dihydro-pyrrol-2-one (2.3 mmol, 0.3 g) and potassium hydroxide (4.6 mmol, 0.26 g) in water (1 ml), was dissolved in DMSO (2 ml) and stirred at 60 °C under argon atmosphere for 12 hours. The reaction mixture was then poured into water and neutralized with 37% HCl to allow the precipitation of the product. The solid was filtered to obtain 0.16 g (50%) of an orange solid.
^{1}H-NMR (400 MHz, DMSO-D_6): δ 15.30 (s, 1H), 10.28 (s, 1H), 9.04 (s, 1H), 8.31 (d, *J* = 8.4 Hz, 1H), 7.91 (s, 1H), 7.80 (d, *J* = 8.5 Hz, 1H), 6.41 (s, 1H), 4.16 (s, 3H), 2.31 (q, *J* = 7.2 Hz, 2H), 2.14 (s, 3H), 1.04 (t, *J* = 7.5 Hz, 3H).
^{13}C-NMR (100 MHz, DMSO-D_6): δ 177.2, 172.9, 166.1, 150.3, 141.7, 140.7, 140.7, 140.5, 133.9, 127.0, 125.7, 123.5, 117.9, 107.4, 105.9, 41.6, 16.3, 13.2, 9.4.
HR-MS (ESI, [M-H]-): Calcd. for C19H18N2O4 - H: 337.1194; Found: 337.1198

Sodium 7-((4-ethyl-3-methyl-5-oxo-1,5-dihydro-2H-pyrrol-2-ylidene)methyl)-1-methyl-4-oxo-1,4-dihydroquinoline-3-carboxylate (9b):

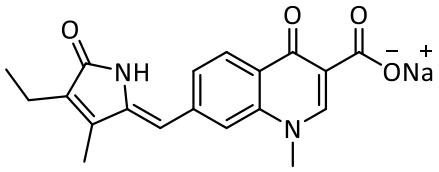

Compound **9a** (0.15 mmol, 0.05g) was dissolved in a solution containing sodium hydroxide (0.15 mmol, 6 mg) in water (1 ml). The solvent was removed *in vacuo* to obtain 54 mg (100%) of the sodium salt as an orange solid.

^{1}H-NMR (400 MHz, D_2O): δ 8.20 (s, 1H), 8.00 (d, *J* = 8.5 Hz, 1H), 7.35 (d, *J* = 8.5 Hz, 1H), 7.31 (s, 1H), 5.68 (s, 1H), 3.66 (s, 3H), 2.02 (q, *J* = 7.4 Hz, 2H), 1.72 (s, 3H), 0.86 (t, *J* = 7.4 Hz, 3H).

^{13}C-NMR (100 MHz, D_2O): δ 177.2, 176.6, 172.6, 149.5, 144.1, 140.9, 140.2, 139.6, 133.9, 126.7, 126.2, 125.1, 117.8, 117.7, 109.9, 41.6, 16.9, 13.3, 9.4.

HR-MS (ESI, [M+H]+): Calcd. for C19H17N2NaO4: 361.1159; Found: 361.1157

***Tert*-butyl 2-tosylhydrazine-1-carboxylate (10)**:[30]

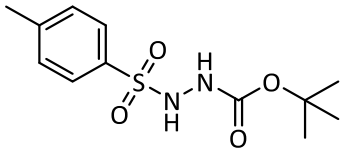

tert-butyl carbazate (7.5 mmol, 1 g) was dissolved in DMF (10 ml) at 0 °C and potassium carbonate (8.3 mmol, 1.2 g), and *p*-toluenesulfonyl chloride (7.5 mmol, 1.4 g) were added in three portions. The mixture was allowed to reach room temperature and subsequently was stirred for 1 hour. After that time, the reaction mixture was diluted with EtOAc (5 ml), quenched with saturated aqueous ammonium chloride (5 ml) and partitioned between EtOAc and H_2O. The aqueous layer was extracted with EtOAc (40 ml) twice, and the combined organic layers were washed with brine (40 ml) twice and dried with anhydrous $MgSO_4$. The solvent was evaporated *in vacuo*, and the residue was purified by flash column chromatography (Hexane:EtOAc 5:1) to obtain 1.2 g (55%) of a white solid.

^{1}H-NMR (400 MHz, $CDCl_3$): δ 7.81 (d, *J* = 8.2 Hz, 2H), 7.31 (d, *J* = 8.2 Hz, 2H), 6.50 (brs, 2H), 2,42 (s, 3H), 1.24 (s, 9H).

^{1}H-NMR spectrum in agreement with published data.[30]

***Tert*-butyl 2-(1-ethyl-7-methyl-4-oxo-1,4-dihydro-1,8-naphthyridine-3-carbonyl) -2-tosylhydrazine-1-carboxylate (12)**:[30]

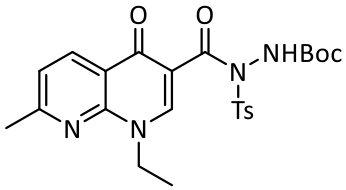

A mixture of nalidixic acid **11** (5.1 mmol, 1.2 g), TBTU (5.7 mmol, 1.8 g), DMAP (0.9 mmol, 0.1 g), DIPEA (7.0 mmol, 0.9 g), and hydrazine **10** (4.7 mmol, 1.3 g) were dissolved in DCM and stirred at room temperature for 2 hours. After that time, the reaction was quenched with saturated aqueous ammonium chloride (15 ml) and partitioned between EtOAc and H_2O. The aqueous layer was extracted with EtOAc (50 ml) twice, and the combined organic layers were washed with brine (50 ml) twice. The organic layer was dried over anhydrous $MgSO_4$, filtered and the solvent was removed *in vacuo*. The residue was purified by flash column chromatography (Hexane: EtOAc 9:1 to 6:4) to result in 1.4 g (60%) of a white solid.

^{1}H-NMR (400 MHz, $CDCl_3$): δ 8.62 (d, *J* = 8.3 Hz, 1H), 8.47 (s, 1H), 8.21 (s, 1H), 8.06 (d, *J* = 8.2 Hz, 2H), 7.33 (d, *J* = 8.3 Hz, 2H), 7.29 (d, *J* = 8.2 Hz, 1H), 4.49 (qd, *J* = 13.3, 7.3 Hz, 1H), 4.35 (qd, *J* = 13.3, 7.3 Hz, 1H), 2.68 (s, 3H), 2.43 (s, 3H), 1.40 (t, *J* = 7.3 Hz, 3H), 1.18 (s, 9H).

^{1}H-NMR spectrum in agreement with published data.[30]

***N*-(1-ethyl-7-methyl-4-oxo-1,4-dihydro-1,8-naphthyridine-3-carbonyl)-4-methylbenzenesulfonohydrazide (13)**:[30]

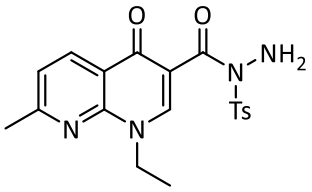

Compound **12** (2.8 mmol, 1.4 g) was dissolved in a mixture of 1:1 TFA:DCM and stirred at room temperature for 2 hours. After that time, the reaction was neutralized with saturated aqueous potassium carbonate to allow the precipitation of the product. The solid was filtered to give 1.0 g (94%) of a yellow solid.

^{1}H-NMR (400 MHz, $CDCl_3$): δ 8.55 (d, *J* = 7.8 Hz, 1H), 8.12 (s, 1H), 8.00 (d, *J* = 8.2 Hz, 2H), 7.34 (d, *J* = 8.2 Hz, 2H), 7.24 (d, J = 8.2 Hz, 1H), 4.91 (brs, 2H), 4.45 (q, *J* = 7.3 Hz, 2H), 2.66 (s, 3H), 2.42 (s, 3H), 1.45 (t, *J* = 8.2 Hz, 3H).

^{1}H-NMR spectrum in agreement with published data.[30]

1-ethyl-7-methyl-4-oxo-1,4-dihydro-1,8-naphthyridine-3-carbaldehyde (14):[30]

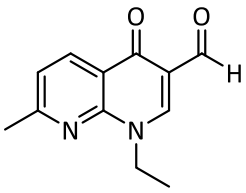

A mixture of **13** (1 mmol, 0.4 g) and TMS-imidazole (3 mmol, 0.4 g) in toluene (2 ml) was stirred at room temperature for 5 minutes. After that time, imidazole (2 mmol, 0.14 g) was added, and the reaction was stirred at 55 °C for 20 hours. Next, 1M citric acid (20 ml) was added, and the reaction was stirred for an additional 2 hours. The resulting mixture was partitioned between EtOAc (20 ml) and saturated sodium bicarbonate (25 ml). The aqueous layer was extracted with EtOAc twice. The combined organic layers were washed with brine (50 ml) and dried over anhydrous $MgSO_4$. The solvent was removed *in vacuo*, and the resulting residue was purified by flash column chromatography (Hexane:EtOAc 1:1) to give 0.11 g (53%) of a white powder.

^{1}H-NMR (400 MHz, $CDCl_3$): δ 10.4 (s, 1H), 8.65 (d, *J* = 8.2 Hz, 1H), 8.45 (s, 1H), 7.29 (d, *J* = 8.2 Hz, 1H), 4.50 (q, *J* = 6.9 Hz, 2H), 2.69 (s, 3H), 1.51 (t, *J* = 6.9 Hz, 3H)

^{1}H-NMR spectrum in agreement with published data.[30]

1-ethyl-3-((4-ethyl-3-methyl-5-oxo-1,5-dihydro-2H-pyrrol-2-ylidene)methyl)-7-methyl-1,8-naphthyridin-4(1H)-one (15):

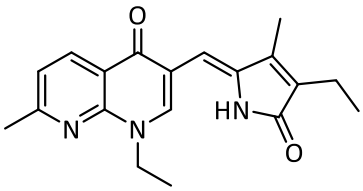

A mixture of aldehyde **14** (0.5 mmol, 0.1 g), 3-ethyl-4-methyl-1,5-dihydro-pyrrol-2-one (1 mmol, 0.12 g) and potassium hydroxide (2 mmol, 0.11 g) in water (1 ml), was dissolved in DMSO (2 ml) and stirred at 60 °C under argon atmosphere for 12 hours.The reaction mixture was then poured into water and neutralized with 37% HCl to allow the precipitation of the product. The solid was filtered to obtain 0.15 g (94%) of a yellow solid.

^{1}H-NMR (400 MHz, CD_3OD): δ 8.58 (d, *J* = 8.2 Hz, 1H), 8.41 (s, 1H), 7.36 (d, *J* = 8.2 Hz, 1H), 6.04 (s, 1H), 4.57 (q, *J* = 7.1 Hz, 2H), 2.68 (s, 3H), 2.37 (q, *J* = 7.5 Hz, 2H), 2.14 (s, 3H), 1.49 (t, *J* = 7.1 Hz, 3H), 1.10 (t, *J* = 7.5 Hz, 3H).

^{13}C-NMR (100 MHz, CD_3OD): δ 177.2, 172.9, 164.8, 149.1, 148.7, 142.3, 138.2, 137.3, 134.8, 122.1, 120.3, 129.2, 106.7, 47.5, 25.2, 17.7, 15.4, 13.8, 9.6.

HR-MS (ESI, [M+H]+): Calcd. for C19H21N3O2 + H: 324.1707; Found: 324.1699

1-ethyl-7-formyl-4-oxo-1,4-dihydro-1,8-naphthyridine-3-carboxylic acid (16):

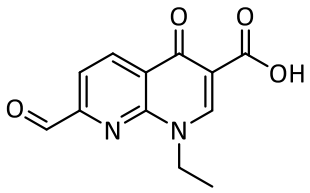

A mixture of nalidixic acid **11** (1.8 mmol, 0.4 g) and selenium dioxide (2.6 mmol, 0.30 g) was dissolved in DMSO (3 ml) and stirred at 175 °C during 1 hour. After that time, the solvent was evaporated *in vacuo*. The solid obtained was dissolved in hot $CHCl_3$ and filtered. The filtrate was washed twice with water (50 ml), and the organic layer was dried over anhydrous $MgSO_4$. The solvent was removed *in vacuo*, and the resulting solid was purified by column chromatography (DCM:Hexane:EtOH:AcOH 3:2:0.4:0.1) to give 0.1 g (23%) of a dark green solid.

^{1}H-NMR (300 MHz, $CDCl_3$): δ 10.11 (s, 1H), 9.37 (s, 1H), 8.96 (dd, *J* = 8.1, 0.8 Hz, 1H), 8.13 (d, *J* = 8.1 Hz, 1H), 4.74 (q, *J* = 7.1 Hz, 2H), 1.48 (t, *J* = 7.1 Hz, 3H).

1-ethyl-7-((4-ethyl-3-methyl-5-oxo-1,5-dihydro-2H-pyrrol-2-ylidene)methyl)-4-oxo-1,4-dihydro-1,8-naphthyridine-3-carboxylic acid (17a):

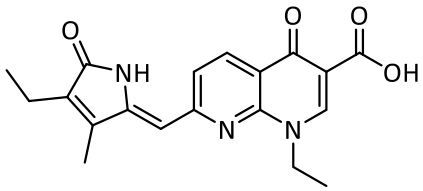

A mixture of aldehyde **16** (0.4 mmol, 0.1 g), 3-ethyl-4-methyl-1,5-dihydro-pyrrol-2-one (0.8 mmol, 0.1 g) and potassium hydroxide (1.6 mmol, 0.09 g) in water (1 ml), was dissolved in DMSO (2 ml) and stirred at 60 °C under argon atmosphere for 12 hours.The reaction mixture was then poured into water and neutralized with 37% HCl to allow the precipitation of the product. The solid was filtered to obtain 0.07 g (50%) of a yellow solid.

^{1}H-NMR (400 MHz, $CDCl_3$): δ 14.51 (s, 1H), 9.64 (s, 1H), 8.91 (s, 1H), 8.75 (d, *J* = 7.9 Hz, 1H), 7.45 (d, *J* = 8.4 Hz, 1H), 6.06 (s, 1H), 4.57 (q, *J* = 6.7 Hz, 2H), 2.44 (q, *J* = 7.6 Hz, 2H), 2.16 (s, 3H), 1.70 (t, *J* = 6.8 Hz, 3H), 1.17 (t, *J* = 7.5 Hz, 3H).

^{13}C-NMR (100 MHz, $CDCl_3$): δ 178.3, 171.9, 166.4, 160.1, 149.2, 148.8, 146.6, 140.9, 137.1, 136.9, 123.5, 119.1, 110.4, 101.7, 48.8, 17.2, 14.8, 13.3, 9.7.

HR-MS (ESI, [M+H]+): Calcd. for C19H19N3O4 + H: 354.1448; Found: 354.1452

Sodium -1-ethyl-7-((4-ethyl-3-methyl-5-oxo-1,5-dihydro-2H-pyrrol-2-ylidene) methyl)-4-oxo-1,4-dihydro-1,8-naphthyridine-3-carboxylate (17b):

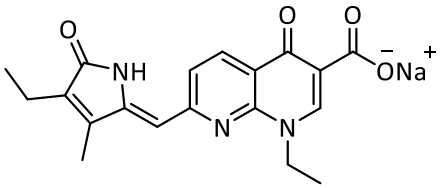

Compound **17a** (0.14 mmol, 0.05g) was dissolved in a solution containing sodium hydroxide (0.14 mmol, 5.5 mg) in water (1 ml). The solvent was removed in vacuo to obtain 52 mg (100%) of the sodium salt as an orange solid.

^{1}H-NMR (300 MHz, D_2O): δ 8.20 (s, 1H), 7.87 (d, *J* = 8.0 Hz, 1H), 6.64 (d, *J* = 8.2 Hz, 1H), 5.17 (s, 1H), 3.61 (m, 2H), 1.82 (m, 2H), 1.41 (s, 3H), 0.96 (t, *J* = 6.3 Hz, 3H), 0.72 (t, *J* = 6.9 Hz, 3H).

^{13}C-NMR (100 MHz, D_2O): δ 176.5, 173.4, 171.4, 157.1, 148.4, 148.0, 142.9, 142.9, 136.9, 135.4, 123.3, 120.5, 118.7, 104.9, 47.3, 16.8, 13.7, 13.0, 9.1.

HR-MS (ESI, [M+H]+): Calcd. for C19H18N3NaO4 +H : 376.1268; Found: 376.1269

4.5 References

1. *Antimicrobial consumption in the EU/EEA, annual epidemiological report for 2018*; ECDC: Stockholm 2019.
2. Emmerson, A. M.; Jones, A. M., The quinolones: decades of development and use. *Journal of Antimicrobial Chemotherapy* **2003,** *51* (suppl_1), 13-20.
3. Drusano, G.; Labro, M.-T.; Cars, O.; Mendes, P.; Shah, P.; Sörgel, F.; Weber, W., Pharmacokinetics and pharmacodynamics of fluoroquinolones. *Clinical Microbiology and Infection* **1998,** *4* (s2), 2S27-2S41.
4. Lesher, G. Y.; Froelich, E. J.; Gruett, M. D.; Bailey, J. H.; Brundage, R. P., 1,8-Naphthyridine Derivatives. A New Class of Chemotherapeutic Agents. *Journal of Medicinal and Pharmaceutical Chemistry* **1962,** *5* (5), 1063-1065.
5. Ronald, A. R.; Turck, M.; Petersdorf, R. G., A Critical Evaluation of Nalidixic Acid in Urinary-Tract Infections. *New England Journal of Medicine* **1966,** *275* (20), 1081-1089.
6. Mitscher, L. A., Bacterial Topoisomerase Inhibitors: Quinolone and Pyridone Antibacterial Agents. *Chemical Reviews* **2005,** *105* (2), 559-592.
7. Almalki, Z. S.; Yue, X.; Xia, Y.; Wigle, P. R.; Guo, J. J., Utilization, Spending, and Price Trends for Quinolones in the US Medicaid Programs: 25 Years' Experience 1991–2015. *PharmacoEconomics - Open* **2017,** *1* (2), 123-131.

8. Domagala, J. M., Structure-activity and structure-side-effect relationships for the quinolone antibacterials. *Journal of Antimicrobial Chemotherapy* **1994,** *33* (4), 685-706.
9. Walker, R. C., The Fluoroquinolones. *Mayo Clinic Proceedings* **1999,** *74* (10), 1030-1037.
10. Stahlmann, R.; Lode, H., Toxicity of Quinolones. *Drugs* **1999,** *58* (2), 37-42.
11. Lipsky, B. A.; Baker, C. A., Fluoroquinolone Toxicity Profiles: A Review Focusing on Newer Agents. *Clinical Infectious Diseases* **1999,** *28* (2), 352-361.
12. Aldred, K. J.; Kerns, R. J.; Osheroff, N., Mechanism of Quinolone Action and Resistance. *Biochemistry* **2014,** *53* (10), 1565-1574.
13. Hooper, D. C., Mode of Action of Fluoroquinolones. *Drugs* **1999,** *58* (2), 6-10.
14. Baeyer, A., Vorläufige Notiz über das Hydantoïn. *Justus Liebigs Annalen der Chemie* **1861,** *117* (2), 178-180.
15. Konnert, L.; Lamaty, F.; Martinez, J.; Colacino, E., Recent Advances in the Synthesis of Hydantoins: The State of the Art of a Valuable Scaffold. *Chemical Reviews* **2017,** *117* (23), 13757-13809.
16. Tian, X.; Peng, X.; Yu, M.; Huang, Y.; Wang, X.; Zhou, L.; Qiu, M., Hydantoin and thioamide analogues from Lepidium meyenii. *Phytochemistry Letters* **2018,** *25*, 70-73.
17. Wang, Q.; Tang, X.; Luo, X.; de Voogd, N. J.; Li, P.; Li, G., (+)- and (−)-Spiroreticulatine, A Pair of Unusual Spiro Bisheterocyclic Quinoline-imidazole Alkaloids from the South China Sea Sponge Fascaplysinopsis reticulata. *Organic Letters* **2015,** *17* (14), 3458-3461.
18. Yasuda, T.; Araki, A.; Kubota, T.; Ito, J.; Mikami, Y.; Fromont, J.; Kobayashi, J. i., Bromopyrrole Alkaloids from Marine Sponges of the Genus Agelas. *Journal of Natural Products* **2009,** *72* (3), 488-491.
19. Leitch, J. A.; Cook, H. P.; Bhonoah, Y.; Frost, C. G., Use of the Hydantoin Directing Group in Ruthenium(II)-Catalyzed C–H Functionalization. *The Journal of Organic Chemistry* **2016,** *81* (20), 10081-10087.
20. Kondoh, A.; Ota, Y.; Komuro, T.; Egawa, F.; Kanomata, K.; Terada, M., Chiral Brønsted acid-catalyzed enantioselective Friedel–Crafts reaction of 2-methoxyfuran with aliphatic ketimines generated in situ. *Chemical Science* **2016,** *7* (2), 1057-1062.
21. Oyaizu, K.; Ohtani, Y.; Shiozawa, A.; Sugawara, K.; Saito, T.; Yuasa, M., Highly Stable Gold(III) Complex with a Hydantoin Ligand in Alkaline Media. *Inorganic Chemistry* **2005,** *44* (20), 6915-6917.

22. Rai, R. K.; Jayakrishnan, A., Synthesis and polymerization of a new hydantoin monomer with three halogen binding sites for developing highly antibacterial surfaces. *New Journal of Chemistry* **2018,** *42* (14), 12152-12161.
23. Martínez-López, D.; Yu, M.-L.; García-Iriepa, C.; Campos, P. J.; Frutos, L. M.; Golen, J. A.; Rasapalli, S.; Sampedro, D., Hydantoin-Based Molecular Photoswitches. *The Journal of Organic Chemistry* **2015,** *80* (8), 3929-3939.
24. Lamparter, T.; Krauß, N.; Scheerer, P., Phytochromes from Agrobacterium fabrum. *Photochemistry and Photobiology* **2017,** *93* (3), 642-655.
25. Velazquez Escobar, F.; Piwowarski, P.; Salewski, J.; Michael, N.; Fernandez Lopez, M.; Rupp, A.; Qureshi, B. M.; Scheerer, P.; Bartl, F.; Frankenberg-Dinkel, N.; Siebert, F.; Andrea Mroginski, M.; Hildebrandt, P., A protonation-coupled feedback mechanism controls the signalling process in bathy phytochromes. *Nature Chemistry* **2015,** *7* (5), 423-430.
26. Davis, S. J.; Vener, A. V.; Vierstra, R. D., Bacteriophytochromes: Phytochrome-Like Photoreceptors from Nonphotosynthetic Eubacteria. *Science* **1999,** *286* (5449), 2517-2520.
27. Bhoo, S.-H.; Davis, S. J.; Walker, J.; Karniol, B.; Vierstra, R. D., Bacteriophytochromes are photochromic histidine kinases using a biliverdin chromophore. *Nature* **2001,** *414* (6865), 776-779.
28. Starostzik, C.; Marwan, W., A photoreceptor with characteristics of phytochrome triggers sporulation in the true slime mould Physarum polycephalum. *FEBS Letters* **1995,** *370* (1-2), 146-148.
29. García-Iriepa, C.; Ernst, H. A.; Liang, Y.; Unterreiner, A.-N.; Frutos, L. M.; Sampedro, D., Study of Model Systems for Bilirubin and Bilin Chromophores: Determination and Modification of Thermal and Photochemical Properties. *The Journal of Organic Chemistry* **2016,** *81* (15), 6292-6302.
30. Iwai, Y.; Ozaki, T.; Takita, R.; Uchiyama, M.; Shimokawa, J.; Fukuyama, T., Modified McFadyen–Stevens reaction for a versatile synthesis of aliphatic/aromatic aldehydes: design, optimization, and mechanistic investigations. *Chemical Science* **2013,** *4* (3), 1111-1119.
31. Kuhn, H. J.; Braslavsky, S. E.; Schmidt, R., Chemical actinometry (IUPAC Technical Report). *Pure and Applied Chemistry* **2004,** *76* (12), 2105-2146.
32. Briales, A.; Rodríguez-Martínez, J. M.; Velasco, C.; Díaz de Alba, P.; Domínguez-Herrera, J.; Pachón, J.; Pascual, A., In vitro effect of qnrA1, qnrB1, and qnrS1 genes on fluoroquinolone activity against isogenic Escherichia coli isolates with mutations in gyrA and parC. *Antimicrobial Agents and Chemotherapy* **2011,** *55* (3), 1266-1269.

33. Microbiology, European Comitee for Antimicrobial Susceptibility Testing (EUCAST) of the European Society of Clinical Microbiology and Infectious; Diseases (ESCMID), Determination of minimum inhibitory concentrations (MICs) of antibacterial agents by broth dilution. *Clinical Microbiology and Infection* **2003,** *9* (8), ix-xv.
34. Gazieva, G. A.; Kravchenko, A. N.; Strelenko, Y. A., Unusual reactions of 6,8-dialkyl-3-thia-2,4,6,8-tetraazabicyclo[3.3.0]octan-7-one 3,3-dioxides under conditions of acid hydrolysis and acetylation. *Mendeleev Communications* **2000,** *10* (6), 232-233.

Chapter 5

Irreversible Control of Quinolone Derivatives Using Oxime Esters

5.1 Introduction

The controlled release of a drug in a specific target is another strategy currently used to avoid many of the problems that conventional drugs present. The irreversible control of a drug can be achieved by covalently attaching a protective group in the structure of the pharmaceutical agent. This group should be linked in a position that cancels the activity of the drug. Initially, the inactive form will be obtained, which upon release of the protective group will result in the active form. Moreover, if the control wants to be induced by using light as a stimulus, the protective group should be photoresponsive, meaning that when it is irradiated with the adequate wavelength, the release reaction is produced. This reaction can only take place in one direction, as opposed to the reversible systems explained in chapter 4. Once the pharmaceutical agent is released, the inactive form can no longer be obtained, which makes this process irreversible. The use of the caging strategy presents an alternative to the irreversible control of drugs seen in the previous chapter.

In this chapter, the irreversible control of quinolone derivatives will be studied, from the design of the molecules to the synthesis and study of their photochemical properties. Two components form this irreversible system, an antibiotic part, and a photoreleasable protective group. By combining both, it is expected to create a system whose antibacterial properties could be optically controlled in a non-reversible way.

5.1.1 Oxime esters

Oxime esters are present in many bioactive compounds with a range of activities like antibacterial,[1-2] antifungal,[3] anti-inflammatory,[4] and cytotoxic.[5-6] Oximes can be easily made by the treatment of an aldehyde or ketone of choice with hydroxylamine hydrochloride and a base. Subsequently, transformation into the oxime ester can be achieved in a one-step reaction of the oxime with an acyl halide or anhydride.[7] Besides their simple synthesis, oxime esters can be made in large scales and stored for a long time under adequate conditions. These compounds have many uses in organic synthesis as they can be transformed among others in amines,[8-9] amides,[10-11] and heteroaromatic systems.[12-13] Furthermore, they are relevant starting materials in the preparation of photosensitive compositions.[14]

The primary photochemical process of oxime esters is a homolytic scission of the weak N-O bond. This fragmentation results in an iminyl radical and an oxygen-centered radical. In addition, a second process of isomerization of the N=C double

bond can be photoinduced, resulting in two isomers *Z* and *E*. These two processes can compete with each other.

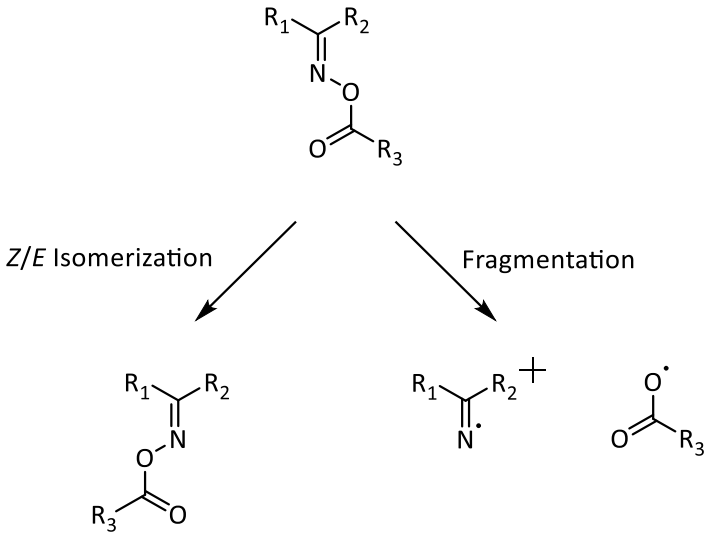

Figure 1. Possible reaction pathways of oxime esters upon light irradiation. On the left, the N=C double bond can undergo *Z*/*E* isomerization. On the right, the N-O bond can be cleaved, generating two radicals.

In order to cleave the N-O bond, it is necessary to irradiate with UV light, since these molecules present strong absorption in the 250-350 nm range. The dissociation of the bond is a homolytic fission that produces two fragments with one of the originally bonded electrons. Apart from the isomerization, no additional fragmentation processes compete under normal conditions.

The scission of the N-O bond results in two radicals, which in turn, can follow different pathways. The iminyl radical can terminate by bimolecular combination to give the corresponding hydrazine.[15] Besides, it can undergo dissociation, resulting in the analogous nitrile and the release of a C-centered radical by β-scission.[15] The iminyl radical can also abstract hydrogen atoms to obtain imines.[16] Finally, if the iminyl radical has an alkenyl side chain, it can go through cyclization with the formation of pyrrolomethyl type radicals.[17]

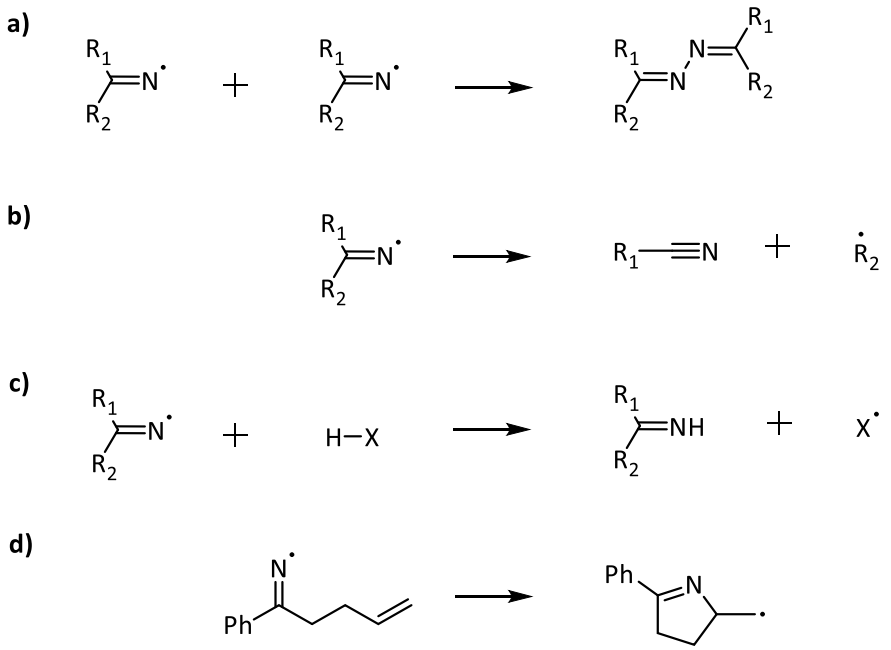

Figure 2. Photoinduced pathways for the iminyl radical: a) bimolecular combination, b) dissociation, c) H-atom abstraction, d) cyclization.

Regarding the oxygen-centered radical, also known as acyloxyl radical, the most common reaction is a decarboxylation process followed by the release of a C-centered radical.[18-19] However, if the lifetime of the radical is sufficient, it can participate in other processes like abstraction, addition or cyclization.[20-22]

Oxime esters have been used in biological applications as protective groups for drug delivery. The bioactive molecule can be caged by the formation of the N-O bond with an oxime, which later, can be released upon application of the adequate stimulus. Among these stimuli are pH[23] and light irradiation.[5, 24] More specifically, their use as photoprotective groups has been directed towards DNA cleavage and DNA binding due to their ability to act as metal-free DNA photocleavers. The homolysis of the N-O bond generates acyloxyl radicals able to attack DNA.[20]

5.2 Results

5.2.1 Design of photoreleasable antibiotics using oxime esters

The design of our photoreleasable antibiotics can be described as a combination of two parts: a quinolone antibiotic and an oxime. Based on our previous studies about quinolone derivatives (see chapter 4), we realized that upon modification of the acid group at position 3, the antibacterial properties of the molecule were severely affected to the point of deactivation of the antibiotic. Having these results in mind, we conceived that the incorporation of a photoreleasable group in that position would

have a similar effect to the one previously reported, blocking the antibacterial properties. Hence, the release of the quinolone would afford spatial and temporal control over the antibiotic activity. Moreover, the acid group at position 3 can be easily transformed into an oxime ester in a few steps. In order to carry out this study, we chose ciprofloxacin, a broad-spectrum quinolone, as the antibiotic part. As to the photoreleasable group, several oximes were designed with the purpose of achieving a bathochromic shift in the absorption spectra. This shift would imply the use of longer wavelengths to induce the release, which, in turn, would make the process compatible with biological applications. By combining both parts, ciprofloxacin and the corresponding oxime, the acid group of ciprofloxacin can be converted into an oxime ester. It was expected that upon irradiation, the release reaction would take place to give the iminyl and acyloxyl radicals and generating subsequently, the molecule of ciprofloxacin. Thus, creating an irreversible system that would allow the optical control of the selected quinolone.

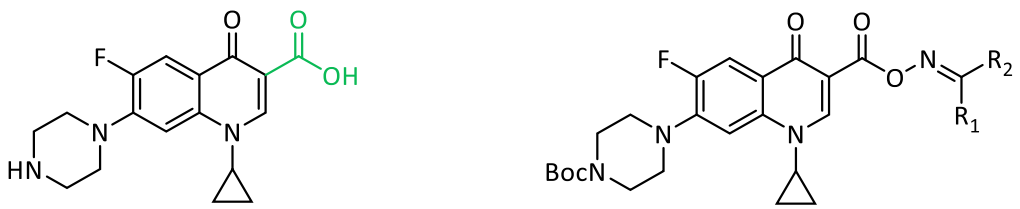

Ciprofloxacin **Oxime ester of BOC-ciprofloxacin**

Figure 3. Irreversible control of ciprofloxacin derivatives. On the left, structure of ciprofloxacin a second-generation quinolone antibiotic. Position 3 is highlighted in green. On the right, general motif of oxime esters of Boc-ciprofloxacin. The oxime ester is generated at position 3.

5.2.2 Synthesis

The synthesis of oxime esters can be separated into two routes. First, the oxime part was made either through procedure A or B described in scheme 1.

Scheme 1

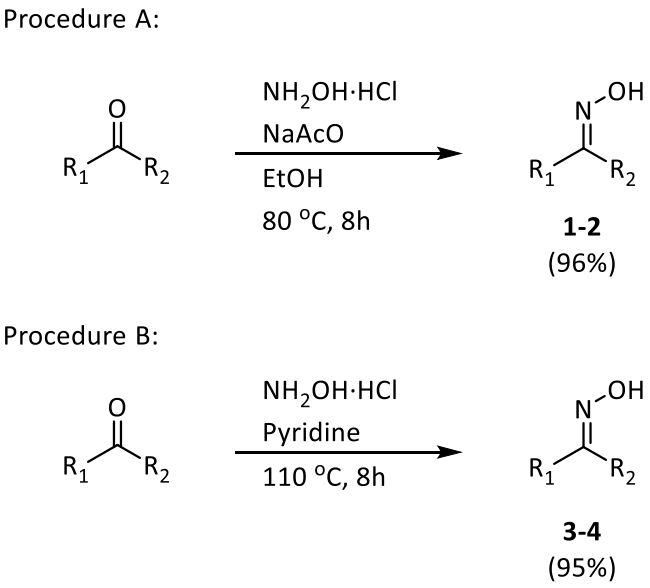

Both procedures involve the condensation of a ketone with hydroxylamine. In procedure A, the base employed was sodium acetate with ethanol as a solvent, whereas procedure B used pyridine as base and solvent, which allowed higher temperature conditions.

Once the oximes were synthesized, the oxime esters can be easily generated following the procedure described in scheme 2.

Scheme 2

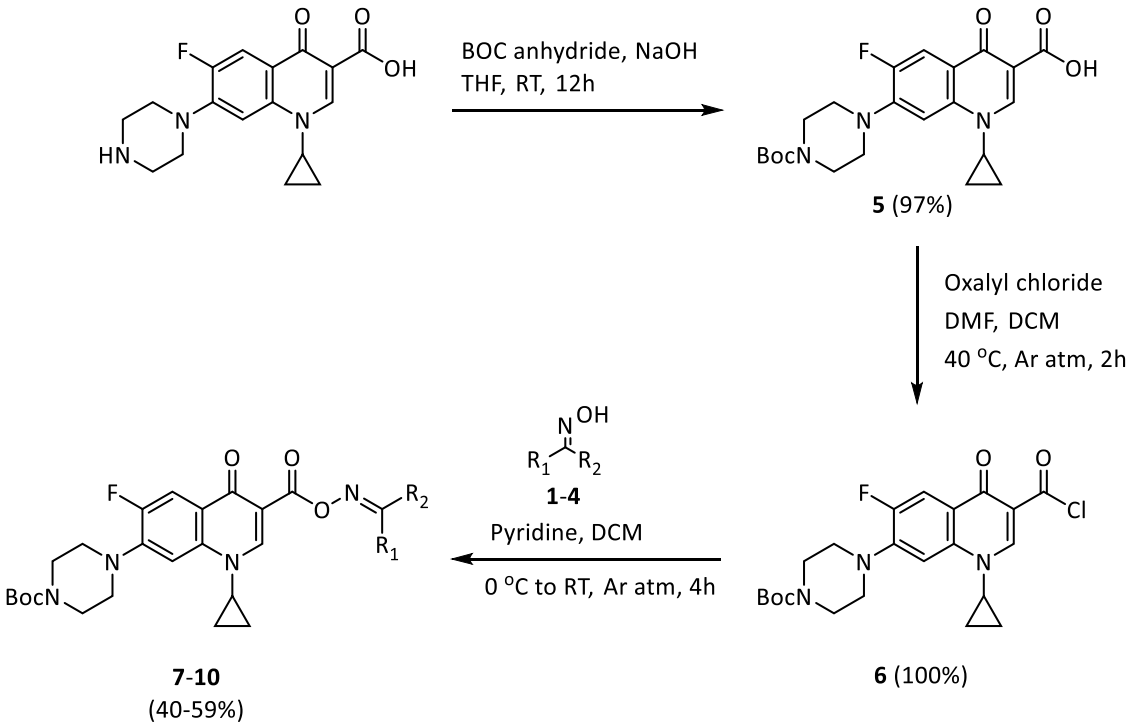

The route started by protecting the secondary amine group in the piperazine unit of ciprofloxacin with a Boc group, to avoid possible side reactions of the amine in the next steps. Then, acyl chloride **6** was synthesized from carboxylic acid **5** using oxalyl chloride with DMF as a catalyst. Finally, the acyl chloride **6** combined with an oxime (**1**-**4**) gave the corresponding oxime ester (**7**-**10**).

5.2.3 Photochemical properties

After successfully synthesizing several oxime esters of ciprofloxacin, a study to evaluate their photochemical properties was performed. This study provided information about the requirements of the photocleavable group to carry out the release reaction. Besides, some interesting features were observed and will be discussed in the next paragraphs.

With the purpose of knowing the range of absorption of these compounds, UV-Vis spectroscopy was employed to record the absorption spectrum of all of them. The samples were prepared in concentrations close to 5E-5M, and all of them were dissolved in dichloromethane. The information provided by the UV-Vis spectra allowed to choose a suitable light source to carry out the irradiation of the samples and induce the release reaction.

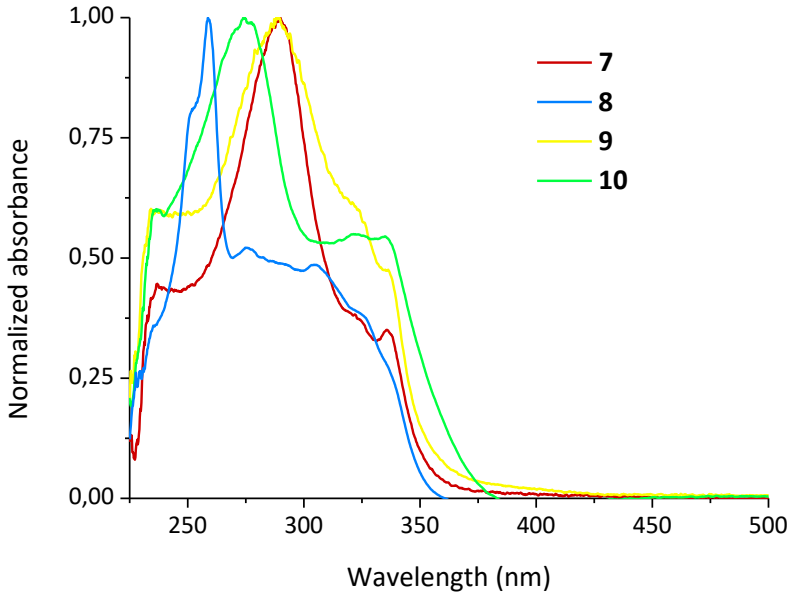

Figure 4. UV-Vis spectra of the different oxime esters of Boc-ciprofloxacin. All compounds (**7**-**10**) dissolved in DCM in a concentration close to 5E-5M.

As shown in figure 4, all oxime esters presented a similar absorption centered in the UV region. Compounds **7** and **9** corresponding to the benzophenone and 2-

aminobenzophenone oximes presented the maximum absorption at slightly longer wavelengths (290 nm) compared with the other two structures (259 and 274 nm for **8** and **10** respectively). Unfortunately, neither of the molecules displayed absorption in the visible region, and the most extended band barely reached 375 nm for the oxime of tetraphenylcyclopentadienone **10**. The information obtained in this experiment, such as the absorption maximum or the molar extinction coefficient, is collected in table 1.

Table 1. Maximum absorption and molar extinction coefficient of the oxime esters of Boc-ciprofloxacin.

Compound	λ_{max} (nm)	ε ($M^{-1}cm^{-1}$)
7	290	38300
8	259	42300
9	290	38200
10	274	34200

After considering these results, two types of light sources emitting in the UV region were selected to carry out the irradiation of the samples: a 125W medium-pressure Hg lamp and a photoreactor provided with UVA lamps. When the Hg lamp was used, samples were protected with a Pyrex filter to avoid radiation at wavelengths shorter than 290 nm. Even though all of the compounds presented absorption under 290 nm, this action was taken to avoid non-desired reactions caused by more energetic transitions. This step was no necessary when irradiating with the UVA lamps since their emission starts at 280 nm. The emission spectra of both light sources are displayed in figure 5. All samples were prepared in a 0.1M concentration in deuterated solvents, and the irradiation process was followed by ^{1}H-NMR and mass spectroscopy.

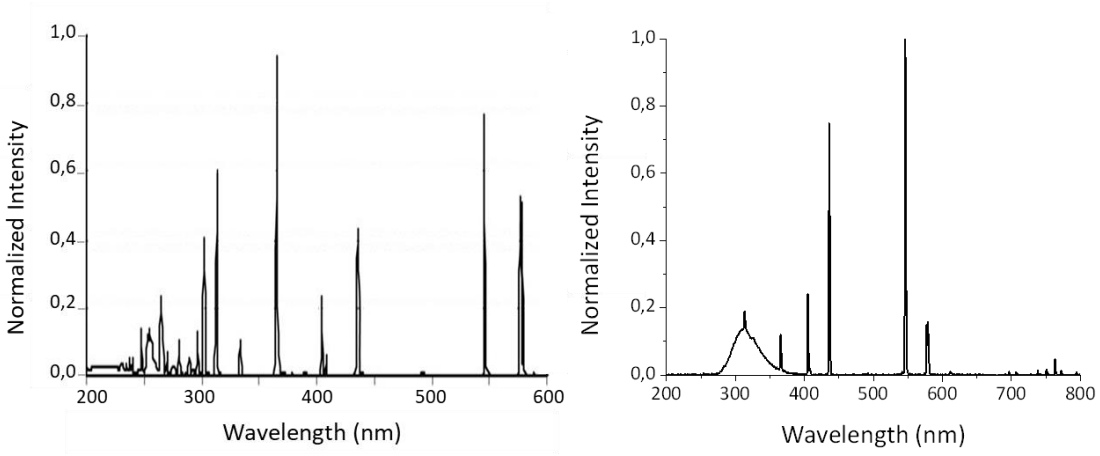

Figure 5. Emission spectra of the UV light sources employed to induce the release process. On the left, the emission spectrum of medium-pressure Hg lamp; the use of a Pyrex filter removes the shorter wavelengths (λ < 290 nm). On the right, the emission spectrum of UVA lamps.

Compound **7** was irradiated in two different solvents, methanol and acetonitrile, with the 125W medium-pressure Hg lamp. These two solvents were selected with the purpose of testing the differences between protic and aprotic solvents. Results showed that the oxime ester in methanol was able to release Boc-ciprofloxacin (> 95%) in 10 minutes. For the compound dissolved in acetonitrile the release took place at a slower pace, and it was necessary to irradiate for 20 minutes to obtain Boc-ciprofloxacin (92%). When UVA lamps were used to induce the release of the antibiotic in acetonitrile, longer times were required due to the lower potency of these lamps compared to the Hg one. Regarding the solvent selection, it was expected for the protic solvent to display a higher release yield than the aprotic one. This can be explained when taking into consideration the mechanism of the reaction. As shown in figure 6, when the oxime ester is irradiated, two radicals are generated, the iminyl and the acyloxyl radicals. The acyloxyl radical, corresponding to the antibiotic part, can undergo a decarboxylation process, or it can abstract a hydrogen atom from the solvent to regenerate the Boc-ciprofloxacin structure. This last option was the one observed, and no product of decarboxylation was found. Hence, to generate the antibiotic molecule, hydrogen atoms are needed in the medium, which are easier to be provided for the protic solvent than the aprotic one. As to the iminyl radical, its general reactivity has been explained in the previous section (see figure 2). After carrying out the photorelease of compound **7**, it was found by mass spectroscopy that the iminyl radical of benzophenone went through a bimolecular combination to give the corresponding hydrazine.

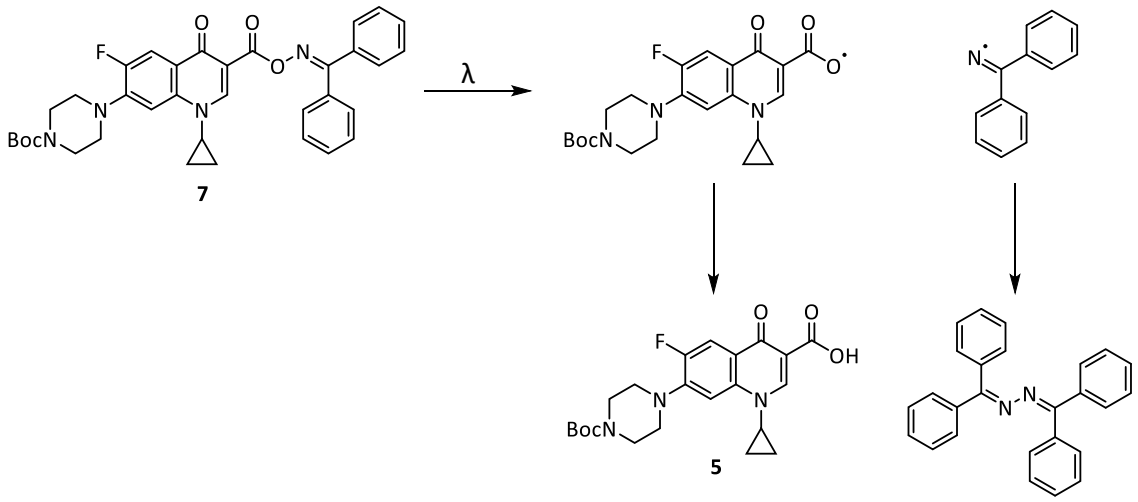

Figure 6. Reaction pathway for compound **7**. After light irradiation, the acyloxyl and iminyl radicals are obtained. The acyloxyl radical can abstract a hydrogen atom from the medium to generate Boc-ciprofloxacin (**5**), the antibiotic part. The iminyl radical undergoes a bimolecular combination to give a hydrazine.

Compound **8** was also irradiated using both lamps. For the Hg lamp, acetonitrile and chloroform were used as solvents due to product solubility. Irradiation in acetonitrile showed faster release rates (92% yield in 17 minutes) than chloroform, with a similar yield obtained for an irradiation time of 35 minutes. The photocleaved acyloxyl radical formed Boc-ciprofloxacin **5**, and no signs of decarboxylation were observed either through ^{1}H-NMR, or mass spectroscopy. Regarding the iminyl radical, the product corresponding to the bimolecular combination was found by mass spectroscopy. When the UVA lamps were employed, slower release rates were observed, similarly to **7**.

The irradiation of compound **9** could not be studied because the product was found to be unstable in solution. Assays involving short times like ^{1}H-NMR, UV-Vis, or mass spectroscopy were performed. However, studies requiring more extended times, like ^{13}C-NMR or light irradiation of the sample were not possible due to product decomposition.

Finally, compound **10** was irradiated using acetonitrile as a solvent with both lamps. One more time, the Hg lamp showed a faster release (90% yield in 30 minutes), whereas the irradiation time was 3 times longer to achieve the same release percentage with the UVA lamps. The acyloxyl radical generated Boc-ciprofloxacin **5**, and no signals of decarboxylation were observed. Unlike previous examples **7** and **8**, the iminyl radical did not undergo bimolecular combination. Probably due to steric hindrance since the N-centered radical is surrounded by two bulky groups. However, the product of abstraction of a hydrogen atom to generate the tetraphenylcyclopentadienone imine was detected by mass spectroscopy.

Table 2. Summary of data related to the release process of each compound.

Compound	Solvent	Release yield (%)	Irradiation time (min)
7	CD_3OD	95[a]	10[a]
	CD_3CN	92[a]	20[a]
	CD_3CN	92[b]	50[b]
8	CD_3CN	92[a]	18[a]
	$CDCl_3$	92[a]	35[a]
	$CDCl_3$	92[b]	120[b]
9	n/a	n/a[c]	n/a[c]
10	CD_3CN	90[a]	30[a]
	CD_3CN	90[b]	100[b]

[a]: Irradiation with 125W medium-pressure Hg lamp using Pyrex filter. [b]: Irradiation with UVA lamps. [c]: Irradiation of the sample could not be carried out due to the decomposition of the sample in solution.

After studying the behavior of the synthesized compounds when exposed to UV light, we discovered a very interesting property of these molecules. When they were exposed to stoichiometric amounts of an acid, a new band in the visible region appeared. The most plausible explanation for this new band is the protonation of the nitrogen in the N-O bond of the oxime ester.

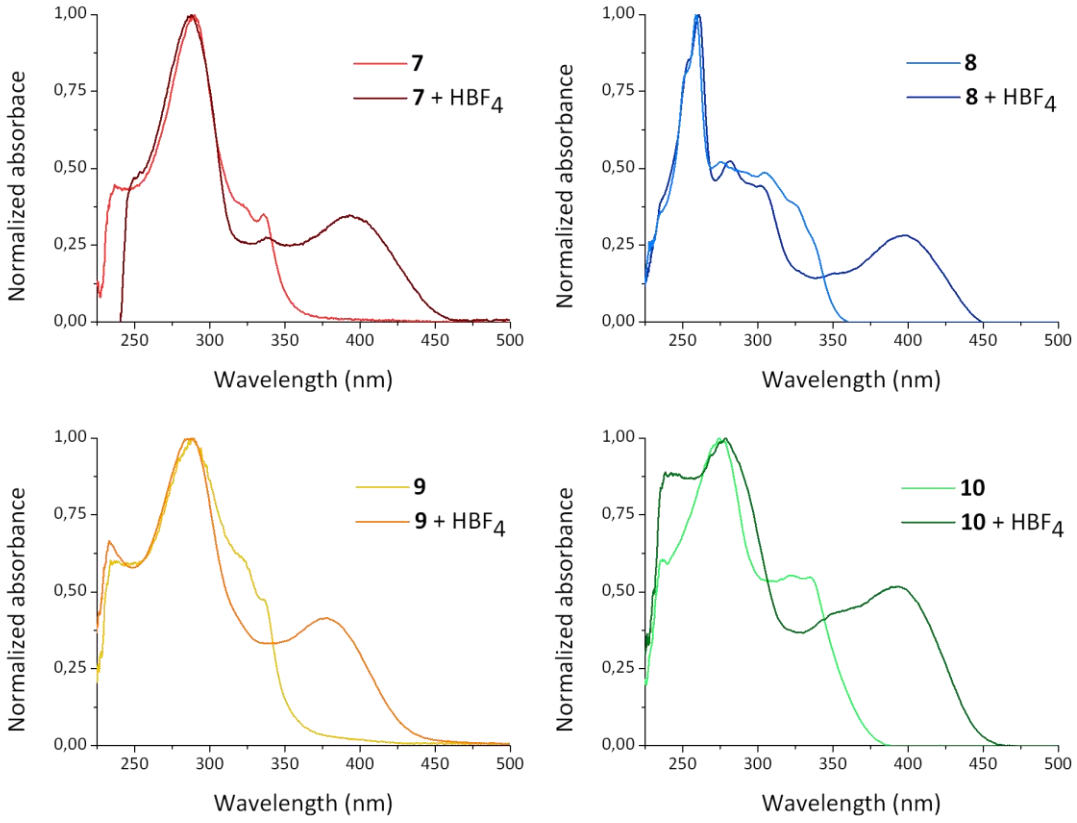

Figure 7. UV-Vis spectra of the different oxime esters of ciprofloxacin before and after the addition of a stoichiometric amount of tetrafluoroboric acid. All compounds (**7**-**10**) dissolved in DCM in a concentration close to 5E-5M.

It should be mentioned that the development of this new band only took place when halogenated solvents like dichloromethane or chloroform were used. The presence of acid in polar solvents such as dimethyl sulfoxide or acetonitrile did not produce changes in the UV-Vis spectrum.

As can be seen in figure 7, the new band displayed absorption between 350-450 nm with a maximum near to 400 nm. This new finding offered the possibility to carry out the irradiation of the samples with new light sources emitting in the visible region. In order to test this possibility, compound **10** was selected as a representative molecule to irradiate in the visible region. Two light sources were selected to induce the release process, a 500 mW LED with the emission centered around 390 nm, and a 30 W RGB LED in blue mode with emission between 430-500 nm. The emission spectra of both light sources are represented in figure 8. The samples were prepared at 0.1M concentration using deuterated chloroform as a solvent, and a stoichiometric amount of tetrafluoroboric acid was added to achieve protonation of the nitrogen atom. The irradiation process was followed by ^{1}H-NMR and mass spectroscopy, like previous examples.

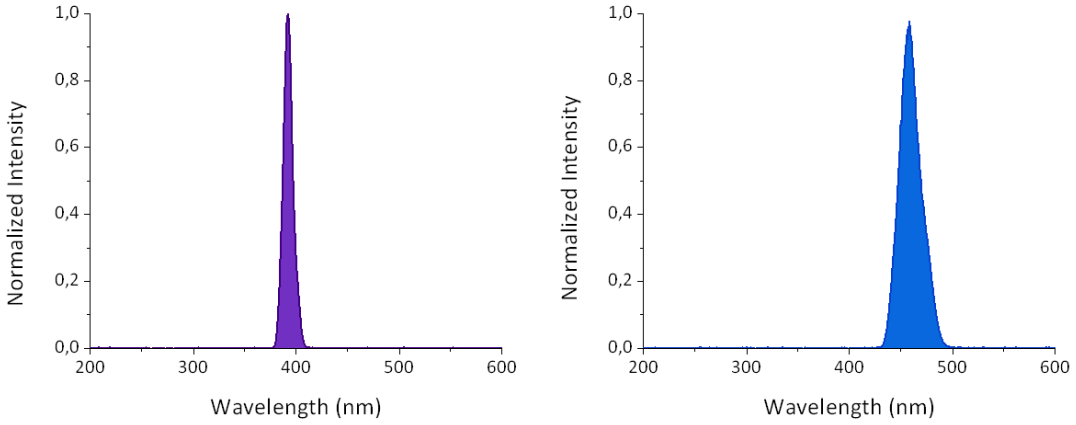

Figure 8. Emission spectra of the visible light sources employed to induce the release process of compound **10**. On the left, the emission spectrum of the 390 nm LED lamp. On the right, the emission spectrum of the blue LED lamp.

The release of the antibiotic part was possible with both LEDs, albeit slower than when using UV light. A 70% release was observed for both samples with an irradiation time of 700 and 450 min for the 390 nm and the blue LEDs, respectively. The significant time difference as a result of the disparity in the potency of the two LEDs. No product of decarboxylation was observed.

5.2.4 Enhancing water solubility

One of the problems for the use of oxime esters in biological applications is their low solubility in water. However, oxime esters are not an isolated case, as the solubility of drugs in aqueous media is a major concern in the pharmaceutical industry. More than 40% of NCEs (new chemical entities) developed in this industry are practically insoluble in water.[25] Solubility is an important parameter related to drug concentration in the systemic circulation, which is essential for achieving a good pharmacological response. Hence, the drug needs to be in aqueous solution at the site of absorption.[25] Many approaches have been developed to enhance the water solubility of these compounds. These techniques can be divided into three categories: physical modifications, chemical modifications, and other techniques. Physical modifications are based on methods that reduce the particle size of the drug or create dispersions in different carriers. Meanwhile, chemical modifications make changes in the structure of the molecule through pH variations, derivatization, complexation, etc. Belonging to this group is also salt formation, which is the most common approach to improve the water solubility of acidic and basic drugs. This technique has been applied previously in chapter 4, where the sodium salt of the photodrug was synthesized to improve its water solubility. The last group includes procedures like the use of surfactants, solubilizers, or supercritical fluids.

Surfactants can be used to enhance water solubility of poorly soluble drugs by reducing the surface tension. Micelle formation occurs when the surfactant concentration exceeds their critical micelle concentration (CMC). This value is typically between 0.05-0.10% for most surfactants. If the drug is present in the solution, micelle formation will entrap it within the micelles. There are many surfactants available in the market that have been employed to encapsulate drugs with low solubility.[26-28] Among all these examples, polymers have become of great interest in micelle formation.[29-31]

Polymeric micelles mimic aspects of biological transport systems in terms of structure and function.[32] They offer great versatility as their chemical structure can be modified to change properties such as specificity for an organ or tissue or make them responsive to an external stimulus.[33] Pluronic® polymers have emerged in recent years as promising candidates for drug delivery, and they are approved by the FDA for pharmaceutical and medical applications. Their structure consists of a hydrophilic part of ethylene oxide (EO) and a hydrophobic part of propylene oxide (PO), which are arranged in a triblock structure EO_x-PO_y-EO_x often described as PEO-PPO-PEO. The ethylene oxide part can have a length between 2-130 units, and the propylene oxide part can vary between 16-70 units. Because of their excellent properties, Pluronic® F-127 was selected to form micelles containing the oxime esters. A schematic representation of the experimental procedure is described in figure 9. A more detailed version of the procedure can be found in section 5.4.1.

a)

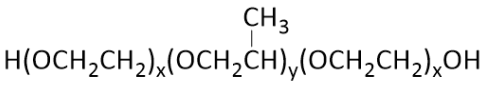

b)

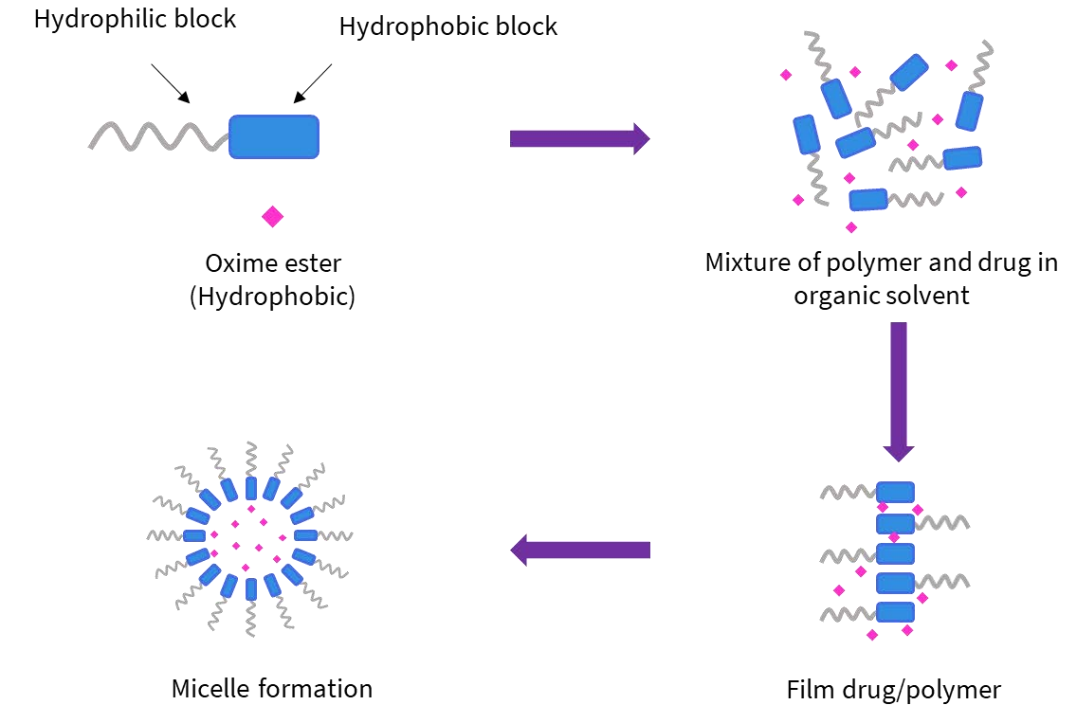

Figure 9. Use of polymeric micelles to enhance water solubility of oxime esters. a) Structure of Pluronic® F-127(x and y with averaged values of 101 and 56 units, respectively). b) Method of encapsulation of the cargo inside the micelle. Oxime esters were encapsulated using the solvent evaporation method. The polymer and the cargo are initially dissolved in a volatile organic solvent. Evaporation of the solvent leads to the formation of a drug/polymer film. Finally, the film is reconstituted in water by vigorous shaking to allow micelle formation.

Compound **7** was selected to study its solubility change upon micellar encapsulation. Initial attempts to dissolve **7** in water led to turbid solutions with solid particles in suspension, proving the low solubility of the oxime ester. Nonetheless, when **7** was inside the polymeric micelles, the water solubility changed drastically, resulting in a clear solution of this compound in water. Micelle encapsulation was also controlled by UV-Vis spectroscopy. The resulting spectra, as well as pictures of the samples, are shown in figure 10.

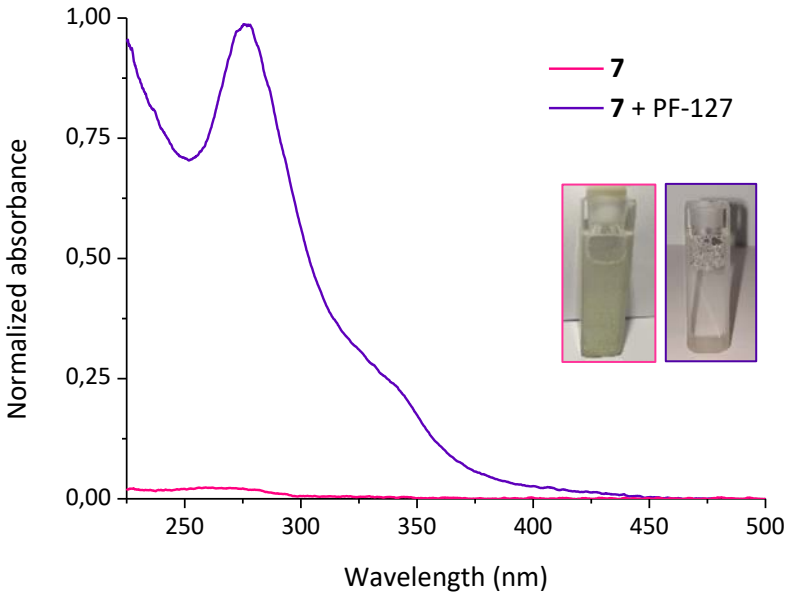

Figure 10. UV-Vis spectra of **7** in water. In pink, spectrum of compound **7** before micelle encapsulation and a picture of the cuvette containing the sample. In purple, spectrum of compound **7** after forming polymeric micelles, which facilitates its water solubility and a picture of the cuvette containing the sample.

As can be seen in the UV-Vis spectra, initial efforts at solubilizing **7** in water were unsuccessful, with the compound displaying no absorption due to its low solubility. However, when polymeric micelles were formed, the UV-Vis spectrum changed drastically, displaying the absorption of the compound thanks to its solubilization in water. This result proved that the oxime ester was successfully trapped within the micelle. Additionally, the protonated version of **7** was also effectively trapped inside the polymeric micelles, but unfortunately, the spectrum did not show absorption in the visible region, and the result was similar to the non-protonated version. It should not be forgotten that this was also observed when polar solvents were used to dissolve the oxime esters, and the development of the new band in the visible region was not detected.

No further experiments were performed as these data did not offer the prospects we were initially looking for, which included absorption in the visible region and moderate to high water solubility. Thus, the characteristics displayed by the oxime esters made the study of their properties *in vivo* not suitable.

5.3 Conclusions

In this chapter, several photoreleasable derivatives of ciprofloxacin have been studied. The synthesis has been designed to generate an oxime ester in position 3 of ciprofloxacin, which is crucial for the activity of the antibiotic. The procedures to obtain these compounds involve only 4 steps which can be easily achieved. Once the oxime esters were prepared, their photochemical properties were evaluated. The irradiation of the photoreleasable derivatives of ciprofloxacin was initially carried out using UV light, giving release yields between 90-95%, and no product of decarboxylation was detected in any case. Additionally, it was observed that in the presence of stoichiometric amounts of acid in halogenated solvents, a new band appeared in the visible region. This discovery opened the possibility of visible light irradiation, which was tested in one derivative. The irradiation with visible light induced the antibiotic's release with a yield of 70%, although longer times were needed. Moreover, oxime esters of ciprofloxacin have low solubility in water; for this reason, a method to enhance their solubility was employed. One of the photoreleasable drugs was successfully encapsulated in polymeric micelles of Pluronic® F-127, making possible their solution in water. However, once within the micelle, the protonated oxime ester no longer presented absorption in the visible region, which made it not possible to carry out biological assays of the samples.

5.4 Experimental section

5.4.1 Preparation of oxime ester loaded micelles

Micelles were prepared following the solvent evaporation method. Polymer and oxime ester solutions were prepared in a 10:1 w/w ratio. Compound **7** (11 mg, 0.018 mmol) and Pluronic® F-127 (111 mg) were dissolved separately in DCM (5 and 10 ml, respectively). The solution containing **7** was added over the polymer solution and stirred for 30 minutes. After that time, the solvent was removed *in vacuo* to obtain a thin film of oxime ester/polymer. For the micelle formation, an ultrasound bath heated at 50 °C was employed. The film container was introduced in the heated bath, and water (10 ml) at 50 °C was added. The sample was sonicated for 10 minutes. Non-encapsulated oxime ester was separated by centrifugation of the micelle suspension, followed by filtration of the supernatant using a 0.2 μm filter.

For micelle formation of compound **7** in the presence of acid, tetrafluoroboric acid was added in a stoichiometric amount to the solution containing the oxime ester in DCM. After that, the same procedure was followed.

5.4.2 Synthesis

5.4.2.1 General information

For details about general experimental information, see Appendix, section A.

5.4.2.2 Synthetic procedure

Benzophenone oxime (1):

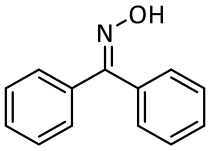

Benzophenone oxime was synthesized following procedure A (see scheme 1). Sodium acetate (0,50 g, 6.1 mmol) was dissolved in water (4 ml) and added over a solution of hydroxylamine hydrochloride (0.42 g, 6.1 mmol) in water (4 ml). The resulting mixture was added over benzophenone (1 g, 5.5 mmol) dissolved in ethanol (10 ml) and heated at 35 °C. Next, the sample was stirred for 8 hours at 80 °C. After that time, the reaction was cooled at room temperature, and cold water was added to allow the precipitation of 1.04 g (96%) of **1** as a white solid.
^{1}H-NMR (300 MHz, $CDCl_3$): δ 7.5-7.43 (m, 7H), 7.37-7.30 (m, 3H).
^{1}H-NMR spectrum in agreement with published data.[34]

9-fluorenone oxime (2):

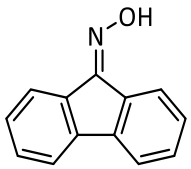

9-fluorenone oxime was synthesized following procedure A (see scheme 1). Sodium acetate (0.50 g, 6.1 mmol) was dissolved in water (4 ml) and added over a solution of hydroxylamine hydrochloride (0.42 g, 6.1 mmol) in water (4 ml). The resulting mixture was added over 9-fluorenone (1 g, 5.5 mmol) dissolved in ethanol (10 ml) and heated at 35 °C. Next, the sample was stirred for 8 hours at 80 °C. After that time, the reaction was cooled at room temperature, and cold water was added to allow the precipitation of 1.04 g (96%) of **2** as a white solid.
^{1}H-NMR (300 MHz, $CDCl_3$): δ 8.40 (dt, *J* = 7.6, 0.9 Hz, 1H), 8.33 (brs, 1H), 7.74 (dt, *J* = 7.5, 0.9 Hz, 1H), 7.69 – 7.61 (m, 2H), 7.48 – 7.28 (m, 4H).

2-aminobenzophenone oxime (3):

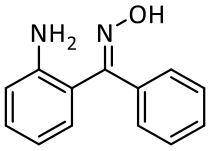

2-aminobenzophenone oxime was synthesized following procedure B (see scheme 1). 2-amino benzophenone (1 g, 5.1 mmol) was dissolved in pyridine (15 ml), and hydroxylamine hydrochloride was added (1.8 g, 25.4 mmol). The reaction was then stirred for 8 hours at 110 °C. After that time, the solvent was removed *in vacuo* and re-dissolved in EtOAc (50 ml). The organic phase was then washed with 0.5M HCl (50 ml) and twice with H_2O (50 ml), dried over anhydrous $MgSO_4$, and filtered. The solvent was evaporated *in vacuo* to give 1.02 g (95%) of white solid.
^{1}H-NMR (300 MHz, $CDCl_3$): δ 7.52 – 7.42 (m, 3H), 7.36 – 7.31 (m, 2H), 7.12 (ddd, *J* = 8.2, 7.2, 1.6 Hz, 1H), 6.76 (ddd, J = 13.6, 8.1, 1.2 Hz, 2H), 6.58 (td, J = 8.2, 7.7, 1.2 Hz, 1H), 5.99 (brs, 2H).

Tetraphenylcyclopentadienone oxime (4):

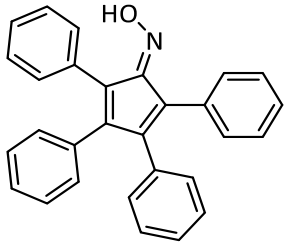

Tetraphenylcyclopentadienone oxime was synthesized following procedure B (see scheme 1). Tetraphenylcyclopentadienone (1 g, 2.6 mmol) was dissolved in pyridine (15 ml), and hydroxylamine hydrochloride was added (0.9 g, 13 mmol). The reaction was then stirred for 8 hours at 110 °C. After that time, the solvent was removed *in vacuo* and re-dissolved in DCM (50 ml). The organic phase was then washed with 0.5M HCl (50 ml) and twice with H_2O (50 ml), dried over anhydrous $MgSO_4$, and filtered. The solvent was evaporated *in vacuo* to give 0.98 g (95%)of dark purple solid.
^{1}H-NMR (300 MHz, $CDCl_3$): δ 7.32 – 7.18 (m, 10H), 7.13 – 6.98 (m, 7H), 6.87 – 6.76 (m, 4H).

7-(4-(*tert*-butoxycarbonyl)piperazin-1-yl)-1-cyclopropyl-6-fluoro-4-oxo-1,4-dihydroquinoline-3-carboxylic acid (5):

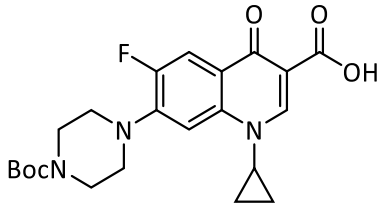

Ciprofloxacin (2 g, 6.0 mmol) and di-*tert*-butyl dicarbonate (1.4 g, 6.6 mmol) were dissolved in THF (60 ml). Next, a solution of sodium hydroxide (0.48 g, 12.0 mmol) in water (12 ml) was added, and the mixture was stirred overnight at room temperature. After that time, the solvent was removed *in vacuo*, and the residue was taken into aqueous saturated ammonium chloride (200 ml). The aqueous phase was extracted with DCM (200 ml) three times. The organic phase was washed with brine (400 ml), dried over anhydrous $MgSO_4$, and filtered. The solvent was evaporated *in vacuo* to obtain 2.51 g (97%) of white solid.

^{1}H-NMR (300 MHz, $CDCl_3$): δ 14.94 (s, 1H), 8.71 (s, 1H), 7.96 (d, *J* = 12.9 Hz, 1H), 7.35 (d, *J* = 7.1 Hz, 1H), 3.72 – 3.61 (m, 4H), 3.59-3.50 (m, 1H), 3.34 – 3.21 (m, 4H), 1.49 (s, 9H), 1.41-1.35 (m, 2H), 1.26 – 1.15 (m, 2H).

^{1}H-NMR spectrum in agreement with published data.[35]

***Tert*-butyl 4-(3-(chlorocarbonyl)-1-cyclopropyl-6-fluoro-4-oxo-1,4-dihydro quinolin-7-yl)piperazine-1-carboxylate (6):**

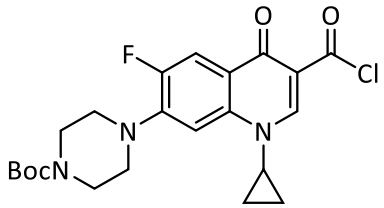

To a solution of compound **6** (0.2 g, 0.46 mmol) in dry DCM (5 ml) under argon atmosphere, oxalyl chloride (0.17 g, 1.38 mmol) and one drop of DMF were added. The reaction was stirred for 2 hours at 40 °C. After that time, the solvent was removed *in vacuo* to give 0.21 g (100%) of an orange solid that was immediately used in the next step.

***Tert*-butyl 4-(1-cyclopropyl-3-((((diphenylmethylene)amino)oxy)carbonyl)-6-fluoro-4-oxo-1,4-dihydroquinolin-7-yl)piperazine-1-carboxylate (7):**

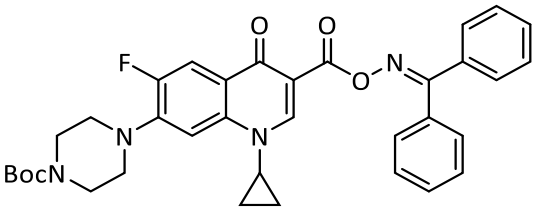

To a solution of compound **6** (0.21g, 0.46 mmol) in dry DCM (5 ml) under argon atmosphere, oxime **1** (0.09 g, 0.46 mmol) and pyridine (74 μl, 0.92 mmol) were added. The reaction was stirred at room temperature for 4 hours. Next, the solvent was removed *in vacuo*, and the resulting residue was purified by column chromatography (Hexane:THF 1:1), to give 0.17 g (59%) of white solid.

^{1}H-NMR (400 MHz, $CDCl_3$): δ 7.96 (s,1H), 7.83 (d, *J* = 13.2 Hz, 1H), 7.62 – 7.58 (m, 2H), 7.53 – 7.45 (m, 5H), 7.44 – 7.39 (m, 1H), 7.37 – 7.31 (m, 2H), 7.16 (d, *J* = 7.1 Hz, 1H), 3.64 – 3.57 (m, 4H), 3.37 – 3.30 (m, 1H), 3.20 – 3.14 (m, 4H), 1.49 (s, 9H), 1.20 – 1.13 (m, 2H), 0.94 – 0.87 (m, 2H).

^{13}C-NMR (100 MHz, $CDCl_3$): δ 172.6, 164.5, 161.3, 154.7, 151.7, 147.7, 144.3, 137.8, 135.0, 133.2, 130.8, 129.6, 129.2, 129.1, 128.4, 128.4, 122.8, 113.0, 108.2, 105.3, 80.2, 50.0, 43.6, 34.7, 28.5, 8.1.

HR-MS (ESI, [M+H]+): Calcd. for C35H35FN4O5 + H: 611.2664; Found: 611.2659

***Tert*-butyl 4-(3-((((9H-fluoren-9-ylidene)amino)oxy)carbonyl)-1-cyclopropyl-6-fluoro-4-oxo 1,4-dihydroquinolin-7-yl)piperazine-1-carboxylate (8):**

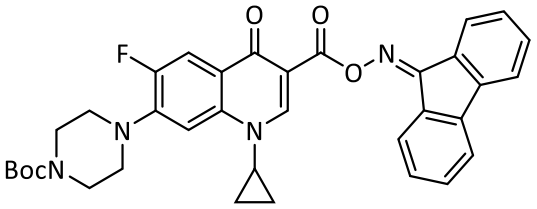

To a solution of compound **6** (0.21g, 0.46 mmol) in dry DCM (5 ml) under argon atmosphere, oxime **2** (0.09 g, 0.46 mmol) and pyridine (74 μl, 0.92 mmol) were added. The reaction was stirred at room temperature for 4 hours. Next, the solvent was removed *in vacuo*, and the resulting residue was purified by column chromatography (DCM:EtOAc 2:1), to give 0.14 g (51%) of white solid.

^{1}H-NMR (400 MHz, $CDCl_3$): δ 9.39-9.30 (m, 1H), 8.69 (s, 1H), 8.07 (d, *J* = 13.1 Hz, 1H), 7.98 (d, *J* = 7.5 Hz, 1H), 7.62 - 7.55 (m, 2H), 7.50 - 7.45 (m, 2H), 7.41 (td, *J* = 7.5, 1.0 Hz, 1H), 7.31 - 7.23 (m, 2H), 3.66 - 3.60 (m, 4H), 3.53 - 3.43 (m, 1H), 3.24 - 3.13 (m, 4H), 1.49 (s, 9H), 1.36 - 1.30 (m, 2H), 1.22 - 1.15 (m, 2H).

^{13}C-NMR (100 MHz, $CDCl_3$): δ 172.5, 164.8, 158.8, 154.7, 152.3, 149.7, 144.6, 142.2, 141.5, 138.1, 135.1, 132.5, 131.5, 131.5, 130.1, 129.3, 128.2, 123.4, 123.4, 120.1, 119.9, 113.7, 109.2, 105.2, 80.3, 50.0, 43.5, 34.9, 28.5, 8.3.
HR-MS (ESI, [M+H]+): Calcd. for C35H33FN4O5 + H: 609.2508; Found: 609.2502

***Tert*-butyl-4-(3-(((((2-aminophenyl)(phenyl)methylene)amino)oxy)carbonyl)-1-cyclopropyl-6-fluoro-4-oxo-1,4-dihydroquinolin-7-yl)piperazine-1-carboxylate (9):**

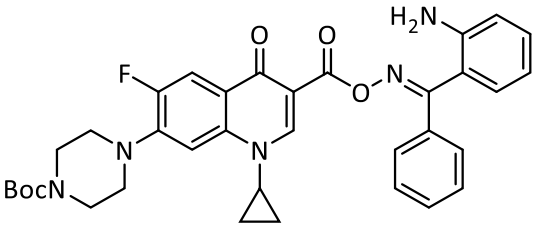

To a solution of compound **6** (0.21g, 0.46 mmol) in dry DCM (5 ml) under argon atmosphere, oxime **3** (0.10 g, 0.46 mmol) and pyridine (74 μl, 0.92 mmol) were added. The reaction was stirred at room temperature for 4 hours. Next, the solvent was removed *in vacuo*, and the resulting residue was purified by column chromatography (DCM:EtOAc 2:1), to give 0.14 g (49%) of white solid.
^{1}H-NMR (300 MHz, $CDCl_3$): δ 8.82 (s, 1H), 8.26 (d, *J* = 8.1 Hz, 1H), 8.05 (d, *J* = 13.2 Hz, 1H), 7.58 – 7.53 (m, 2H), 7.51 – 7.42 (m, 1H), 7.30 - 7.26 (m, 4H), 7.23 – 7.11 (m, 2H), 3.68 – 3.58 (m, 4H), 3.47 – 3.35 (m, 1H), 3.26 – 3.16 (m, 4H), 1.49 (s, 9H), 1.35 -1.28 (m, 2H), 1.16 – 1.06 (m, 2H).
^{13}C-NMR data are not available due to product decomposition in solution for long periods of time.
HR-MS (ESI, [M+H]+): Calcd. for C35H36FN5O5 + H: 626.2773; Found: 626.2797

***Tert*-butyl 4-(1-cyclopropyl-6-fluoro-4-oxo-3-((((2,3,4,5-tetraphenylcyclopenta-2,4-dien-1-ylidene)amino)oxy)carbonyl)-1,4-dihydroquinolin-7-yl)piperazine-1-carboxylate (10):**

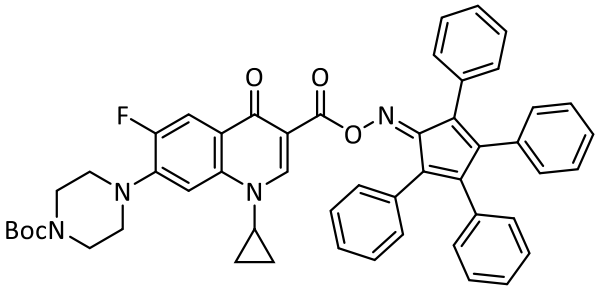

To a solution of compound **6** (0.21g, 0.46 mmol) in dry DCM (5 ml) under argon atmosphere, oxime **4** (0.18 g, 0.46 mmol) and pyridine (74 μl, 0.92 mmol) were added.

The reaction was stirred at room temperature for 4 hours. Next, the solvent was removed *in vacuo*, and the resulting residue was purified by column chromatography (DCM:EtOAc 2:1), to give 0.15 g (40%) of yellow solid.

^{1}H-NMR (300 MHz, $CDCl_3$): δ 7.90 (d, *J* = 13.1 Hz, 1H), 7.41 – 7.37 (m, 2H), 7.34 (s, 1H), 7.24 – 7.00 (m, 14H), 6.93 (tt, *J* = 7.4, 1.3 Hz, 1H), 6.86 (dt, *J* = 6.9, 1.4 Hz, 2H), 6.77 (dt, *J* = 7.0, 1.3 Hz, 2H), 3.67 – 3.59 (m, 4H), 3.23 – 3.11 (m, 5H), 1.50 (s, 9H), 1.20 – 1.14 (m, 2H), 0.93 – 0.88 (m, 2H).

^{13}C-NMR (75 MHz, $CDCl_3$): δ 172.7, 165.0, 160.1, 155.1, 154.7, 152.9, 151.8, 147.1, 146.9, 144.4, 137.8, 137.8, 136.3, 134.0, 133.3, 132.9, 132.2, 131.4, 130.4, 130.1, 129.9, 127.9, 127.9, 127.8, 127.8, 127.7, 127.5, 127.3, 126.2, 124., 122.70, 113.4, 108.1, 105.2, 80.3, 50.0, 43.4, 34.7, 28.5, 8.6.

HR-MS (ESI, [M+H]+): Calcd. for C51H45FN4O5 + H: 813.3447; Found: 813.3445

5.5 References

1. Gao, Y.; Song, J.; Shang, S.; Wang, D.; Li, J., Synthesis and antibacterial activity of oxime esters from dihydrocumic acid. *Bioresources* **2012,** *7*.
2. Liu, X.-H.; Cui, P.; Song, B.-A.; Bhadury, P. S.; Zhu, H.-L.; Wang, S.-F., Synthesis, structure and antibacterial activity of novel 1-(5-substituted-3-substituted-4,5-dihydropyrazol-1-yl)ethanone oxime ester derivatives. *Bioorganic & Medicinal Chemistry* **2008,** *16* (7), 4075-4082.
3. Zhao, H.; Zhou, M.; Duan, L.; Wang, W.; Zhang, J.; Wang, D.; Liang, X., Efficient Synthesis and Anti-Fungal Activity of Oleanolic Acid Oxime Esters. *Molecules* **2013,** *18*, 3615-3629.
4. Bednarczyk-Cwynar, B.; Zaprutko, L.; Marciniak, J.; Lewandowski, G.; Szulc, M.; Kaminska, E.; Wachowiak, N.; Mikolajczak, P. L., The analgesic and anti-inflammatory effect of new oleanolic acid acyloxyimino derivative. *European Journal of Pharmaceutical Sciences* **2012,** *47* (3), 549-555.
5. Chowdhury, N.; Dutta, S.; Dasgupta, S.; Singh, N. D. P.; Baidya, M.; Ghosh, S. K., Synthesis, photophysical, photochemical, DNA cleavage/binding and cytotoxic properties of pyrene oxime ester conjugates. *Photochemical & Photobiological Science* **2012,** *11* (7), 1239-1250.
6. Mukherjee, R.; Jaggi, M.; Siddiqui, M. J. A.; Srivastava, S. K.; Rajendran, P.; Vardhan, A.; Burman, A. C., Synthesis and cytotoxic activity of 3-O-acyl/3-hydrazine /2-bromo/20,29-dibromo betulinic acid derivatives. *Bioorganic & Medicinal Chemistry Letters* **2004,** *14* (15), 4087-4091.

7. Gass, L.; Bope, F. W., The Preparation of Some Derivatives of Oximes**College of Pharmacy, The Ohio State University, Columbus 10. *Journal of the American Pharmaceutical Association (Scientific ed.)* **1959,** *48* (3), 186-189.
8. Hassner, A.; Catsoulacos, P., A new synthesis of amines with diborane. *Chemical Communications (London)* **1967,** (12), 590-591.
9. Feuer, H.; Braunstein, D. M., Reduction of oximes, oxime ethers, and oxime esters with diborane. Novel synthesis of amines. *The Journal of Organic Chemistry* **1969,** *34* (6), 1817-1821.
10. Kumar, P.; Mukerjee, A. K., Acylation of Primary Amines by O-Acyl Oximes. *Synthesis* **1979,** *1979* (09), 726-727.
11. Fernández, S.; Menéndez, E.; Gotor, V., Oxime Esters as Acylating Agents in the Aminolysis Reaction. A Simple and Chemoselective Method for the Preparation of Amides from Amino Alcohols. *Synthesis* **1991,** *1991* (09), 713-716.
12. Hironori, T.; Koichi, N., Synthesis of Pyrrole Derivatives by the Heck-Type Cyclization of γ,δ-Unsaturated Ketone O-Pentafluorobenzoyloximes. *Chemistry Letters* **1999,** *28* (1), 45-46.
13. Tang, X.; Huang, L.; Qi, C.; Wu, W.; Jiang, H., An efficient synthesis of polysubstituted pyrroles via copper-catalyzed coupling of oxime acetates with dialkyl acetylenedicarboxylates under aerobic conditions. *Chemical Communications* **2013,** *49* (83), 9597-9599.
14. Xu, J.; Ma, G.; Wang, K.; Gu, J.; Jiang, S.; Nie, J., Synthesis and photopolymerization kinetics of oxime ester photoinitiators. *Journal of Applied Polymer Science* **2012,** *123* (2), 725-731.
15. Griller, D.; Mendenhall, G. D.; Van Hoof, W.; Ingold, K. U., Kinetic applications of electron paramagnetic resonance spectroscopy. XV. Iminyl radicals. *Journal of the American Chemical Society* **1974,** *96* (19), 6068-6070.
16. Hwang, H.; Jang, D.-J.; Chae, K. H., Photolysis reaction mechanism of dibenzophenoneoxime hexamethylenediurethane, a new type of photobase generator. *Journal of Photochemistry and Photobiology A: Chemistry* **1999,** *126* (1), 37-42.
17. Uchiyama, K.; Hayashi, Y.; Narasaka, K., Synthesis of dihydropyrroles by the intramolecular addition of alkylideneaminyl radicals generated from O-2,4-dinitrophenyloximes of γ,δ-unsaturated ketones. *Tetrahedron* **1999,** *55* (29), 8915-8930.
18. Groenenboom, C. J.; Hageman, H. J.; Oosterhoff, P.; Overeem, T.; Verbeek, J., Photoinitiators and photoinitiation Part 11. The photodecomposition of some O-acyl 2-oximinoketones. *Journal of Photochemistry and Photobiology A: Chemistry* **1997,** *107* (1), 261-269.

19. Miyake, Y.; Takahashi, H.; Akai, N.; Shibuya, K.; Kawai, A., Structure and Reactivity of Radicals Produced by Photocleavage of Oxime Ester Compounds Studied by Time-resolved Electron Paramagnetic Resonance Spectroscopy. *Chemistry Letters* **2014,** *43* (8), 1275-1277.
20. Karamtzioti, P.; Papastergiou, A.; Stefanakis, J. G.; Koumbis, A. E.; Anastasiou, I.; Koffa, M.; Fylaktakidou, K. C., O-Benzoyl pyridine aldoxime and amidoxime derivatives: novel efficient DNA photo-cleavage agents. *Medicinal Chemistry Communications* **2015,** *6* (4), 719-726.
21. McBurney, R. T.; Harper, A. D.; Slawin, A. M. Z.; Walton, J. C., An all-purpose preparation of oxime carbonates and resultant insights into the chemistry of alkoxycarbonyloxyl radicals. *Chemical Science* **2012,** *3* (12), 3436-3444.
22. McBurney, R. T.; Eisenschmidt, A.; Slawin, A. M. Z.; Walton, J. C., Rapid and selective spiro-cyclisations of O-centred radicals onto aromatic acceptors. *Chemical Science* **2013,** *4* (5), 2028-2035.
23. Upadhayaya, R. S.; Shinde, P. D.; Kadam, S. A.; Bawane, A. N.; Sayyed, A. Y.; Kardile, R. A.; Gitay, P. N.; Lahore, S. V.; Dixit, S. S.; Földesi, A.; Chattopadhyaya, J., Synthesis and antimycobacterial activity of prodrugs of indeno[2,1-c]quinoline derivatives. *European Journal of Medicinal Chemistry* **2011,** *46* (4), 1306-1324.
24. Pasolli, M.; Dafnopoulos, K.; Andreou, N.-P.; Gritzapis, P. S.; Koffa, M.; Koumbis, A. E.; Psomas, G.; Fylaktakidou, K. C., Pyridine and p-Nitrophenyl Oxime Esters with Possible Photochemotherapeutic Activity: Synthesis, DNA Photocleavage and DNA Binding Studies. *Molecules* **2016,** *21*, 864.
25. Savjani, K. T.; Gajjar, A. K.; Savjani, J. K., Drug solubility: importance and enhancement techniques. *ISRN Pharm* **2012,** *2012*, 195727-195727.
26. Le Garrec, D.; Ranger, M.; Leroux, J.-C., Micelles in anticancer drug delivery. *American Journal of Drug Delivery* **2004,** *2* (1), 15-42.
27. Seedher, N.; Kanojia, M., Micellar solubilization of some poorly soluble antidiabetic drugs: a technical note. *AAPS PharmSciTech* **2008,** *9* (2), 431-436.
28. Wang, Q.; Jiang, J.; Chen, W.; Jiang, H.; Zhang, Z.; Sun, X., Targeted delivery of low-dose dexamethasone using PCL–PEG micelles for effective treatment of rheumatoid arthritis. *Journal of Controlled Release* **2016,** *230*, 64-72.
29. Kedar, U.; Phutane, P.; Shidhaye, S.; Kadam, V., Advances in polymeric micelles for drug delivery and tumor targeting. *Nanomedicine: Nanotechnology, Biology and Medicine* **2010,** *6* (6), 714-729.
30. Gou, M.; Men, K.; Shi, H.; Xiang, M.; Zhang, J.; Song, J.; Long, J.; Wan, Y.; Luo, F.; Zhao, X.; Qian, Z., Curcumin-loaded biodegradable polymeric micelles for colon cancer therapy in vitro and in vivo. *Nanoscale* **2011,** *3* (4), 1558-1567.

31. Zhang, W.; Shi, Y.; Chen, Y.; Ye, J.; Sha, X.; Fang, X., Multifunctional Pluronic P123/F127 mixed polymeric micelles loaded with paclitaxel for the treatment of multidrug resistant tumors. *Biomaterials* **2011,** *32* (11), 2894-2906.
32. Lavasanifar, A.; Samuel, J.; Kwon, G. S., Poly(ethylene oxide)-block-poly(l-amino acid) micelles for drug delivery. *Advanced Drug Delivery Reviews* **2002,** *54* (2), 169-190.
33. Aliabadi, H. M.; Lavasanifar, A., Polymeric micelles for drug delivery. *Expert Opinion on Drug Delivery* **2006,** *3* (1), 139-162.
34. Liu, S.; Yu, Y.; Liebeskind, L. S., N-Substituted Imines by the Copper-Catalyzed N-Imination of Boronic Acids and Organostannanes with O-Acyl Ketoximes. *Organic Letters* **2007,** *9* (10), 1947-1950.
35. Ji, C.; Miller, P. A.; Miller, M. J., Syntheses and Antibacterial Activity of N-Acylated Ciprofloxacin Derivatives Based on the Trimethyl Lock. *ACS Medicinal Chemistry Letters* **2015,** *6* (6), 707-710.

Chapter 6

Irreversible Control of Quinolone Derivatives Using BODIPYs

6.1 Introduction

Gaining control over a drug's activity using a photoreleasable protective group is a widely used strategy that allows the activation of the pharmaceutical agent in a specific target. Nowadays, the development of new photocleavable groups is evolving towards molecules absorbing in the visible region, since these types of PPGs have been less explored than its analogs absorbing in the UV region. What makes this property extremely interesting in the photocontrol of bioactive molecules is the possibility of using light inside the therapeutic window to carry out the release process, which will allow their use in living tissues.

This chapter is a continuation of the previous one, where initial studies about the irreversible control of quinolone derivatives were described. Herein, a new PPG will be used to try to solve some of the drawbacks of oxime esters. The new photolabile group will be covalently attached to the structure of a quinolone to generate an irreversible system whose antibacterial properties could be controlled using light.

6.1.1 BODIPYs

Boron-dipyrromethenes, also known as BODIPYs, are becoming a popular protective group for the photorelease of bioactive molecules. Among their characteristics, BODIPYs have sharp and tunable absorption throughout the visible/NIR region, they are thermally stable in the dark and have high molar absorption coefficients. As has been previously mentioned, BODIPYs have three different positions where the leaving group can be linked (see chapter 2, section 2.5.3). However, in this chapter, only *meso*-substituted BODIPYs will be discussed.

The *meso*-methyl BODIPY PPG was discovered in 2015 by Winter[1] and Weinstain.[2] The structure of these molecules is a derivatization of the boron dipyrromethene core that introduces a methylhydroxy moiety at the *meso*-position. Several molecules of interest can be linked through this position, including acids,[3] alcohols,[3] and amines.[4] The versatility of this PPG makes it of great interest to cage different bioactive compounds.

The mechanism of the release reaction is not fully understood yet, but some propositions have been made. It was suggested that the release of the leaving group occurs through a photochemical S_N1 reaction via a carbocation intermediate and consecutive nucleophilic attack of the solvent.[5] The leaving group is released in a heterolytic fission that results in a *meso*-methyl cation as an intermediate. This carbocation can either recombine to regenerate the starting material, which may be

the major nonradiative deactivation process, or be attacked by a nucleophile. When the solvent acts as the nucleophile, a solvolysis reaction takes place.

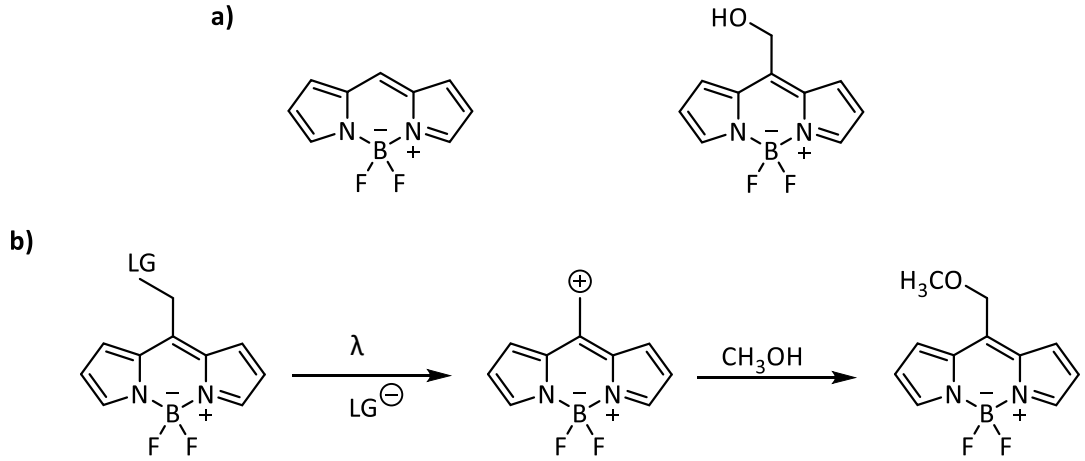

Figure 1. Structure and release process of *meso*-methyl BODIPY. a) On the left, boron dipyrromethene core. On the right, substitution at the *meso*-position with the methylhydroxy moiety enables the attachment of a leaving group. b) Proposed mechanism of photorelease. The irradiation of the BODIPY results in the release of the leaving group (LG) and the generation of a carbocation at the secondary position, which suffers a nucleophilic attack by the solvent.

Despite being a new type of PPG, *meso*-substituted BODIPYs have been already employed in drug release to achieve spatial and temporal control of some pharmacological agents.

In 2020, Szymanski, Feringa, and co-workers designed a red-sensitive BODIPY able to control heart rhythm.[6] Extending the π-system of boron dipyrromethene by adding styryl groups, they achieved a significant bathochromic shift in the absorption of the compound. Additionally, the fluorinated atoms on the boron in the BODIPY core were exchanged by methyl groups to increase the quantum yield of release. The selected drug to be released was dopamine, which plays an important role in regulating cardiac function. The activity of the BODIPY containing dopamine was tested before and after irradiation with red light on *in vitro* beating human embryonic stem cell (hESC). The activity of the compound after irradiation was similar to the activity of dopamine, although the compound before irradiation still exhibited some residual activity. The results obtained proved that BODIPYs could have a potential used in medical therapy as PPGs.

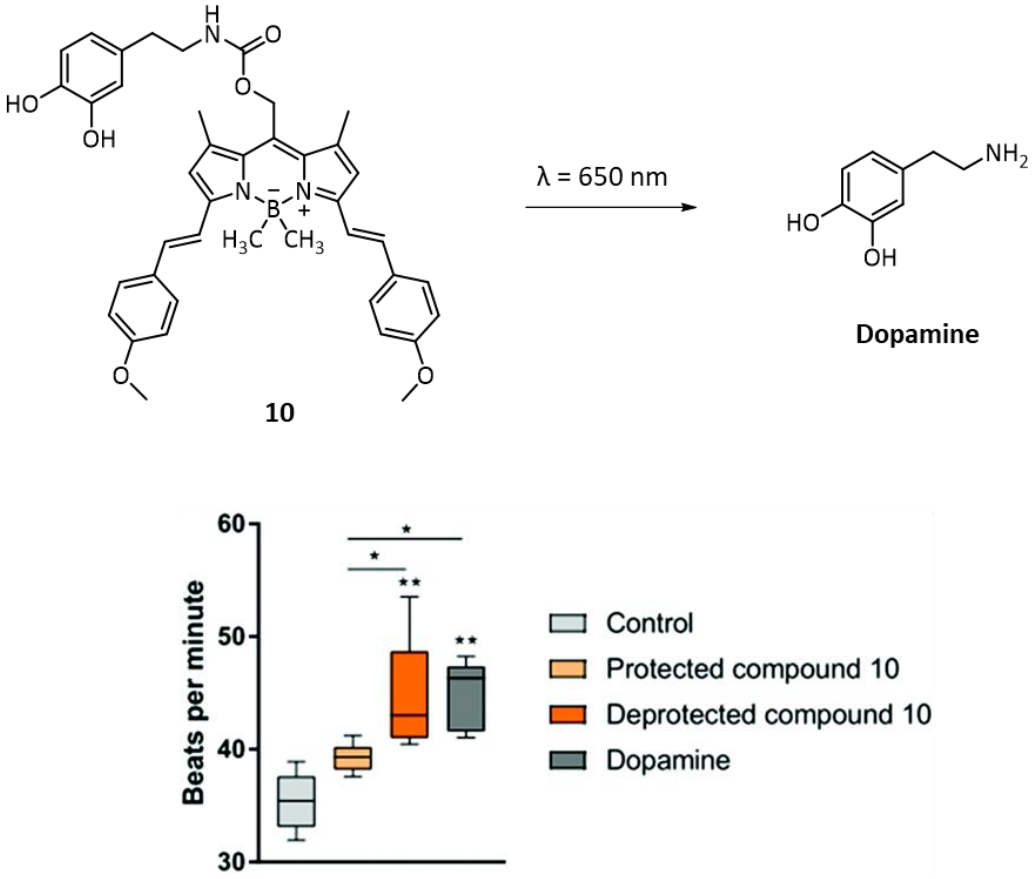

Figure 2. Control of heart rhythm using light. When protected dopamine (**10**) is irradiated with red light (650 nm), the deprotected drug is obtained. The graphic shows the results obtained. The protected form of **10** (BODIPY containing dopamine) displayed some residual activity as the beats per minute measured were slightly higher than those for the control. When compound **10** is irradiated with red light, dopamine is released (deprotected compound **10**), which exhibited similar values as the one obtained for the dopamine control. Adapted by permission from reference 6. Copyright © The Royal Society of Chemistry 2020.

Besides this work, *meso*-substituted BODIPYs have been employed to achieve controlled release of some anticancer drugs.[7-8] Although there are not many examples in the bibliography of their use as PPG for drugs, due to their recent discovery, BODIPYs are promising candidates in this area.

6.2 Results

6.2.1 Design of photoreleasable antibiotics using BODIPYs

The design of these photoreleasable antibiotics displays some similarities with the ones explained in the previous chapter. Their structure can be divided into two parts: a quinolone antibiotic and a PPG, which in this case, is a BODIPY. As the antibiotics part, nalidixic acid and ciprofloxacin were selected, both belonging to the quinolone family. Regarding the protective group, we chose BODIPYs because of their ability to

carry out the release process with visible light. Different *meso*-substituted BODIPYs were synthesized in order to achieve a bathochromic shift in their absorption range, as well as to improve their water solubility. Thanks to the methylhydroxy moiety, the antibiotic part can be combined with the PPG through the acid group at position 3. We envisioned that once the corresponding quinolone was protected with the BODIPY, its antibiotic properties would be severely affected, ideally, to the point of deactivation. Subsequently, when the protected antibiotic would be irradiated with visible light, the quinolone would be released in its acid form, recovering its properties. This would create an irreversible system that would allow the optical control of quinolones and, could be compatible with biological applications.

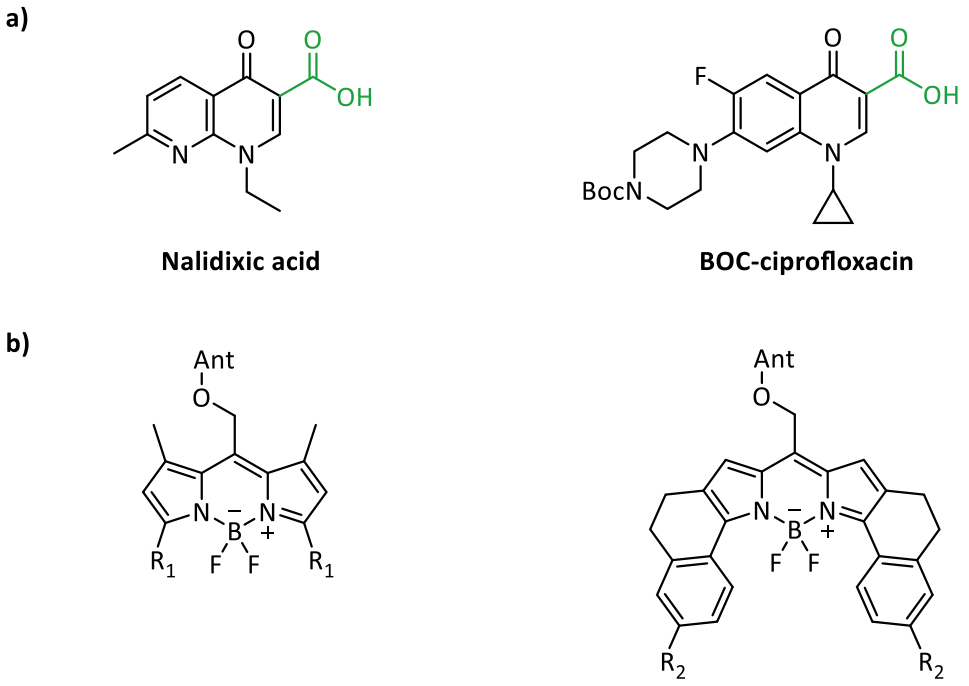

Figure 3. Structures of quinolone antibiotics and their photoreleasable derivatives. a) Structure of nalidixic acid and Boc-ciprofloxacin, first- and second-generation quinolones. Position 3 with the acid group is highlighted in green. b) Structure of BODIPY protected antibiotics. The antibiotic part is represented as Ant to simplify.

6.2.2 Synthesis

The synthesis of photoreleasable quinolones using BODIPYs as PPGs is described in the next paragraphs. First, two different photoreleasable groups were synthesized following the procedure described by Winter and co-workers for the synthesis of *meso*-substituted BODIPYs.[3]

Scheme 1

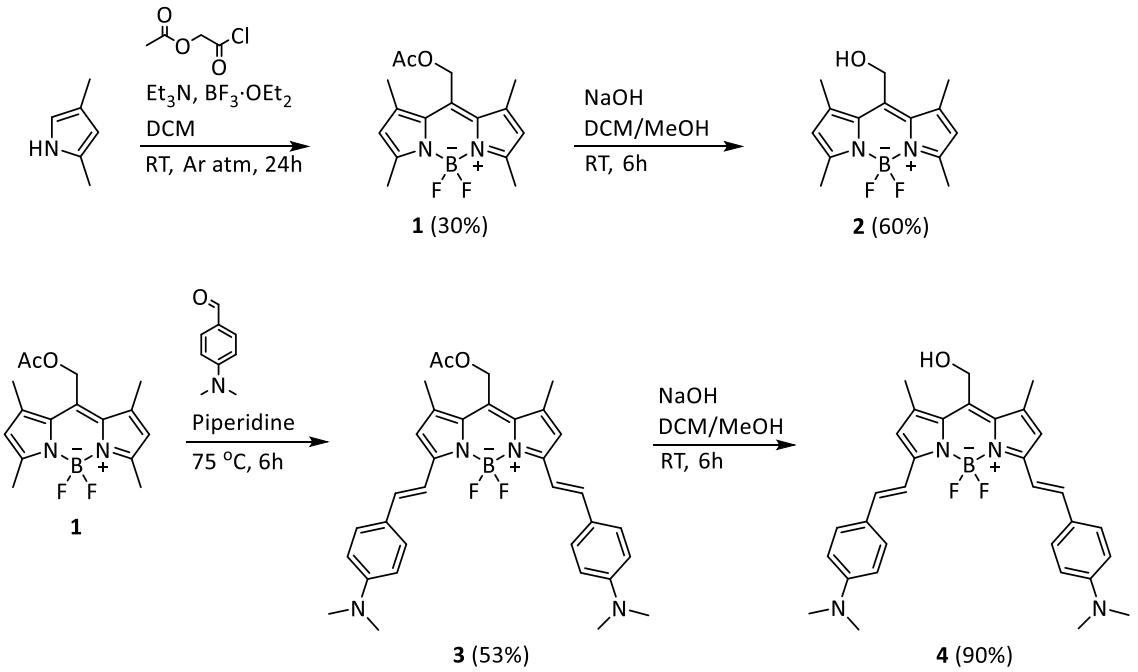

The first step was a condensation between acetoxyacetyl chloride and 2,4-dimethylpyrrole followed by *in situ* complexation with boron trifluoride diethyl etherate in the presence of a base to give **1**. Next, conversion to the *meso*-methylhydroxy BODIPY **2** was achieved upon ester hydrolysis.

For the second protective group synthesis, a condensation reaction was carried out between compound **1** and 4-(dimethylamino)benzaldehyde in the presence of piperidine as a catalyst to obtain **3**. Lastly, conversion to the *meso*-methylhydroxy form upon ester hydrolysis gave **4**.

Then, the protection of the antibiotics with the two synthesized BODIPYs was carried out. Unfortunately, the procedure described in the bibliography for this step,[3] which involved an acid group and a coupling agent in the presence of a base, did not work. Because no final product was observed, it seemed like this was not an effective method for the coupling between the quinolone and the BODIPY. Hence, a new route was designed for this step. By taking advantage of the reactivity studied in the previous chapter, the acyl chloride of the antibiotics was prepared, and the coupling reaction with the BODIPY was made in the presence of a base. The synthesis of the photoreleasable derivatives of nalidixic acid is described in scheme 2.

Scheme 2

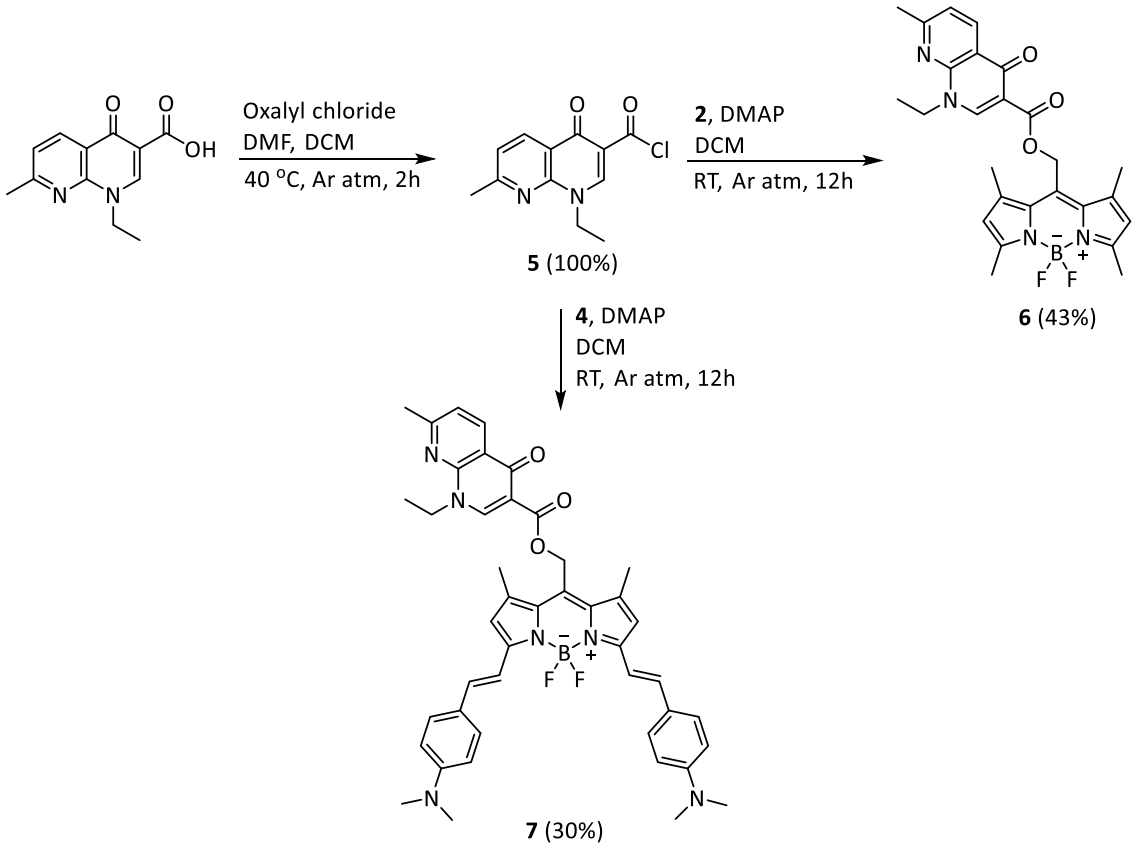

The route started with nalidixic acid, a commercially available quinolone. The acyl chloride form **5** was prepared using oxalyl chloride and DMF as a catalyst. Subsequently, the coupling with the BODIPY moiety was made in the presence of a base to give **6** and **7**.

A similar procedure was used to achieve the ciprofloxacin derivatives. The route is described in scheme 3.

Scheme 3

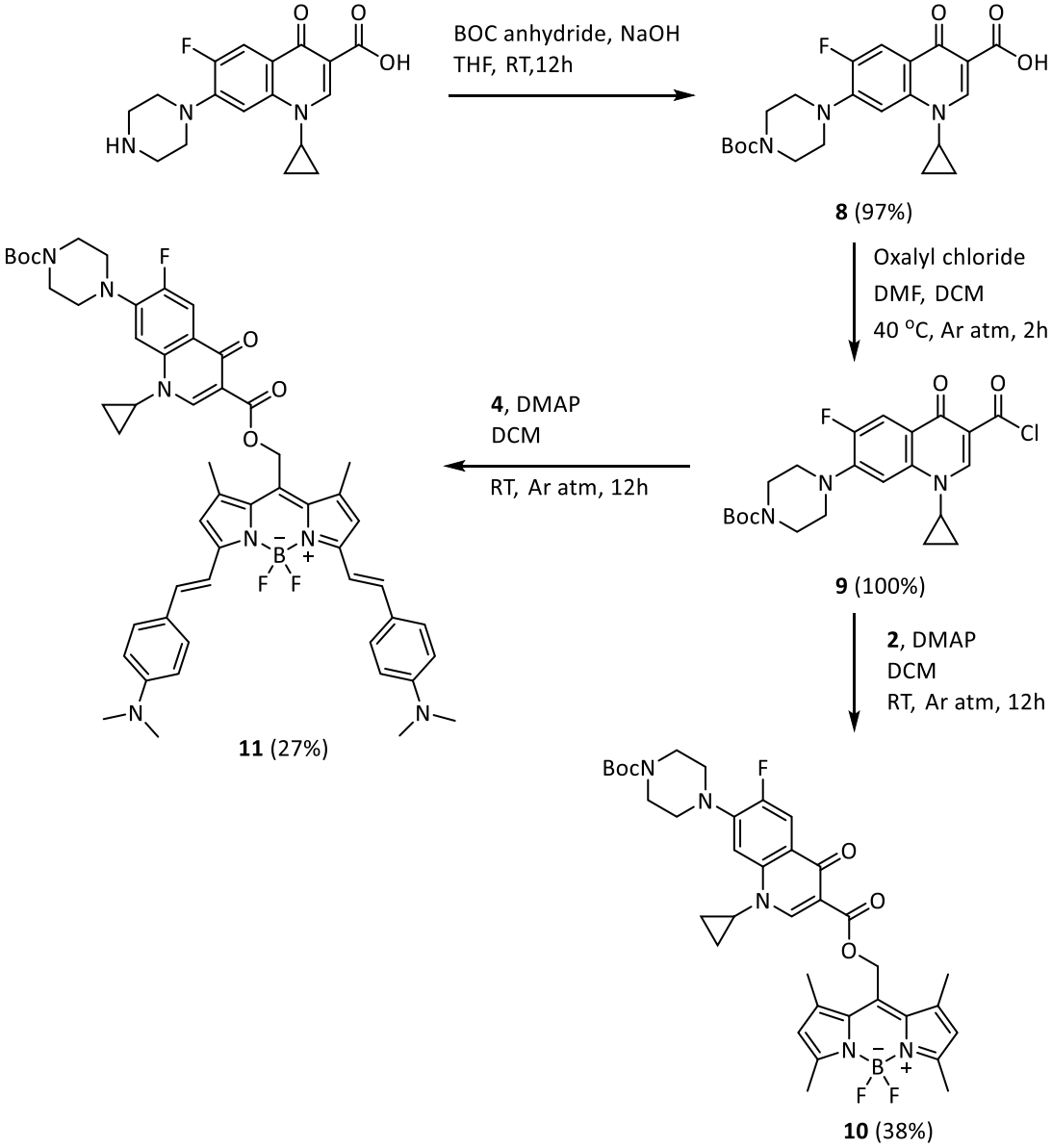

In the case of ciprofloxacin, a previous step to protect the secondary amine in the piperazine unit was performed. The protection was carried out using Boc anhydride to form **8**. Next, the acyl chloride was made using oxalyl chloride and DMF as a catalyst to give **9**. Finally, the coupling reaction with both BODIPY moieties was possible in the presence of a base to obtain **10** and **11**.

6.2.3 Photochemical properties

Once the photoreleasable quinolone derivatives were synthesized, their photochemical properties were explored. As explained in previous chapters, the data obtained from this study gives information about the conditions needed to induce the

photoreaction, which in this case involves the release of the antibiotics. Besides, the performance of the different photoreleasable groups was evaluated.

When designing the molecules, the BODIPY part was chosen according to the data displayed in the bibliography.[3] Thus, a simpler structure (**2**) was initially synthesized to test the viability of the route. Then, a second structure (**4**) was selected based on its range of absorption, well above the lower limit for the therapeutic window. After the coupling reaction of Boc-ciprofloxacin or nalidixic acid with the corresponding BODIPY, the UV-Vis spectra of the final products were recorded. The samples were prepared in concentrations close to 5E-5M, and all of them were dissolved in dichloromethane.

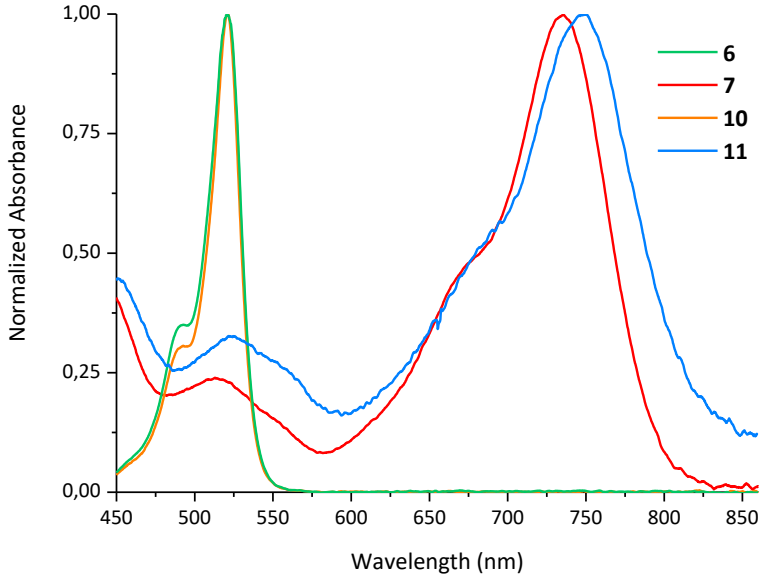

Figure 4. UV-Vis spectra of the photoreleasable quinolones derivatives. All compounds were dissolved in DCM in a concentration close to 5E-5M.

The results displayed in figure 4 are in agreement with the ones found in the bibliography. Compounds **6** and **10** bearing the BODIPY with a simpler structure displayed absorption in the green region of the spectrum, both with the maximum absorption at 520 nm. A large bathochromic shift took place when the conjugation of the BODIPY part was elongated through the addition of two (dimethylamino)-styryl groups. Compounds **7** and **11**, bearing this BODIPY displayed absorption in the red/NIR region of the spectrum with the maximum absorption at 735 and 744 nm, respectively. Hence, the presence of the (dimethylamino)-styryl groups, induces a shift of more than 200 nm in the maximum absorption.

Besides, all the compounds presented high molar absorption coefficients, a common feature of BODIPYs. A summary of the information obtained from the UV-Vis spectra can be found in table 1.

Table 1. Maximum absorption and molar extinction coefficient of photoreleasable quinolone derivatives

Compound	λ_{max} (nm)	ε ($M^{-1}cm^{-1}$)
6	520	60500
7	735	58400
10	520	56200
11	744	52900

The selection of adequate light sources to carry out the irradiation of the samples was made according to the information obtained from this experiment. For compounds **6** and **10**, a 30 W RGB LED lamp was employed in green light mode. Compound **7** and **11** were irradiated using a 515 mW far-red LED lamp. The emission spectra of both light sources are displayed in figure 5. All samples were irradiated in a concentration close to 256 μg/ml of antibiotic, considering a total release, and the sample volume was 1 ml. Compounds were dissolved in mixtures of dimethyl sulfoxide and water in different proportions, 60:40 for **6** and **10**, and 80:20 for **7** and **11**. The irradiation process was followed by mass spectroscopy and HPLC over time (see figure 6).

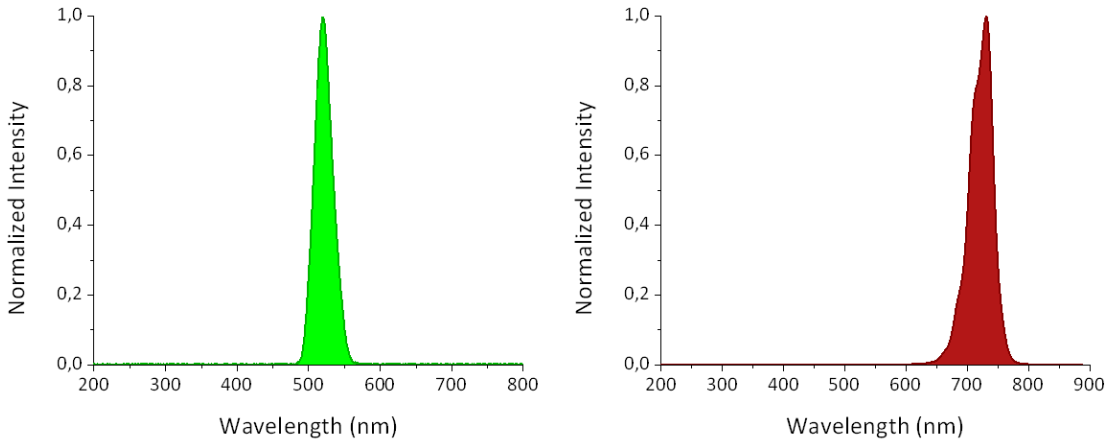

Figure 5. Emission spectra of the visible light sources employed to induce the release of the antibiotics. On the left, emission spectrum of the 30 W RGB LED lamp in green mode. On the right, emission spectrum of the 515 mW far-red LED lamp.

Compounds **6** and **10** showed a total release of the antibiotic when irradiated with the green LED lamp in 24 and 18 hours, respectively. Compounds **7** and **11** achieved a total release of the antibiotic in 58 and 44 hours, respectively, when irradiated with the far-red LED. This increment of time due to the lower potency of the LED lamp employed. In all cases, the release reaction was carried out until completion, and no products of decomposition were observed.

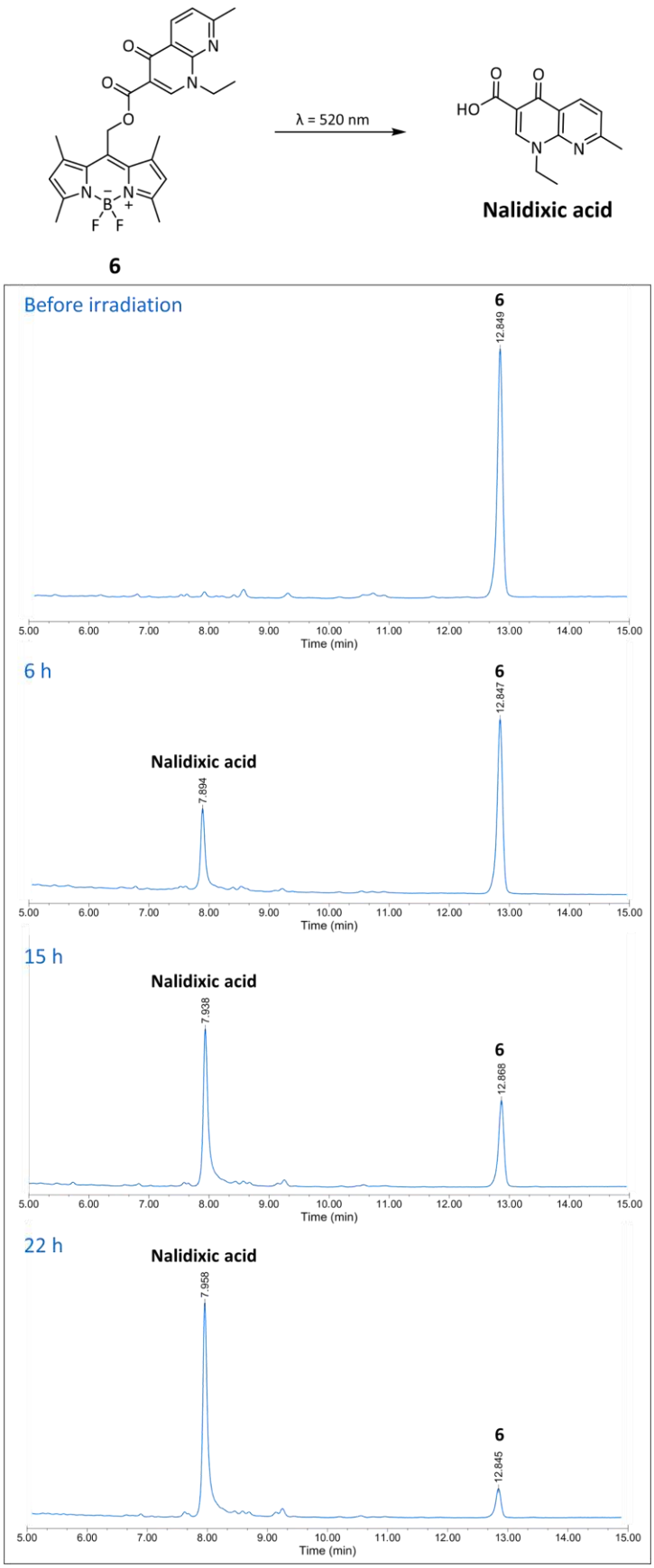

Figure 6. Irradiation of compound **6** followed by HPLC at 0, 6, 15, and 22 hours of exposure to the green LED lamp. As the release process takes place, the peak corresponding to the antibiotic (t_R = 7.9 min) increases while the peak of the protected compound **6** (t_R = 12.8 min) decreases.

Initially, the irradiation times to obtain a total release might seem long, but this is due to the sample concentration employed for this assay. Whereas higher concentrations allow better visualization of the results with the techniques employed to follow the irradiation process, in reality, biological applications require considerably lower volumes and concentrations of the antibiotic.

Additionally, the stability of the compounds at room temperature was measured. The samples were kept in the dark for 5 days, and no release or products of decomposition were observed by ^{1}H-NMR or HPLC after that time.

To finishing the photochemical study, the quantum yield of release was measured for all the derivatives. This factor relates the number of antibiotic molecules released with the number of photons absorbed by the photocleavable system. The resulting value is the number of photons that effectively participate in the fission of the C-O bond to release the leaving group.

$$\Phi = \frac{\text{number of molecules of antibiotic released}}{\text{number of photons absorbed by the photoreleasable system}}$$

Equation 2. Equation expressing the quantum yield of release in the photocleavable system.

The quantum yield of compounds **6** and **10** was calculated using potassium diamminetetrakis(thiocyanato-*N*) chromate, commonly known as Reinecke's salt, as an actinometer. Reinecke's salt was selected because its quantum yield was known accurately at 504 nm, which is close to the maximum absorption of the compounds under study.[9] The experimental procedure for the measures of the quantum yield is described in section 6.6.2.1.

The quantum yield for the release of the antibiotics of compounds **6** and **10** was 0.008% in both cases. Although this number is low, the value is in agreement with the published data by Winter and co-workers.[3]

The use of Reinecke's salt in the red/NIR region of the spectrum is limited due to its low absorbance. Thus, compounds **7** and **11** required a different method for measuring their quantum yield since their maximum absorption appears at 735 and 744 nm. Inspired by the work of Riedle and co-workers,[10] the quantum yield of these two compounds was measured instrumentally. The photonic flux emitted by the light source, as well as the number of photons not absorbed by the sample, were determined using an Ocean Optics USB4000-UV-Vis detector equipped with a cosine corrector. The light source from a 515 mW far-red LED (see figure 5) was imaged into the sample contained in a quartz cuvette of 1 cm path length with a focusing lens. The

use of the lens assures an efficient utilization of the available photons as well as a bigger control and reproducibility of the measurement. In order to ensure the correct irradiation of the total volume of the sample, the cuvette was provided with a magnetic stirrer. Last, a second lens focused the light not absorbed by the sample into the cosine corrector. A schematic representation of the setup used can be seen in figure 7. Additional details about the experimental procedure followed for this method can be found in section 6.6.2.2.

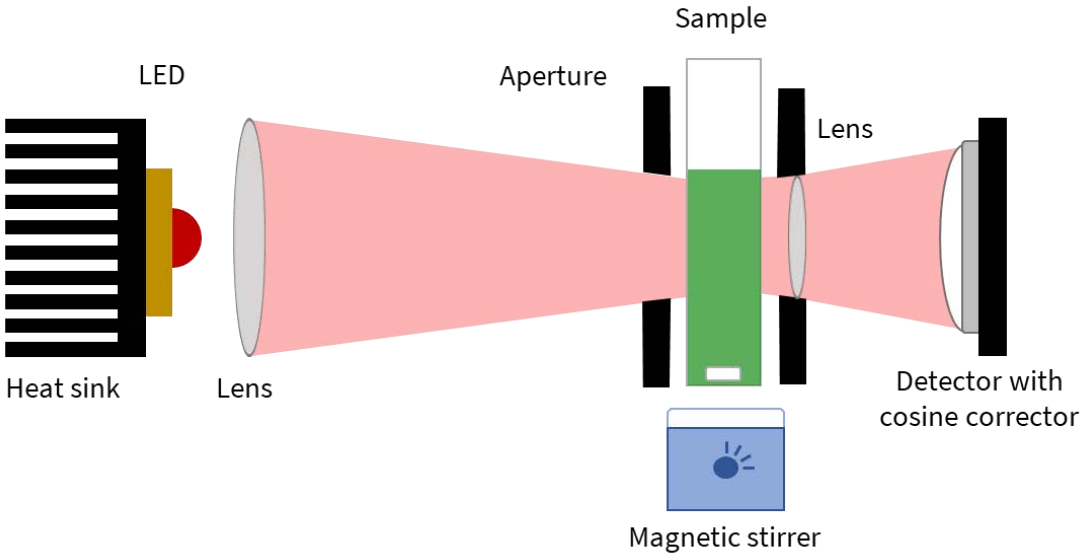

Figure 7. Schematic representation of the instrumental setup used to measure the quantum yield, inspired by Riedle's work.[10] The light emitted by the LED is focused through a lens and imaged into the sample equipped with a magnetic stirrer. The radiation not absorbed by the sample is collected by a cosine corrector.

The estimated values of quantum yield for the release of the antibiotics of compounds **7** and **11** were 0.003% in both cases. These values are lower than the ones obtained for the compounds absorbing in the green region, which means that the release process is less efficient.

In addition, this method was also employed to calculate the quantum yield of the compounds absorbing in the green region **6** and **10**, previously done with the actinometer. The resulting quantum yield with the instrumental setup was 0.006% for both compounds. which is close to the previous value 0.008% measured with the actinometer. However, both methods should not be directly compared since they have different sources of error associated.

6.3 Design of a new *meso*-substituted BODIPY structure

This section of the thesis was developed during a pre-doctoral stay in the group of Professor Arthur Winter at Iowa State University. The name of Professor Winter has been mentioned several times during this chapter as one of the discoverers of the *meso*-substituted BODIPY PPG. Not only that but, in recent years, Winter's work has become one of the main contributions of this topic in high impact scientific journals.

The objective of this pre-doctoral stay was to design, synthesize, and study the photochemical properties of a new type of *meso*-substituted BODIPY. Some of the desired characteristics of this new compound were absorption inside the therapeutic window, water solubility to ensure its safe use in biological applications, and better release efficiency. With the aim to fulfill these requisites, the structure of the new BODIPY included an extended π-system and glycol chains. The synthetic route of this new derivative is described in scheme 4. A more detailed version can be found in section 6.6.4.2.

Scheme 4

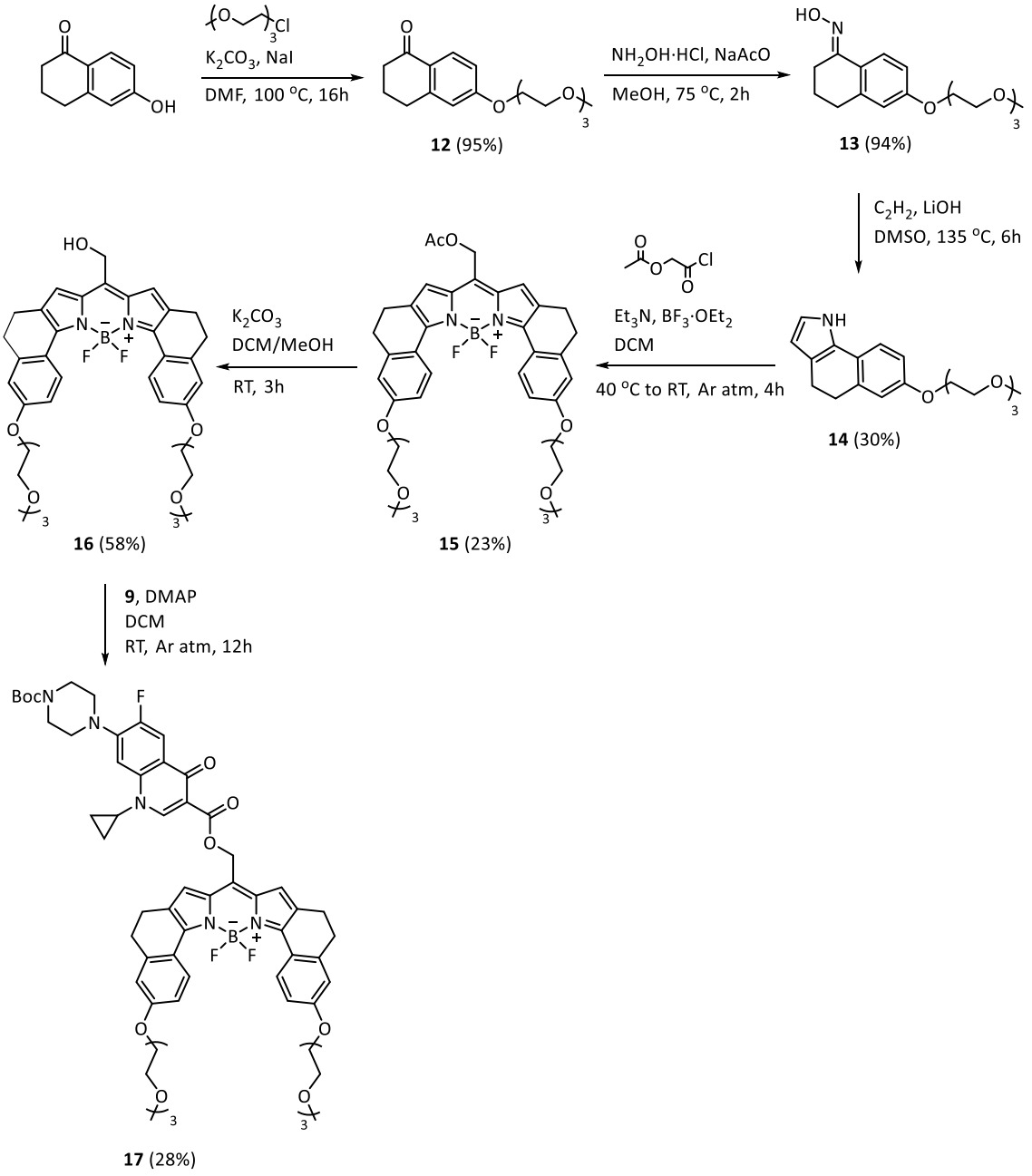

The first step was an O-alkylation of 6-hydroxy-1-tetralone to introduce the glycol chain and give ketone **12**. Next, oxime **13** was obtained by condensation of ketone **12** with hydroxylamine. Then, pyrrole **14** was formed via a Trofimov reaction between oxime **13** and acetylene in the presence of a strong base. The synthesis of the BODIPY was carried out following the common methodology, which involves a condensation between acetoxyacetyl chloride and pyrrole **14**, followed by *in situ* complexation with boron trifluoride diethyl etherate in the presence of a base resulting in **15**. After that, conversion to the *meso*-methylhydroxy BODIPY **16** was achieved upon ester hydrolysis. Finally, the coupling reaction between the acyl

chloride form of Boc-ciprofloxacin **9**, and **16** gave the protected form of the antibiotic **17**.

After the synthesis of compound **17**, a photochemical study was performed. Initially, the UV-Vis spectrum was recorded in order to know the range of absorption.

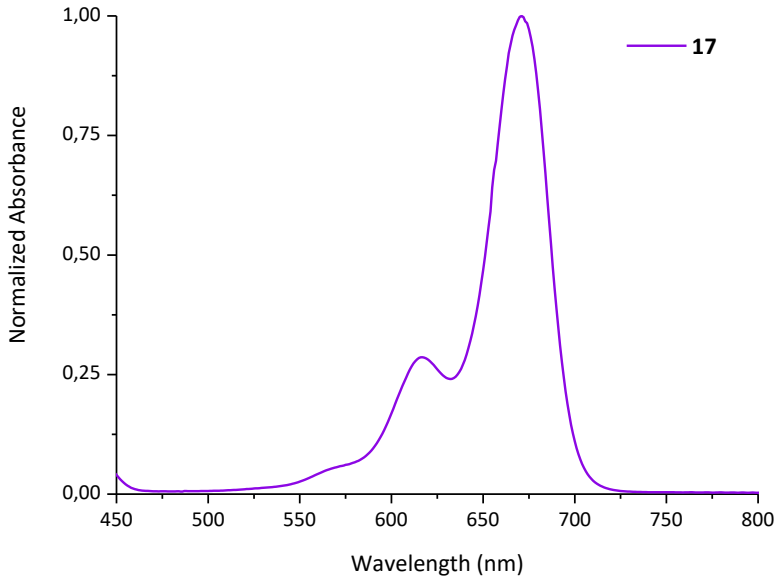

Figure 8. UV-Vis spectra of compound **17**, a photoreleasable derivative of Boc-ciprofloxacin. The sample was prepared in a concentration close to 5E-5M using DCM as a solvent.

As shown in figure 8, the new derivative displayed strong absorption in the visible region, and more importantly, inside the therapeutic window. The range of absorption was centered between 600-700 nm, with the maximum absorption at 671 nm. As in previous examples, compound **17** had a high molar extinction coefficient of 80500 $M^{-1}cm^{-1}$.

The irradiation of the BODIPY was carried out using a halogen lamp with a water filter to prevent heating of the sample and was followed by ^{1}H-NMR over time. The sample was prepared in a concentration of 256 μg/ml of antibiotic, considering a total release, and a volume of 1 ml.

The new derivative was able to release the antibiotic completely after 260 minutes of irradiation. The evolution of the irradiation can be seen in figure 9. As the irradiation time increases, the release process advances, and the signals corresponding to the antibiotic grow. At the same time, the signals corresponding to the protected compound **17** decrease. The byproduct of the photocage was not soluble at the concentration required for ^{1}H-NMR and precipitated.

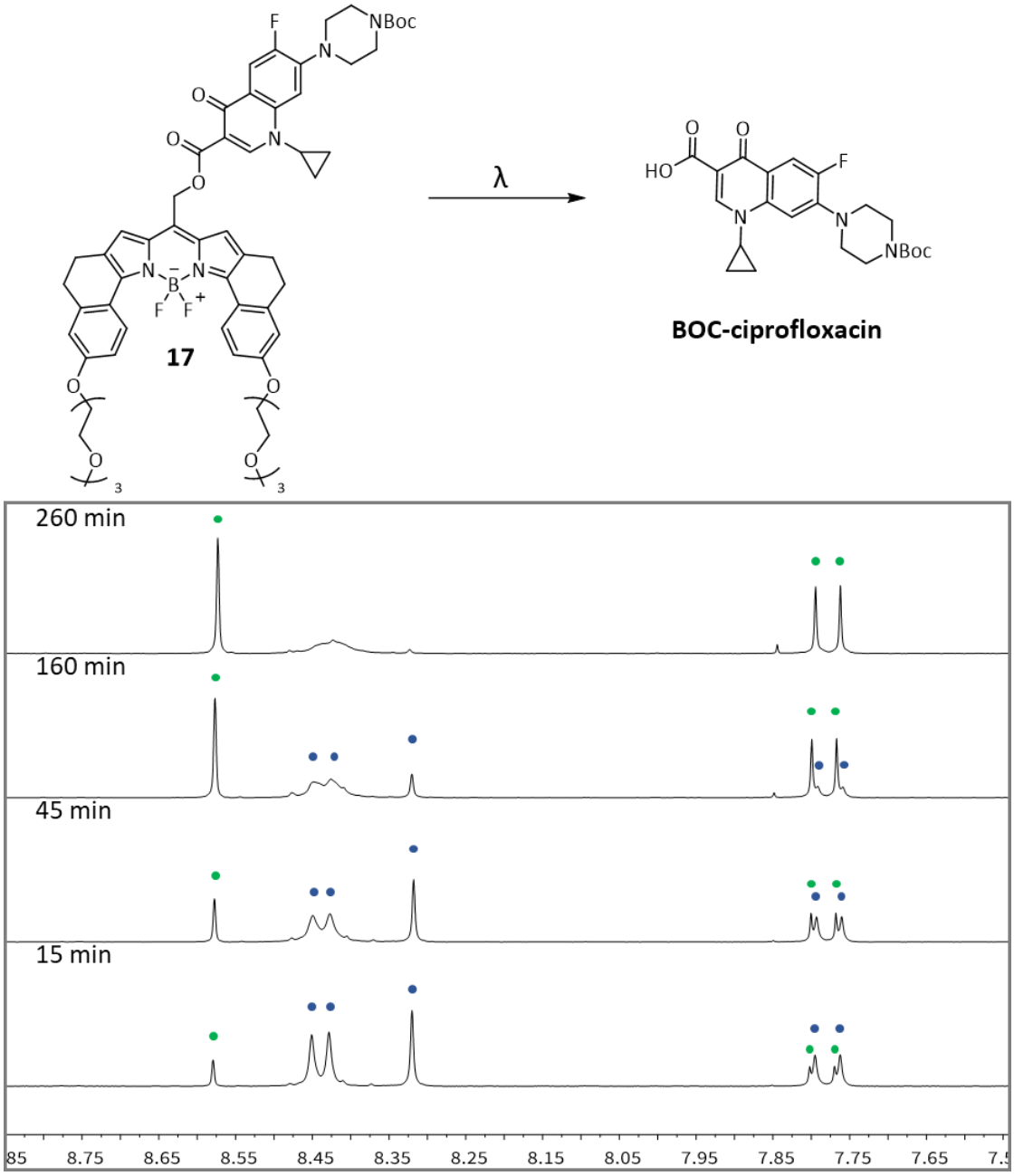

Figure 9. Irradiation of compound **17** followed by ^{1}H-NMR at 15, 45, 160, and 260 minutes of exposure to the halogenated lamp. As the release process takes place, the signals corresponding to the antibiotic (in green) increase, whereas the signals of the protected compound **17** (in blue) decrease.

After achieving the release of the ciprofloxacin derivative, a fraction of the final compound was sent to the University of La Rioja to complete the photochemical study by measuring its quantum yield and, finally, to test its antibacterial activity.

As with previous samples absorbing in the red region in the spectrum, the quantum yield of compound **17** was measured instrumentally. In this occasion, a 30 W RGB LED lamp in red light mode was employed to induce the photoreaction. The emission spectrum of the red LED can be seen in figure 10. Although this lamp did not

cover the maximum absorption region, a significant part of the emitted light was inside the absorption range of **17**.

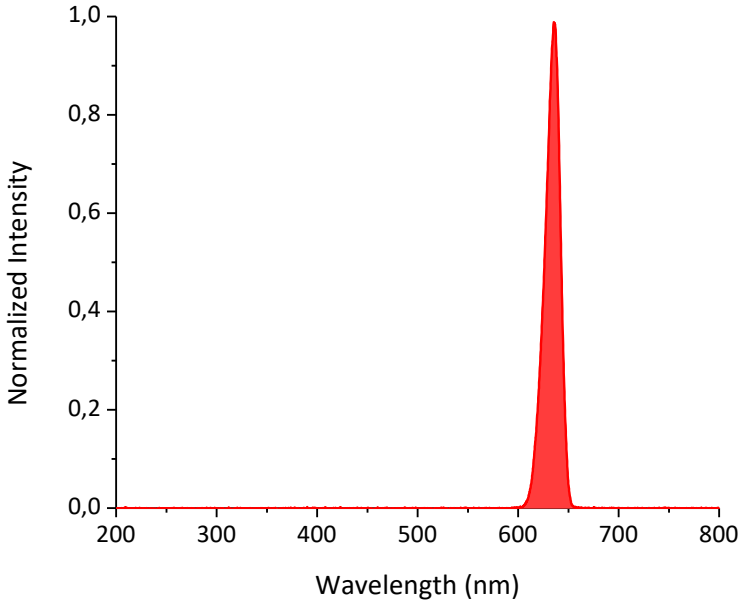

Figure 10. Emission spectra of the 30 W RGB LED lamp in red light mode, employed to carry out the release of the antibiotic in compound **17**.

The sample was dissolved in a mixture of DMSO and water 60:40, which makes its solubility similar to those activated with green light, but better than the ones activated with far-red light. The calculated quantum yield for **17** was 0.006%, which means that the release efficiency is similar to those activated by green light and better than those activated with far-red light. The total release of the antibiotic was achieved with red light in 35 hours. These results suppose a moderate improvement in the performance of the BODIPYs activated with light inside the therapeutic window (600-1200 nm). Moreover, as mentioned, the light source used to induce the release of the antibiotic was not the most optimal, because it only covered a fraction of the absorbance region where the compound has low absorption. It is expected that irradiation with a lamp emitting in the range of 675 nm will give fasters release rates.

6.4 Antibacterial activity

To testing the antibacterial activity of the photoreleasable quinolones, their MICs were evaluated. The synthesized compounds were studied before and after irradiation. Quinolone sensitive *Escherichia coli* ATCC 25922,[11] was incubated with different concentrations either of the protected form (BODIPY linked to the antibiotic) or the deprotected form (irradiated samples where the antibiotic was released). MIC was

determined visually by the presence or absence of turbidity in the well, as shown in figure 12. If the well is clear, it means that the compound studied in that concentration has a bacteriostatic effect, inhibiting the growth of new bacteria. If the well is turbid, it means the opposite. The results obtained for each compound are explained next.

Table 2. MIC values of photoreleasable quinolones

Compound	**6**	**7**	**10**	**11**	**17**
$MIC_{protected}$ (μg/ml)	>32	32	8-16	16	16
$MIC_{deprotected}$ (μg/ml)	4	4	0,5	2	0,5

As mentioned in a previous chapter, when performing a study of the antibacterial properties, the solvent used to prepare the samples should be water ideally. The use of other organic solvents could affect the results if it interferes with the bacterium survival rate. In this study, due to the solubility of the synthesized structures, it was necessary to employ a mixture of water and DMSO to ensure total solubility of the samples. Hence, a stock solution of each compound in a concentration of 256 μg/ml of the corresponding antibiotic, was prepared either in 80:20 DMSO/H_2O for **7** and **11**, or 60:40 DMSO:H_2O for **6**, **10**, and **17**. Subsequent dilutions to achieve lower concentrations were made with Mueller Hinton broth so that the amount of organic solvent was significantly cut down. Therefore, in order to check the survival of the bacterium with the solvents employed, a control test was made. Solvents were found to not affect the bacterium growth as both mixtures employed (80:20 and 60:40) resulted in MIC > 32 μg/ml. This control proved that the MIC values obtained for all the compounds under study were not affected by the use of DMSO.

The derivatives of nalidixic acid **6** and **7**, showed an 8-fold and 6-fold change in activity when they were irradiated ($MIC_{\mathbf{6}protected}$ > 32 μg/ml *vs.* $MIC_{\mathbf{6}deprotected}$ = 4 μg/ml, $MIC_{\mathbf{7}protected}$ = 32 μg/ml *vs.* $MIC_{\mathbf{7}deprotected}$ = 4 μg/ml). These values were in agreement with the control of nalidixic acid, which reported a value of 4 μg/ml, indicating that after irradiation, the antibiotic was completely released.

Boc-ciprofloxacin derivatives showed a 10-fold difference in activity in **10** and **17** ($MIC_{\mathbf{10}protected}$ = 8-16 μg/ml *vs.* $MIC_{\mathbf{10}deprotected}$ = 0.5 μg/ml, $MIC_{\mathbf{17}protected}$ = 16 μg/ml *vs.* $MIC_{\mathbf{17}deprotected}$ = 0.5 μg/ml), and 6-fold change in **11** ($MIC_{\mathbf{11}protected}$ = 16 μg/ml *vs.*

$MIC_{11deprotected}$ = 2 μg/ml).These results were in agreement with the controls made for Boc-ciprofloxacin which reported MIC values of 0.5 and 2 μg/ml when the stock solution (256 μg/ml) was dissolved in 60:40 and 80:20 DMSO:H_2O. The values once again demonstrated that upon irradiation the release yield of the antibiotic was 100%.

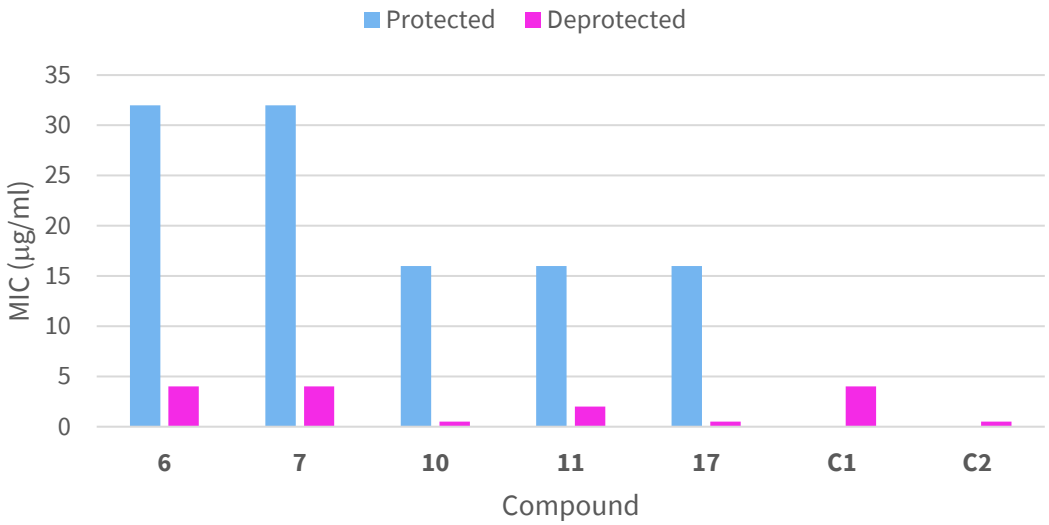

Figure 11. Graphic comparing MICs on *E. coli* ATCC 25922 of the protected and deprotected forms of the photoreleasable quinolones. In blue is represented the protected form (BODIPY linked to the antibiotic). In pink is represented the activated form (after irradiation of the sample which induces the release of the antibiotic). C1 and C2 refer to the control experiments of the antibiotics (C1 = Nalidixic acid, C2 = Boc-ciprofloxacin).

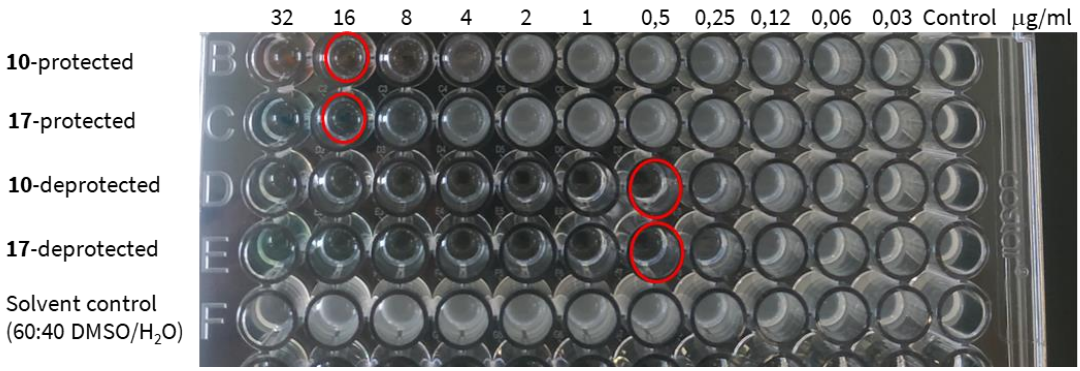

Figure 12. MIC study on *E. coli* ATCC 25922 of the two derivatives showing better results (**10** and **17**). MIC is depicted with a red circle. The protected compounds showed higher MIC values than the deprotected ones, which indicates that upon light irradiation, the antibiotic regains its activity. The solvent control did not affect bacterial growth.

6.5 Conclusions

In this chapter, several photoreleasable derivatives of quinolones have been designed. The photoreleasable group employed, allowed to protect position 3 of the quinolone antibiotics, which is crucial for their activity. Different BODIPY structures were synthesized in order to induce a bathochromic shift, as well as to try to improve their water solubility and release efficiency. The new photoreleasable derivatives displayed strong absorption in the visible region. More importantly, three of them were inside the therapeutic window, absorbing up to 800 nm. One of the properties that remain to be improved is their quantum yield. However, despite showing low values, the release process was induced using visible light to completely generate the unprotected form of the antibiotic in all cases. These excellent results allowed us to test the antibacterial properties of the synthesized molecules *in vitro*. Although the use of mixtures of DMSO and water were needed to achieve total solubility, it was found that this did not affect the final results of this study. The MIC assay showed a significant deactivation of the antibiotics when they were linked to the BODIPY scaffold. When the samples were irradiated, causing the release of the antibiotic, the antibacterial activity was recovered in all cases. The best results were obtained for two Boc-ciprofloxacin derivatives, which upon irradiation suffered a 10-fold difference in activity. This work opens the possibility of activation of antibiotic molecules with visible light inside the therapeutic window. Even though some properties need to be improved, faster activation processes can be accomplished using adequate instrumentation. For example, the lasers employed in PDT, combined with fiber optic delivery systems can ensure a high potency of the light source in a reduced area of irradiation, which would result in a much faster release of the drug.

6.6 Experimental section

6.6.1 HPLC conditions

A Phenomenex C_{18} column (250 mm x 4.6 mm x 5 μm) was employed as the stationary phase. The mobile phase consisted of different mixtures of acetonitrile and water containing 0.1% of trifluoroacetic acid. The flow in all cases was 1 ml/minute, and the injection volume was 20 μl, previously filtered through a 0.45 μm PTFE membrane filter. The gradient methods used for each compound are described next.

Table 3. HPLC method A, used for the analysis of compounds **6** and **10**

Time (min)	Mobile phase composition (%)	
	Acetonitrile	Water (0.1% TFA)
0	80	20
5	40	60
7	40	60
14	10	90
15	10	90

For compounds **6** and **10**, the detection was carried out in dual-mode at 254 or 282, and 520 nm to monitor the release of the antibiotic as well as the remaining protected compound. Retention times are indicated next: $t_{R\mathbf{6}}$ = 12.8 min, $t_{R\mathbf{10}}$ = 14.7 min, $t_{R\mathbf{Nalidixic\ acid}}$ = 8.0 min, $t_{R\mathbf{Boc\text{-}ciprofloxacin}}$ = 11.3 min.

Table 4. HPLC method B, used for the analysis of compounds **7**, **11**, and **17**

Time (min)	Mobile phase composition (%)	
	Acetonitrile	Water (0.1% TFA)
0	80	20
5	40	60
7	40	60
14	10	90
20	10	90

For compounds **7** and **11**, the detection was carried out in dual-mode at 254 or 282, and 730 nm in order to monitor the release of the antibiotic and the remaining protected compound. For compound **17**, the selected wavelengths in dual-mode were 282 and 675 nm. Retention times are indicated next: $t_{R\mathbf{7}}$ = 15.8 min, $t_{R\mathbf{11}}$= 16.8 min, $t_{R\mathbf{17}}$ = 15.9 min, $t_{R\mathbf{Nalidixic\ acid}}$ = 8.0 min, $t_{R\mathbf{Boc\text{-}ciprofloxacin}}$ = 11.3 min.

6.6.2 Quantum yield

6.6.2.1 Reinecke's salt

Reinecke's salt is a popular actinometer for the visible region as it is commercially available and affordable. However, the experimental procedure is not easy and must be precisely followed in order to avoid possible errors in the final value.[12] The photochemical reaction involving Reinecke's salt is expressed in equation 2.

$$[Cr(NH_3)_2(NCS)_4]^- + H_2O \rightarrow [Cr(NH_3)_2(NCS)_3H_2O] + NCS^-$$

Equation 2. Photochemical reaction of Reinecke's salt. Upon light irradiation, an isothiocyanate ion is released and is substituted by a water molecule.

According to equation 2, the rate of photodissociation is equal to the production of the thiocyanate ion. Thus, the amount of thiocyanate ion produced during an irradiation time (t), enables the monitoring of the kinetics of the photoreaction. For this purpose, several thiocyanate standard solutions between 4E-4 and 4E-3 M were prepared using potassium thiocyanate. Additionally, an iron reagent solution containing 0.1M $Fe(NO_3)_3 \cdot 9H_2O$ and 0.5 M $HClO_4$ was prepared. Then, to a volume of thiocyanate solution were added 3 ml of iron reagent and distilled water up to 10 ml. The concentration of thiocyanate ion was determined spectroscopically, as it forms a colored complex with iron.

Table 5. Data of calibration line for the determination of [SCN^-]

[KSCN] (M)	Volume of KSCN (ml)	Volume of iron reagent (ml)	Absorbance (452 nm)
4E-4	2	3	0.322
8E-4	2	3	0.594
2.4E-3	1	3	0.920
3.2E-3	1	3	1.165
4E-3	1	3	1.414

By plotting the absorbance at 452 nm and the concentration of thiocyanate ion of the measured solution, a calibration line was obtained.

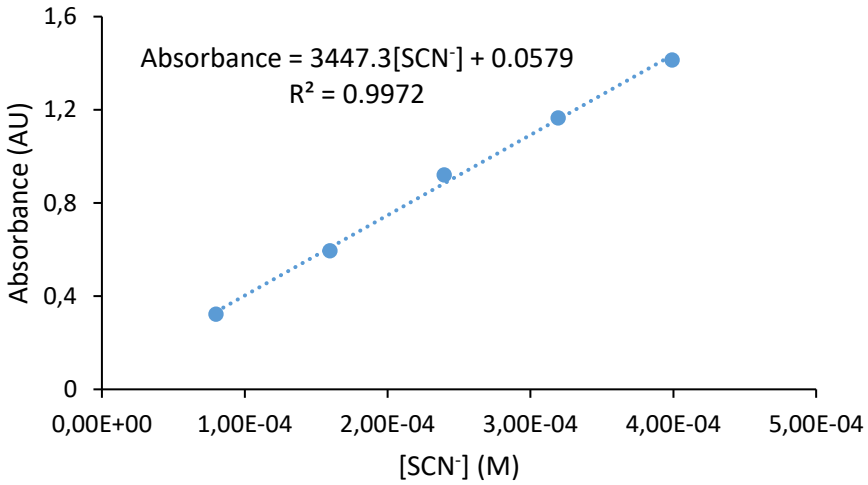

Figure 13. Calibration line obtained for the determination of [SCN^-] through UV-Vis spectroscopy at 452 nm.

The calibration line obtained in figure 13 gives an equation that allows the calculation of the concentration of thiocyanate ion for a given value of absorbance at 452 nm.

$$Absorbance_{(452nm)} = 3447.3[SCN^-] + 0.0579$$

Equation 3. Equation obtained from the calibration line for the determination of [SCN^-].

Next, Reinecke's salt was treated before its use. This salt is commercially available as the ammonium salt and must be converted into the potassium salt since ammonia quenches the photochemical reaction. This is possible by dissolving Reinecke's salt in an aqueous solution of 0.1M potassium hydroxide, obtaining a final concentration of 0.015M of the actinometer. The solution was stirred for a few minutes and subsequently cooled in an ice bath and shaken manually to strip ammonia. Note that the whole procedure must be performed in the absence of light. Once the ammonium salt was obtained, the sample was irradiated at different times with a 30W RGB LED in green mode. At last, the spectrometric analysis sample was prepared as follows: 0.5 ml of the irradiated solution, 3 ml of the iron reagent, and 6.5 ml of distilled water. The concentration of thiocyanate ion was determined spectroscopically at 452 nm. The conversion should be below 10% to avoid secondary reactions, such as more than one thiocyanate ion substituted by molecules of water.

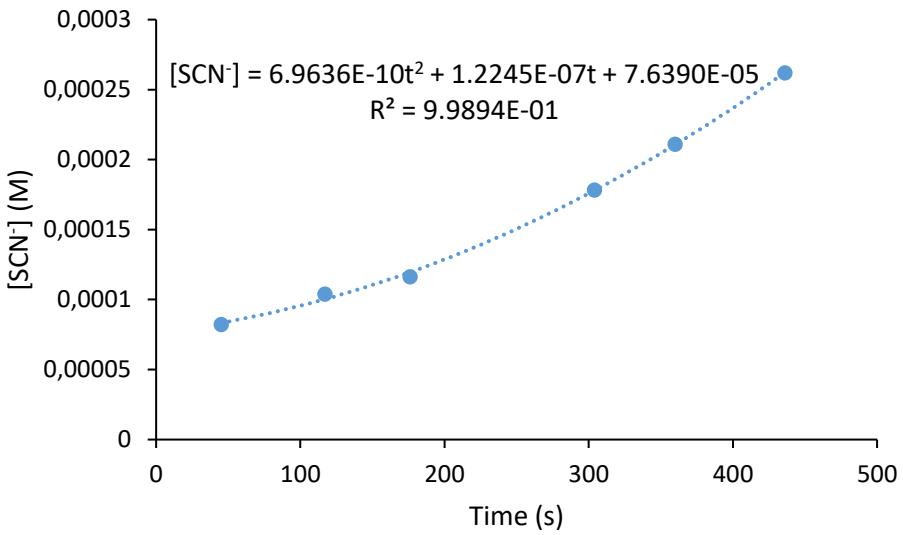

Figure 14. Evolution of [SCN^-] in time. Upon photoreaction of Reinecke's salt, one molecule of SCN^- is substituted by a water molecule. Irradiation carried out using the green LED.

To calculating the concentration of thiocyanate ion, equation 3 was employed. From the graphic shown in figure 14, a polynomic equation of second degree is obtained.

$$[SCN^-] = 6.9636E\text{-}10t^2 + 1.2245E\text{-}7t + 7.6390E\text{-}5$$

Equation 4. Equation obtained from the irradiation of Reinecke's salt. This formula allows to calculate the amount of SCN^- produced when the actinometer is irradiated for a known time (t).

By calculating the slope of the polynomic equation, the value of k_0 was obtained, m = k_0 = 1.2245E-7. Finally, at 520 nm the quantum yield of the actinometer is 0.286. Substituting both values in equation 5 the resulting photonic flux had a value of 4.28E-7 einstein $L^{-1}\,s^{-1}$.

$$I_0 = \frac{k_0}{\Phi}$$

Equation 5. Equation expressing the photonic flux of the lamp. k_0 is the slope of the polynomic function obtained from the photoreaction of Reinecke's salt (equation 4), Φ can be found in the bibliography for different wavelengths.[9]

Once the value of I_0 is known, equation 5 can be used to calculate the quantum yield of the photoreleasable quinolone derivative by finding k_0 for the release process. With this purpose, a solution of compound **6** or **10** was prepared by adjusting the absorbance value at 520 nm to the one displayed by the actinometer. Then the sample was irradiated at different times using the same light source as the one used for the actinometer. The conversion should be below 10% to avoid competitive absorption

between the initial compound and the byproduct of the photocage. The release process was quantified by HPLC using method A, described in section 6.6.1.

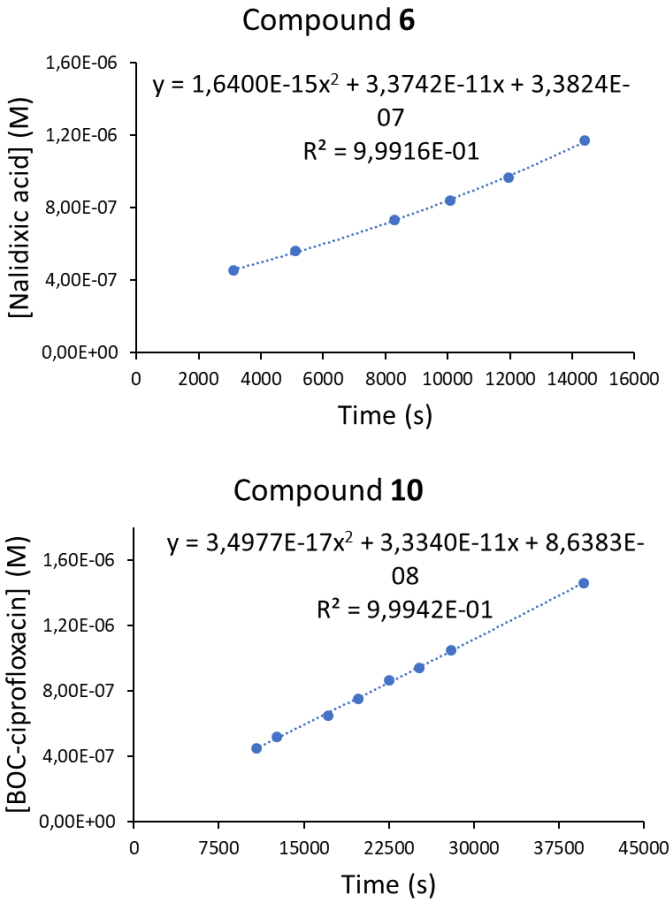

Figure 15. Photorelease course of quinolone derivatives. Upon irradiation of compounds **6** and **10**, nalidixic acid and Boc-ciprofloxacin respectively are released.

As has been described for Reinecke's salt, the value of k_0 for compound **6** and **10** can be calculated from the slope of the polynomic equations obtained for the release of the antibiotic (figure 15, compound **6** k_0 = 3.37E-11 and compound **7** k_0 = 3.33E-11). After that, equation 5 was used to calculate the quantum yield of release of each compound.

6.6.2.2 Instrumental setup

First, the adequate light source was selected according to the sample under study. Compounds **6** and **10** were irradiated with green light using a 30 W RGB LED. Compounds **7** and **11** were irradiated using a 515 mW far-red LED. Compound **17** was irradiated with a 30 W RGB LED in red light mode. The LED of choice was incorporated in the setup represented in figure 7. Samples were prepared in a concentration close to 5E-5M and dissolved in different mixtures of DMSO and water according to their

solubility. All samples were equipped with a magnetic stirrer to ensure homogeneous irradiation of the total volume. Prior to the irradiation process, the sample was analyzed by HPLC to check that the protected form of the antibiotic was being irradiated. The HPLC conditions for each compound can be found in section 6.6.1.

Once the LED was placed in the setup, the light was blocked with a laser dimming paper in front of the lens. This allowed the determination of the ambient light, which was later substrate from subsequent measurements.

Next, the paper was removed, and a reference cuvette containing the solvent used to dissolve the samples was inserted. The light not absorbed by the sample was collected by a cosine corrector coupled to an Ocean Optics USB4000-UV-Vis detector. The transmitted radiant flux (P_{ref}), was obtained in moles of photons·s^{-1}·m^{-2}.

Then, the reference was exchanged by a cuvette containing the sample that was irradiated for a determined time. During that time, the light not absorbed by the sample (P_{sample}) was monitored by continuous acquisition of the transmitted radiant flux in moles of photons·s^{-1}·m^{-2}. Note that upon irradiation, the conversion from the protected antibiotic to the released form should be below 10% to avoid competitive absorption between the initial product and the byproduct of the photocage. After irradiation, the sample's conversion was quantified by HPLC, which allowed the calculation of the number of antibiotic molecules released.

The light absorbed by the sample can be calculated as the difference between the light not absorbed by the reference and the light not absorbed by the sample, as expressed in equation 6:

$$P_{abs} = P_{ref} - P_{sample}$$

Equation 6. Equation expressing the moles of photons·s^{-1}·m^{-2} absorbed by the sample. P_{ref} corresponds with the transmitted radiant flux measured for the reference with solvent, P_{sample} refers to the transmitted radiant flux recorded when the sample was inserted in the setup.

To conclude the experiment, the number of photons absorbed by the sample, as well as the number of molecules of antibiotic released, were introduced in equation 1 to obtain the quantum yield (see section 6.2.3).

6.6.3 Antibacterial activity

To testing the antibacterial activity of the synthesized compounds, a MIC assay was performed on *Escherichia coli* ATCC 25922 strain following the microdilution method in cation adjusted Mueller Hinton broth, according to CLSI protocol (CLSI, 2019).[13]

Escherichia coli ATCC 25922 strain was cultured in Brain-Heart Infusion agar (Becton Dickinson) for 24 hours at 37 °C. Overnight colonies were used to prepare an inoculum adjusted to the turbidity of a 0.5 McFarland in sterile saline (equivalent to 1 x 10^8 CFU/ml). All compounds were dissolved in mixtures of DMSO/H_2O depending on their solubility to prepare the stock solution in a concentration of 256 μg/ml of the corresponding antibiotic considering total release. Serial two-fold dilutions of the stock solution were made in a range of concentrations from 32 to 0.03 μg/ml. The bacterial suspension was diluted in cation adjusted Mueller-Hinton broth to give a final organism density of 5 x 10^5 CFU/ml and exposed to serial twofold dilutions of each compound tested (0.03-32 μg/ml) with a final volume of 0.1 ml in a 96 well microdilution tray. The MIC value was the lowest concentration of compound where no visible growth was apparent after 20-24 hours of incubation at 37 °C. Compounds were tested before and after irradiation with visible light, green light in **6** and **10**, far-red light in **7** and **11**, and red light in **17**. Additional controls of the antibiotics (Nalidixic acid and Boc-ciprofloxacin), as well as the solvents used, were made.

6.6.4 Synthesis

6.6.4.1 General information

For details about general experimental information, see Appendix, section A.

6.6.4.2 Synthetic procedure

(5,5-difluoro-1,3,7,9-tetramethyl-5*H*-4l4,5l4-dipyrrolo[1,2-*c*:2',1'-*f*][1,3,2] diazaborinin-10-yl)methyl acetate (1):[4]

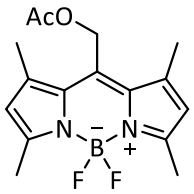

To a solution of 2,4-dimethylpyrrole (10.5 mmol, 1.08 ml) in dry DCM (40 ml) under argon atmosphere, was added acetoxyacetyl chloride (6.0 mmol, 0.64 ml) and the mixture was stirred in the dark at room temperature for 24 hours. Then, TEA (31.5 mmol, 4.4 ml) was added. The resulting mixture was allowed to stir for 15 minutes. Next, boron trifluoride diethyl etherate (47.2 mmol, 5.8 ml) was added. After 1 hour of stirring, another portion of TEA (31.5 mmol, 4.4 ml) and boron trifluoride diethyl etherate (47.2 mmol, 5.8 ml) were added, and the stirring continued for one more hour. After that time, silica was added to the flask, and the solvents were evaporated

in vacuo. The obtained solid was purified by column chromatography (Et_2O:Hexane 1:1) to give 0.5 g (30%) of a solid as red-gold crystals.
^{1}H-NMR (300 MHz, $CDCl_3$): δ 6.08 (s, 2H), 5.30 (s, 2H), 2.53 (s, 6H), 2.36 (s, 6H), 2.13 (s, 3H).
^{1}H-NMR spectrum in agreement with published data.[4]

(5,5-difluoro-1,3,7,9-tetramethyl-5*H*-4l4,5l4-dipyrrolo[1,2-*c*:2',1'-*f*][1,3,2] diazaborinin-10-yl)methanol (2):[4]

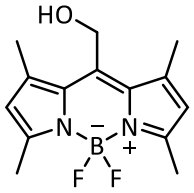

Sodium hydroxide (0.25 mmol, 10 mg) was dissolved in a mixture of water (2.5 ml) and methanol (12 ml) and stirred for 10 minutes and then was added to a solution of compound **1** (0.63 mmol, 0.2 g) in DCM (12 ml). The reaction mixture was stirred for 6 hours in the dark at room temperature. Then, the organic solvents were evaporated *in vacuo*, and the residue was extracted with EtOAc (30 ml) three times. The combined organic layers were washed with 1M HCl (15 ml) twice and brine (15 ml) and dried over anhydrous $MgSO_4$. The solvent was removed *in vacuo*, and the solid obtained was purified by column chromatography (Et_2O:Hexane 1:1 to 1:0) to obtain 0.1 g (60%) of solid as red crystals.
^{1}H-NMR (300 MHz, $CDCl_3$): δ 6.09 (s, 2H), 4.91 (s, 2H), 2.53 (s, 6H), 2.51 (s, 6H).
^{1}H-NMR spectrum in agreement with published data.[4]

(3,7-bis(4-(dimethylamino)styryl)-5,5-difluoro-1,9-dimethyl-5*H*-4l4,5l4-dipyrrolo[1,2-*c*:2',1'-*f*][1,3,2]diazaborinin-10-yl)methyl acetate (3):[3]

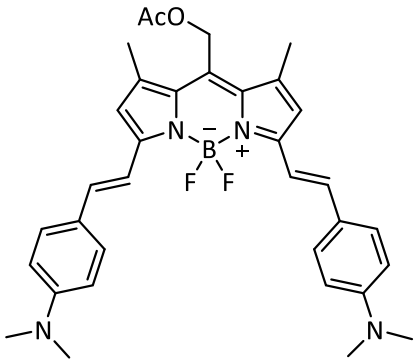

Compound **1** (0.31 mmol, 0.1 g) and 4-(dimethylamino)benzaldehyde (3.4 mmol, 0.51 g) were added to a 24 ml scintillation vial. Then, one drop of piperidine was added, and the vial was rotated under vacuum while heated at 75 °C for 6 hours. After that

time, the resulting solid was purified by column chromatography (DCM:MeOH 50:0.1) to give 0.1 g (53%) of a dark green solid.
^{1}H-NMR (300 MHz, DMSO-D_6): δ 7.50-7.43 (m, 6H), 7.27 (d, *J* = 16.2 Hz, 2H), 7.00 (s, 2H), 6.79 (d, *J* = 8.9 Hz, 4H), 5.29 (s, 2H), 3.01 (s, 12H), 2.39 (s, 6H), 2.13 (s, 3H).
^{1}H-NMR spectrum in agreement with published data.[3]

(3,7-bis(4-(dimethylamino)styryl)-5,5-difluoro-1,9-dimethyl-5*H*-4l4,5l4-dipyrrolo[1,2-*c*:2',1'-*f*][1,3,2]diazaborinin-10-yl)methanol (4):[3]

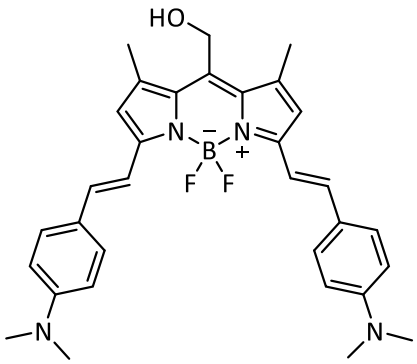

To a solution of compound **3** (0.17 mmol, 0.1 g) in a mixture of DCM (50 ml) and MeOH (50 ml) was added a solution of sodium hydroxide (1.0 mmol, 41 mg) in water (10 ml). The reaction mixture was stirred in the dark at room temperature for 6 hours. After that time, the organic solvent was removed *in vacuo*, and the residue was extracted with DCM (40 ml) twice. Next, the combined organic layers were washed with 1M HCl (20 ml) and brine (20 ml). The organic layer was dried over anhydrous $MgSO_4$, and the solvent was removed *in vacuo*. The resulting residue was purified by column chromatography (DCM:EtOAc 5:0.15) to obtain 83 mg (90%) of a dark green solid.
^{1}H-NMR (300 MHz, DMSO-D_6): δ 7.48-7.43 (m, 6H), 7.27 (d, *J* = 16 Hz, 2H), 6.94 (s, 2H), 6.79 (d, *J* = 8.9 Hz, 4H), 5.45 (t, *J* = 4.9 Hz, 1H), 4.74 (d, *J* = 4.8 Hz, 2H), 3.00 (s, 12H), 2.54 (s, 6H).
^{1}H-NMR spectrum in agreement with published data.[3]

1-ethyl-7-methyl-4-oxo-1,4-dihydro-1,8-naphthyridine-3-carbonyl chloride (5):

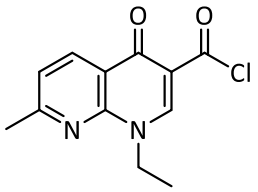

To a solution of nalidixic acid (0.43 mmol, 0.1 g) in dry DCM (4 ml) under argon atmosphere was added oxalyl chloride (1.29 mmol, 0.11 ml) and one drop of DMF. The resulting mixture was stirred for 2 hours at 40 °C. After that time, the solvent was

evaporated *in vacuo* to give 0.11 g of a dark blue solid that was immediately used in the next step.

(5,5-difluoro-1,3,7,9-tetramethyl-5*H*-4l4,5l4-dipyrrolo[1,2-*c*:2',1'-*f*][1,3,2] diazaborinin-10-yl)methyl 1-ethyl-7-methyl-4-oxo-1,4-dihydro-1,8-naphthyridine-3-carboxylate (6):

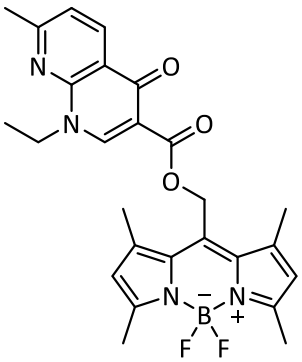

Compound **2** (80 mg, 0.29 mmol) was dissolved in dry DCM (4 ml) under argon atmosphere and 4-(dimethylamino)pyridine (70 mg, 0.58 mmol) was added. This mixture was added over a solution containing compound **5** (111 mg, 0.43 mmol) in dry DCM (3 ml) under argon atmosphere. The reaction mixture was stirred in the dark for 12 hours at room temperature. After that time, the solvent was evaporated *in vacuo*, and the resulting residue was purified by column chromatography (DCM:EtOAc 5:2) to obtain 61 mg (43%) of a red solid.

^{1}H-NMR (400 MHz, $CDCl_3$): δ 8.63 (d, *J* = 8.1 Hz, 1H), 8.55 (s, 1H), 7.24 (d, *J* = 8.1 Hz, 1H), 6.08 (s, 2H), 5.51 (s, 2H), 4.46 (q, *J* = 7.1 Hz, 2H), 2.65 (s, 3H), 2.54 (s, 6H), 2.44 (s, 6H), 1.47 (t, *J* = 7.1 Hz, 3H).

^{13}C-NMR (100 MHz, $CDCl_3$): δ 174.8, 164.2, 163.0, 156.6, 148.7, 142.1, 137.0, 134.0, 133.1, 122.4, 121.6, 121.5, 110.6, 58.1, 47.0, 25.2, 15.9, 15.4, 14.8.

HR-MS (ESI, [M+H]+): Calcd. for C26H27BF2N4O3 + H: 493.2217; Found: 493.2226

(3,7-bis(4-(dimethylamino)styryl)-5,5-difluoro-1,9-dimethyl-5*H*-4l4,5l4-dipyrrolo[1,2-*c*:2',1'-*f*][1,3,2]diazaborinin-10-yl)methyl 1-ethyl-7-methyl-4-oxo-1,4-dihydro-1,8-naphthyridine-3-carboxylate (7):

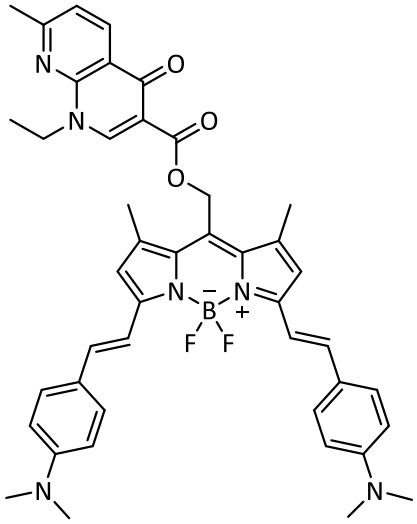

Compound **4** (83 mg, 0.15 mmol) was dissolved in dry DCM (4 ml) under argon atmosphere and 4-(dimethylamino)pyridine (37 mg, 0.30 mmol) was added. This mixture was added over a solution containing compound **5** (56 mg, 0.23 mmol) in dry DCM (3 ml) under argon atmosphere. The reaction mixture was stirred in the dark for 12 hours at room temperature. After that time, the solvent was evaporated *in vacuo*, and the resulting residue was purified by column chromatography (DCM:EtOAc:Toluene 2:3:1) to obtain 34 mg (30%) of a dark green solid.

^{1}H-NMR (300 MHz, $CDCl_3$): δ 8.64 (d, *J* = 8.1 Hz, 1H), 8.57 (s, 1H), 7.53 (d, *J* = 8.9 Hz, 6H), 7.25-7.15 (m, 3H), 6.71 (d, *J* = 8.9 Hz, 6H), 5.53 (s, 2H), 4.45 (q, *J* = 7.1 Hz, 2H), 3.04 (s, 12H), 2.64 (s, 3H), 2.46 (s, 6H), 1.45 (t, *J* = 7.1 Hz, 3H).

^{13}C-NMR (75 MHz, $CDCl_3$): δ 175.0, 163.7, 162.9, 153.4, 151.1, 148.7, 148.6, 139.5, 137.2, 137.0, 129.4, 129.3, 125.2, 121.5, 121.4, 118.4, 115.0, 112.2, 110.6, 58.4, 46.9, 40.4, 25.2, 16.1, 15.4.

HR-MS (ESI, [M+Na]+): Calcd. for C44H45BF2N6O3 +Na: 777.3514; Found: 777.3497

7-(4-(*tert*-butoxycarbonyl)piperazin-1-yl)-1-cyclopropyl-6-fluoro-4-oxo-1,4-dihydroquinoline-3-carboxylic acid (8):

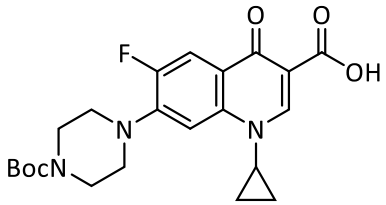

Ciprofloxacin (2 g, 6.0 mmol) and di-*tert*-butyl decarbonate (1.4 g, 6.6 mmol) were dissolved in THF (60 ml). Next, a solution of sodium hydroxide (0.48 g, 12.0 mmol) in water (12 ml) was added, and the mixture was stirred overnight at room temperature. After that time, the solvent was removed *in vacuo*, and the residue was taken into aqueous saturated ammonium chloride (200 ml). The aqueous phase was extracted with DCM (200 ml) three times. The organic layer was washed with brine (400 ml) and dried over anhydrous $MgSO_4$. The solvent was evaporated *in vacuo* to obtain 2.51 g (97%) of white solid.

^{1}H-NMR (300 MHz, $CDCl_3$): δ 14.94 (s, 1H), 8.71 (s, 1H), 7.96 (d, *J* = 12.9 Hz, 1H), 7.35 (d, *J* = 7.1 Hz, 1H), 3.72 – 3.61 (m, 4H), 3.59-3.50 (m, 1H), 3.34 – 3.21 (m, 4H), 1.49 (s, 9H), 1.41-1.35 (m, 2H), 1.26 – 1.15 (m, 2H).

^{1}H-NMR spectrum in agreement with published data.[14]

***Tert*-butyl 4-(3-(chlorocarbonyl)-1-cyclopropyl-6-fluoro-4-oxo-1,4-dihydroquinolin-7-yl)piperazine-1-carboxylate (9):**

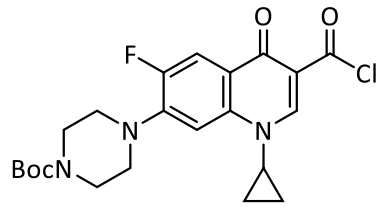

To a solution of compound **8** (0.15 g, 0.35 mmol) in dry DCM (5 ml) under argon atmosphere, oxalyl chloride (88 µl, 1.05 mmol) and one drop of DMF were added. The reaction was stirred for 2 hours at 40 °C. After that time, the solvent was removed *in vacuo* to give 0.16 g (100%) of an orange solid that was immediately used in the next step.

(5,5-difluoro-1,3,7,9-tetramethyl-5*H*-4l4,5l4-dipyrrolo[1,2-*c*:2',1'-*f*][1,3,2] diazaborinin-10-yl)methyl 7-(4-(*tert*-butoxycarbonyl)piperazin-1-yl)-1 cyclopropyl-6-fluoro-4-oxo-1,4-dihydroquinoline-3-carboxylate (10):

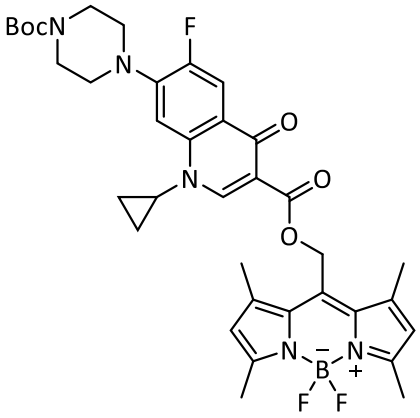

Compound **2** (67 mg, 0.24 mmol) was dissolved in dry DCM (4 ml) under argon atmosphere and 4-(dimethylamino)pyridine (57 mg, 0.47 mmol) was added. This mixture was added over a solution containing compound **9** (160 mg, 0.36 mmol) in dry DCM (3 ml) under argon atmosphere. The reaction mixture was stirred in the dark for 12 hours at room temperature. After that time, the solvent was evaporated *in vacuo*, and the resulting residue was purified by column chromatography (DCM:EtOAc 5:2) to obtain 63 mg (38%) of a red solid.

^{1}H-NMR (300 MHz, $CDCl_3$): δ 8.45 (s, 1H), 8.05 (d, *J* = 13.1 Hz, 1H), 7.24 (d, 1H), 6.08 (s, 2H), 5.51 (s, 2H), 3.68 – 3.60 (m, 4H), 3.45 – 3.33 (m, 1H), 3.24 – 3.16 (m, 4H), 2.53 (s, 6H), 2.45 (s, 6H), 1.49 (s, 9H), 1.34 – 1.26 (m, 2H), 1.12 – 1.02 (m, 2H).

^{13}C-NMR (75 MHz, $CDCl_3$): δ 173.1, 164.6, 156.5, 155.2, 154.7, 151.9, 148.2, 144.8, 142.1, 138.1, 134.1, 133.1, 122.4, 113.8, 109.3, 105.1, 80.4, 58.1, 50.1, 43.6, 34.7, 28.6, 15.9, 14.8, 8.5.

HR-MS (ESI, [M+H]+): Calcd. for C36H41BF3N5O5 +H: 692.3225; Found: 692.3235

(3,7-bis(4-(dimethylamino)styryl)-5,5-difluoro-1,9-dimethyl-5*H*-4l4,5l4-dipyrrolo[1,2-*c*:2',1'-*f*][1,3,2]diazaborinin-10-yl)methyl 7-(4-(*tert*-butoxycarbonyl)piperazin-1-yl)-1-cyclopropyl-6-fluoro-4-oxo-1,4-dihydroquinoline-3-carboxylate (11):

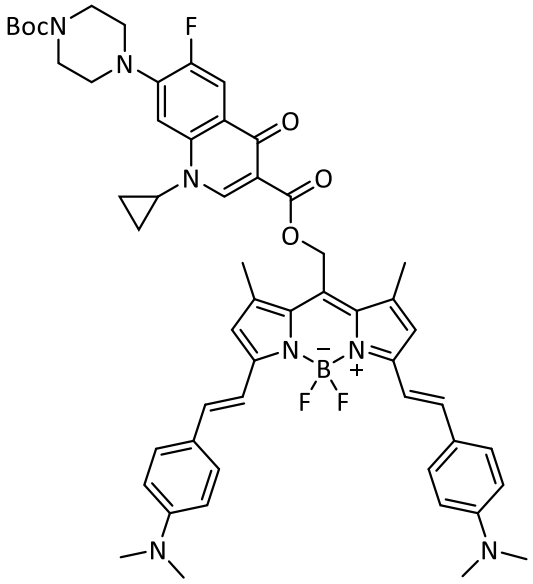

Compound **4** (83 mg, 0.15 mmol) was dissolved in dry DCM (4 ml) under argon atmosphere and 4-(dimethylamino)pyridine (37 mg, 0.30 mmol) was added. This mixture was added over a solution containing compound **9** (103 mg, 0.23 mmol) in dry DCM (3 ml) under argon atmosphere. The reaction mixture was stirred in the dark for 12 hours at room temperature. After that time, the solvent was evaporated *in vacuo*, and the resulting residue was purified by column chromatography (DCM:EtOAc:Toluene 2:3:1) to obtain 34 mg (30%) of a dark green solid.

^{1}H-NMR (300 MHz, $CDCl_3$): δ 8.45 (s, 1H), 8.07 (d, *J* = 13.1 Hz, 1H), 7.53 (d, *J* = 8.9 Hz, 6H), 7.25 – 7.17 (m, 3H), 6.71 (d, *J* = 8.7 Hz, 6H), 5.54 (s, 2H), 3.66 – 3.59 (m, 4H), 3.42 – 3.32 (m, 1H), 3.22 – 3.16 (m, 4H), 3.03 (s, 12H), 2.48 (s, 6H), 1.49 (s, 9H), 1.26 – 1.21 (m, 2H), 1.09 – 1.02 (m, 2H).

^{13}C-NMR (75 MHz, $CDCl_3$): δ 173.3, 164.1, 154.8, 153.4, 151.1, 148.0, 144.7, 144.6, 139.6, 138.1, 137.1, 134.8, 129.4, 129.3, 127.9, 125.2, 123.3, 118.4, 115.0, 113.9, 113.6, 112.2, 109.4, 105.2, 80.3, 58.4, 50.1, 43.6, 40.4, 34.7, 28.6, 16.1, 8.6.

HR-MS (ESI, [M+H]+): Calcd. for C54H59BF3N7O5 +H: 954.4704; Found: 954.4659

6-(2-(2-(2-methoxyethoxy)ethoxy)ethoxy)-3,4-dihydronaphthalen-1(2H)-one (12):

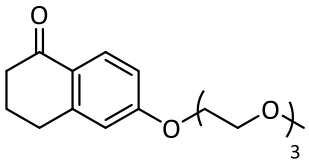

To a solution of 6-hydroxy-1-tetralone (1 g, 6.2 mmol) in anhydrous DMF (15 ml)under argon atmosphere was added sodium carbonate (1.3 g, 12.3 mmol), 1-chloro-2-[2-(2-methoxyethoxy)ethoxy]ethane (1.2 g, 6.7 mmol), and sodium iodide as a catalyst. The resulting mixture was stirred for 16 hours at 100 °C. After that time, the solvent was removed *in vacuo*, and the resulting product was neutralized with 1M HCl. Then, it was extracted with DCM (60 ml) twice, and the organic layers were washed with brine (60 ml). Next, the organic layer was dried over anhydrous $MgSO_4$, and the solvent was evaporated *in vacuo* to give 1.8 g (95%) of a clear oil.

^{1}H-NMR (400 MHz, $CDCl_3$): δ 7.99 (d, *J* = 8.7 Hz, 1H), 6.83 (dd, *J* = 8.8, 2.5 Hz, 1H), 6.71 (d, *J* = 2.5 Hz, 1H), 4.20 – 4.15 (m, 2H), 3.88-3.84 (m, 2H), 3.75-3.72 (m, 2H), 3.70 – 3.61 (m, 4H), 3.56-3.53 (m, 2H), 3.37 (s, 3H), 2.92-2.89 (m, 2H), 2.62-2.58 (m, 2H), 2.10 (quint, *J* = 6.4 Hz, 2H).

^{13}C-NMR (100 MHz, $CDCl_3$): δ 197.3, 162.9, 147.0, 129.7, 126.6, 113.6, 113.4, 72.1, 71.0, 70.8, 70.7, 69.7, 67.7, 59.2, 39.0, 30.3, 23.5.

HR-MS (ESI, [M+H]+): Calcd. for C17H24O5 +H: 309.1697; Found: 309.1701

6-(2-(2-(2-methoxyethoxy)ethoxy)ethoxy)-3,4-dihydronaphthalen-1(2H)-one oxime (13):

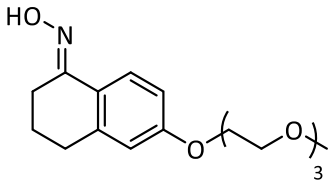

Sodium acetate (0,29 g, 3.6 mmol) was dissolved in water (3 ml) and added over a solution of hydroxylamine hydrochloride (0.25 g, 3.6 mmol) in water (3 ml). The resulting mixture was added over a solution of compound **12** (1 g, 3.2 mmol) in methanol (10 ml) and heated at 35 °C. Next, the sample was stirred for 2 hours at 80 °C. After that time, the reaction was cooled at room temperature, and the solvent was removed *in vacuo*. Next, water (30 ml) was added to the residue, and the aqueous phase was extracted with DCM (50 ml) twice. The combined organic layers were washed with brine (50 ml) and dried over anhydrous $MgSO_4$. Then, the solvent was evaporated *in vacuo* to result in 0.99 g (94%) of a clear oil.

^{1}H-NMR (400 MHz, $CDCl_3$): δ 7.77 (d, *J* = 8.7 Hz, 1H), 6.76 (dd, *J* = 8.8, 2.7 Hz, 1H), 6.66 (d, *J* = 2.6 Hz, 1H), 4.16 – 4.09 (m, 2H), 3.87 – 3.82 (m, 2H), 3.75 – 3.71 (m, 2H), 3.70 – 3.62 (m, 4H), 3.58 – 3.52 (m, 2H), 3.37 (s, 3H), 2.79 (t, *J* = 6.6 Hz, 2H), 2.70 (t, *J* = 6.1 Hz, 2H), 1.85 (quint, *J* = 6.5 Hz, 2H).
^{13}C-NMR (100 MHz, $CDCl_3$): δ 159.6, 155.2, 141.6, 125.7, 123.5, 113.8, 113.6, 72.0, 70.9, 70.8, 70.7, 69.8, 67.4, 59.1, 30.2, 23.9, 21.5.
HR-MS (ESI, [M+H]+): Calcd. for C17H25NO5 +H: 324.1805; Found: 324.1811

7-(2-(2-(2-methoxyethoxy)ethoxy)ethoxy)-4,5-dihydro-1H-benzo[g]indole (14):

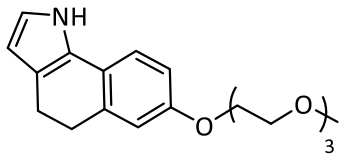

In a three-neck flask, under argon atmosphere, compound **13** (1 g, 3.1 mmol) was dissolved in DMSO (25 ml). Next, lithium hydroxide monohydrate (0.7 g, 16.7 mmol) was added, and a light flow of acetylene was passed through the reaction mixture. The mixture was heated at 135 °C while keeping the acetylene flow for 6 hours. After that time, the reaction mixture was allowed to reach room temperature, and distilled water (60 ml) was added. Then, the aqueous phase was extracted with diethyl ether (100 ml) five times. The combined organic layers were extracted with water (100 ml) once. Finally, the solvent was removed *in vacuo*, and the obtained residue was purified by column chromatography (DCM:EtOAc 5:1)to give 0.31 g (30%) of a clear oil.
^{1}H-NMR (400 MHz, $CDCl_3$): δ 8.34 (s, 1H), 7.06 (d, *J* = 8.3 Hz, 1H), 6.80 (d, *J* = 2.5 Hz, 1H), 6.72 (d, *J* = 2.7 Hz, 1H), 6.71 (t, *J* = 2.7 Hz, 1H), 6.10 (t, *J* = 2.5 Hz, 1H), 4.14 – 4.07 (m, 2H), 3.86 – 3.82 (m, 2H), 3.76 – 3.72 (m, 2H), 3.71-3.64 (m, 4H), 3.59 – 3.52 (m, 2H), 3.38 (s, 3H), 2.89 (t, *J* = 7.5 Hz, 2H), 2.72 (t, *J* = 7.3 Hz, 2H).
^{13}C-NMR (100 MHz, $CDCl_3$): δ 156.6, 136.8, 127.8, 123.1, 119.3, 118.5, 117.4, 115.6, 112.1, 108.0, 72.1, 70.9, 70.8, 70.7, 69.9, 67.6, 59.2, 30.6, 21.9.
HR-MS (ESI, [M+H]+): Calcd. for C19H25NO4 +H: 332.1856; Found: 332.1855

8-((acetyloxy)methyl)-17,17-difluoro-3,13-bis(2-(2-(2-methoxyethoxy)ethoxy) ethoxy)-5,10,11,17-tetrahydro-6H benzo[g]benzo[6',7']indolo[1',2':3,4] [1,3,2] diazaborinino[1,6-a]indol-16-ium (15):

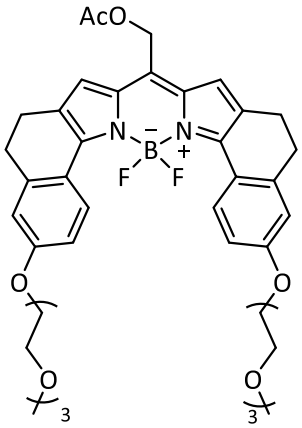

To a solution of compound **14** (0.94 mmol, 0.31 g) in dry DCM (10 ml) under argon atmosphere, was added acetoxyacetyl chloride (0.56 mmol, 60 μl) and the mixture was stirred in the dark at 40 °C for 2 hours. Then, TEA (1.7 mmol, 0.23 ml) was added. The resulting mixture was allowed to stir for 15 minutes. Next, boron trifluoride diethyl etherate (1.7 mmol, 0.21 ml) was added. After 1 hour of stirring, another portion of TEA (1.7 mmol, 0.23 ml) and boron trifluoride diethyl etherate (1.7 mmol, 0.21 ml) were added, and the stirring continued for one more hour. After that time, the solvent was evaporated *in vacuo*, and the obtained residue was purified by column chromatography (DCM:MeOH 32:1) to give 85 mg (23%) of a deep blue-green solid.

^{1}H-NMR (400 MHz, $CDCl_3$): δ 8.68 (d, *J* = 9.0 Hz, 2H), 6.98 (s, 2H), 6.95 (dd, *J* = 8.9, 2.7 Hz, 2H), 6.82 (d, *J* = 2.7 Hz, 2H), 5.25 (s, 2H), 4.24 – 4.19 (m, 4H), 3.91 – 3.86 (m, 4H), 3.78 – 3.73 (m, 4H), 3.72 – 3.65 (m, 8H), 3.58 – 3.53 (m, 4H), 3.38 (s, 6H), 2.88 (t, *J* = 7.0 Hz, 4H), 2.73 (t, *J* = 6.4 Hz, 4H), 2.10 (s, 3H).

^{13}C-NMR (100 MHz, $CDCl_3$): δ 170.7, 160.2, 152.6, 143.1, 136.2, 132.6, 130.4, 128.3, 122.1, 121.6, 115.1, 113.1, 72.1, 71.0, 70.8, 70.7, 69.7, 67.5, 59.9, 59.2, 31.0, 22.5, 21.1.

HR-MS (ESI, [M+H]+): Calcd. for C42H51BF2N2O10 +H: 790.3568; Found: 790.3562

17,17-difluoro-8-(hydroxymethyl)-3,13-bis(2-(2-(2-methoxyethoxy)ethoxy) ethoxy)-5,10,11,17-tetrahydro-6H-benzo[g]benzo[6',7']indolo[1',2':3,4] [1,3,2]diazaborinino [1,6-a]indol-16-ium (16):

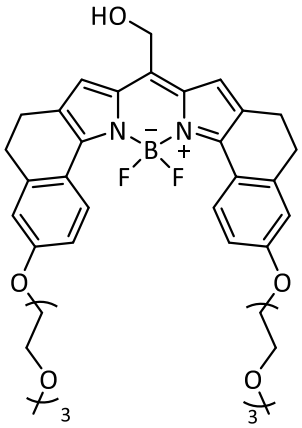

To a solution of compound **15** (0.11 mmol, 85 mg) in a mixture of DCM (25 ml) and MeOH (10 ml) was added a solution of potassium carbonate (0.39 mmol, 53 mg) in water (1 ml). The reaction mixture was stirred in the dark at room temperature for 3 hours. After that time, the organic solvent was removed *in vacuo*, and the residue was extracted with DCM (40 ml) twice. Next, the combined organic layers were washed with 1M HCl (10 ml) and brine (20 ml). The organic layer was dried over anhydrous $MgSO_4$, and the solvent was removed *in vacuo*. The resulting residue was purified by column chromatography (DCM:MeOH 40:1) to obtain 48 mg (58%) of a dark green solid.

^{1}H-NMR (400 MHz, $CDCl_3$): δ 8.68 (d, *J* = 9.0 Hz, 2H), 7.04 (s, 2H), 6.96 (dd, *J* = 8.9, 2.7 Hz, 2H), 6.82 (d, *J* = 2.7 Hz, 2H), 4.81 (s, 2H), 4.28 – 4.14 (m, 4H), 3.93 – 3.84 (m, 4H), 3.80 – 3.72 (m, 4H), 3.72 – 3.64 (m, 8H), 3.59 – 3.52 (m, 4H), 3.38 (s, 6H), 2.88 (t, *J* = 7.0 Hz, 4H), 2.73 (t, *J* = 7.0 Hz, 4H).

^{13}C-NMR (100 MHz, $CDCl_3$): δ 160.1, 152.4, 143.0, 135.5, 133.5, 132.4, 121.8, 121.8, 121.7, 115.1, 113.1, 72.1, 71.0, 70.8, 70.7, 69.8, 67.6, 59.9, 59.2, 31.0, 22.6.

HR-MS (ESI, [M+H]+): Calcd. for C40H49BF2N2O9 +H: 790.3568; Found: 790.3562

8-((((7-(4-(*tert*-butoxycarbonyl)piperazin-1-yl)-1-cyclopropyl-6-fluoro-4-oxo-1,4-dihydroquinolin-3-yl)carbonyl)oxy)methyl)-17,17-difluoro-3,13-bis(2-(2-(2-methoxyethoxy)ethoxy)ethoxy)-5,10,11,17-tetrahydro-6H benzo[g]benzo [6',7'] indolo [1',2':3,4][1,3,2]diazaborinino[1,6-a]indol-16-ium (17):

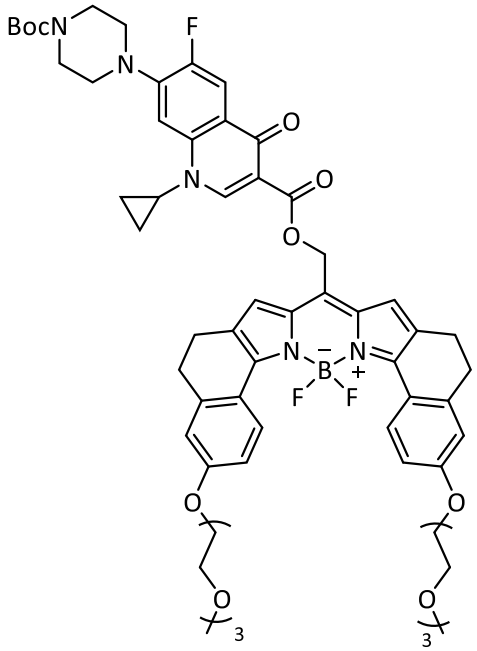

Compound **16** (48 mg, 0.06 mmol) was dissolved in dry DCM (3 ml) under argon atmosphere and 4-(dimethylamino)pyridine (16 mg, 0.13 mmol) was added. This mixture was added over a solution containing compound **9** (39 mg, 0.09 mmol) in dry DCM (2 ml) under argon atmosphere. The reaction mixture was stirred in the dark for 12 hours at room temperature. After that time, the solvent was evaporated *in vacuo*, and the resulting residue was purified by column chromatography (DCM:MeOH 40:1) to obtain 21 mg (28%) of a dark green solid.

^{1}H-NMR (400 MHz, $CDCl_3$): δ 8.68 (d, *J* = 9.0 Hz, 2H), 8.46 (s, 1H), 8.07 (d, *J* = 13.1 Hz, 1H), 7.24 (d, *J* = 7.0 Hz, 1H), 7.18 (s, 2H), 6.95 (dd, *J* = 8.9, 2.7 Hz, 2H), 6.82 (d, *J* = 2.7 Hz, 2H), 5.49 (s, 2H), 4.25 – 4.16 (m, 4H), 3.91 – 3.81 (m, 4H), 3.79 – 3.73 (m, 4H), 3.72 – 3.61 (m, 12H), 3.59 – 3.52 (m, 4H), 3.38 (s, 6H), 3.45-3.33 (m, 1H), 3.20 (m, 4H), 2.88 (t, *J* = 6.2 Hz, 4H), 2.74 (t, *J* = 7.1 Hz, 4H), 1.49 (s, 9H), 1.31 – 1.26 (m, 2H), 1.10-1.05 (m, 2H).

^{13}C-NMR (100 MHz, $CDCl_3$): δ 173.2, 164.3, 160.1, 154.8, 154.7, 152.4, 152.3, 148.5, 144.6, 143.1, 138.1, 136.2, 132.6, 130.3, 129.3, 122.6, 121.7, 115.1, 113.8, 113.6, 113.1, 109.5, 105.3, 80.4, 72.1, 71.0, 70.8, 70.7, 69.8, 67.5, 60.1, 59.2, 53.6, 50.1, 34.8, 31.0, 29.8, 28.5, 22.6, 8.4.

HR-MS (ESI, [M+H]+): Calcd. for C62H73BF3N5O13 +H: 1163.5359; Found: 1163.5340

6.7 References

1. Goswami, P. P.; Syed, A.; Beck, C. L.; Albright, T. R.; Mahoney, K. M.; Unash, R.; Smith, E. A.; Winter, A. H., BODIPY-Derived Photoremovable Protecting Groups Unmasked with Green Light. *Journal of the American Chemical Society* **2015,** *137* (11), 3783-3786.
2. Rubinstein, N.; Liu, P.; Miller, E. W.; Weinstain, R., meso-Methylhydroxy BODIPY: a scaffold for photo-labile protecting groups. *Chemical Communications* **2015,** *51* (29), 6369-6372.
3. Peterson, J. A.; Wijesooriya, C.; Gehrmann, E. J.; Mahoney, K. M.; Goswami, P. P.; Albright, T. R.; Syed, A.; Dutton, A. S.; Smith, E. A.; Winter, A. H., Family of BODIPY Photocages Cleaved by Single Photons of Visible/Near-Infrared Light. *Journal of the American Chemical Society* **2018,** *140* (23), 7343-7346.
4. Sitkowska, K.; Feringa, B. L.; Szymański, W., Green-Light-Sensitive BODIPY Photoprotecting Groups for Amines. *The Journal of Organic Chemistry* **2018,** *83* (4), 1819-1827.
5. Slanina, T.; Shrestha, P.; Palao, E.; Kand, D.; Peterson, J. A.; Dutton, A. S.; Rubinstein, N.; Weinstain, R.; Winter, A. H.; Klán, P., In Search of the Perfect Photocage: Structure–Reactivity Relationships in meso-Methyl BODIPY Photoremovable Protecting Groups. *Journal of the American Chemical Society* **2017,** *139* (42), 15168-15175.
6. Sitkowska, K.; Hoes, M. F.; Lerch, M. M.; Lameijer, L. N.; van der Meer, P.; Szymański, W.; Feringa, B. L., Red-light-sensitive BODIPY photoprotecting groups for amines and their biological application in controlling heart rhythm. *Chemical Communications* **2020**.
7. Jang, Y.; Kim, T.-I.; Kim, H.; Choi, Y.; Kim, Y., Photoactivatable BODIPY Platform: Light-Triggered Anticancer Drug Release and Fluorescence Monitoring. *ACS Applied Bio Materials* **2019,** *2* (6), 2567-2572.
8. Liu, M.; Meng, J.; Bao, W.; Liu, S.; Wei, W.; Ma, G.; Tian, Z., Single-Chromophore-Based Therapeutic Agent Enables Green-Light-Triggered Chemotherapy and Simultaneous Photodynamic Therapy to Cancer Cells. *ACS Applied Bio Materials* **2019,** *2* (7), 3068-3076.
9. Kuhn, H.; Braslavsky, S.; Schmidt, R., Chemical actinometry (IUPAC Technical Report). *Pure and Applied Chemistry - Pure and Applied Chemistry* **2004,** *76*, 2105-2146.
10. Megerle, U.; Lechner, R.; König, B.; Riedle, E., Laboratory apparatus for the accurate, facile and rapid determination of visible light photoreaction quantum yields. *Photochemical & Photobiological Sciences* **2010,** *9* (10), 1400-1406.

11. Briales, A.; Rodríguez-Martínez, J. M.; Velasco, C.; Díaz de Alba, P.; Domínguez-Herrera, J.; Pachón, J.; Pascual, A., In vitro effect of qnrA1, qnrB1, and qnrS1 genes on fluoroquinolone activity against isogenic Escherichia coli isolates with mutations in gyrA and parC. *Antimicrobial Agents and Chemotherapy* **2011,** *55* (3), 1266-1269.
12. Cornet, J.-F.; Marty, A.; Gros, J.-B., Revised Technique for the Determination of Mean Incident Light Fluxes on Photobioreactors. *Biotechnology Progress* **1997,** *13* (4), 408-415.
13. CLSI, *Performance Standards for Antimicrobial Susceptibility Testing*. 30th ed.; Clinical and Laboratory Standards Institute: Wayne, PA, 2020.
14. Ji, C.; Miller, P. A.; Miller, M. J., Syntheses and Antibacterial Activity of N-Acylated Ciprofloxacin Derivatives Based on the Trimethyl Lock. *ACS Medicinal Chemistry Letters* **2015,** *6* (6), 707-710.

Chapter 7
Conclusions/Conclusiones

In this doctoral thesis, several quinolone derivatives have been designed, synthesized, and evaluated. To gain control over their antibacterial activity using light as a stimulus, two different methods have been followed. The first method, inside the photopharmacological approach, is based on the use of molecular switches linked to the antibiotic part to generate a reversible system. The second method, the caging technique, relies on the use of a photoreleasable protective group attached to the antibiotic molecule to create an irreversible system.

From the photopharmacological approach, followed in chapter 4, the following conclusions can be drawn:

- The synthetic routes have been designed either to create the antibiotic part from scratch with a molecular switch in position 7, or to modify a commercially available antibiotic and link the molecular switch in two different positions, 3 or 7.
- It has been proved that all derivatives are able to carry out the isomerization process when irradiated with UV or visible light, reaching different PSS in short times. Furthermore, most of them are able to revert to the initial isomer by thermal relaxation.
- In one specific case (**9a**), additional studies have been performed that have proved the excellent stability of the derivative as well as the high efficiency of the isomerization process.
- Out of the six candidates, two of them (**9a** and **9b**) have demonstrated to change their activity upon light irradiation, with a 4-fold change in activity as the best result found for the MIC assay.

From the caging technique, followed in chapter 5 and 6, the following conclusions can be drawn:

- The synthetic routes of both groups, oxime esters and BODIPYs, have been designed to link the photoprotective group at position 3 of the quinolone antibiotic.
- The release reaction of oxime esters has been successfully carried out with both visible and UV light.
- In the case of BODIPYs, the release reaction has been carried out with visible light. More importantly, some of them can be used inside the therapeutic window with a total release of the antibiotic part.
- Both photoprotective groups have shown high stability when they are kept in the dark.

- Solubility in water has been achieved by micelle entrapment of one oxime ester derivative. Regarding BODIPY derivatives, partial water solubility has been achieved, although DMSO is needed for a complete solution.
- The biological studies performed of BODIPY derivatives have proved a strong deactivation of the antibacterial properties when the antibiotic is caged. Upon light irradiation, the antibiotic activity is recovered with the best results showing a 10-fold change in activity for the MIC assay.

En esta tesis doctoral, se han diseñado, sintetizado y evaluado varios derivados de la familia de las quinolonas. Con el fin de obtener control sobre la actividad antibacteriana utilizando la luz como estímulo, se han seguido dos métodos distintos. El primer método, dentro del enfoque fotofarmacológico, está basado en el uso de interruptores moleculares unidos a una parte antibiótica. El segundo método, la técnica de enjaulado, se basa en el uso de un grupo protector fotoliberable unido a la molécula antibiótica para crear un sistema irreversible.

A partir del enfoque fotofarmacológico, seguido en el capítulo 4, se pueden obtener las siguientes conclusiones:

- Se han diseñado rutas sintéticas que, o bien crean la parte antibiótica desde cero con un interruptor molecular en la posición 7, o modifican un antibiótico disponible comercialmente para unir el interruptor molecular en dos posiciones diferentes 3 o 7.
- Se ha demostrado que todos los derivados son capaces de llevar a cabo el proceso de isomerización cuando son irradiados con luz UV o visible, alcanzando distintos estados fotoestacionarios en tiempos cortos. Además, la mayoría de ellos son capaces de revertir al isómero inicial mediante relajación térmica.
- En uno de los casos (**9a**), se han realizado estudios adicionales que han probado la excelente estabilidad del derivado, así como la alta eficiencia del proceso de isomerización.
- De los seis candidatos, dos de ellos (**9a** y **9b**) han demostrado un cambio en su actividad tras su irradiación con luz. El mejor resultado encontrado fue de 4 órdenes de diferencia en el ensayo de la CMI.

A partir de la técnica de enjaulado, seguida en los capítulos 5 y 6, se pueden obtener las siguientes conclusiones:

- Las rutas sintéticas de ambos grupos, ésteres de oxima y BODIPYs, se han diseñado para unir el grupo fotoprotector en la posición 3 de la quinolona.
- La reacción de liberación de los ésteres de oxima se ha llevado a cabo exitosamente con luz visible y UV.
- En el caso de los BODIPYs, la reacción de liberación se ha llevado a cabo con luz visible. Más importante, algunos de ellos pueden usarse dentro de la ventana terapéutica con una liberación total de la parte antibiótica.
- Ambos grupos fotoprotectores han mostrado tener una alta estabilidad cuando se encuentran en la oscuridad.

- La solubilidad en agua se ha conseguido encapsulando un éster de oxima dentro de una micela polimérica. En cuanto a los derivados de BODIPY, se ha conseguido una solubilidad parcial en agua, aunque es necesario utilizar DMSO para una total disolución.
- Los estudios biológicos realizados a los derivados de BODIPY han probado una fuerte desactivación de las propiedades antibacterianas cuando el antibiótico está enjaulado. Tras su irradiación con luz, se recupera la actividad antibiótica. Los mejores resultados mostraron un cambio en la actividad de 10 órdenes en el ensayo de la CMI.

Appendix

General Information and Characterization Data

A. General information

For synthesis, all chemicals were obtained from commercial sources and used as received unless stated otherwise. Room temperature reactions were carried out between 22-25 °C. Thin-layer chromatography (TLC) was performed using silica gel 60 pre-coated aluminum plates (Macherey-Nagel 0.20 mm thickness) with a fluorescence indicator UV_{254}. Solvents were ACS grade and used without further purification. For the detection of components, UV light at 254 nm was used. All chromatographic solvents were ACS grade and used without further purification. Column chromatography was performed on silica gel 60 (0.040-0.063 mm) and the indicated eluent in each case.

^{1}H and ^{13}C NMR spectra were recorded on a Bruker AVANCE III HD (300 MHz) or a Bruker AVANCE (400 MHz) spectrometers at 25 °C. ^{1}H and ^{13}C spectra performed at Iowa State University were recorded on a Bruker AVANCE NEO (400 MHz) spectrometer at 25 °C. Chemical shifts (δ) are reported in parts per million (ppm) with the solvent resonance as the internal standard (δ_H 7.26 for $CHCl_3$, 3.31 for CH_3OH, 4.79 for H_2O, and 2.50 for DMSO; δ_C 77.16 for $CHCl_3$, 49.00 for CH_3OH, and 39.52 for DMSO). Coupling constants (*J*) are reported in Hertz (Hz). The following abbreviations are used to indicate signal multiplicity: s (singlet), d (doublet), t (triplet), q (quartet), m (multiplet), brs (broad singlet), dd (doublet of doublets), qd (quartet of doublets), and quint (quintet).

Molecular absorption spectra were obtained by using a spectrometer provided with an Ocean Optics USB4000-UV-Vis detector and coupled to a deuterium/tungsten halogen lamp. Quartz cuvettes with 1 cm optical path length were used. Solutions were prepared in a concentration range of 5E-5 M approximately.

High-resolution electrospray mass spectra (HR ESI-MS) were recorded on a Bruker MicrOTOF-Q spectrometer. Accurate mass measurements were achieved by using sodium formate as an external reference. HR ESI-MS performed at Iowa State University were recorded on an Agilent QTOF 6540 spectrometer.

B. Characterization data of selected compounds in chapter 4

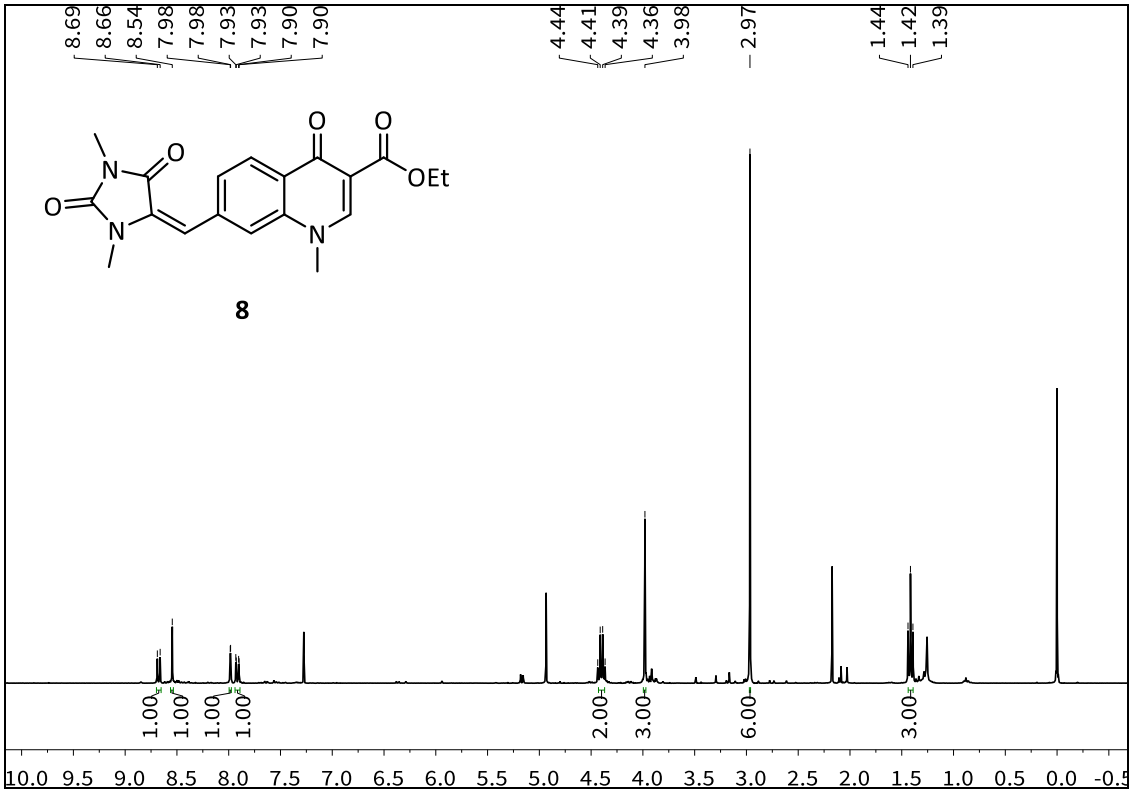

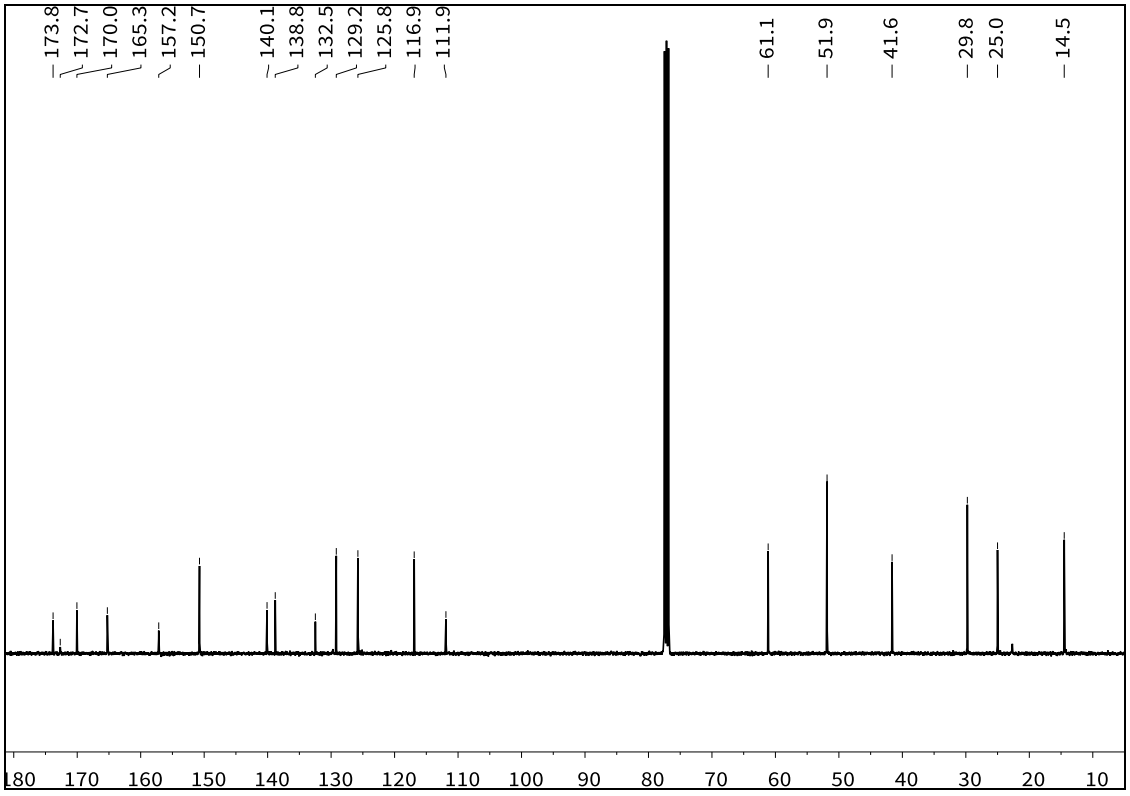

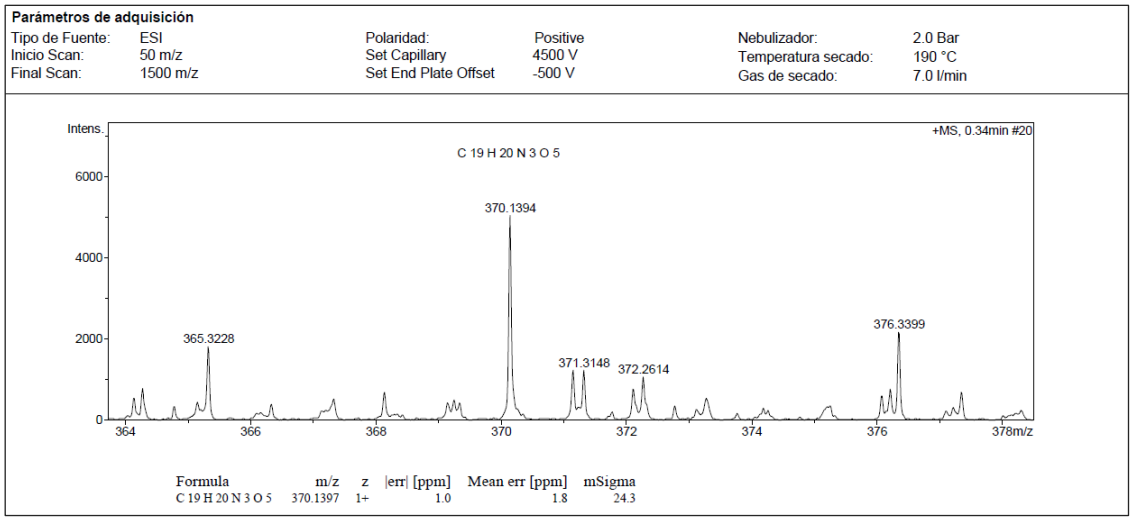
Parámetros de adquisición
Tipo de Fuente: ESI
Inicio Scan: 50 m/z
Final Scan: 1500 m/z
Polaridad: Positive
Set Capillary 4500 V
Set End Plate Offset -500 V
Nebulizador: 2.0 Bar
Temperatura secado: 190 °C
Gas de secado: 7.0 l/min
Intens.
+MS, 0.34min #20
C 19 H 20 N 3 O 5
370.1394
365.3228
371.3148
372.2614
376.3399
Formula m/z z |err| [ppm] Mean err [ppm] mSigma
C 19 H 20 N 3 O 5 370.1397 1+ 1.0 1.8 24.3

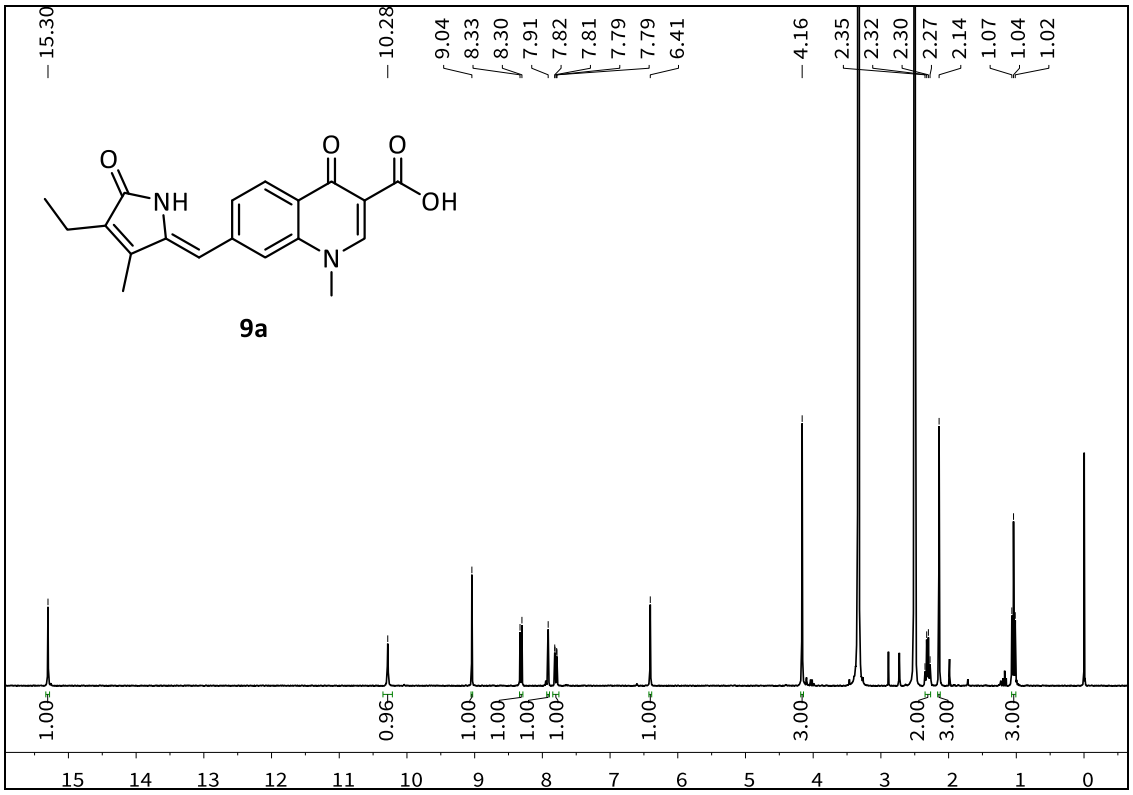
15.30
10.28
9.04
8.33
8.30
7.91
7.82
7.81
7.79
7.79
6.41
4.16
2.35
2.32
2.30
2.27
2.14
1.07
1.04
1.02
9a

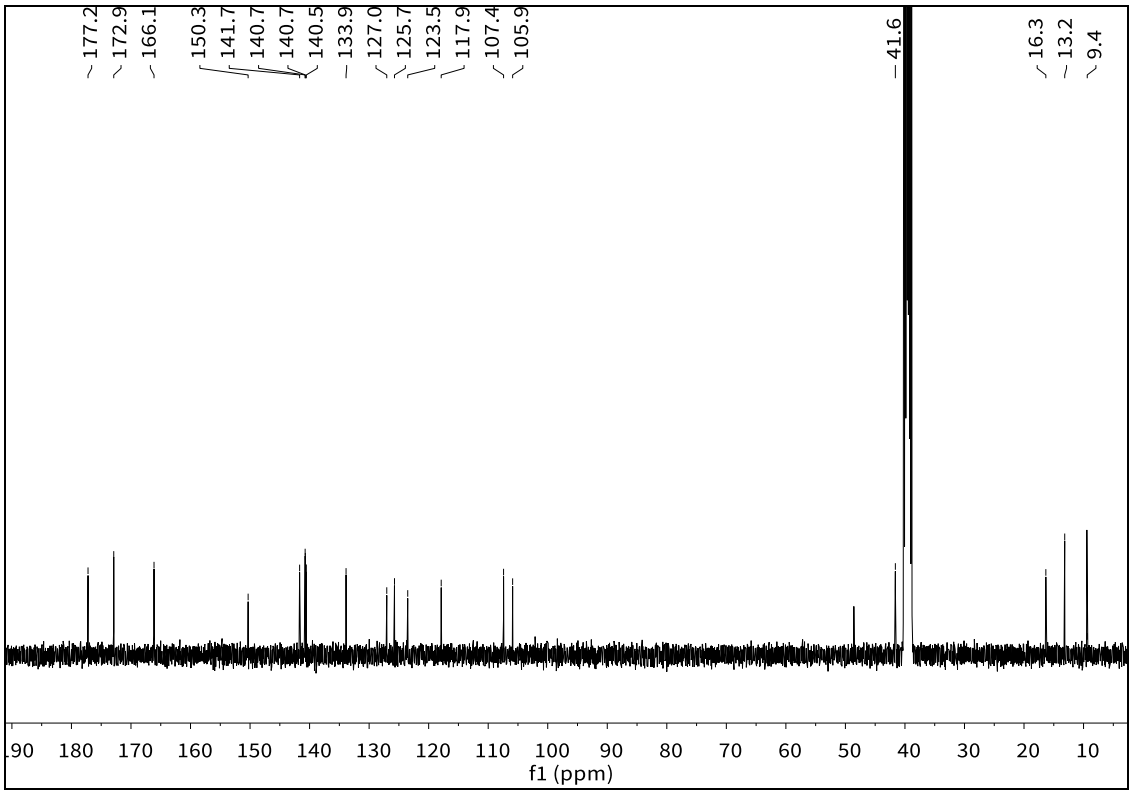
177.2
172.9
166.1
150.3
141.7
140.7
140.7
140.5
133.9
127.0
125.7
123.5
117.9
107.4
105.9
41.6
16.3
13.2
9.4
f1 (ppm)

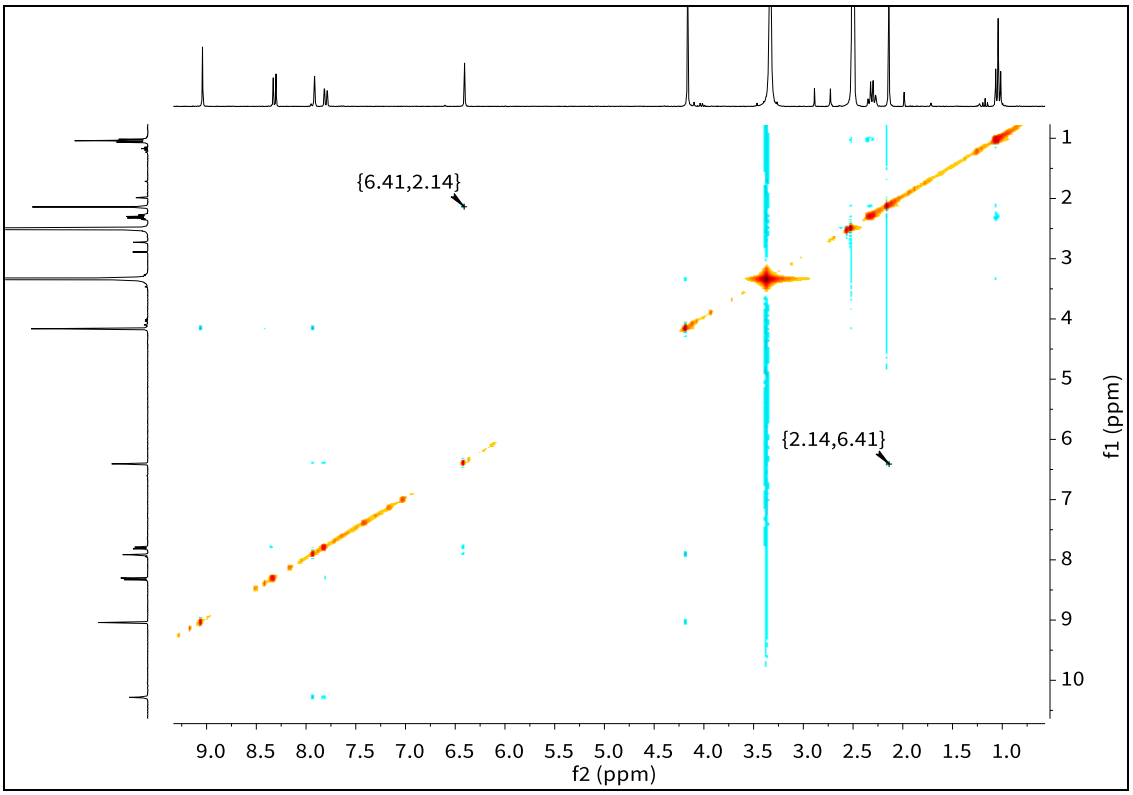
{6.41,2.14}
{2.14,6.41}
f2 (ppm)
f1 (ppm)

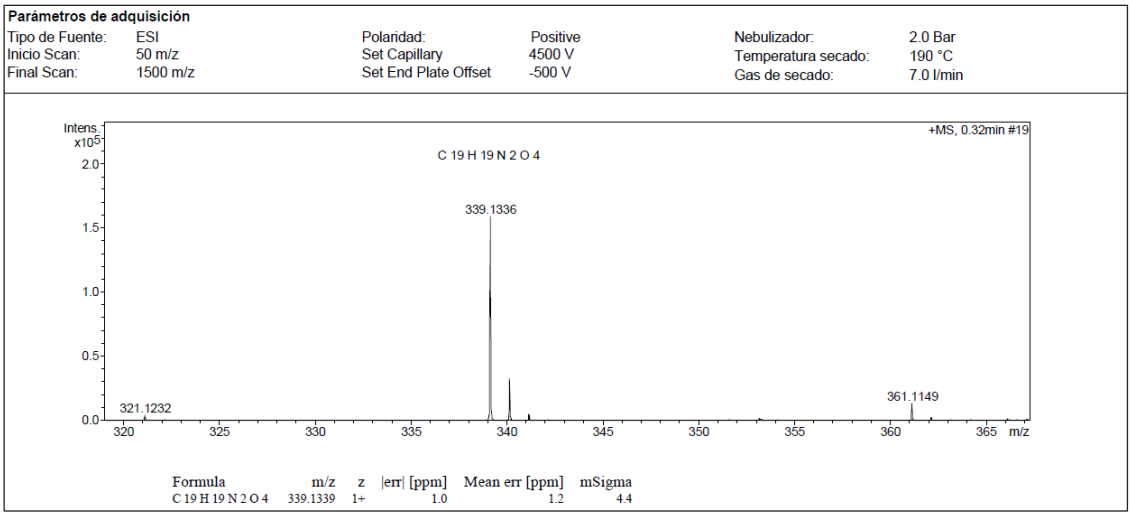
Parámetros de adquisición
Tipo de Fuente: ESI
Inicio Scan: 50 m/z
Final Scan: 1500 m/z
Polaridad: Positive
Set Capillary 4500 V
Set End Plate Offset -500 V
Nebulizador: 2.0 Bar
Temperatura secado: 190 °C
Gas de secado: 7.0 l/min
Intens. x10^5
+MS, 0.32min #19
C 19 H 19 N 2 O 4
339.1336
321.1232
361.1149
m/z
Formula m/z z |err| [ppm] Mean err [ppm] mSigma
C 19 H 19 N 2 O 4 339.1339 1+ 1.0 1.2 4.4

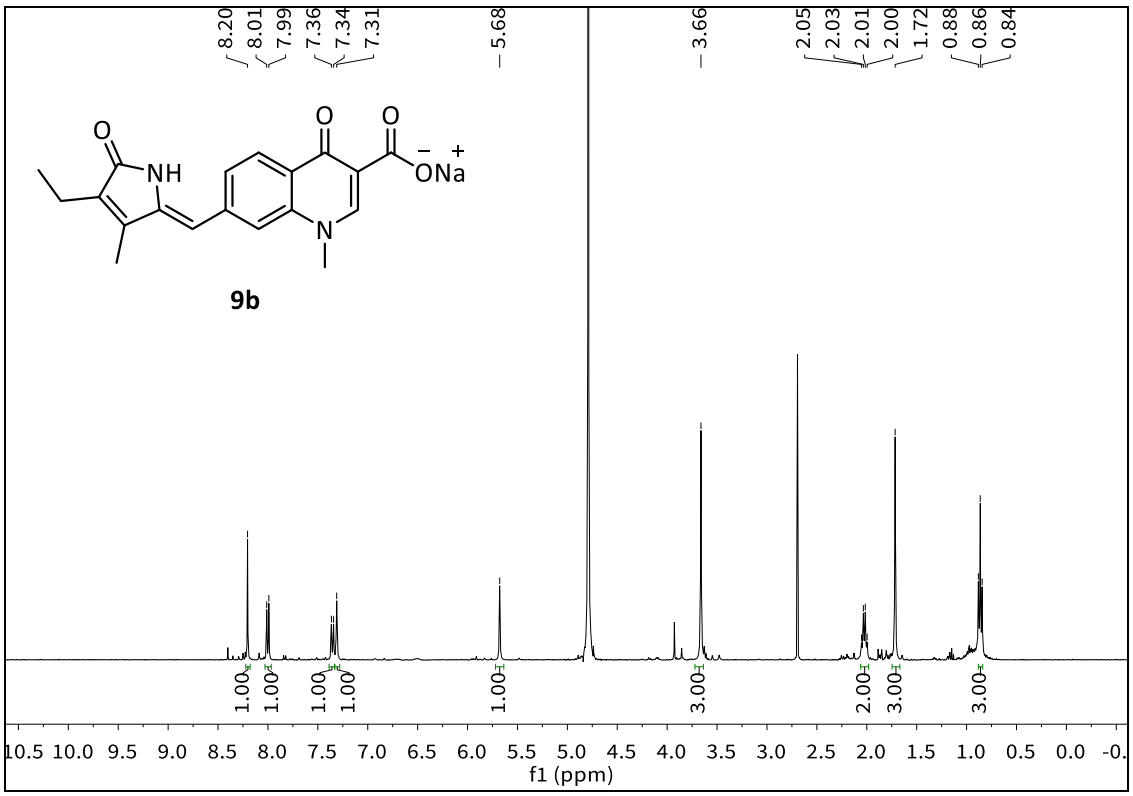
8.20
8.01
7.99
7.36
7.34
7.31
5.68
3.66
2.05
2.03
2.01
2.00
1.72
0.88
0.86
0.84
NH
ONa
9b
1.00
1.00
1.00
1.00
1.00
3.00
2.00
3.00
3.00
f1 (ppm)

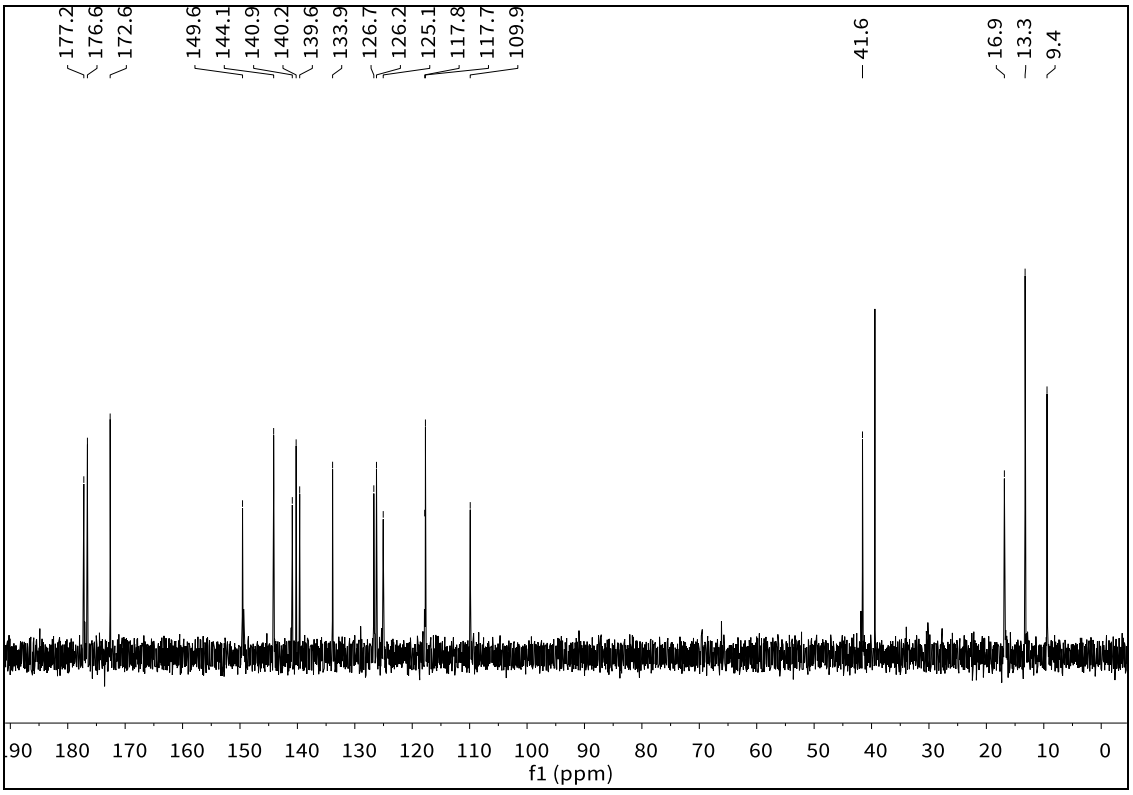

Parámetros de adquisición

Tipo de Fuente:	ESI	Polaridad:	Positive	Nebulizador:	2.0 Bar
Inicio Scan:	50 m/z	Set Capillary	4500 V	Temperatura secado:	190 °C
Final Scan:	1500 m/z	Set End Plate Offset	-500 V	Gas de secado:	7.0 l/min

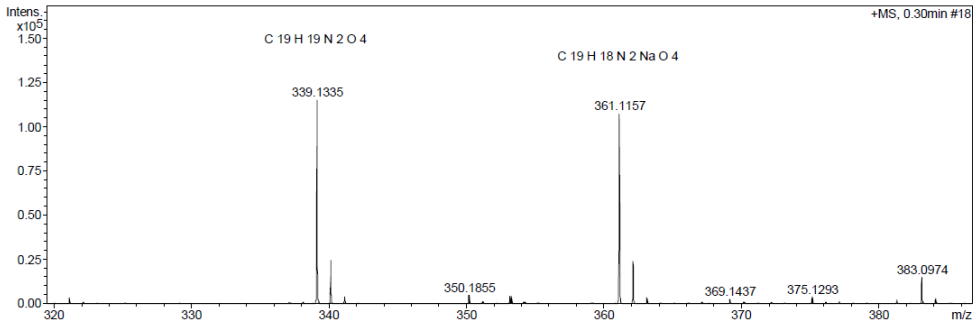

Formula	m/z	z	|err| [ppm]	Mean err [ppm]	mSigma
C 19 H 18 N 2 Na O 4	361.1159	1+	0.4	0.6	7.3
C 19 H 19 N 2 O 4	339.1339		1.2	1.0	3.0

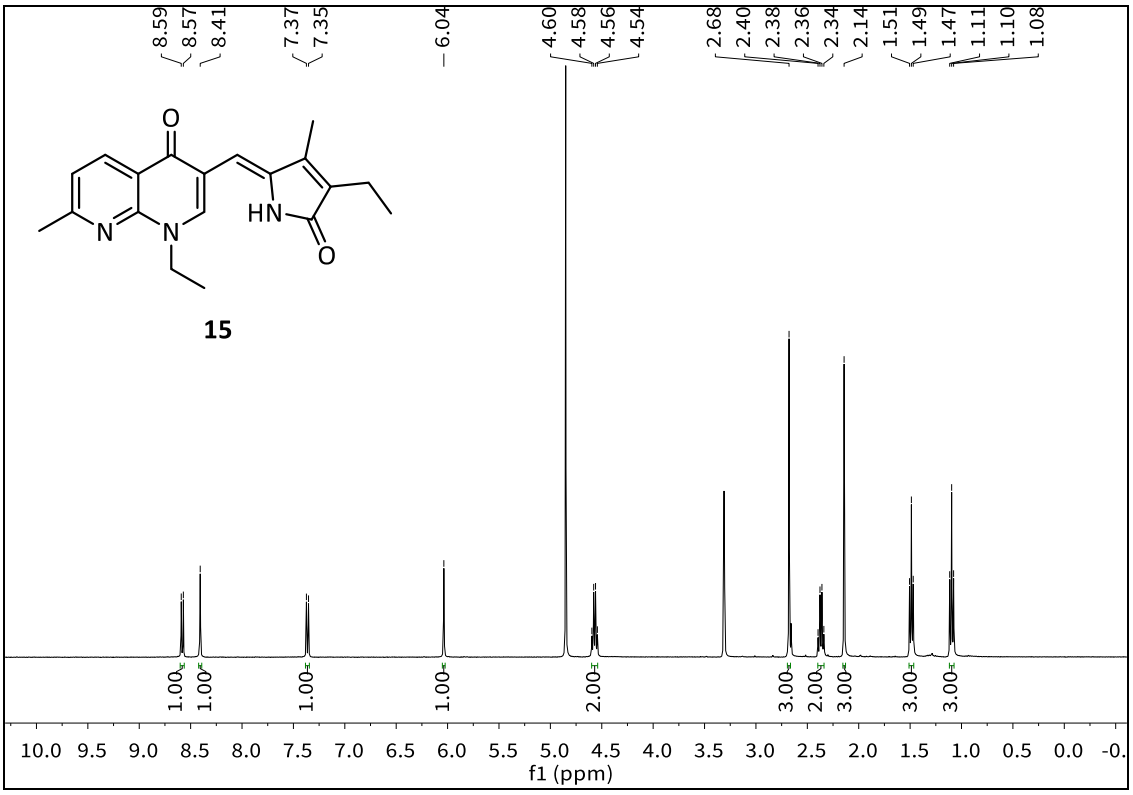
8.59
8.57
8.41
7.37
7.35
6.04
4.60
4.58
4.56
4.54
2.68
2.40
2.38
2.36
2.34
2.14
1.51
1.49
1.47
1.11
1.10
1.08
O
N
N
HN
O
15
1.00
1.00
1.00
1.00
2.00
3.00
2.00
3.00
3.00
3.00
10.0 9.5 9.0 8.5 8.0 7.5 7.0 6.5 6.0 5.5 5.0 4.5 4.0 3.5 3.0 2.5 2.0 1.5 1.0 0.5 0.0
f1 (ppm)

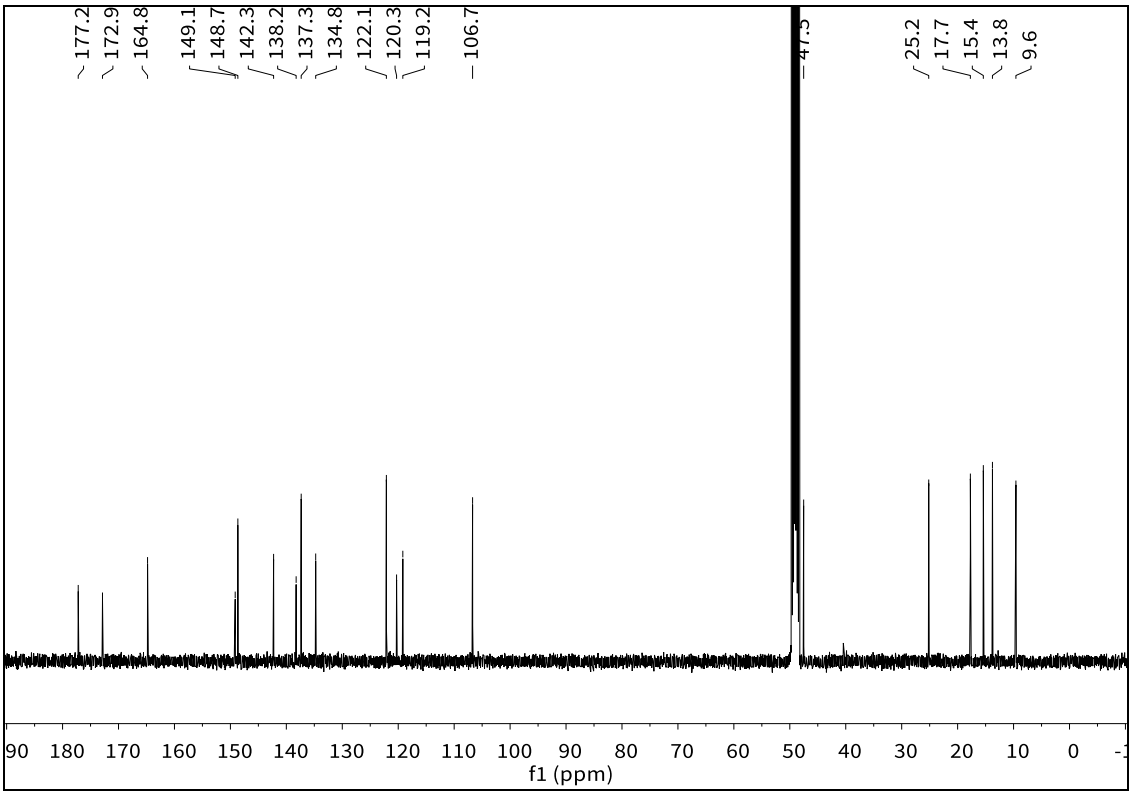
177.2
172.9
164.8
149.1
148.7
142.3
138.2
137.3
134.8
122.1
120.3
119.2
106.7
47.5
25.2
17.7
15.4
13.8
9.6
90 180 170 160 150 140 130 120 110 100 90 80 70 60 50 40 30 20 10 0
f1 (ppm)

Parámetros de adquisición

Tipo de Fuente:	ESI	Polaridad:	Positive	Nebulizador:	2.0 Bar
Inicio Scan:	50 m/z	Set Capillary	4500 V	Temperatura secado:	190 °C
Final Scan:	1500 m/z	Set End Plate Offset	-500 V	Gas de secado:	7.0 l/min

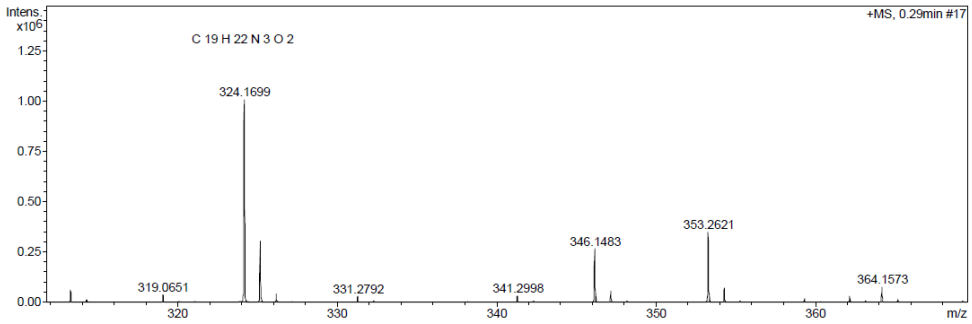

Formula	m/z	z	|err| [ppm]	Mean err [ppm]	mSigma
C 19 H 22 N 3 O 2	324.1707	1+	2.3	3.8	50.9

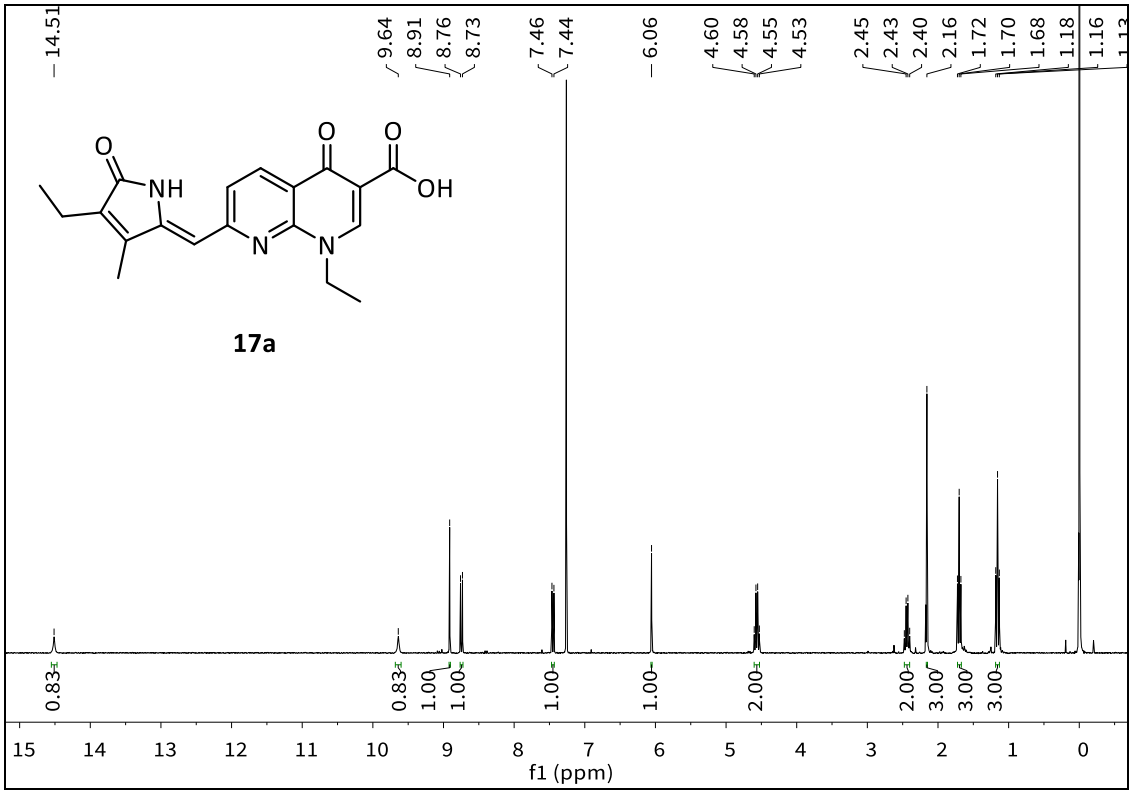

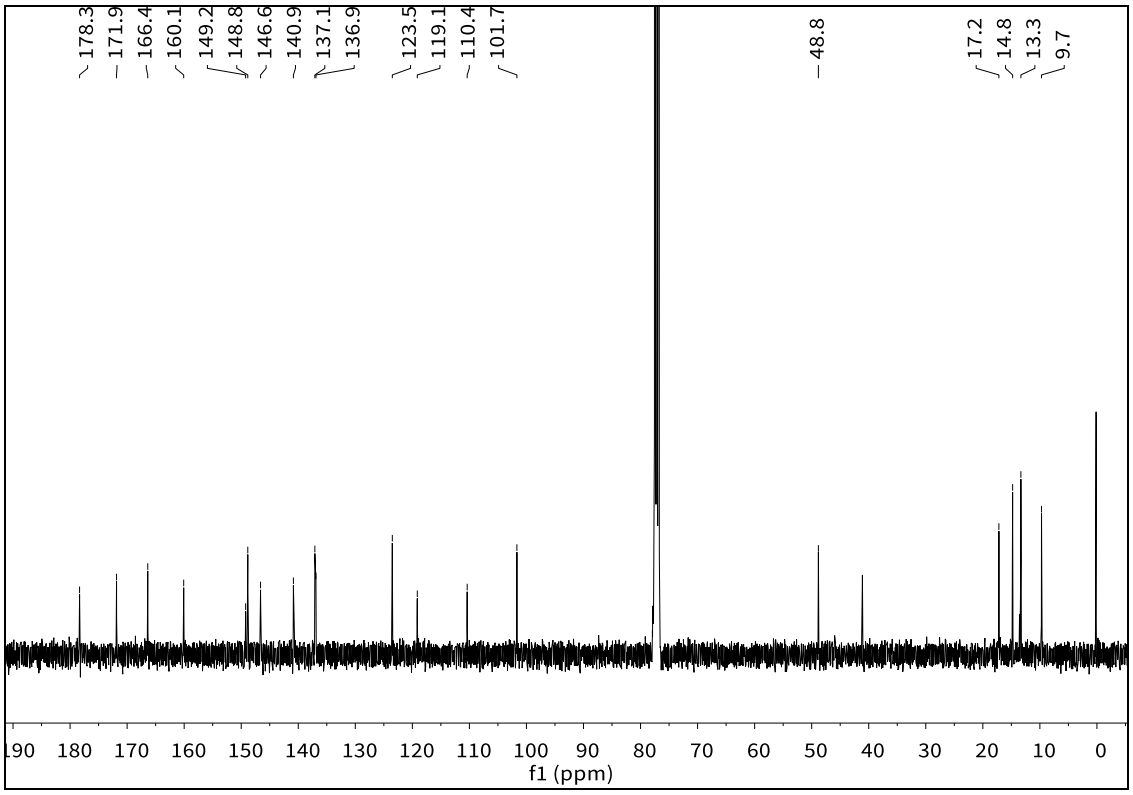
178.3
171.9
166.4
160.1
149.2
148.8
146.6
140.9
137.1
136.9
123.5
119.1
110.4
101.7
48.8
17.2
14.8
13.3
9.7
190 180 170 160 150 140 130 120 110 100 90 80 70 60 50 40 30 20 10 0
f1 (ppm)

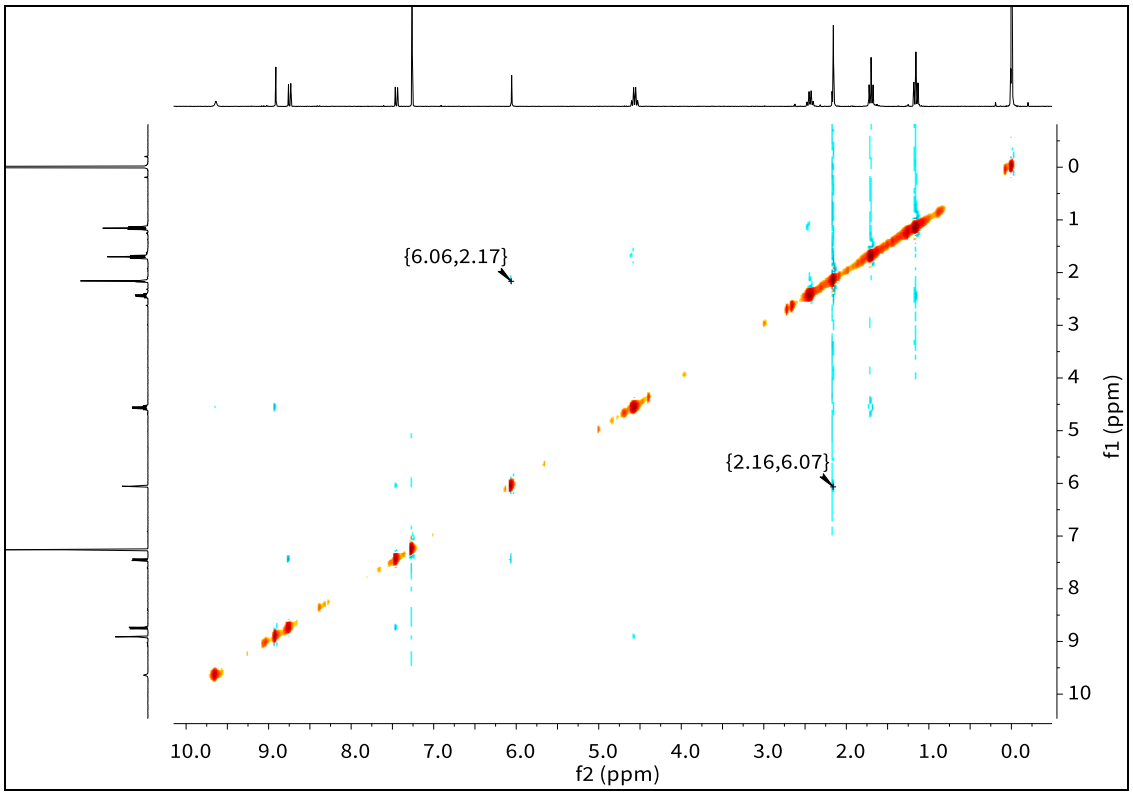
{6.06,2.17}
{2.16,6.07}
0 1 2 3 4 5 6 7 8 9 10
f1 (ppm)
10.0 9.0 8.0 7.0 6.0 5.0 4.0 3.0 2.0 1.0 0.0
f2 (ppm)

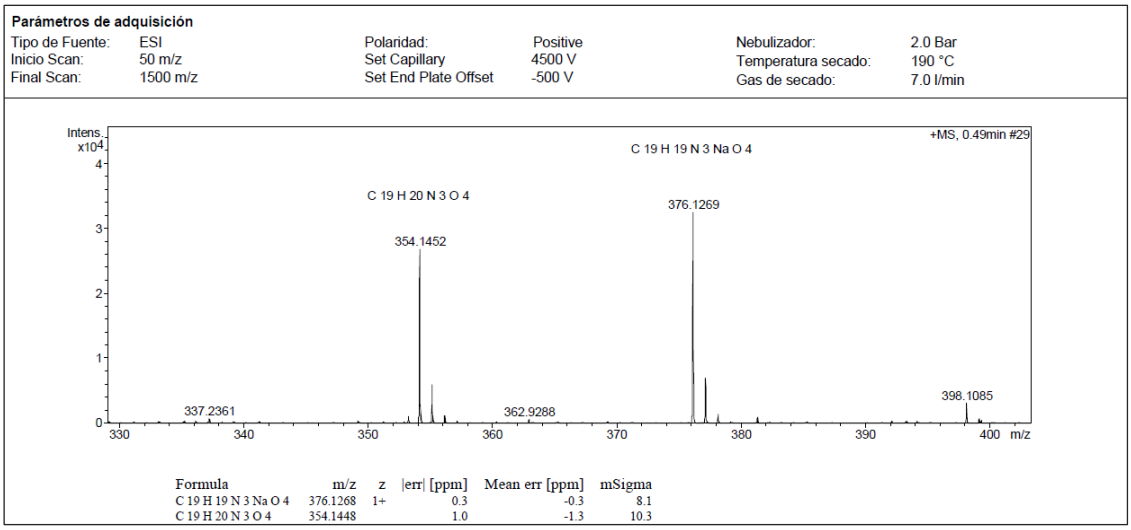
Parámetros de adquisición
Tipo de Fuente: ESI
Inicio Scan: 50 m/z
Final Scan: 1500 m/z
Polaridad: Positive
Set Capillary 4500 V
Set End Plate Offset -500 V
Nebulizador: 2.0 Bar
Temperatura secado: 190 °C
Gas de secado: 7.0 l/min
Intens. x10^4
+MS, 0.49min #29
C 19 H 19 N 3 Na O 4
C 19 H 20 N 3 O 4
376.1269
354.1452
337.2361
362.9288
398.1085
m/z
Formula m/z z |err| [ppm] Mean err [ppm] mSigma
C 19 H 19 N 3 Na O 4 376.1268 1+ 0.3 -0.3 8.1
C 19 H 20 N 3 O 4 354.1448 1.0 -1.3 10.3

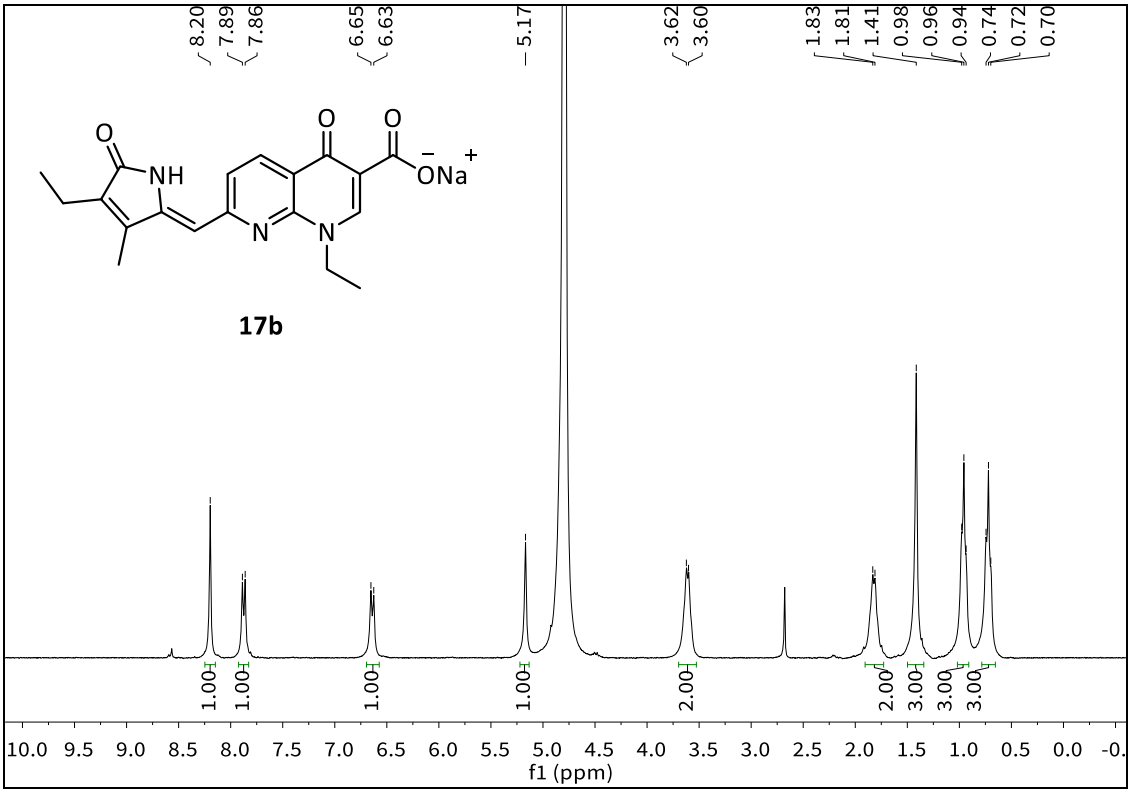
8.20
7.89
7.86
6.65
6.63
5.17
3.62
3.60
1.83
1.81
1.41
0.98
0.96
0.94
0.74
0.72
0.70
NH
ONa
17b
1.00
1.00
1.00
1.00
2.00
2.00
3.00
3.00
3.00
f1 (ppm)

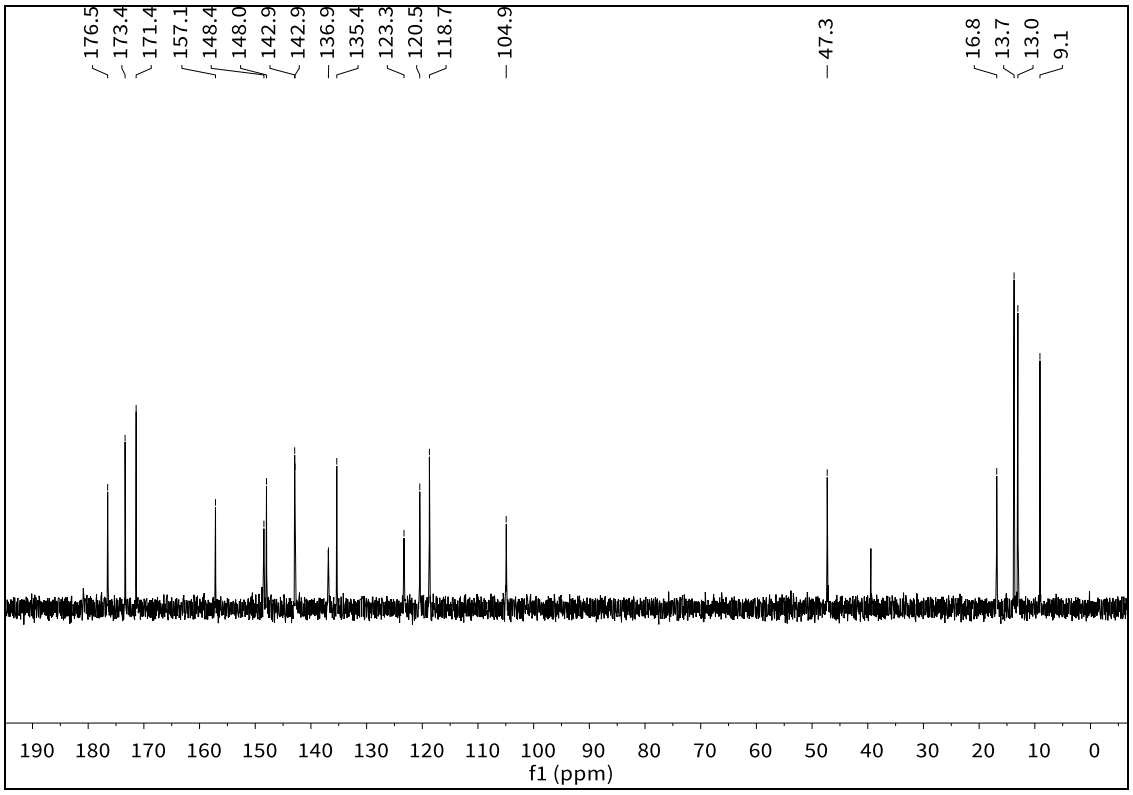

Parámetros de adquisición

Tipo de Fuente:	ESI	Polaridad:	Positive	Nebulizador:	2.0 Bar
Inicio Scan:	50 m/z	Set Capillary	4500 V	Temperatura secado:	190 °C
Final Scan:	1500 m/z	Set End Plate Offset	-500 V	Gas de secado:	7.0 l/min

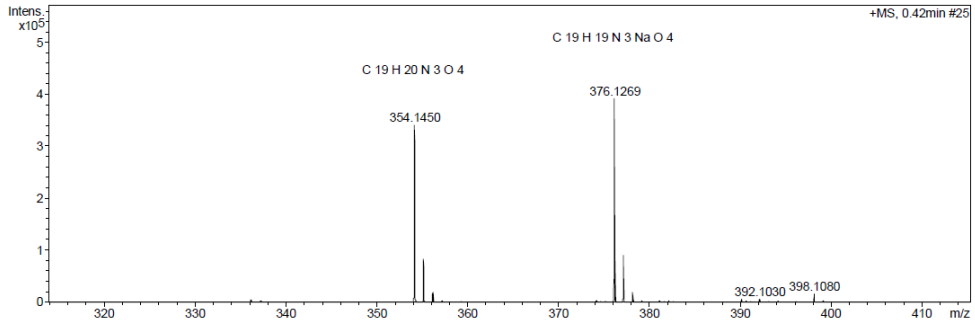

Formula	m/z	z	|err| [ppm]	Mean err [ppm]	mSigma
C 19 H 19 N 3 Na O 4	376.1268	1+	0.4	-0.2	13.9
C 19 H 20 N 3 O 4	354.1448		0.4	-0.4	20.9

C. Characterization data of selected compounds in chapter 5

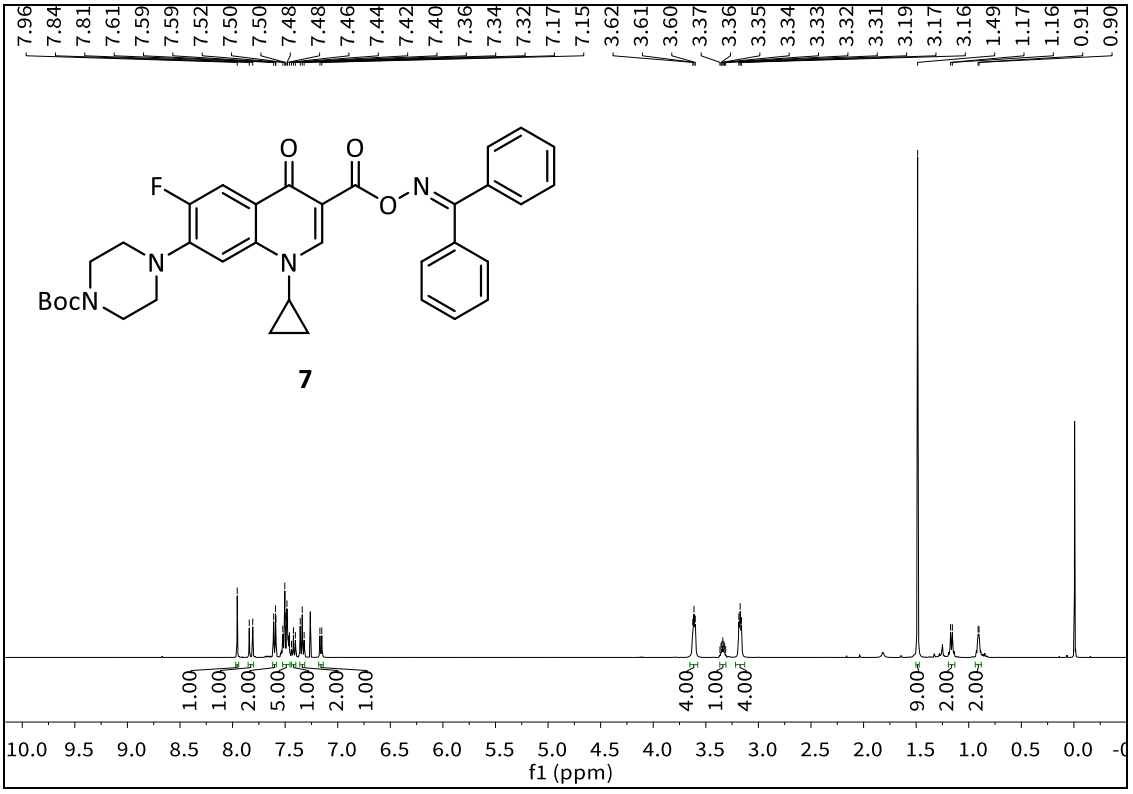

7

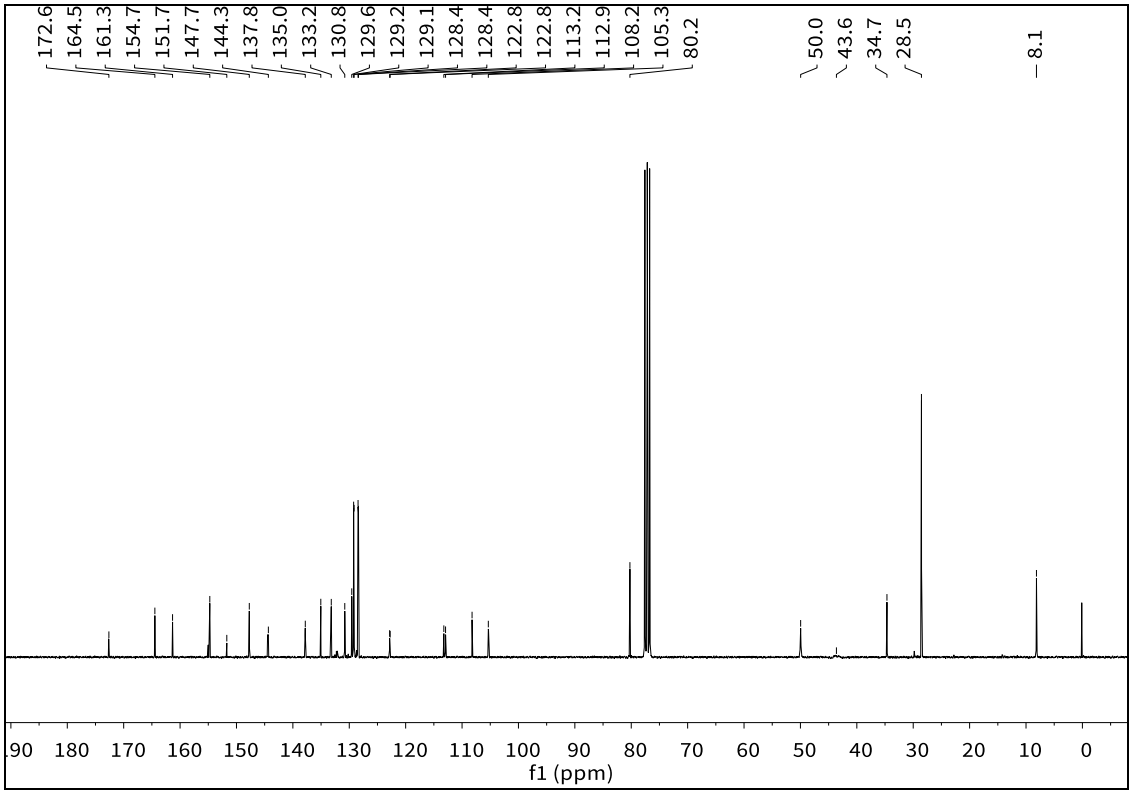

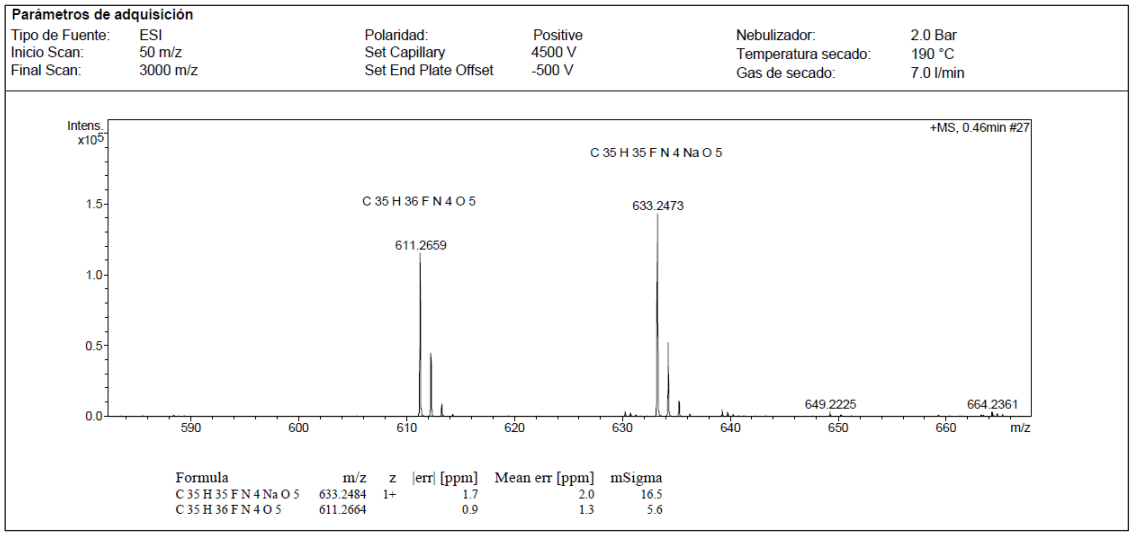
Parámetros de adquisición
Tipo de Fuente: ESI
Inicio Scan: 50 m/z
Final Scan: 3000 m/z
Polaridad: Positive
Set Capillary 4500 V
Set End Plate Offset -500 V
Nebulizador: 2.0 Bar
Temperatura secado: 190 °C
Gas de secado: 7.0 l/min
Intens. x10^5
+MS, 0.46min #27
C 35 H 35 F N 4 Na O 5
C 35 H 36 F N 4 O 5
633.2473
611.2659
649.2225
664.2361
m/z
Formula m/z z |err| [ppm] Mean err [ppm] mSigma
C 35 H 35 F N 4 Na O 5 633.2484 1+ 1.7 2.0 16.5
C 35 H 36 F N 4 O 5 611.2664 0.9 1.3 5.6

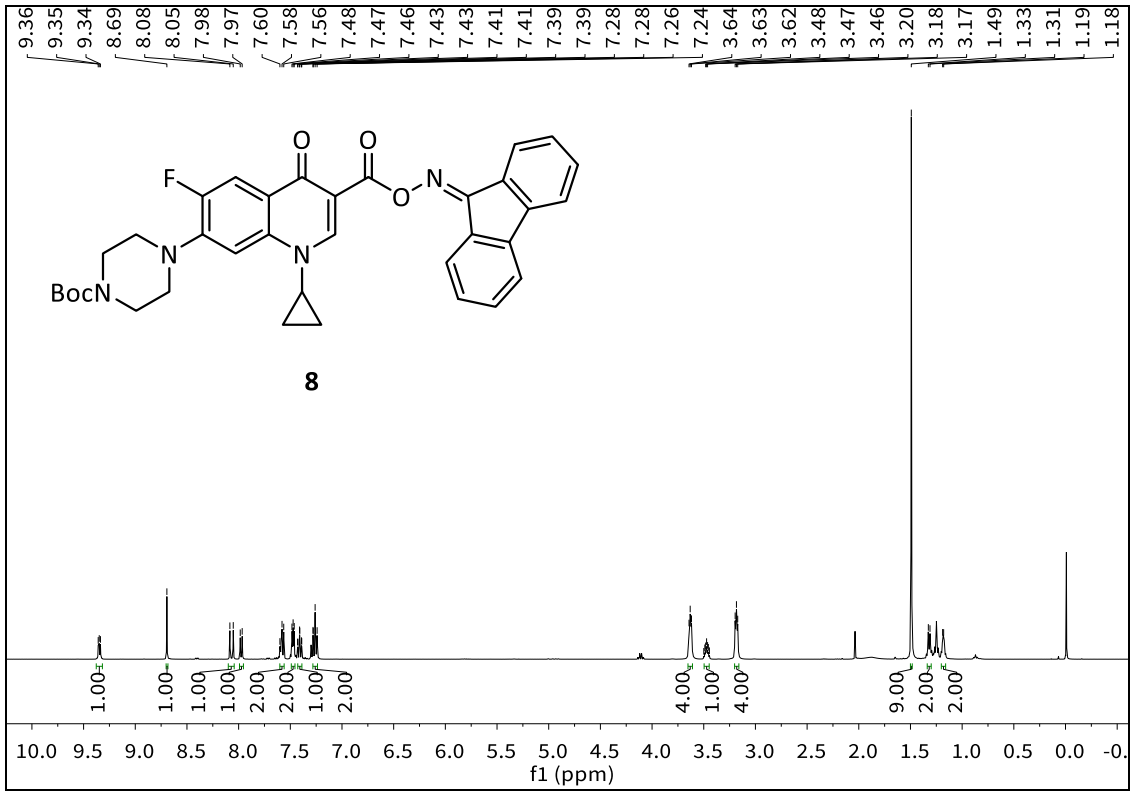
9.36 9.35 9.34 8.69 8.08 8.05 7.98 7.97 7.60 7.58 7.56 7.48 7.47 7.46 7.43 7.43 7.41 7.41 7.39 7.39 7.28 7.28 7.26 7.24 3.64 3.63 3.62 3.48 3.47 3.46 3.20 3.18 3.17 1.49 1.33 1.31 1.19 1.18
F
O
O
O
N
N
N
BocN
8
1.00 1.00 1.00 1.00 2.00 2.00 1.00 2.00 4.00 1.00 4.00 9.00 2.00 2.00
10.0 9.5 9.0 8.5 8.0 7.5 7.0 6.5 6.0 5.5 5.0 4.5 4.0 3.5 3.0 2.5 2.0 1.5 1.0 0.5 0.0 -0.
f1 (ppm)

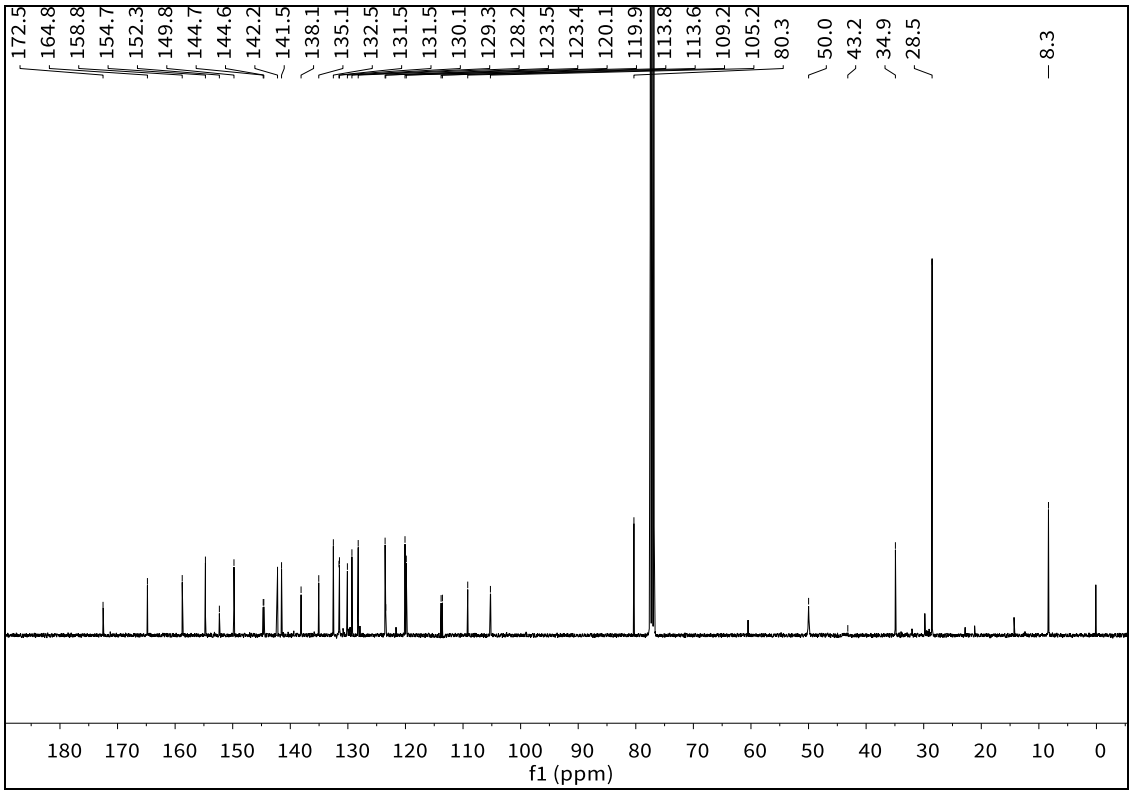

Parámetros de adquisición

Tipo de Fuente:	ESI	Polaridad:	Positive	Nebulizador:	2.0 Bar
Inicio Scan:	50 m/z	Set Capillary	4500 V	Temperatura secado:	190 °C
Final Scan:	3000 m/z	Set End Plate Offset	-500 V	Gas de secado:	7.0 l/min

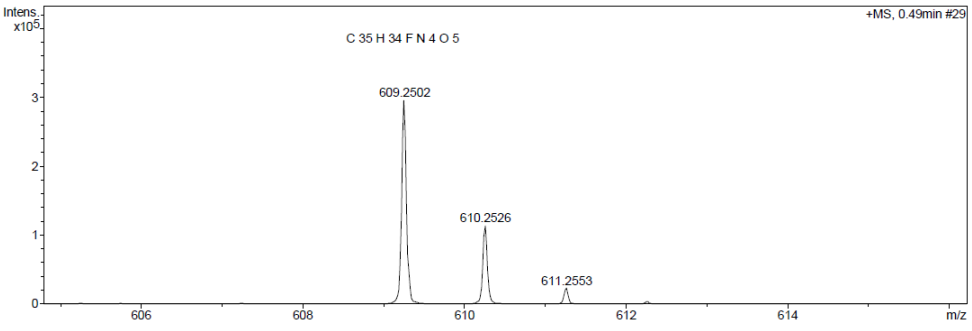

Formula	m/z	z	|err| [ppm]	Mean err [ppm]	mSigma
C 35 H 34 F N 4 O 5	609.2508	1+	0.9	1.5	7.5

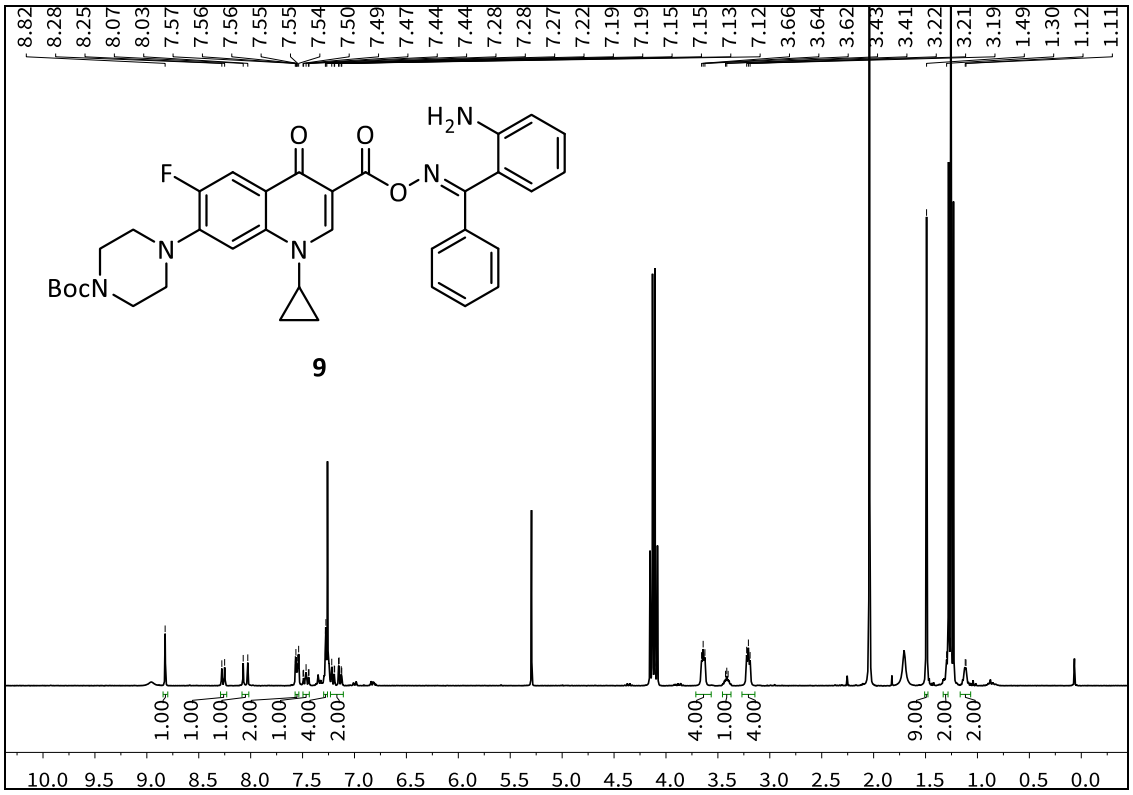

9

Parámetros de adquisición

Tipo de Fuente:	ESI	Polaridad:	Positive	Nebulizador:	2.0 Bar
Inicio Scan:	50 m/z	Set Capillary	4500 V	Temperatura secado:	190 °C
Final Scan:	3000 m/z	Set End Plate Offset	-500 V	Gas de secado:	7.0 l/min

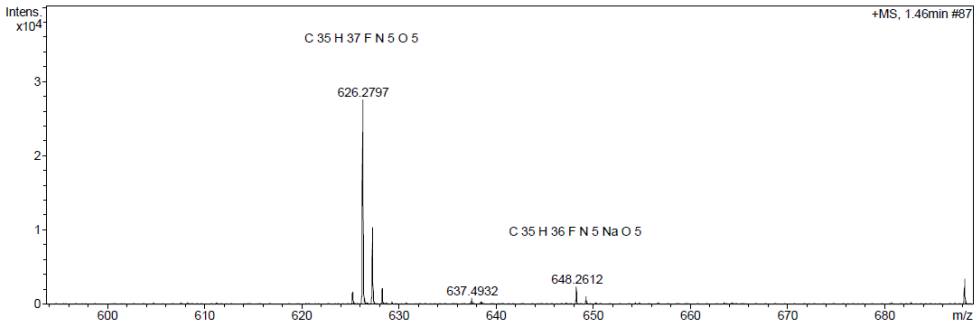

Formula	m/z	z	|err| [ppm]	Mean err [ppm]	mSigma
C 35 H 36 F N 5 Na O 5	648.2593	1+	3.0	-3.1	16.4
C 35 H 37 F N 5 O 5	626.2773		3.8	-3.2	13.6

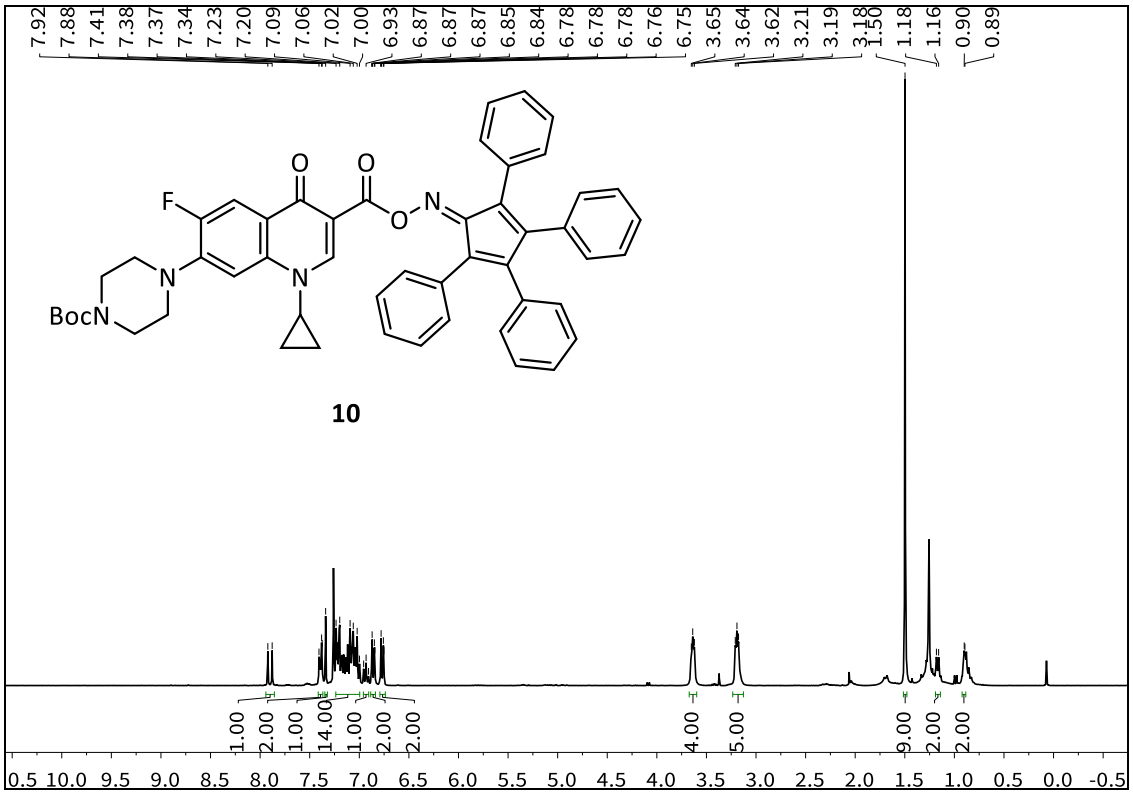
7.92
7.88
7.41
7.38
7.37
7.34
7.23
7.20
7.09
7.06
7.02
7.00
6.93
6.87
6.87
6.87
6.85
6.84
6.78
6.78
6.78
6.76
6.75
3.65
3.64
3.62
3.21
3.19
3.18
1.50
1.18
1.16
0.90
0.89
O
O
F
O
N
N
N
BocN
1.00
2.00
1.00
14.00
1.00
2.00
2.00
4.00
5.00
9.00
2.00
2.00
0.5 10.0 9.5 9.0 8.5 8.0 7.5 7.0 6.5 6.0 5.5 5.0 4.5 4.0 3.5 3.0 2.5 2.0 1.5 1.0 0.5 0.0 -0.5

10

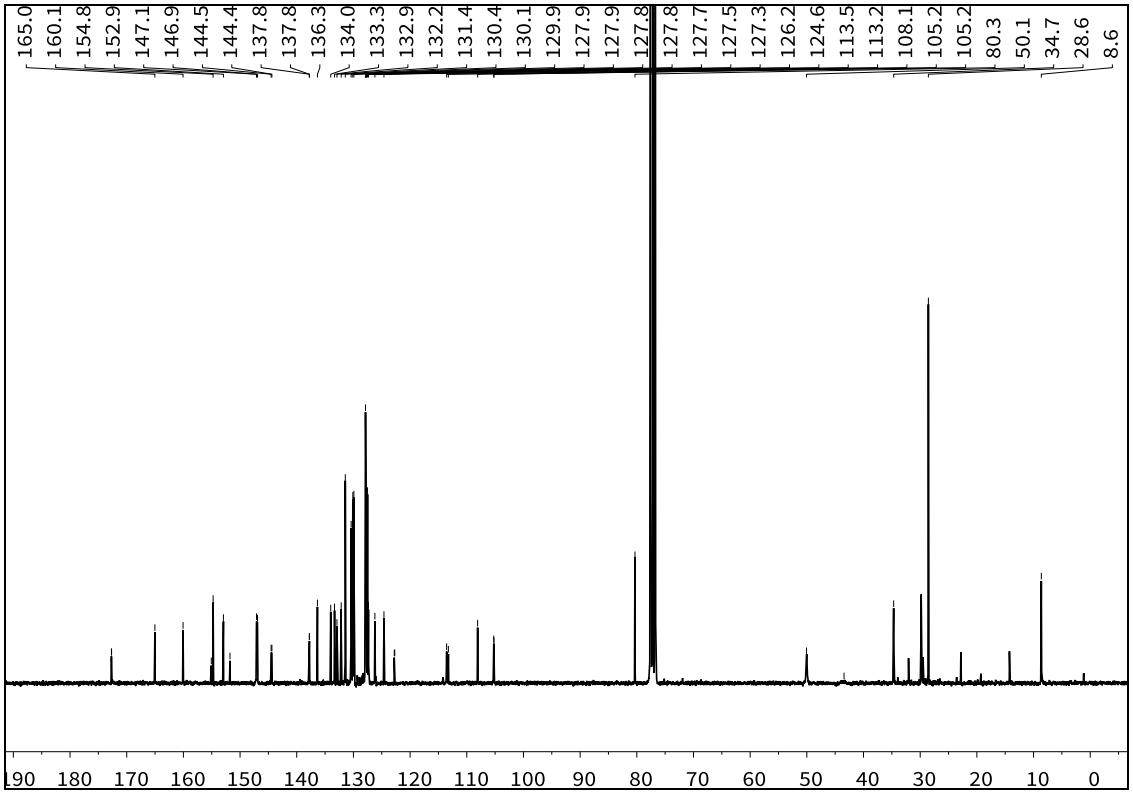
165.0
160.1
154.8
152.9
147.1
146.9
144.5
144.4
137.8
137.8
136.3
134.0
133.3
132.9
132.2
131.4
130.4
130.1
129.9
127.9
127.9
127.8
127.8
127.7
127.5
127.3
126.2
124.6
113.5
113.2
108.1
105.2
105.2
80.3
50.1
34.7
28.6
8.6
190 180 170 160 150 140 130 120 110 100 90 80 70 60 50 40 30 20 10 0

Parámetros de adquisición

Tipo de Fuente:	ESI	Polaridad:	Positive	Nebulizador:	2.0 Bar
Inicio Scan:	50 m/z	Set Capillary	4500 V	Temperatura secado:	190 °C
Final Scan:	3000 m/z	Set End Plate Offset	-500 V	Gas de secado:	7.0 l/min

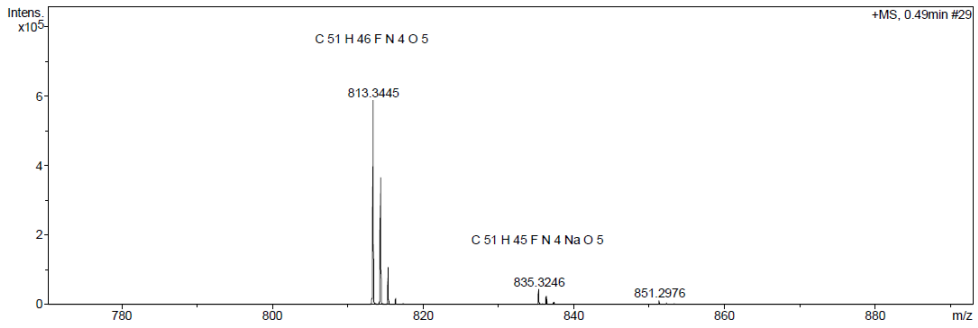

Formula	m/z	z	|err| [ppm]	Mean err [ppm]	mSigma
C 51 H 45 F N 4 Na O 5	835.3266	1+	2.4	2.5	18.4
C 51 H 46 F N 4 O 5	813.3447		0.2	0.7	25.2

D. Characterization data of selected compounds in chapter 6

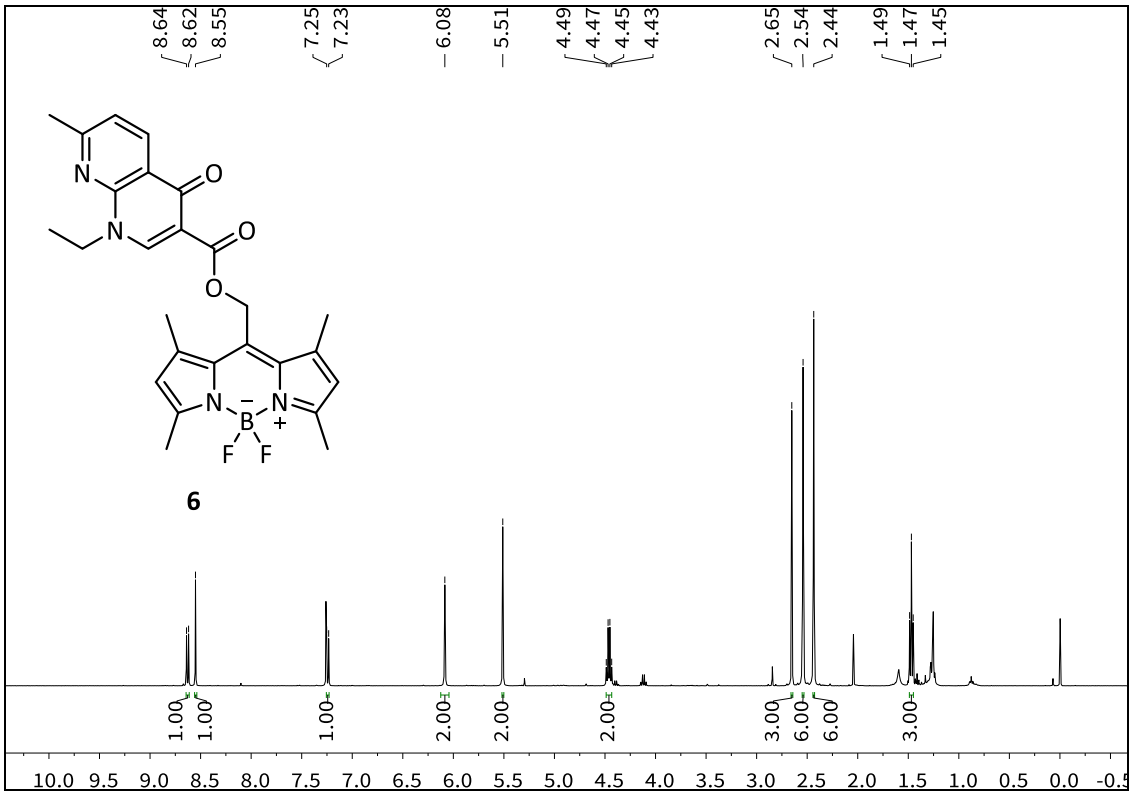

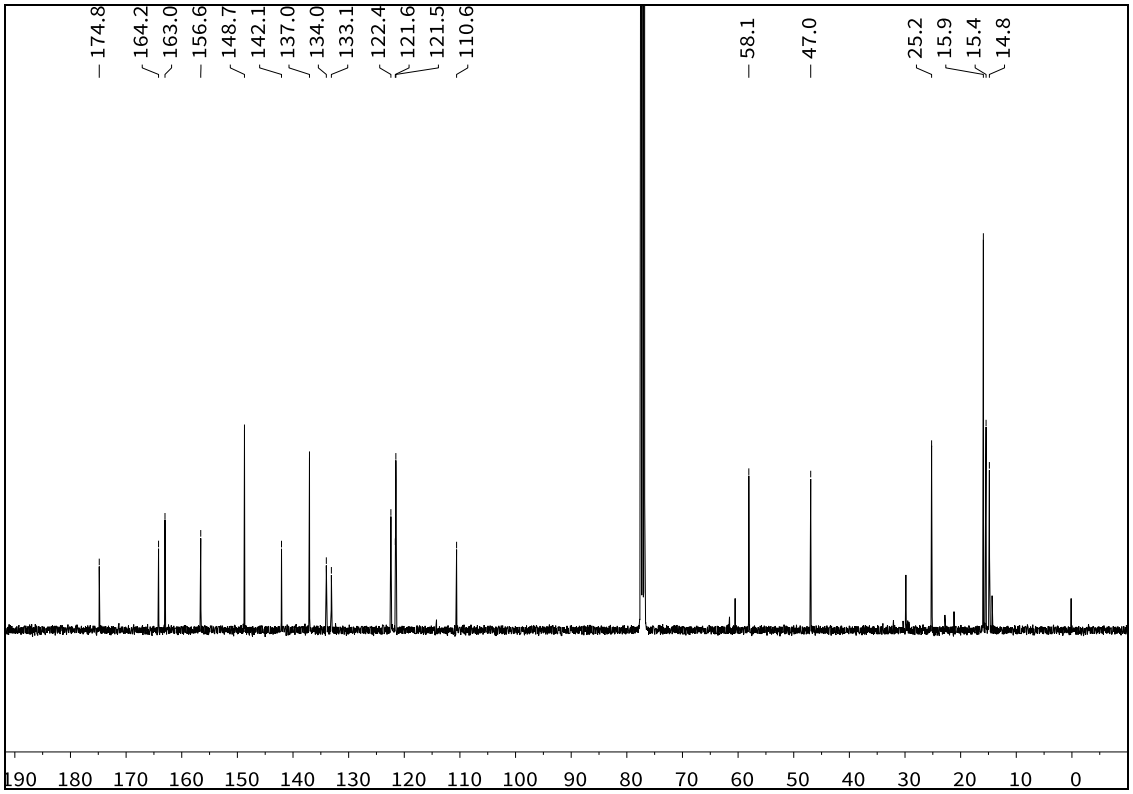

Parámetros de adquisición

Tipo de Fuente:	ESI	Polaridad:	Positive	Nebulizador:	2.0 Bar
Inicio Scan:	50 m/z	Set Capillary	4500 V	Temperatura secado:	190 °C
Final Scan:	3000 m/z	Set End Plate Offset	-500 V	Gas de secado:	7.0 l/min

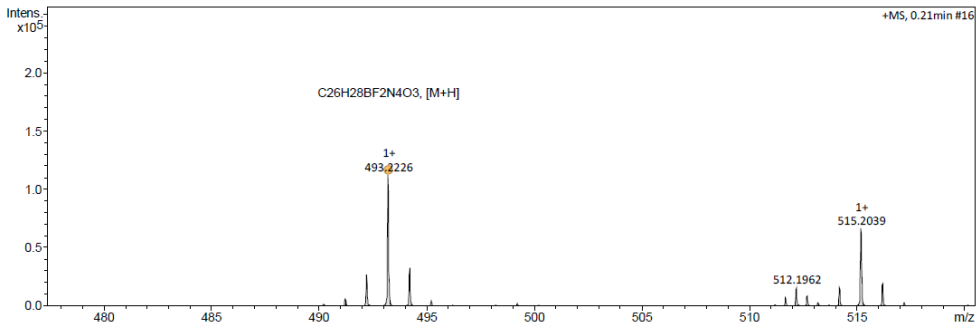

Ion Formula	m/z	z	|err| [ppm]	Mean err [ppm]	mSigma
C26H28BF2N4O3	493.221704	1+	7.8	-3.2	15.4

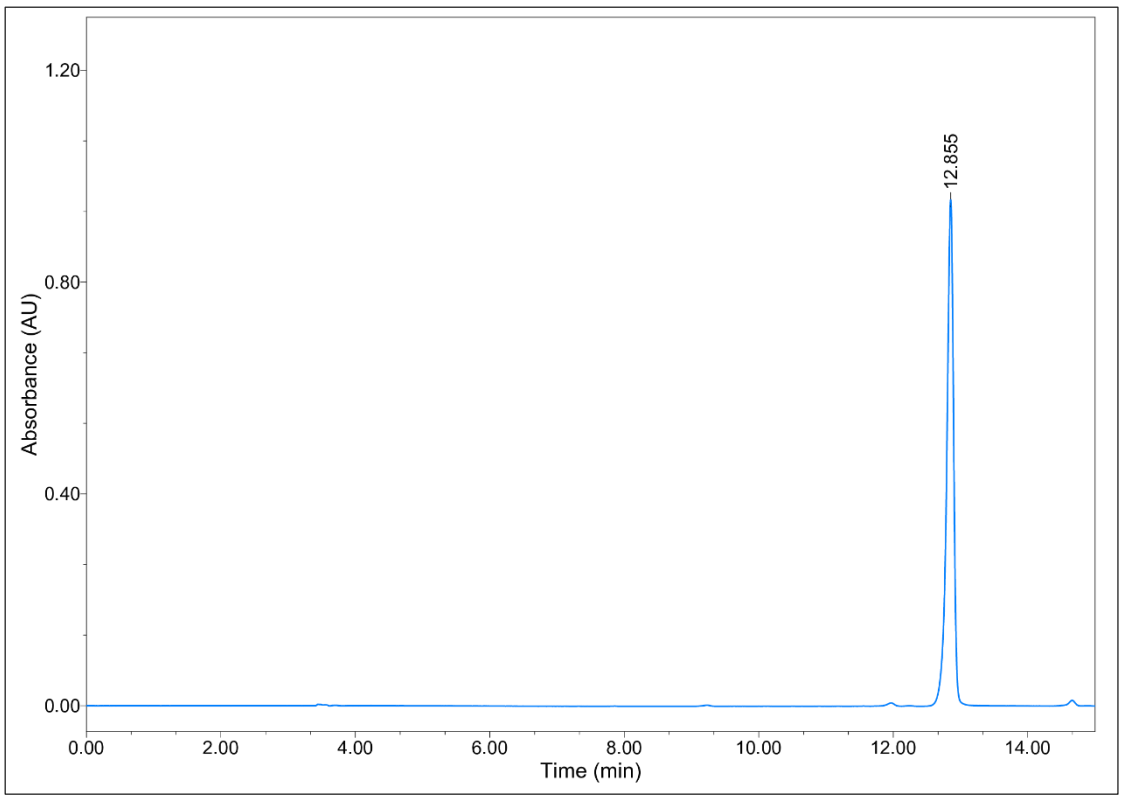

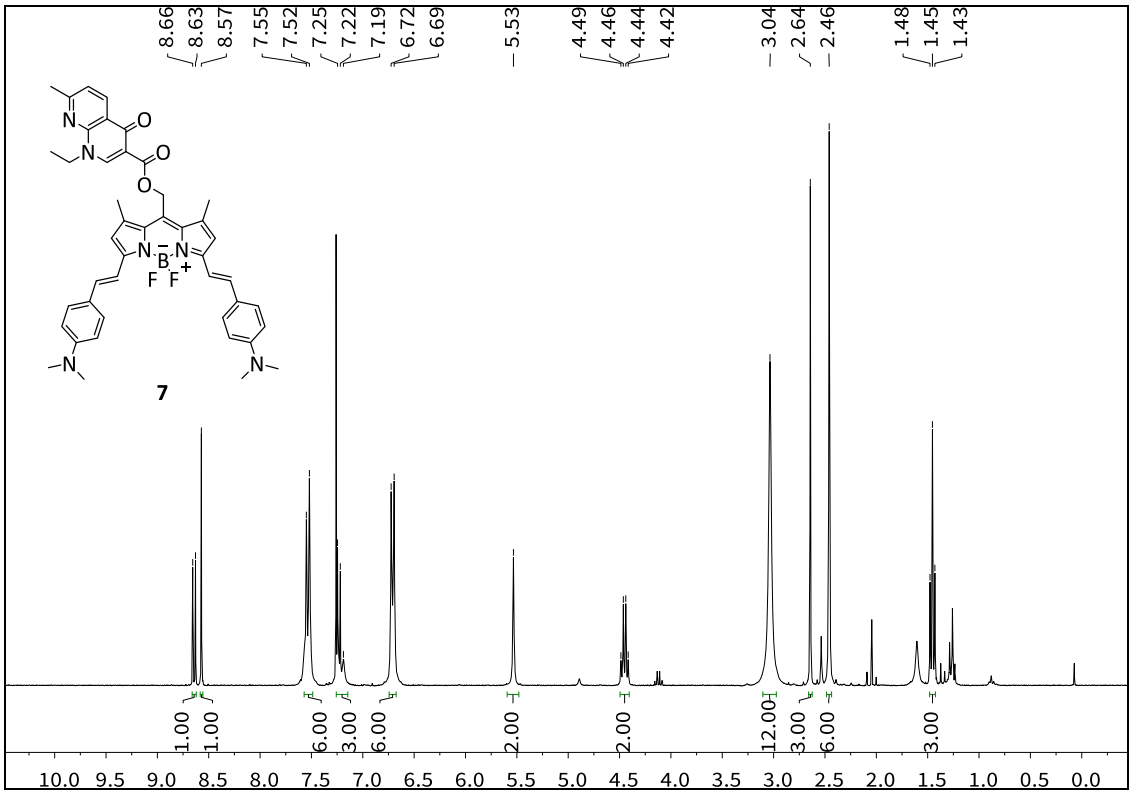
8.66
8.63
8.57
7.55
7.52
7.25
7.22
7.19
6.72
6.69
5.53
4.49
4.46
4.44
4.42
3.04
2.64
2.46
1.48
1.45
1.43
7
1.00
1.00
6.00
3.00
6.00
2.00
2.00
12.00
3.00
6.00
3.00
10.0 9.5 9.0 8.5 8.0 7.5 7.0 6.5 6.0 5.5 5.0 4.5 4.0 3.5 3.0 2.5 2.0 1.5 1.0 0.5 0.0

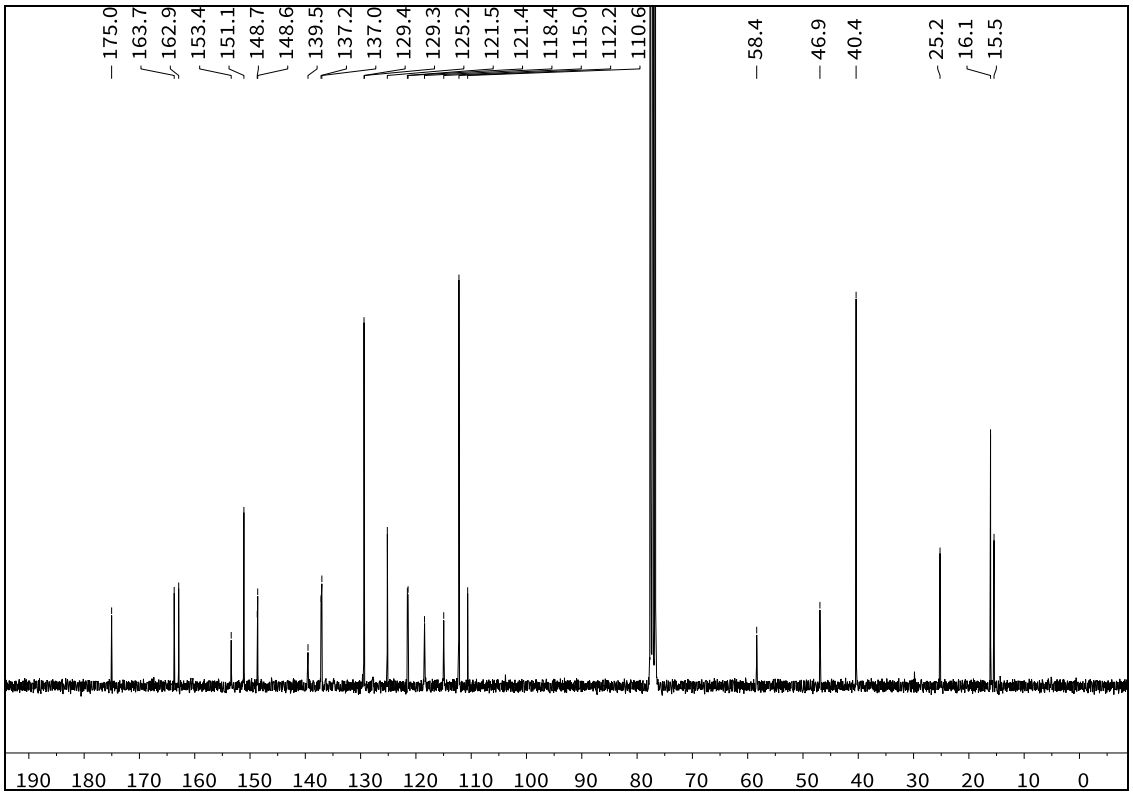
175.0
163.7
162.9
153.4
151.1
148.7
148.6
139.5
137.2
137.0
129.4
129.3
125.2
121.5
121.4
118.4
115.0
112.2
110.6
58.4
46.9
40.4
25.2
16.1
15.5
190 180 170 160 150 140 130 120 110 100 90 80 70 60 50 40 30 20 10 0

Parámetros de adquisición

Tipo de Fuente:	ESI	Polaridad:	Positive	Nebulizador:	2.0 Bar
Inicio Scan:	50 m/z	Set Capillary	4500 V	Temperatura secado:	190 °C
Final Scan:	3000 m/z	Set End Plate Offset	-500 V	Gas de secado:	7.0 l/min

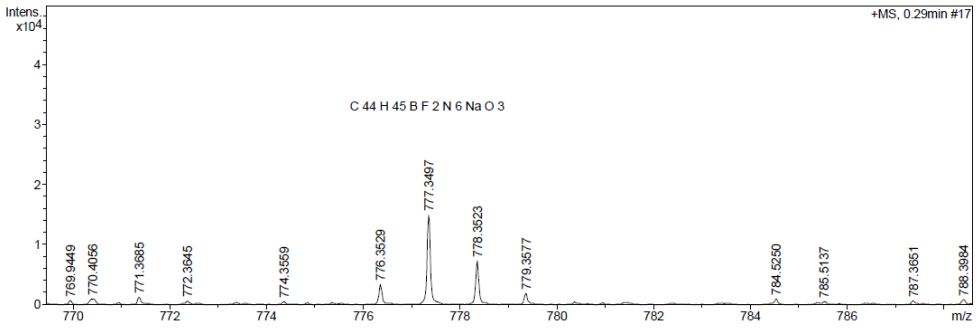

Formula	m/z	z	|err| [ppm]	Mean err [ppm]	mSigma
C 44 H 45 B F 2 N 6 Na O 3	777.3514	1+	1.2	1.5	10.2

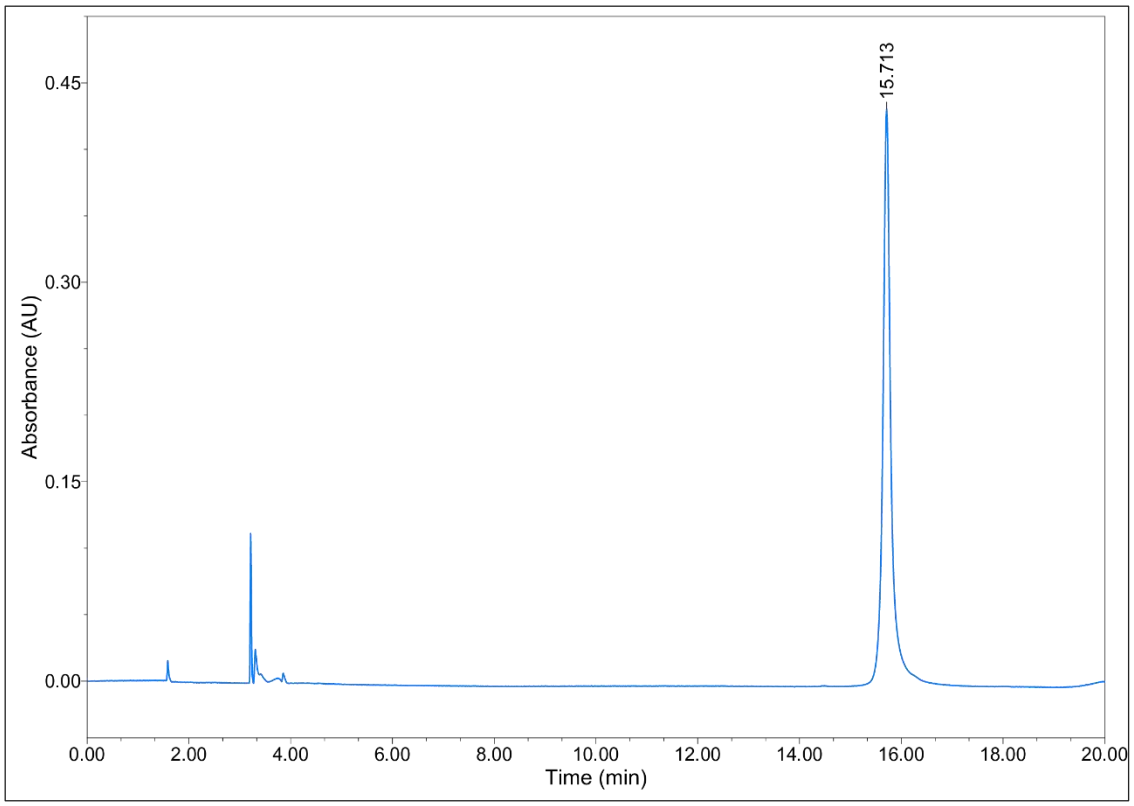

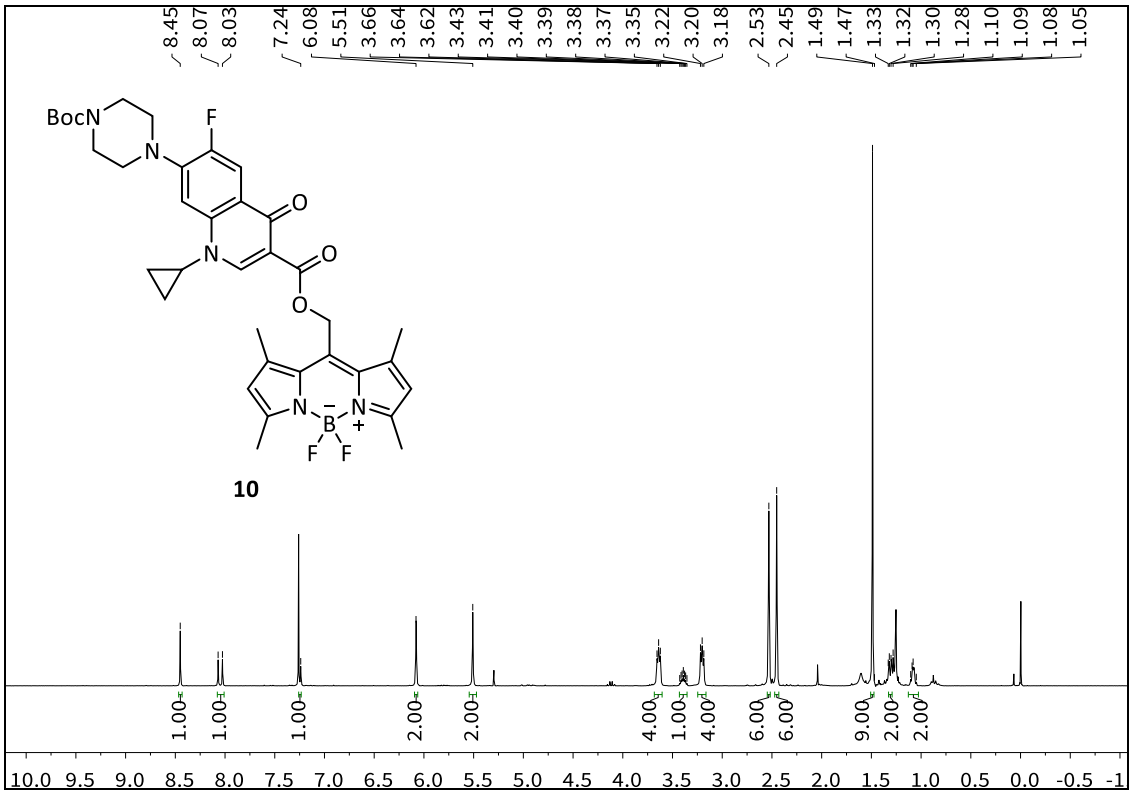
8.45
8.07
8.03
7.24
6.08
5.51
3.66
3.64
3.62
3.43
3.41
3.40
3.39
3.38
3.37
3.35
3.22
3.20
3.18
2.53
2.45
1.49
1.47
1.33
1.32
1.30
1.28
1.10
1.09
1.08
1.05
BocN
F
N
O
O
O
N
N
B
F
F
10
1.00
1.00
1.00
2.00
2.00
4.00
1.00
4.00
6.00
6.00
9.00
2.00
2.00
10.0 9.5 9.0 8.5 8.0 7.5 7.0 6.5 6.0 5.5 5.0 4.5 4.0 3.5 3.0 2.5 2.0 1.5 1.0 0.5 0.0 -0.5 -1

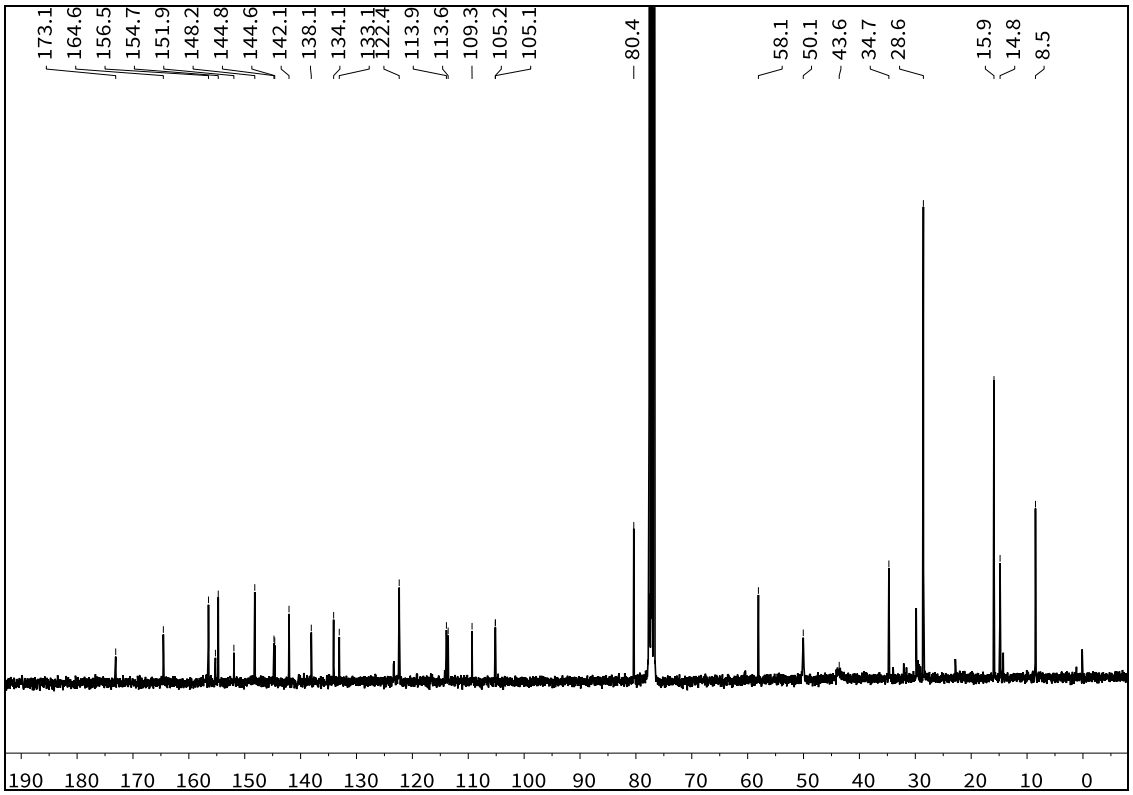
173.1
164.6
156.5
154.7
151.9
148.2
144.8
144.6
142.1
138.1
134.1
133.1
122.4
113.9
113.6
109.3
105.2
105.1
80.4
58.1
50.1
43.6
34.7
28.6
15.9
14.8
8.5
190 180 170 160 150 140 130 120 110 100 90 80 70 60 50 40 30 20 10 0

Parámetros de adquisición

Tipo de Fuente:	ESI	Polaridad:	Positive	Nebulizador:	2.0 Bar
Inicio Scan:	50 m/z	Set Capillary	4500 V	Temperatura secado:	190 °C
Final Scan:	3000 m/z	Set End Plate Offset	-500 V	Gas de secado:	7.0 l/min

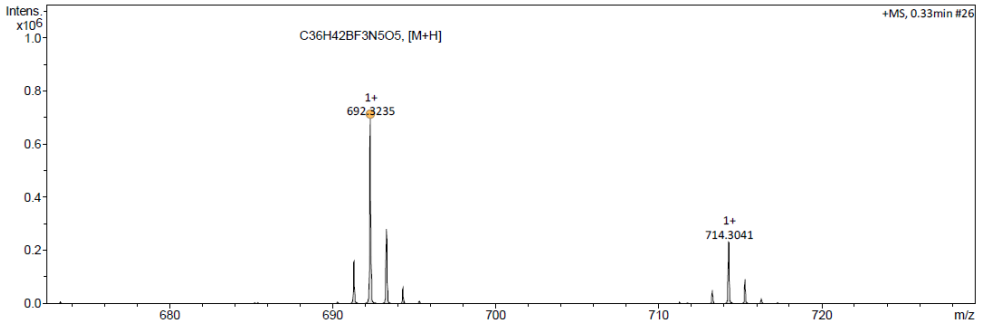

Ion Formula	m/z	z	|err| [ppm]	Mean err [ppm]	mSigma
C36H42BF3N5O5	692.322561	1+	0.4	1.2	4.7

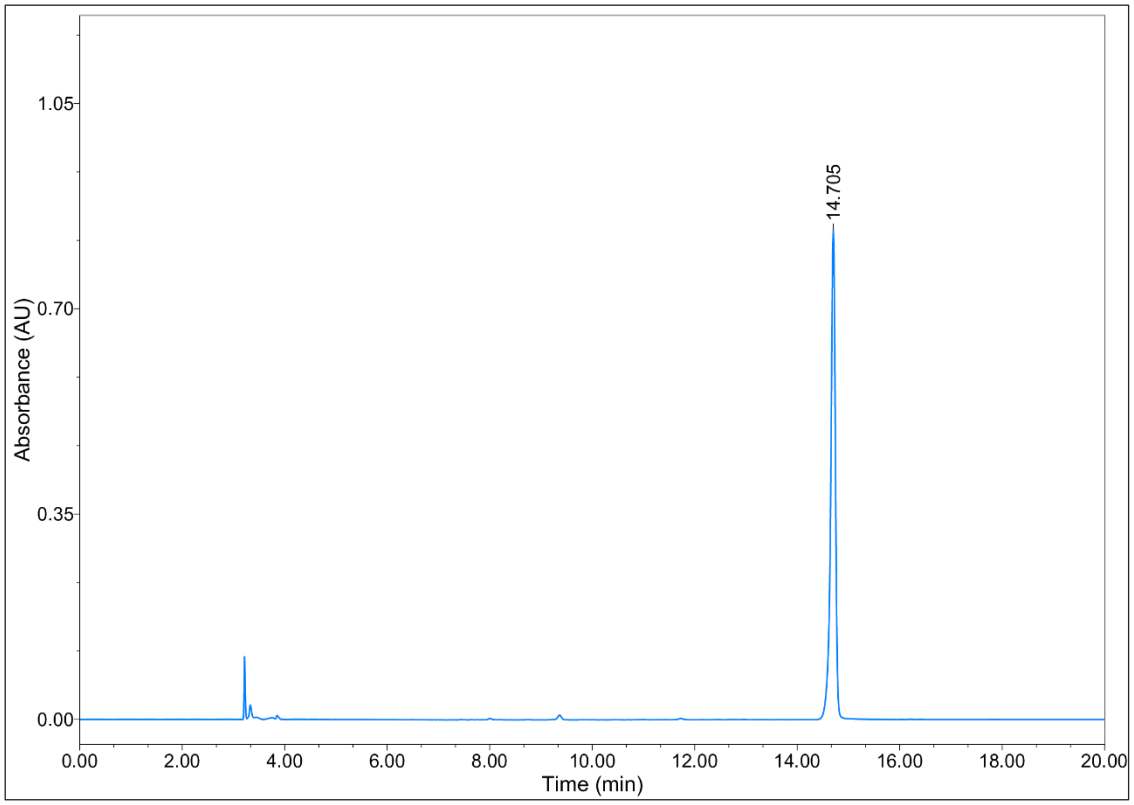

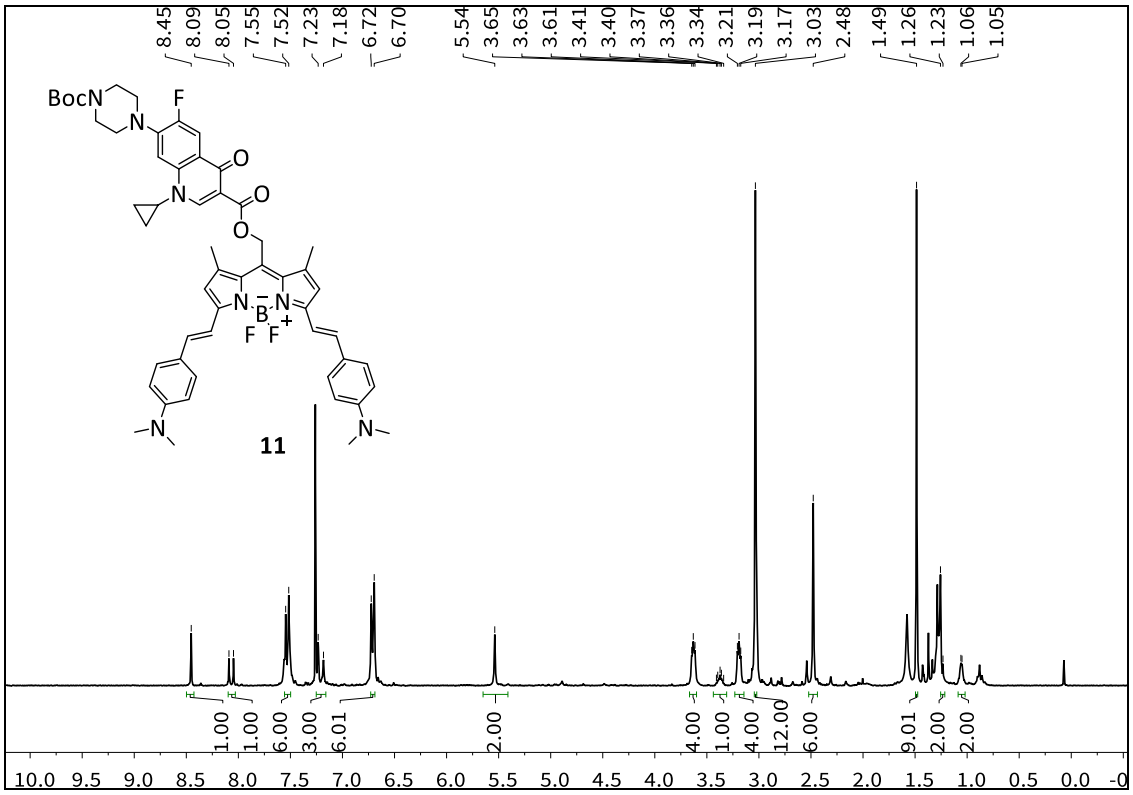
8.45
8.09
8.05
7.55
7.52
7.23
7.18
6.72
6.70
5.54
3.65
3.63
3.61
3.41
3.40
3.37
3.36
3.34
3.21
3.19
3.17
3.03
2.48
1.49
1.26
1.23
1.06
1.05
BocN
F
O
O
O
N
N
N
B
F F
N
N
11
1.00
1.00
6.00
3.00
6.01
2.00
4.00
1.00
4.00
12.00
6.00
9.01
2.00
2.00
10.0 9.5 9.0 8.5 8.0 7.5 7.0 6.5 6.0 5.5 5.0 4.5 4.0 3.5 3.0 2.5 2.0 1.5 1.0 0.5 0.0 -0

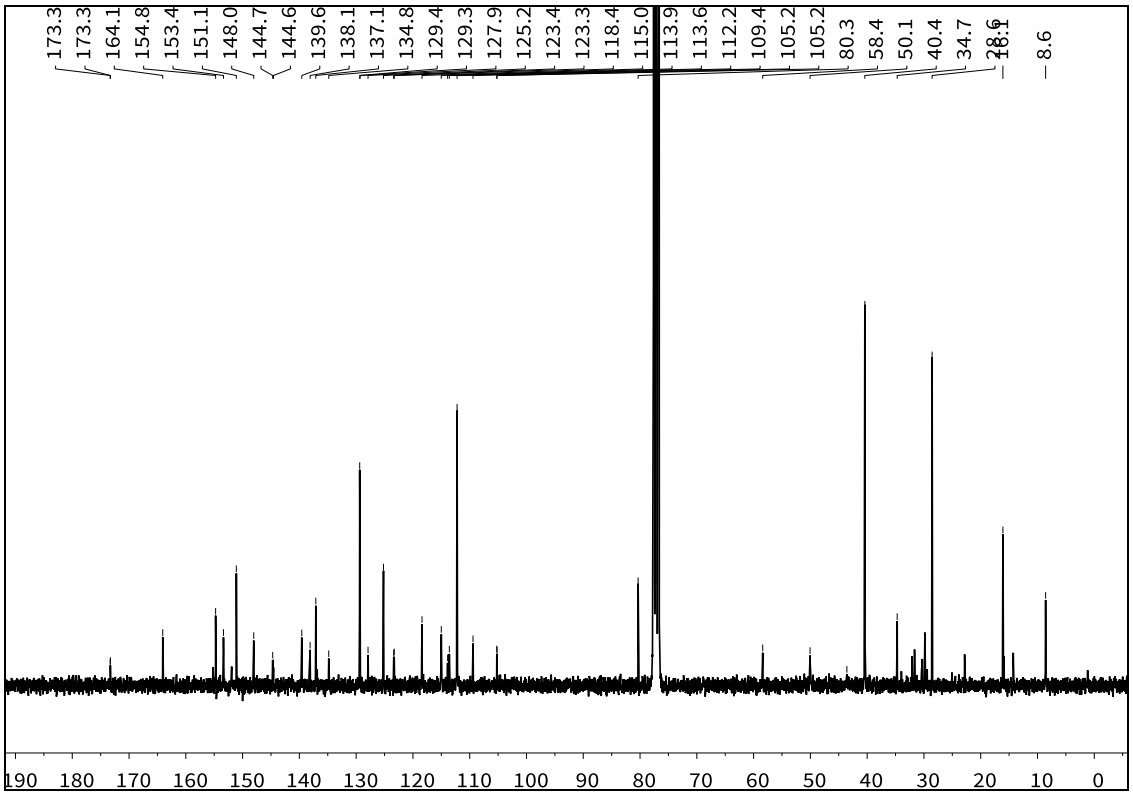
173.3
173.3
164.1
154.8
153.4
151.1
148.0
144.7
144.6
139.6
138.1
137.1
134.8
129.4
129.3
127.9
125.2
123.4
123.3
118.4
115.0
113.9
113.6
112.2
109.4
105.2
105.2
80.3
58.4
50.1
40.4
34.7
28.6
28.1
8.6
190 180 170 160 150 140 130 120 110 100 90 80 70 60 50 40 30 20 10 0

Parámetros de adquisición

Tipo de Fuente:	ESI	Polaridad:	Positive	Nebulizador:	2.0 Bar
Inicio Scan:	50 m/z	Set Capillary	4500 V	Temperatura secado:	190 °C
Final Scan:	3000 m/z	Set End Plate Offset	-500 V	Gas de secado:	7.0 l/min

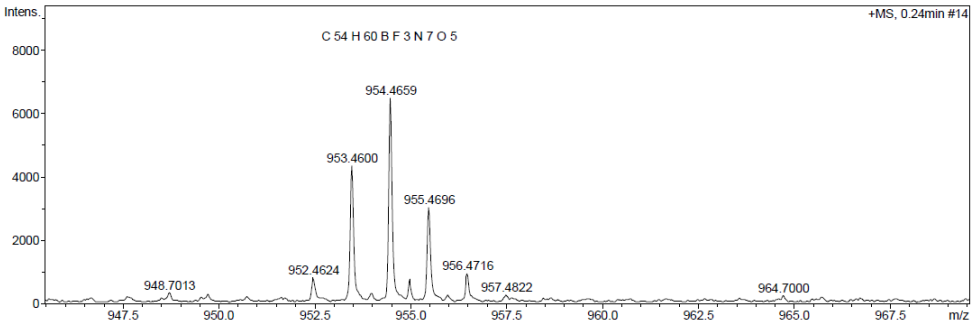

Formula	m/z	z	|err| [ppm]	Mean err [ppm]	mSigma
C 54 H 60 B F 3 N 7 O 5	954.4704	1+	3.8	7.0	193.0

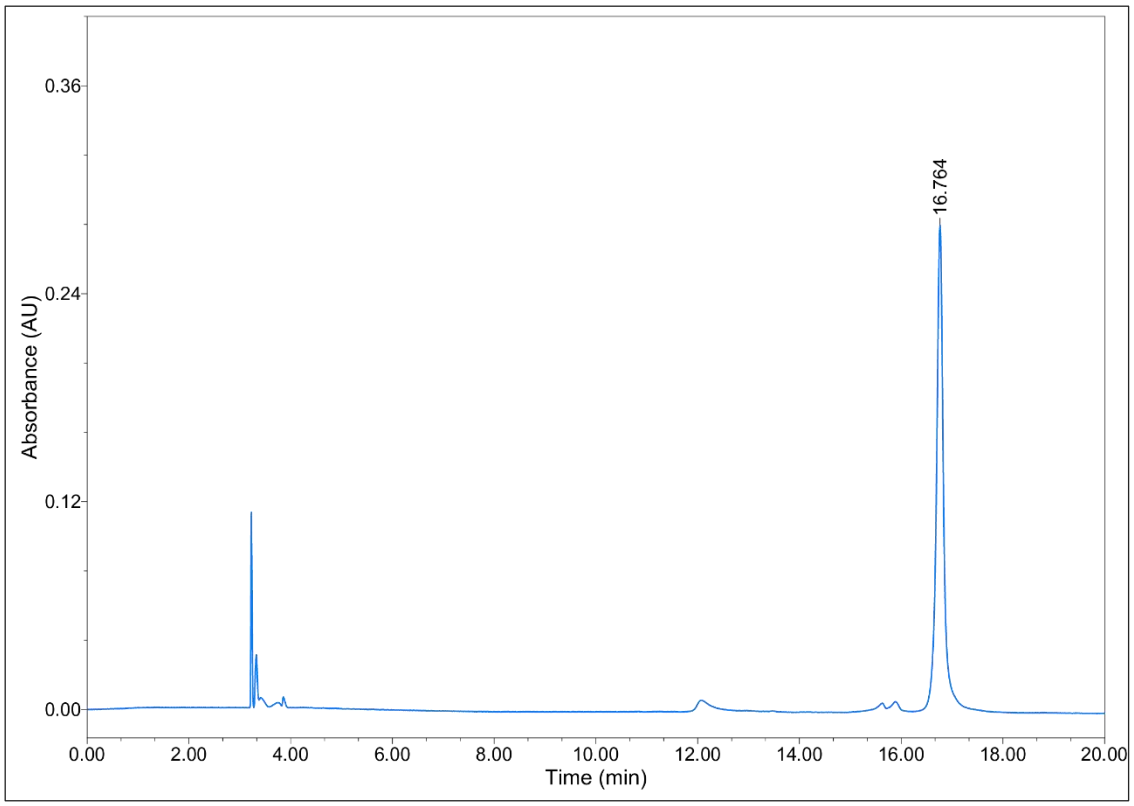

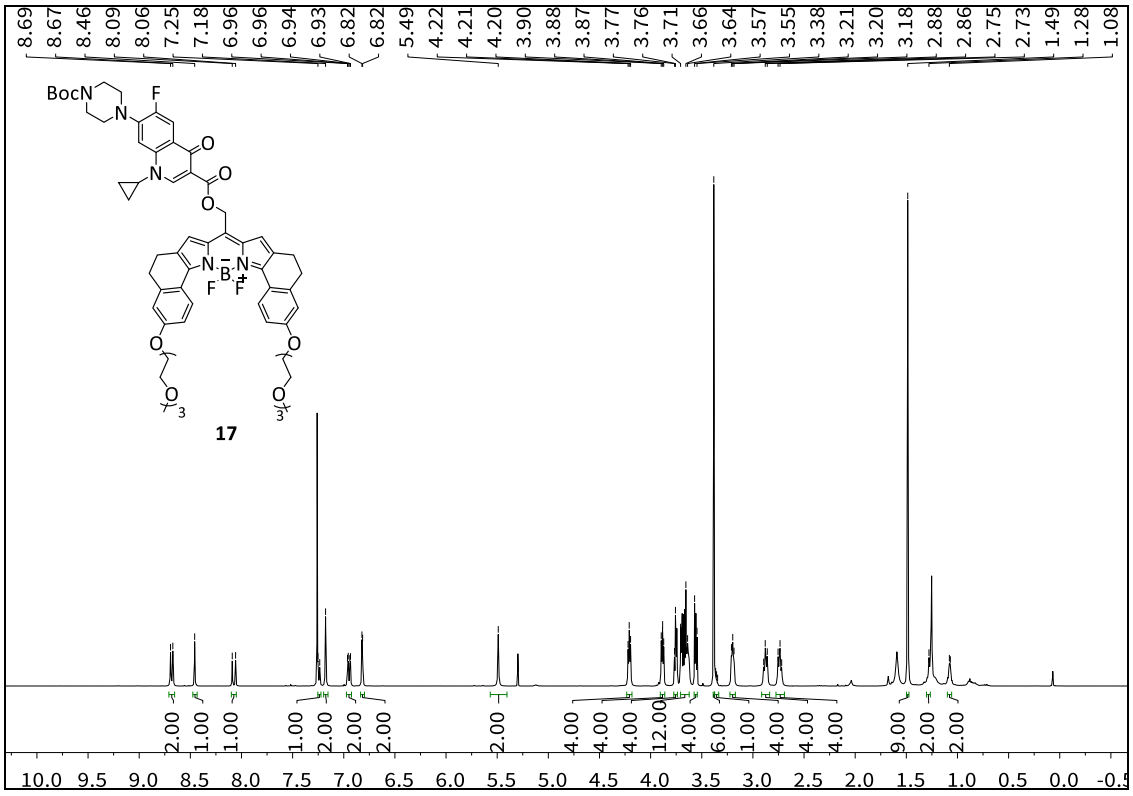
8.69 8.67 8.46 8.09 8.06 7.25 7.18 6.96 6.96 6.94 6.93 6.82 6.82 5.49 4.22 4.21 4.20 3.90 3.88 3.87 3.77 3.76 3.71 3.66 3.64 3.57 3.55 3.38 3.21 3.20 3.18 2.88 2.86 2.75 2.73 1.49 1.28 1.08
BocN
F
O
O
O
N
N
B
F
F
O
O
3
O
O
3
17
2.00 1.00 1.00 1.00 2.00 2.00 2.00 2.00 4.00 4.00 4.00 12.00 4.00 6.00 1.00 4.00 4.00 4.00 9.00 2.00 2.00
10.0 9.5 9.0 8.5 8.0 7.5 7.0 6.5 6.0 5.5 5.0 4.5 4.0 3.5 3.0 2.5 2.0 1.5 1.0 0.5 0.0 -0.5

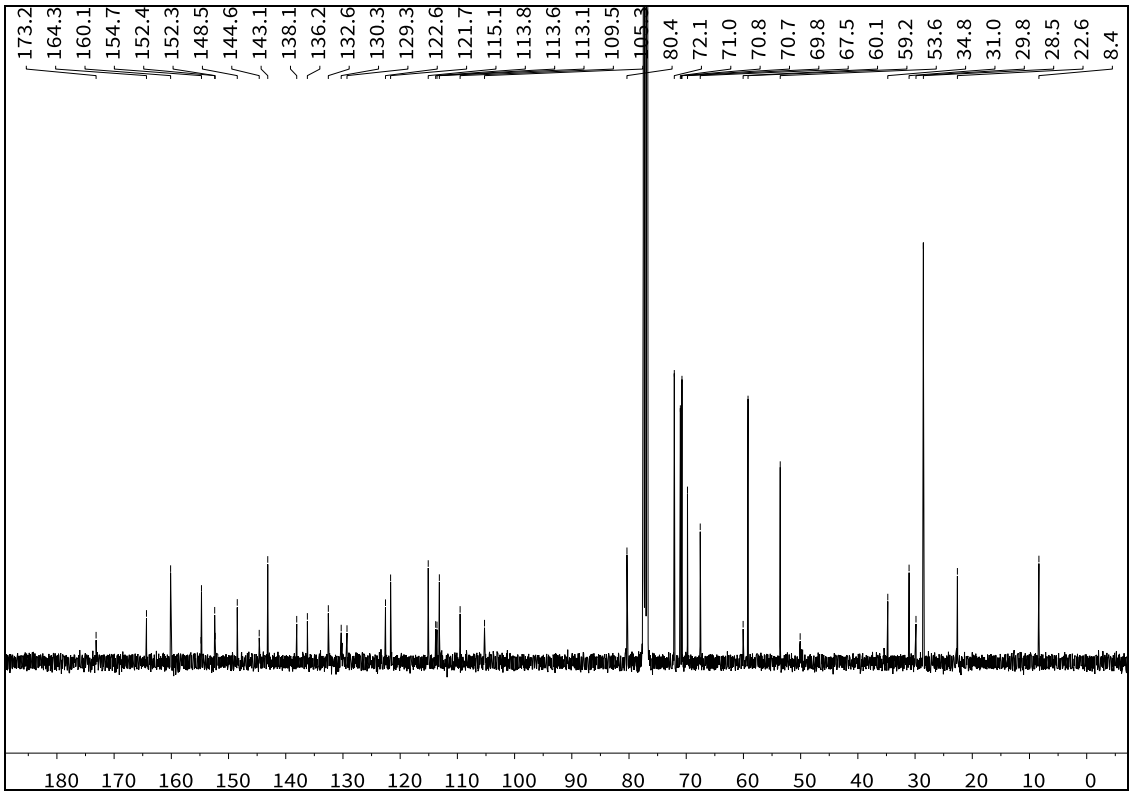
173.2 164.3 160.1 154.7 152.4 152.3 148.5 144.6 143.1 138.1 136.2 132.6 130.3 129.3 122.6 121.7 115.1 113.8 113.6 113.1 109.5 105.3 80.4 72.1 71.0 70.8 70.7 69.8 67.5 60.1 59.2 53.6 34.8 31.0 29.8 28.5 22.6 8.4
180 170 160 150 140 130 120 110 100 90 80 70 60 50 40 30 20 10 0

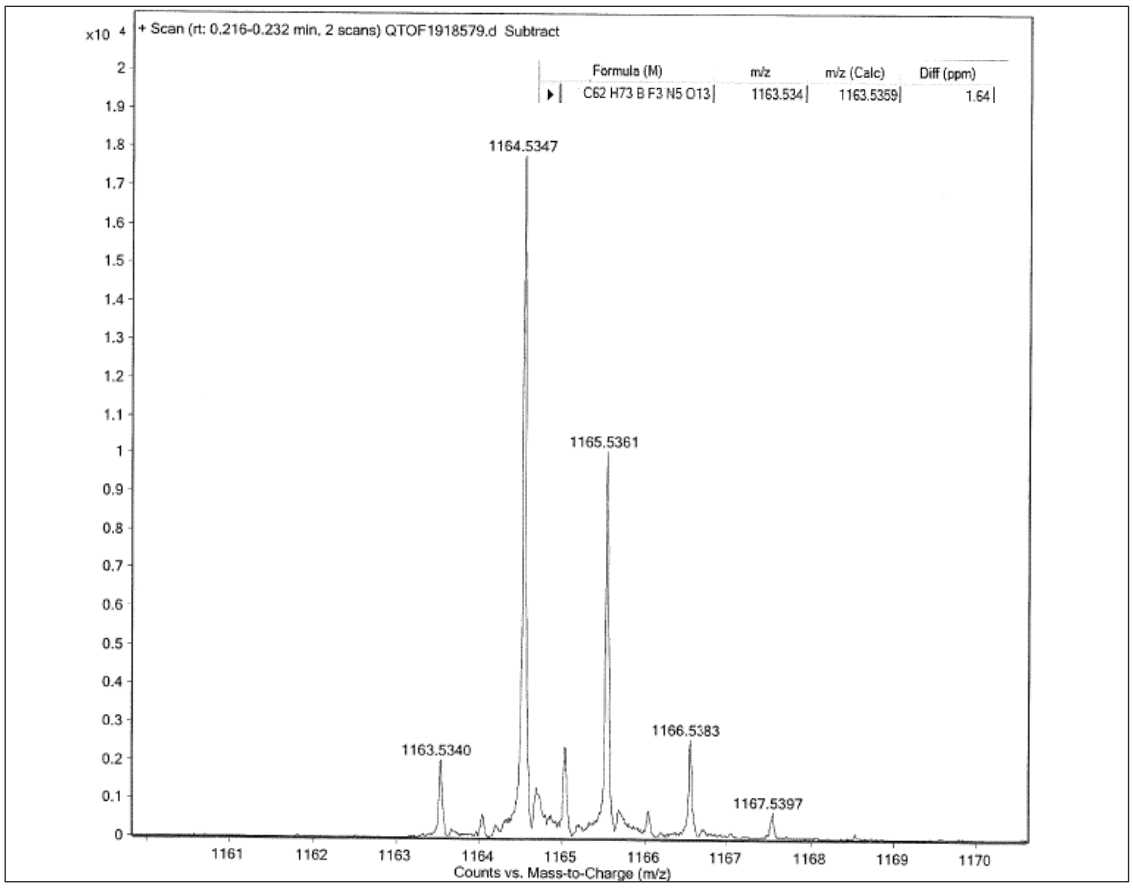
+ Scan (rt: 0.216-0.232 min, 2 scans) QTOF1918579.d Subtract
x10 4
Formula (M)
m/z
m/z (Calc)
Diff (ppm)
C62 H73 B F3 N5 O13
1163.534
1163.5359
1.64
1164.5347
1165.5361
1163.5340
1166.5383
1167.5397
Counts vs. Mass-to-Charge (m/z)

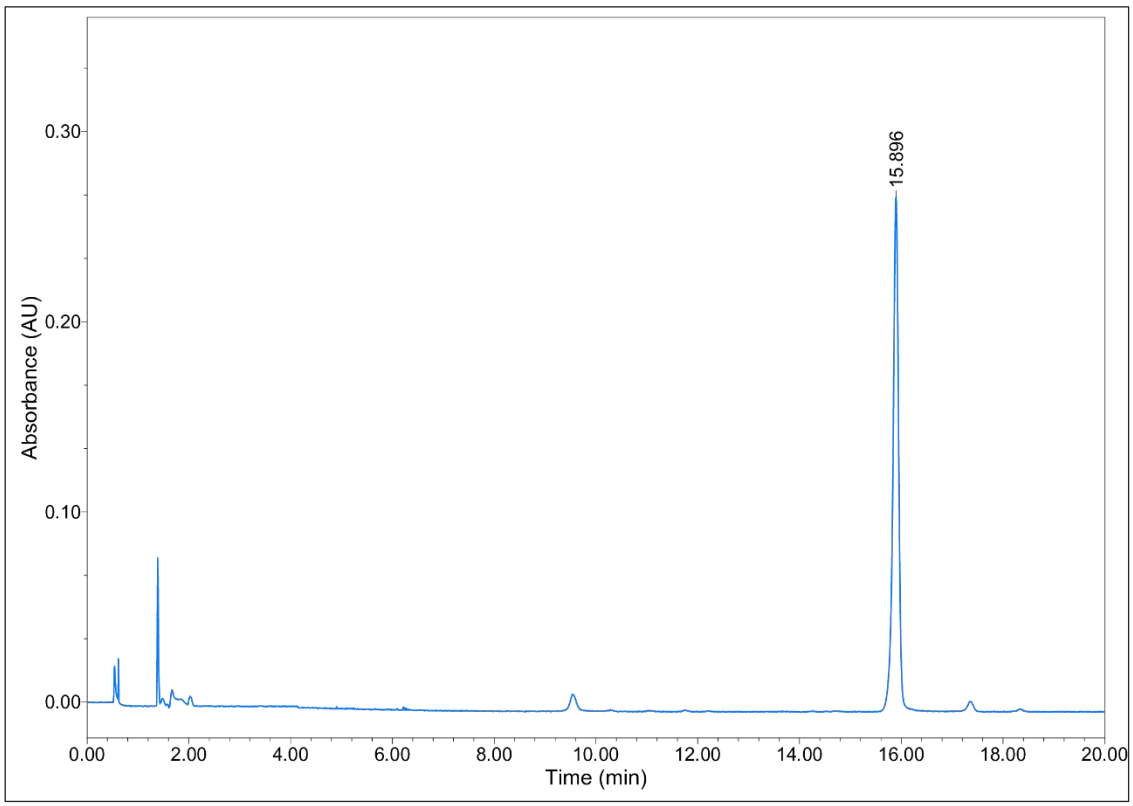
15.896
Absorbance (AU)
Time (min)